The management and conversion of light

Photocatalysis and electrochromics for solar energy conversion and light management

Jensen, Jacob

Publication date:
2014

Document Version
Peer reviewed version

The management and conversion of light

Photocatalysis and electrochromics for solar energy conversion and light management

Ph.D. Thesis

Jacob Jensen

November 2013

The management and conversion of light
Photocatalysis and electrochromics for solar energy conversion and light managemant

November 2013

By
Jacob Jensen

Sponsorship: The project was financed through the Solar Energy section

Academic advisor: Professor Frederik C. Krebs
Solar Energy section, Department of Energy Conversion and Storage

Cover photo: (A) 11 different electrochromic polymers investigated for photochemical stability (B) OPV/ECD demonstrator (C) Spectroelectrochemical analysis(D) ECD comprising silver grid as electrode (E) Roll coating of ECP-magenta

Published by: Department of Energy Conversion and Storage, Frederiksborgvej 399, Building 111, 4000 Roskilde, Denmark

ISBN: [000-00-0000-000-0]

Preface

This thesis presents the highlights of my work carried out as a Ph.D. student at the Technical University of Denmark in the period from August 9th, 2010 until November 6th, 2013 solar energy section; Department of Energy Conversion and Storage. The work has been funded by the section for solar energy and completed under the supervision of Prof. Frederik C. Krebs.

When the former Head of Section Peter Sommer-Larsen called me in July 2010 and told me that I had got a Ph.D. position at the solar energy program, I was naturally very excited as I have always thought highly of Risø as a research institution. But the excitement was just as much due to the fields I was supposed to conduct research in. Photocatalytic reduction of carbon dioxide using titanium dioxide was one of these fields and it is a very fascinating thought to address one of the greatest environmental challenges by shining light onto a mineral. The other part of the project was electrochromic polymers, which is equally fascinating although not as grand. The fascinating thing about electrochromic polymers is that the messy slurry you had a week ago in a separatory funnel can be turned into beautiful thin films that change color by a small applied potential.

I think success in the lab gives every scientist a “hell yearh” feeling. I was warned by Frederik Krebs who at my interview said “most of the stuff we do here don’t work, that’s why it’s called science and not production”. The essence of that is important to remember, as research is always uphill with headwind, but the great thing about doing research is that you contribute to scientific development. Your research might be a parenthesis, but it might also turn out to be important and advance science in general.

I feel very privileged to have conducted research in the SOL group. The SOL group is a great collection of people and I would like to thank the whole group for three exciting years.

I owe a lot of gratitude to my supervisor Professor Frederik Krebs, whom I respect deeply for his knowledge on every aspect of science, and his enthusiastic “let’s do the

experiment" attitude. On top of this Frederik is a really nice guy, and although we have had a few disagreements during the last three years, I like that Frederik always speaks his mind. Kristian Larsen and Torben Kjær also deserve recognition for their technical support and I have benefitted quite a bit from their knowledge on building all kinds of things in metal. Senior Scientist Mikkel Jørgensen always found time to help out with discussion on various aspects of science in general and synthesis in particular. Henrik Friis Dam has helped with crash courses in basic physics and editing this dissertation.

For my external stay I had the opportunity to work in the lab of Professor John. R. Reynolds at Georgia Institute of Technology. They stay in Atlanta was a very good experience for me both personally and professionally. I learned a lot from Professor Reynolds and I would also like to thank him for making me feel welcome in the group. Two other people from Reynolds group deserve notice: Dr. Aubrey Dyer for helping out with everything concerning our stay, being a really good colleague and a good friend. The same goes for Coralie Richards for thoughts on chemistry and life in general.

For proof reading of this manuscript I thank:

Nieves Espinosa, Coralie Richards, Mikkel Jessing, Aubrey Dyer, Mikkel Jørgensen and Bodil Jensen

Roskilde, November 2013

Jacob Jensen

The management and conversion of light

Abstract

Electrochromic conjugated polymers have during the last two decades shown promise as switchable components in displays, windows, signs and other optical applications. Properties such as response time, solubility, electrochemical stability, and color have been fine-tuned, but contrary to their inorganic counterparts there are currently no commercial applications comprising electrochromic polymers. This dissertation addresses several aspects concerning the development of electrochromic devices using polymers coated onto flexible substrates using spray-coating, spin-coating and slot-die coating methods. A key challenge in device fabrication is the development of a suitable electrolyte system, and two electrolyte systems are compared in fully printable and laminated devices on flexible substrates. Devices of various sizes are presented and the transmission contrast, when switched between the fully bleached and fully colored state, are found to be 43 % at Abs_{max} with a response time of less than 10 seconds. To show possible applications, an electrochromic display powered by a printed organic photovoltaic device are demonstrated, that can switch between the two redox states during solar exposure.

In order to reduce production cost, indium-doped tin oxide (ITO) is substituted for two different thin silver grids as electrode material. These grids coated with a commercially available conductive poly(3,4-ethylenedioxythiophene):poly(4-styrenesulfonate acid) formulation (PEDOT:PSS) show sub-second response times for a 30% optical contrast. PEDOT:PSS is found to be superior to the polypyrrole previously employed in electrochromic devices, and in addition the PEDOT:PSS layer increase the conductivity in the hexagonal grid structure. To explore direct photopatterning and multi-film processing a methacrylate substituted poly(ProDOT) is synthesized. Thin films of this polymer crosslink upon UV irradiation and become insoluble in common organic solvents. Electrochemical, spectroelectrochemical, and colorimetric analyses of the crosslinked polymer films are presented, which show that crosslinking does not affect the electrochromic properties.

Electrochromic polymers show appreciable electrochemical stability, but the photochemically stability has never been thoroughly addressed. The stability of thin flexible organic electrochromic films are shown to depend on polymer composition and a hypothesis is presented that shows good correspondence between the experimental results and a simple mathematical model, although there are questions that remain unanswered. The majority of the polymers degrade within 4-5 hours when exposed to solar radiation (AM 1.5 G), and to extend the lifetime of electrochromic devices, oxygen and UV barrier foils are found to drastically slow the photochemical decomposition of the polymer films. When properly protected, the polymer films are sufficiently stable for several years indoors and for a few years under outdoor conditions.

Two photocatalytic reactions are explored; carbon dioxide reduction and water splitting. Practical solutions are presented, and the use of flexible substrates as carrier foils is explored. A key challenge in these conversion systems is the necessary precautions that must be taken when evaluating conversion and this is most convincingly done by using isotopically labelled carbon dioxide. In this regard infrared spectroscopy is found to be a useful analytical tool. The successful photo reduction of isotopically marked carbon dioxide results in a product composition of both ^{13}C and ^{12}C species, and based on similar findings presented in the literature, it is believed that carbonaceous residues that reside on the chamber or catalyst surface contribute to the product composition.

Resume

Elektrokrome konjugerede polymerer har de seneste årtier vist potentiale som farveskiftende materialer i displays, vinduer, skilte samt andre optiske anvendelser. Egenskaber såsom optisk kontrast, opløselighed, elektrokemisk stabilitet og farve er blevet finjusteret, men i modsætning til uorganiske elektrokrome stoffer er der for tiden ingen kommercielle anvendelse af elektrokrome polymerer. Denne afhandling omfatter flere aspekter vedrørende udvikling af elektrokrome komponenter (ved en komponent forstås en funktionel enhed), bestående af polymerer trykt på fleksible folier ved brug af spray-coating, spin-coating og slot-die coating teknikker. En af udfordringerne ved fremstillingen, er udviklingen af et passende elektrolytsystem. To elektrolytsystemer bliver her undersøgt i laminerede enheder bestående af fleksible substrater. Displays af forskellig størrelse fremstilles, og med en skiftetid på mindre end 10 sekunder, ved skift mellem de to redoxstadier (hhv. bleget og farvet) opnås der en optisk kontrast på 43 % ved den maximalt absorberende bølgelængde. For at vise mulige anvendelser demonstreres et elektrokromt display forsynet med en trykt organisk solcelle, som kan facilitere et skift mellem de to redoxstadier ved påvirkning af sollys. For at reducere produktionsomkostningerne erstattes indium-doped tinoxid (ITO) med to forskellige tynde sølvgitre som elektrode materiale. Elektrokrome displays baseret på sådanne sølvgitter elektroder påtrykt en ledende poly(3,4-ethylenedioxythiophene):poly(4-styrenesulfonsyre) (PEDOT:PSS) opløsning, skifter farve på under 1 sekund med en optisk kontrast på 30%. Brugen af PEDOT:PSS har vist sig fordelagtigt i forhold til tidligere anvendte elektrokromiske materialer, og dertil kommer, at PEDOT:PSS forbedrer ledningsevnen. For at undersøge direkte foto-patterning og trykning af flere på hinanden følgende lag er en methacrylate-substituteret poly(ProDOT) blevet syntetiseret. Tynde film af denne polymer krydsforbinder ved UV-bestråling og bliver herved uopløselige i almindelige organiske opløsningsmidler. Elektrokemiske, spektroelektrokemiske og kolorimetriske analyser af de UV bestrålede polymerfilm viser, at krydsforbindingen ikke påvirker de elektrokrome egenskaber.

Elektrokrome polymerer viser generelt god elektrokemisk stabilitet, men fotokemisk stabilitet er ikke nærmere undersøgt. Det er påvist, at stabiliteten af organisk elektrokrome film afhænger af polymersammensætning, og en hypotese præsenteres, som viser god sammenhæng mellem de eksperimentelle resultater og en simpel matematisk model. Hovedparten af polymererne nedbrydes inden for 4-5 timer under påvirkning af sollys (AM 1.5 G), men levetiden af elektrokrome komponenter kan mærkbart forlænges ved brug af ilt- og UV- barrierer folier. Ved en sådan beskyttelse er polymerfilmene stabile i mange år under indendørs forhold og nogle få år udendørs.

To fotokatalytiske reaktioner er undersøgt; reduktion af kuldioxid og vandsplitning. Praktiske løsninger vises, og brugen af fleksible substrater som den bærende folie er undersøges. En væsentlig udfordring ved fotokatalytisk carbondioxid omdannelse er "forurening" med carbon, og de forholdsregler som derfor må tages. Dette gøres mest overbevisende ved brug af isotopmærket kuldioxid og infrarød spektroskopi er dertil fundet at være et nyttigt analytisk værktøj. Den succesfulde fotoreduktion af isotopmærket kuldioxid medfører en produktsammensætning af både ^{13}C og ^{12}C elementer, og baseret på lignende undersøgelser fra andre forskningsgrupper, antages det, at kulstofholdige restmaterialer, som findes på reaktionskammerets eller på katalysatorens overflade, bidrager til produktsammensætningen.

List of publications

This dissertation is based on the following publications, which are found as appendices 3.1 to 3.5.

Appendix 3.1

J. Jensen, H. F. Dam, J. R. Reynolds, A. L. Dyer and F. C. Krebs, *Manufacture and Demonstration of Organic Photovoltaic-Powered Electrochromic Displays Using Roll Coating Methods and Printable Electrolytes*, *J. Polym. Sci. Part B,* 2012, **50,** 536-545.

Appendix 3.2

J. Jensen, A. L. Dyer, D. E. Shen, F. C. Krebs and J. R. Reynolds, *Direct Photopatterning of Electrochromic Polymers*, *Advanced Functional Materials,* 2013, **23,** 3728-3737.

Appendix 3.3

J. Jensen, M. V. Madsen and F. C. Krebs, *Photochemical Stability of Electrochromic Polymers and Devices*, *J. Mater. Chem. C,* 2013, **1,** 4826-4835.

Appendix 3.4

J. Jensen, M. Hösel, I. Kim, J. Yu, J. Jo and F. C. Krebs, *Fast Switching ITO free Electrochromic Devices*, Advanced *Functional Materials,* Article published online Nov. 2013, DOI: 10.1002/adfm.201302320

Appendix 3.5

J. Jensen, M. Mikkelsen and F. C. Krebs, *Flexible Substrates as Basis for Photocatalytic Reduction of Carbon Dioxide, Sol Energ Mater Sol Cells,* 2011, **95,** 2949-2958.

Abbreviations

Abs_{max}	-	Maximum absorbing wavelength
AIBN	-	Azobisisobutyronitrile
A/T	-	Absorptive/transmissive
A/R	-	Absorptive/reflective
BTD	-	2,1,3-benzothiadiazole
C	-	Coulomb (charge)
CAP	-	Chemically amplified photolithography
CIE	-	Commision International l'Eclaire
CB	-	Conducting band
CV	-	Cyclic voltammetry
CT	-	Charge transfer
D-A	-	Donor-acceptor
DCVC	-	Dry column vacuum chromatography
ECD	-	Electrochromic device
ECP	-	Electrochromic conjugated polymer
ECP-magenta		Poly((2,2-bis(2-ethylhexyloxymethyl)-propylene-1,3-dioxy)-3,4-thiophene-2,5-diyl)
Eg	-	Energy gap/band gap
EGDMA	-	Ethyleneglycol dimethacrylate
EtOAc	-	Ethyl acetate
EtOH	-	Ethanol
η	-	Coloration efficiency
η_d	-	Device coloration efficiency
HOMO	-	Highest occupied molecular orbital
I	-	Intensity of transmitted light
I_o	-	Intensity of incident light
IL	-	Ionic liquid
IR	-	Infrared

ITO	-	Indium-doped tin oxide
LUMO	-	Lowest unoccupied molecular orbital
MCCP	-	Minimally color changing polymer poly(N-octadecyl-(propylene-1,3-dioxy)-3,4-pyrrole-2,5-diyl)
Me	-	Methyl
MeOH	-	Methanol
MMA	-	Methyl methacrylate
NCAP	-	Non-chemically amplified photolithography
NIR	-	Near Infrared (app. 800-1500 nm)
NMR	-	Nuclear Magnetic Resonance
OPV	-	Organic photovoltaic
PC	-	Propylene carbonate
PE	-	Polyethylene
PEDOT	-	Poly(3,4-ethylenethiophene)
PEO	-	Polyethylene oxide
PET	-	Polyethylene terephthalate
PMMA	-	Polymethyl methacrylate
ProDOT	-	Propylene dioxythiophene
PSS	-	Polystyrene sulfonate
PWS	-	Photocatalytic water splitting
Q	-	Charge pr. Area
RT	-	Room temperature
ΔT	-	Optical contrast
%T	-	% Transmission
TLC	-	Thin layer chromatography
UV	-	Ultra violet
VB	-	Valence band

Content

Chapter 1

1. Introduction

Due to annual man-made emissions of 24 gigaton CO_2, stemming mainly from the combustion of fossil fuels, the atmospheric content of CO_2 has increased from 270 ppm to 385 ppm, which amounts to around 1 teraton excess carbon dioxide in the atmosphere[1]; proportions that exceeds mankind's capacity for handling by several orders of magnitude. As such, laboratory-scale photocatalytic systems are not particularly useful unless they can be scaled to the required level without any carbon footprint. This fundamental problem has resulted in the passive view that man-made carbon dioxide emissions should be lowered but not reverted. Reduction of CO_2 is done most efficiently directly at the source e.g. flue gasses from coal fired power plants, iron smelters and concrete factories, but extracting the carbon dioxide from the flue gasses is costly, and the carbon sequestration and storage (CSS) costs can be as high as 50 % of the electricity costs. An energy efficient alternative would be through a renewable source that provides the energy to reduce atmospheric carbon dioxide.

The solar energy available at the surface of the earth is around 1000 W m^{-2} (AM 1.5 G), and depending on the local climate one can expect to receive between 1000-2000 kWh m^{-2} $year^{-1}$ from solar irradiation. Based on this, a rational approach seems to be one where the sunlight is used to drive the reduction of carbon dioxide. A solution to the challenge of this scale is through use of flexible substrates as carrier foils. By employing flexible substrates, the large areas necessary for solar exposure conversion can be achieved through fast coating of low cost photocatalysts using roll-to-roll processing at low temperatures.

1.1 Light

In order to understand how the properties of light can be exploited, this dissertation starts with a brief introduction to the nature of electromagnetic irradiation, with a starting point in the 400-800nm range of the electromagnetic spectrum, also known as

the visible light. The electromagnetic spectrum with the visible range highlighted is shown in Figure 1-1.

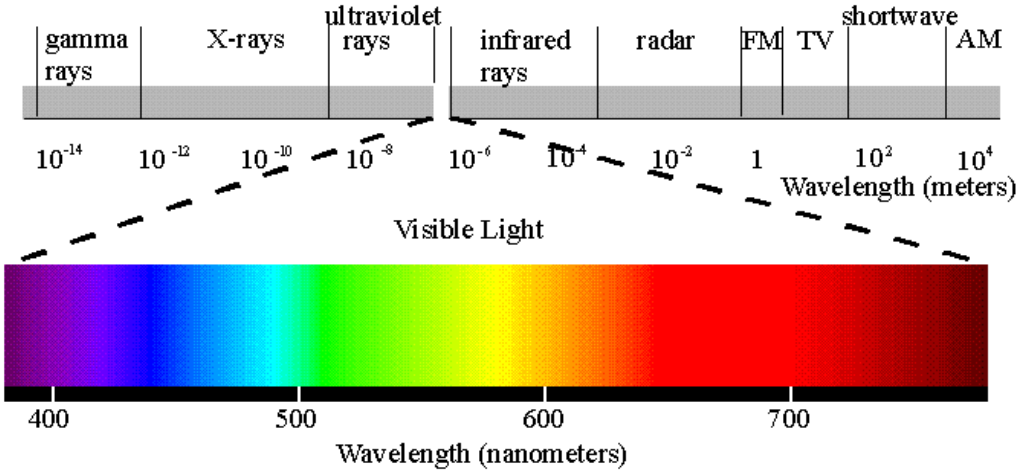

Figure 1-1: The electromagnetic spectrum. The visible region from 400-800 nm has been expanded to show dependence of colors on wavelengths. When all the colors of emitted visible light are added, the resulting light is perceived as white or "normal" light.

As seen the visible is divided into colors dependent on the wavelength, λ. Long wavelengths corresponds to red light and short the wavelengths to blue light.

The wavelength and frequency of the wave are inversely related, with the relationship given by:

$$c = \lambda/\nu$$

Here c denotes the speed of light (app. 3.0×10^8 m/s), λ the wavelength and ν the frequency. In the above description light is be categorized according to wavelength and it follows that light is made up of waves. This is partly true, in that some properties of light is better described using waves, while others are better described when light is regarded as particles called photons. The energy E of such photons is given by Planck's relation:

$$E = h\nu$$

Where h is Planck's constant = $6.6260755 \times 10^{-34}$ Joule x second

This can be rearranged to:

$$E = h\,c/\lambda = 1.986 \times 10^{-25}\ J\,m / \lambda$$

$$E = 1240\ eV\,nm / \lambda\ (nm)$$

Where eV is the energy expressed in electron volts. Since the nominator only contains constants, the essence of this is that that more energy is contained in light of shorter wavelengths than in light of longer wavelengths. To be able to harvest this energy the irradiation must be absorbed by a media. Water is good example of a media that absorbs solar irradiation, but water mainly absorbs radiation of wavelengths longer than those in the visible region. These wavelengths correspond to the vibrational resonance wavelengths in the bindings of a water molecule (and other molecules), and hence the energy from solar radiation is converted to thermal energy as the vibrational motions increases the temperature e.g. in a cup of water standing in the midday sun. This way of capturing solar radiation is the basis for solar water heating systems.[2]

Another way to use the energy in light is through photovoltaics. Photovoltaics make use of that when light of an appropriate energy is absorbed in a material, the energy is transferred to electrons in the valence band (VB, the outermost filled band), whereby they can become excited to the conducting band (CB, the innermost unfilled band). If the excited electrons are separated from the "holes" they leave behind, charge is created that run through an external circuit and hereby solar radiation is converted to electrical energy.[3, 4]

1.2 Semiconductors and band gap

Converting sunlight to electricity cannot be done without energy losses; currently commercial silicon PV modules are able to convert about 16% of the sunlight into electrical energy while organic photovoltaics has an efficiency of up to 3% in large scale applications.[5, 6] This loss represents reflectance from the surface of the material, thermal losses, energy mismatch between the photon energies and the donor band gap and the non-unity absorption of the solar irradiation by the solar cell. The property of a material that defines the wavelengths that is absorbed is the *band gap.* As semiconductors lack coherent energy levels, there is a void region between the valence band

(VB) and the conducting band (CB), where energy transitions are not allowed, known as the band gap. If photons of energy equal to or higher than the band gap reaches the semiconductor surface and is absorbed, an electron is excited to the conducting band leaving behind a positively charged electron vacancy or hole (h^+).[7]

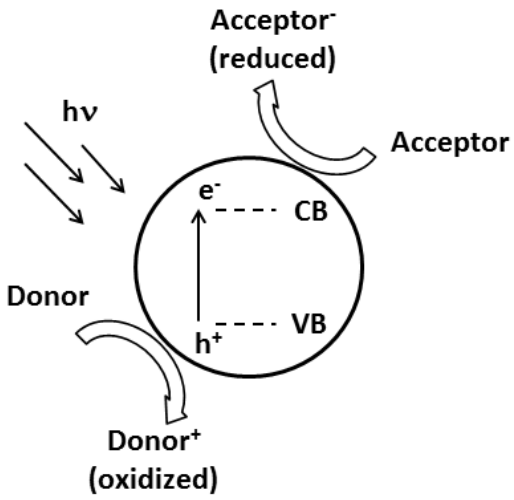

Figure 1-2: General mechanism of photocatalysis in a semiconductor. Solar irradiation excites an electron from the valance band (VB) to the conducting band (CB), whereby an electron deficiency (h^+, a "hole") is created. The excited electron is transferred to an acceptor species that becomes reduced, while a donor species is oxidized as it transfers an electron to the semiconductor.

Figure 1-2 shows how the energy in light is transferred from a donor species via a semiconductor to an acceptor species. As the excited electrons are replenished by a donor the semiconductor functions as a catalyst. This type of light induced reaction is the basis for the photocatalysed carbon dioxide reduction described in chapter 6 and the water splitting reactions described in chapter 7. This conversion stores solar energy as chemical energy (i.e. energy stored in chemical bonds) and resembles the photosynthesis occurring in plant cells whereby solar energy and carbon dioxide are converted into carbohydrates, and hence it is sometimes referred to as artificial photosynthesis.[8]

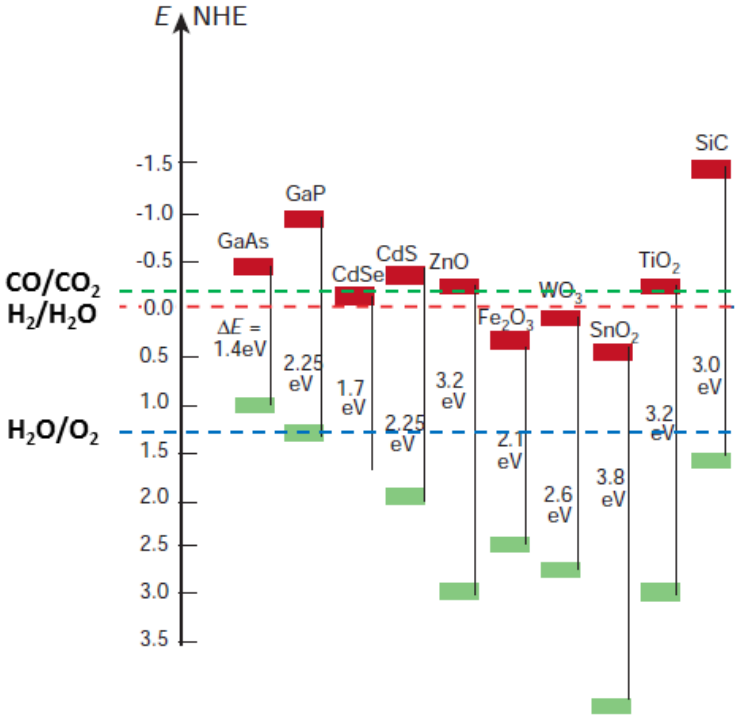

Figure 1-3: Band positions for various semiconductors employed in photocatalysis (in aqueous solution at pH = 1). The red squares represent the CB and the green squares the VB. The band gap (in electron volts) is shown between the two. The reduction potentials of carbon dioxide, water and oxygen relative to the standard hydrogen electrode (pH=1) are shown by the green, red and blue dashed lines respectively. Reprinted by permission from Macmillan Publishers Ltd: Nature,ref 5, copyright (2001).

Transition metal oxides and sulfides semiconductors are commonly employed as photocatalyst. Figure 1-3 shows a selection of semiconductors photocatalyst along with two important properties, the width of the band gap and the band gap positions. The energy levels at the bottom of the semiconductor conducting band is the reduction potential of the excited electron, while the top of the valence band is the oxidation potential of the holes generated. For reduction to occur, the reduction potential of the adsorbed species needs to be higher (more positive) than the conduction band of the photocatalyst, while oxidation requires the reduction potential (of the adsorbed species) to be lower (more negative) than the energy of the valence band holes. From Figure 1-3 several compounds seems ideal for both photocatalytic water splitting and carbon dioxide reduction, but as E = 1240 eV nm / λ (nm) it follows that semiconduc-

tors with band gaps above 3 eV require irradiation of approximately 400 nm and below, which is poorly matched by the solar spectrum.[9] In order to extend the absorption of the photocatalyst so as to better match the solar spectrum two strategies, *doping* and *sensitization*, are employed. While the two terms are used interchangeably sensitization usually refers to the process of making wide band gap semiconductors responsive to visible light using dyes or metal complexes,[10-15] while doping is the term often used when metal or metal ions are deposited on the semiconductor.[16-19] It should be noted that doping are employed for other purposes than solely used for induction of visible light response, e.g. as sites for electron and hole transfer to acceptor and donor species, and to prevent recombination of separated electron-hole pairs oxygen vacancies.

1.3 Carbon dioxide reduction vs. water splitting

While the photocatalytic processes are basically similar whether it is the reduction of carbon dioxide or decomposition of water, the two main differences are the reaction products and the practical challenges associated with handling the reactants. The products of carbon dioxide reduction are small carbon containing molecules such as carbon monoxide, methane, methanol, formic acid etc. commonly known as solar fuels. The majority of these products are liquids at room temperature and atmospheric pressure since and they can more or less be integrated into the infrastructure developed for the currently employed fossil based fuels.[20, 21] In addition to being useable as fuels these carbon species can also be used as precursors for more complex molecules. The products from water decomposition, oxygen and hydrogen are gasses at atmospheric conditions and room temperature, which mean that the energy density is significantly lower if hydrogen is not compressed. The challenge in storing and handling hydrogen is another challenge that has to be solved if hydrogen are to become the fuel of the future. While the reactions products seems to more challenging for water splitting than for carbon dioxide reduction, the situation is opposite for the reactants. As carbon dioxide is a gas under standard conditions it is more challenging to handle than water, and efficiently extracting carbon dioxide from the atmosphere is a significant

challenge.[1] For the purpose of facilitating the handling, photocatalytic reduction has been done on carbon dioxide dissolved in water. This approach is correspondingly difficult since solubility of CO_2 in aqueous solutions is low (33 mM at 25 °C at 1 atm.). The solubility is higher in organic solvents such as methanol, acetonitrile, and propylene carbonate but the conductivity is lower which leads to high Ohmic losses.[22-25] Another problem with using aqueous solution of carbon dioxide is that the reduction potentials of CO/CO_2 and H_2/H_2O are in close proximity to each other as indicated in Figure 1-3 (the other reduction products methane, formic acid etc. has reduction potentials in the same range). Since hydrogen formation is thermodynamically more advantageous than carbon dioxide reduction, the former reaction has to be suppressed in order for efficiently reduction of carbon dioxide.

In this dissertation the challenges associated with photocatalytic conversion of carbon dioxide and water is addressed. Reduction of carbon dioxide is the subject of chapter 6, with focus on the many pitfalls associated with this and especially when using flexible substrates as carrier foils. Photochemical water splitting using organic photovoltaics in combination with a photocatalyst will be covered in chapter 7.

1.4 Light management by electrochromic compounds

In addition to furnishing photocatalytic properties the band gap of certain transition metal oxides also give rise to electrochromism; the alteration of color by electricity.[26] Tungsten oxide (WO_3) is the most notable of the electrochromic (EC) oxides, but Ni, Ta, Ti, V, Mn and other also show electrochromism.[27-29] The valence of these oxides is changed by an applied potential, and this leads to a change in the electronic distribution due to ingress or ejection of electrons (and ion) from the EC film. The result is a change in the band gap and thus a change in the optical absorption (a detailed working mechanism is given in chapter 2).

Figure 1-4: Electrochromic windows from Sage Electrochromics at Siemens wind turbine factory in Hutchinson, Kansas. Reprinted from ref 30.

Electrochromism were at first expected to find application in devices for information displays, but the interest in this faded as liquid crystal displays conquered the market for these applications. But devices based on electrochromism might find renewed interest due to alternative applications. One of these is in the design of windows, where electrochromic compounds can be coated onto to the surface and function as an "electronic curtain" or "smart window".[31, 32] By using EC technology in window design it is possible to save energy by managing the solar radiation passing through a window and EC windows were shown to significantly reduce cooling in buildings due to solar heat and lightning energy use.[33] The company Sage Electrochromics (having recently merged with Saint-Gobain Recherché) is producing electrochromic windows that comprise WO_3 as shown in Figure 1-4.[30, 34, 35]

Other commercial uses of electrochromics involve dimmable windows installed in the Boing 787 "Dreamliner" aircraft, but the most widely used application of electrochromism (and possibly the least obvious) is in car rear-view mirrors. [36, 37] By having an electrochromic system that can attenuate the specular reflection of a polished alloy, it is possible to reduce the headlight glare of cars coming from behind. In addition to operating in an absorptive/reflective mode instead of an absorptive/transmissive mode (a detailed description is provided in chapter 2), another difference in these mirrors compared to the smart windows is that they employ electrochromic organic compounds; thiazines and viologens (bipyridilium species).[38]

As described further in chapter 2, the use of (organic) electrochromic conjugated polymers (ECPs), has opened up a new possibilities for electrochromic applications.

Electrochromic conjugated polymers show a multitude of colors made possible by band gap tuning, and the solubility can be controlled by side chain functionalization.[39, 40] Another advantage is their low fabrication cost and the possibility of using several cheap and low tech deposition techniques, including roll and roll-to-roll coating on flexible substrates. Yet despite these merits, devices comprising electrochromic polymers are still in the laboratory. This dissertation aims to explore how ECPs can be used in functional devices that are commercially interesting. The processability and challenges associated with device fabrication on flexible substrates is the topic of chapter 3. Chapter 4 describes the development of a photo patternable ECP, and the possibilities this provides in processing. Chapter 5 is devoted to the photochemical stability of ECPs, which as all organic compounds decompose when exposed to solar irradiation.

References

1 M. Mikkelsen, M. Jørgensen and F. C. Krebs, *Energy Environ. Sci.,* 2010, **3,** 43-81.

2 J. A. Duffie, *ISA Trans.,* 1976, **15,** 301-305.

3 C. J. Brabec, N. S. Sariciftci and J. C. Hummelen, *Adv. Funct. Mater.,* 2001, **11,** 15-26.

4 H. Hoppe and N. S. Sariciftci, *J Mater Res,* 2004, **19,** 1924-1945.

5 M. Grätzel, *Nature,* 2001, **414,** 338-344.

6 J. E. Carlé and F. C. Krebs, *Sol Energ Mater Sol Cells,* 2013, **119,** 309-310.

7 O. Carp, C. L. Huisman and A. Reller, *Prog Solid State Chem,* 2004, **32,** 33-177.

8 A. Listorti, J. Durrant and J. Barber, *Nature Materials,* 2009, **8,** 929-U22.

9 E. Bundgaard and F. C. Krebs, *Sol Energ Mater Sol Cells,* 2007, **91,** 954-985.

10 T. Kajiwara, K. Hasimoto, T. Kawai and T. Sakata, *J. Phys. Chem.,* 1982, **86,** 4516-4522.

11 T. Shimidzu, T. Iyoda and K. Izaki, *J. Phys. Chem.,* 1985, **89,** 642-645.

12 R. Abe, K. Sayama and H. Arakawa, *J. Photochem. Photobiol. A Chem.,* 2004, **166,** 115-122.

13 M. Grätzel, *J. Photochem. Photobiol. C Photochem. Rev.,* 2003, **4,** 145-153.

14 M. Tahir and N. S. Amin, *Energy Convers. Manage.,* 2013, **76,** 194-214.

15 S. U. M. Khan, M. Al-Shahry and W. B. Ingler Jr., *Science,* 2002, **297,** 2243-2245.

16 M. Anpo and M. Takeuchi, *J. Catal.,* 2003, **216,** 505-516.

17 G. Q. Guan, T. Kida, T. Harada, M. Isayama and A. Yoshida, *Applied Catalysis A-General,* 2003, **249,** 11-18.

18 O. Ozcan, F. Yukruk, E. U. Akkaya and D. Uner, *Appl. Catal. B Environ.,* 2007, **71,** 291-297.

19 O. K. Varghese, M. Paulose, T. J. LaTempa and C. A. Grimes, *Nano Letters,* 2009, **9,** 731-737.

20 G. A. Olah, A. Goeppert and G. K. S. Prakash, *J. Org. Chem.,* 2009, **74,** 487-498.

21 J. C. S. Wu, *Catal. Surv. Asia,* 2009, **13,** 30-40.

22 G. Centi and S. Perathoner, *Top. Catal.,* 2009, **52,** 948-961.

23 N. Furuya, T. Yamazaki and M. Shibata, *J Electroanal Chem,* 1997, **431,** 39-41.

24 C. M. Sánchez-Sánchez, V. Montiel, D. A. Tryk, A. Aldaz and A. Fujishima, *Pure Appl. Chem.,* 2001, **73,** 1917-1927.

25 G. Centi, S. Perathoner, G. Winè and M. Gangeri, *Green Chem.,* 2007, **9,** 671-678.

26 R. J. Mortimer, *Am. Sci.,* 2013, **101,** 38-45.

27 C. G. Granqvist, *Sol Energ Mater Sol Cells,* 2012, **99,** 1-13.

28 G. A. Niklasson and C. G. Granqvist, *J. Mater. Chem.,* 2007, **17,** 127-156.

29 S. K. Deb, *Phil Mag,* 1973, **17,** 801-822.

30 2. Sage, 2013, **2013,** .

31 C. M. Lampert, *Solar Energy Materials,* 1984, **11,** 1-27.

32 C. M. Lampert, *Proc Annu Tech Conf Soc Vac Coaters,* 2005, 675-677.

33 E. S. Lee, S. E. Selkowich, R. D. Clear, D. L. DiBartolomeo, J. H. Klems, L. L. Fernandes, G. J. Ward, V. Inkarojrit and M. Yazdanian, 2006, **CEC-500-2006-052,** .

34 N. Sbar, M. Badding, R. Budziak, K. Cortez, L. Laby, L. Michalski, T. Ngo, S. Schulz and K. Urbanik, *Sol Energ Mater Sol Cells,* 1999, **56,** 321-341.

35 F. Beteille, P. Boire and J. -. Giron, *Proc SPIE Int Soc Opt Eng,* 1999, **3788,** 70-74.

36 2. Gentex, 2013, **2013,** .

37 K. Bange and T. Gambke, *Adv Mater,* 1990, **2,** 10-16.

38 P. M. S. Monk, R. J. Mortimer and D. R. Rosseinsky, *Electrochromism and Electrochromic Devices,* Chamebridge University Press, 2007.

39 C. M. Amb, A. L. Dyer and J. R. Reynolds, *Chem. Mater.,* 2011, **23,** 397-415.

40 A. L. Dyer, E. J. Thompson and J. R. Reynolds, *ACS Appl. Mater. Interfaces,* 2011, **3,** 1787-1795.

Chapter 2

2. Electrochromic polymers and devices

2.1 Introduction

This chapter introduces the fundamentals of conjugated electrochromic polymers (ECPs) and electrochromic devices (ECDs). The first part of the chapter is devoted to the theory underlying the design and synthesis of ECPs. The second part of the chapter describes the use of conjugated electrochromic polymers in devices, starting with the working principle of an ECD, as this influence the choice of materials as well as the manufacturing process and architecture. Since electrochromism is mainly a visual phenomenon I have included a section describing color theory and how the eye perceives color. Also of importance in ECDs are the electrolyte layer and the transparent conducting electrodes, which are described in regards to how these weak points can be improved. The chapter ends with a description of various state of the art ECDs that has yet to reach the market, but show a lot of promise.

Up to now, a major research goal has been to complete the full color circle of ECPs, which has recently been achieved with contributions from several research groups.[1-3] It is my opinion that the challenges and the way forward lie in synthesizing electrochromic processable polymers that contain additional functionalities, with the aim of advancing processing, stability and device manufacture.

2.2 Fundamentals of electrochromism

Electrochromism is the reversible change in the electromagnetic absorption of a compound as a result of an electrochemical induced redox reaction. The name *electrochromic* is short for *electrochromophore* and the definition has throughout the year been expanded so that it now includes changes in the infrared region of the electromagnetic spectrum as well. By application of a suitable potential it is possible to inject or extract electrons, thereby reducing or oxidizing the electrochromic compound. The absorption profile (i.e. color) of a conjugated polymer is due to the band gap between

the valence band (VB) and conducting band (CB) and this leads to colored compounds if the polymer absorbs in the visible region of the electromagnetic spectrum. The band gap is amongst other things determined from the onset of the π–π^* transition in the natural undoped state of the polymer. The observed color of a polymer is complementary to the wavelengths absorbed, e.g. a polymer that absorbs wavelengths around 450-500 nm is seen as orange/red, since the blue light has been filtered out. Figure 2-1 depicts a color wheel showing this. A detailed discussion on color is found in section 2.4.

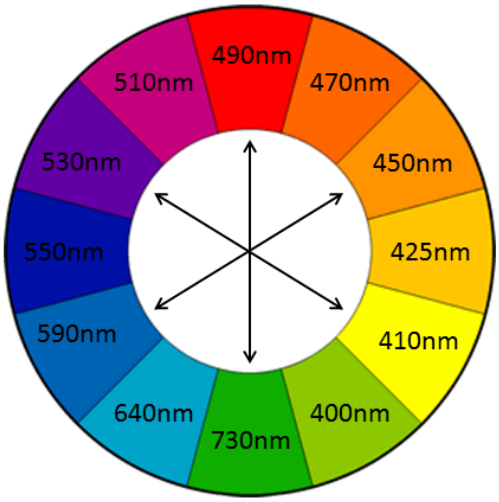

Figure 2-1: Color wheel showing the relationship between approximate absorption wavelength and color (e.g. the color red corresponds to absorption of wavelengths of 490 nm). Colors opposite each other are complementary as exemplified by the arrows.

2.2.1 Redox reactions in ECPs

As ECPs rely on changes in the redox state, two things are of primary importance: the width of the band gap and the position of the valence and conducting bands, determined by the HOMO and LUMO energy levels, respectively. The size of the band gap determines the color of the polymer as described in the introduction and the position of the energy bands determines the potential required for oxidation or reduction, as seen in Figure 2-2.

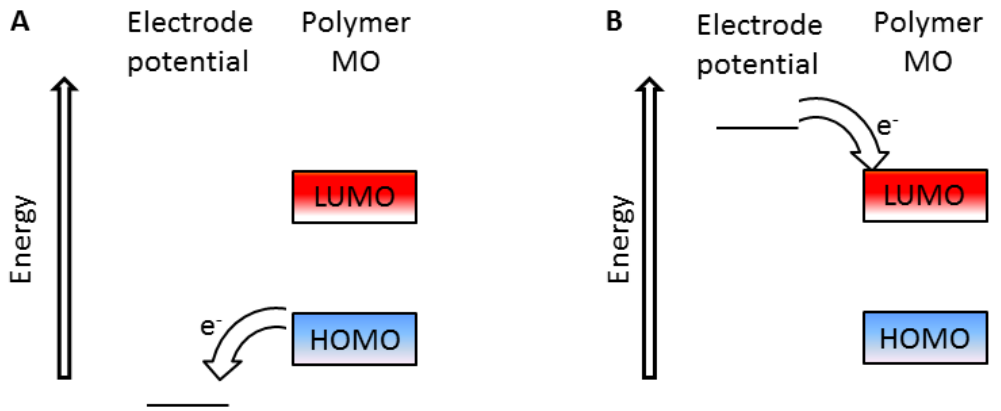

Figure 2-2: Redox reactions in electrochromic polymers. The electrode potential is shown in relation to the LUMO and HOMO molecular orbitals of an ECP. In (A) the electrode potential is lower (more positive) than the HOMO, which causes electrons to flow from the HOMO to the electrode and oxidize the polymer (p-doping). In (B) the electrode potential is higher (more negative) than the LUMO, which causes electrons to flow from the electrode and into the polymer that becomes reduced (n-doping).

By applying a potential more positive than the HOMO of the polymer as shown in Figure 2-2(A) electrons flow from the polymer to the electrode, whereby the polymer becomes oxidized. Contrary to this, a situation where the electrode potential is more negative than the LUMO of the polymer causes electrons to flow into the polymer that becomes reduced (Figure 2-2(B)). The developing charge on the polymers is balanced by counter ions from an electrolyte solution (see section 2.6.1); a process known as *doping* (p-doping for oxidation, n-doping for reduction) in analogy with the term from the semiconductor field, even though the two processes are not identical. In metallic semiconductors a very small amount of impurities (the dopant) are mixed with the semiconductor. The dopant either carries an excess (n-doping) or insufficient (p-doping) amount of valence electrons compared to the semiconductor. In ECPs the term p-doping refers to oxidation of the polymer film, with ingress of anions to balance the developing positive charges; n-doping refers to a reduction, the development of negative charges which are balanced by cations. The ions for charge balance are supplied by an electrolyte/ion storage layer as described in section 2.6.5. Without the ion

storage layer the continuous redox processes would require high capacitive properties of the ECPs.[4]

2.2.2 Redox stability of conjugated polymers

Applying a potential is not the only way to bring about redox reactions in conjugated polymers, which necessitates a closer look at the band positions. The most notable species that can react with the polymers under ambient conditions are oxygen and water (vapor).

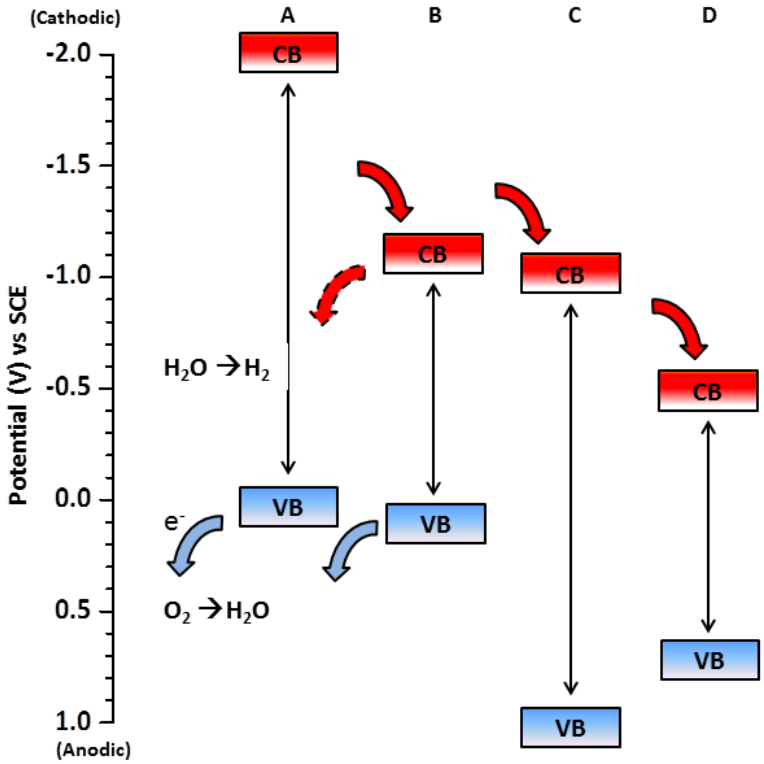

Figure 2-3: Position of band edges for conjugated polymers. VB and CB are the valence band and conducting band, respectively of the polymers. (A) and (C) are examples of high band gap polymers, while (B) and (D) exemplify low band gap polymers. The full red arrows show reduction/n-doping process. The blue arrows and the dashed red arrow show oxidation processes. The formal redox potentials for oxygen/water and water/hydrogen are included.

Figure 2-3 shows a common way of grouping conjugated polymers: The polymers are grouped as being high band gap or low band gap polymers, with either high or low valence band (VB) or conducting band (CB). The distinction between high and low band

gap is rather arbitrary, but polymers having band gaps lower than 1.5 eV are termed low band gap, while those with band gap higher than 2 eV are termed high band gap. The majority of electrochromic polymers belong to group A (as shown at the top of the figure) that has a high band gap (>1.5eV) and a high VB. This group constitutes amongst others PEDOT, polythiophene and polypyrrole. The poly(ProDOTs) that form the basis for many ECPs are intermediate having band gaps from 1.5 eV to 3 eV and are included in group A for this discussion. By virtue of their high lying VB group A polymers are easily oxidized/p-doped, and they are oxidized by O_2 (shown by the blue arrow) under ambient conditions since their formal redox potential is more cathodic than the O_2/H_2O couple. Contrary to the ease of which group A polymers are oxidized, the neutral form is very difficult to reduce due to the high CB, and reduction does not occur at ambient conditions (though electrochemically induced n-doping of PEDOT and polythiophenes at very negative potentials is possible). Group C are also high band gap polymers that are generally not easily doped, but unlike group A the CB of group B polymers is accessible to n-doping.[5, 6] As their VB is more anodic than O_2/H_2O, the neutral form is stable under ambient conditions. The low band gap polymers are generally more easily n-doped (shown by the red arrows) owing to a relatively low lying CB. Low band gap polymers are often used in organic photovoltaics (OPVs) as they are highly absorbing in the visible range, which constitutes 44% of the incoming irradiation from the sun. The position of the CB for these polymers is such that the reduced form is oxidized by water as shown by the dashed red arrow, which means that the neutral from is the stable form under ambient conditions for group D while group B polymers are stable in the oxidized form.

In discussing redox stability of ECPs in relation to band positions it is important to remember that the stability of a given redox state always depend on the chemical environment. A good example of this is ECP-magenta that oxidizes (albeit slowly) to the bleached form under ambient conditions. However, in devices comprising MCCP it is the neutral (colored) form of ECP-magenta, which is the stable form that this polymer reverts to (see section 2.3.3 on memory effect). The oxidation of conjugated polymers creates a radical cation, known as a polaron that is delocalized over a polymer segment

as shown in Figure 2-4(B).[7] The polarons possesses half-filled energy levels and allow lower energy transitions to occur, at the expense of the π–π* transition. Figure 2-4(C) shows the dication/*bipolaron* that is formed on further oxidation. Only low energy transitions are allowed in this form and the π–π* transition is depleted.

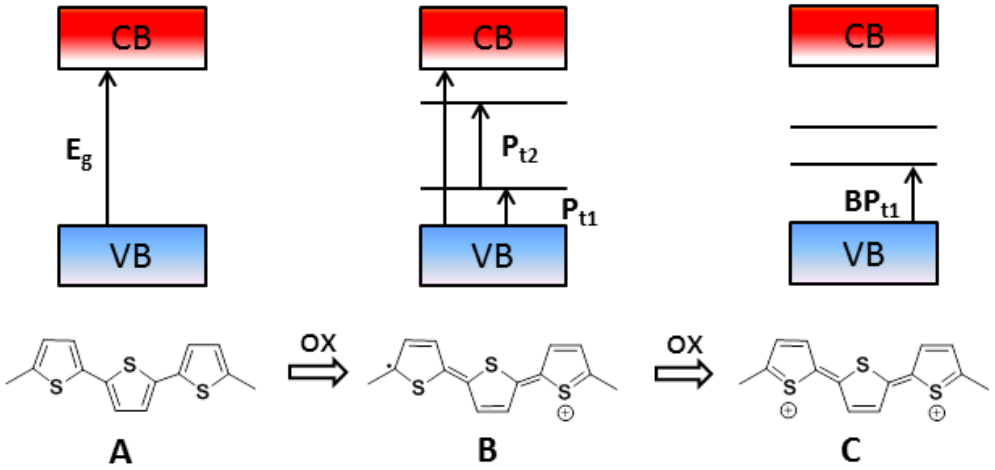

Figure 2-4: Polaron states of a thiophene polymer segment. (A) Shows the neutral undoped state of a thiophene trimer. The π–π* transition is shown as Eg (gap energy). Electrochemical oxidation leads to the polaron state (B). In (B) new low energy transitions are allowed. (C) Shows the bipolaron state, where the π–π* transition is depleted and only transitions from the top of the valence band is allowed.

The development of new energy transitions and the depletion of others are observed as a color change in the polymer (if the changes occur in the visible region). ECPs are frequently designed so that electrochemical switching depletes the absorption in within the visible region while electronic transitions develop outside of this. Hereby the color can be switched on and off (or changed to another color) which can be exploited in electrochromic devices such as displays, signs and light management devices. As redox reactions are always paired (a reduction of one species requires the oxidation of another and vice versa), a change in redox state in an ECP requires the opposite reaction in another species. The strategies to address this is discussed in section 2.6.2

2.3 Electrochromic characteristics and terminology

2.3.1 Optical contrast

The difference in transmittance between the two redox states i.e. the colored and the bleached is referred to as the optical contrast or ΔT. The optical contrast is usually measured at the wavelength of the maximum absorbing peak (Abs_{max}) and is an important parameter as it describes how effective the electrochromic compound is turned "on" and "off". In assessing ECPs several issues regarding the optical contrast is to be noted. Primarily, the optical contrast does not give information on other parts of the spectrum than Abs_{max}, which implies that a high optical contrast not necessarily equals a change from colored to bleached. The reason for this is that while the intensity of the maximum absorbing peak might be reduced by the redox reaction, other peaks might appear or increase in intensity, and in addition tailings from the UV or NIR regions of the electromagnetic spectrum could disrupt complete bleaching.

A three electrode setup is usually employed to measure optical contrast. The ECP is deposited on a conductive substrate, used as the working electrode, which is submerged in a cuvette containing an appropriate electrolyte solution along with a reference and counter electrode. The absorption is measured relative to a blank reference cuvette. A ΔT obtained this way is the maximum contrast obtainable for the *polymer*, but it is important to remember that a polymer is not switchable in a device without electrolyte, electrode substrate and charge balancing polymer, all of which influence the optical contrast.

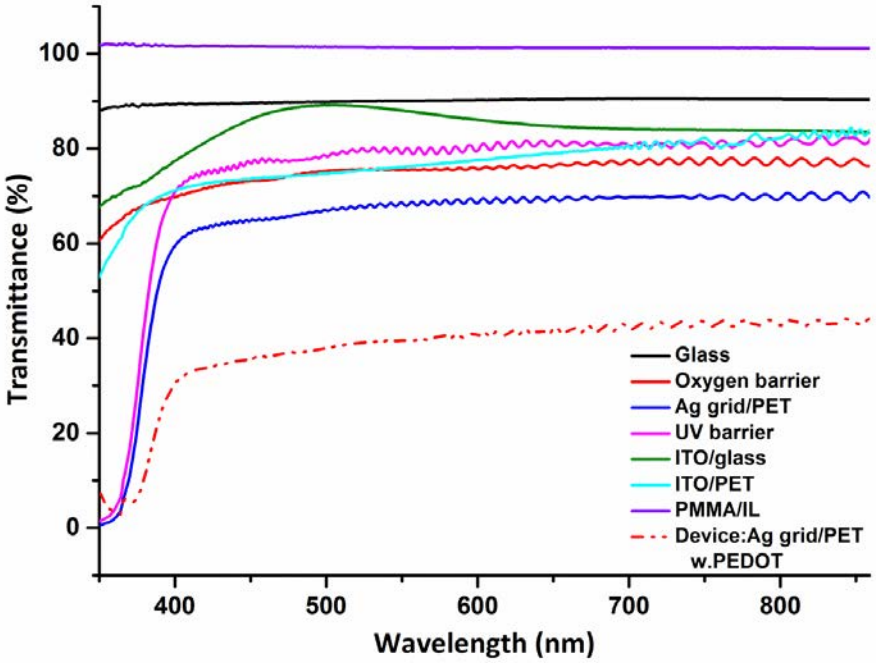

Figure 2-5: Transmittance for materials commonly used in ECDs. The traces show the values for a single substrate. The purple trace from PMMA/IL electrolyte shows a transmittance value above 100%, which is due to reflections from the reference substrate.

Figure 2-5 shows the influence of several common substrates on the transmittance. A 1 mm thick glass substrate without electrode material reduces the transmittance by 10% pr. glass (black trace) while ITO on glass further contributes to an additional 10% reduction (green trace). Flexible electrode substrates such as ITO on PET (thickness 185 μm) reduces the transmittance to roughly 75% (turquoise trace) and PET substrates (72 μm) containing a hexagonal silver grid (used in the ITO free ECDS described in chapter 3) leads to a 40% transmittance decrease (blue trace). The barrier foils that were used to increase the photochemical stability of ECPs (see chapter 5) also absorb light, which reduce the transmittance by 30% (red and pink traces respectively). The PMMA/ionic liquid electrolyte that I used for the majority of ECDs does not influence the transmittance, but this might be different for other electrolyte compositions. It is valuable to keep these numbers in mind when evaluating reported optical contrasts, and to remember that they are given for a single substrate and ECDS employs two such substrates. An example showing this is given by the red dashed trace that shows the

transmittance for a device that comprises two silver grid electrodes on PET each coated with PEDOT and a PMMA/ionic liquid electrolyte. The relatively low transmittance shows that there are certainly challenges associated with using flexible substrates for ECD-window materials as shown by other groups.[8-11]

2.3.2 Response time

Sometimes referred to as switching speed, the response time is a measure of the speed of the color change in response to the applied bias. The response time is important to know, since a change between the two redox states that takes a few minutes are suitable for appliances such as blinds, large area billboards etc., while other devices might require second or sub-second response (clocks, screens etc.). A common protocol on how to report response time does not exist and they are reported differently amongst research groups. The fastest response is naturally linked to the smallest change in transmittance, which highlights the importance in comparing a given response time to the optical contrast obtained. It does however make sense to report a series of response times based on different levels of optical contrast, considering that the majority of the redox reactions occur in the beginning of a switch, e.g. 90% of *full* switch might occur in two seconds while the last 10% takes five seconds to complete. An explanation to this is that when the electric field is first established, the charges and charge balancing ions move quickly, but as the charges move, the field gets screened which limits the movement of charges and charge carriers.[12] Similar to the measurement of optical contrast; a three electrode setup is usually employed for measurements of response time. The response time is obtained by correlating the change in transmittance with time required for that change. Two notable observations are made when electrochemically switching ECPs. Initially the first 5-10 switches are usually quite slow and incomplete. Following this break-in the ECP films reach their maximum response time and optical contrast. This electrochemical improvement is due to incorporation of solvent into the polymer film. The solvent is inserted along with ions upon doping, and is necessary for free ion movement in and out of the film.[4, 13]Secondly, the response time is generally shorter when reducing ECP films compared

to oxidizing them, which is due to the doped state (the oxidized state/p-doped for most ECPs) is electrically conducting and this facilitates charge transport in the initial stages of reduction, contrary to the neutral insulating state.[12-14] In ECDs the response time is affected by several components; with the primary difference (to a standard three electrode set-up) being that ECDs are made up of *two* polymers (or electroactive species) that react complementary to each other, whereby the slowest reaction will be rate limiting. Furthermore, the transport of charge balancing ions through the electrolyte layer is different since a low viscous electrolyte (acetonitrile, propylene carbonate etc.) is usually employed in a standard three electrode set-up, whereas semisolid polymer gels of poly(methyl methacrylate), poly(ethylene oxide) or similar are commonly used for ECDs. The relation between electrolyte viscosity and migration and how this affects the transport of ions is not straight forward, and depends on the interactions between the ions and the polymer chains, with the size of the ions and concentration of polymer as important factors.[14-17] When the maximum optical contrast is obtained, the redox reactions at the two electrodes are complete and no further electron transfer occurs, although a background current is still present.

2.3.3 Memory effect

The memory effect of an electrochromic compound or device is the ability to maintain a redox state when taken to open circuit. This means that an electrochromic window or display can maintain a color state without a continuous power supply; a feature that differentiates ECDs from other display technologies, such as OLED's or LEEC's that require a continuous voltage to operate. Even so, the literature on the memory effect is scarce and even electrochromic textbooks only briefly describe this effect. The memory effect stems from electrons being "trapped" in one redox state of the polymer, when the device is taken to open circuit. This means that the electrons cannot revert, and hence the reversible redox reaction is hindered. As the polymer reacts with the surroundings, a less stable redox state cannot be maintained indefinitely and the memory effect can regarded as the slow reaction of a polymer going from a less stable redox state to a more stable one in reacting with the surrounding chemical environ-

ment. Depending on the application of the ECD, the color can be refreshed by a short potential pulse at certain intervals.[18, 19]

The memory effect is a not just property of the polymer, as it is affected by the surroundings of the polymer. At least two factors influence the memory effect: First, ECDs are electrochemical cells with an electromotive force (EMF) that depends on the equilibrium between the two polymers. In other words, the memory effect of a polymer is dependent on the counter polymer, or more accurately the counter species. This means that memory effect of a polymer can differ whether it is measured in a device where the counter electrode is another polymer or in a three electrode set-up for analysis where the counter electrode is usually made of metal. Secondly, as the electrochemical reaction is hindered due to open circuit, charge transfer through the ions (and possibly moisture) in the electrolyte layer is the only option for reaction to occur. The diffusion of these charge carriers is affected by the viscosity and thickness of the gel that most likely influence the memory effect. In relation to the thickness it is important not to make the electrolyte layer too thin, as this increases the risk of a short circuit during lamination of the flexible substrates. A short circuit will close the circuit allowing electrons to revert the more stable redox state.

2.3.4 Coloration efficiency:

The number of color centers formed as function of the charge used to bring about this change is described by the coloration efficiency, η usually represented in $cm^2 \times C^{-1}$ (area pr. charge) and given by:

$$\eta = (\log (\%T_1 / \%T_2)) / (Q)$$

Where $\%T_1$ and $\%T_2$ refers to the transmission before and after redox switching respectively and Q is the charge consumed pr. area. While high values are desirable for primary electrochromes, low values are advantageous for the charge balancing polymer on the secondary electrode. Coloration efficiencies are reported in several ways, and have so far been seen as a property of a given polymer.[20-22] In the article "Fast switching ITO free electrochromic devices" (appendix 3.2), I challenge this viewpoint

and introduce the *device coloration efficiency* (η_d). η_d describes the number of color centers formed as function of the charge in *a particular device setting* that include contributions due to electrode materials, electrolyte matrix and faradaic side reactions occurring in the device and is related to η by a device correction factor *w*. η_d is then given by:

$$\eta_d = \eta \bullet w$$

As η_d can be used to compare devices with identical polymers, it becomes a tool for evaluating a particular device setting e.g. electrolyte composition or electrode substrate. This representation of coloration efficiency is an attempt to introduce device standards in order to characterize electrochromic devices rather than polymers.

2.4 Color and color spaces

Color can be described in a variety of ways and influenced by several factors and since it is a feature characteristic of an ECP the following section aims to address this. I have included this section primarily to give the reader an understanding of the nature of color, but also to emphasize the use of a more stringent terminology in describing and comparing color. The description of the CIE color space is included as this particular color space is frequently used in the literature on ECPs including my own work on photopatterning, where the color of the newly synthesized ECP was compared to the parent polymer (appendix 3.3).[23-28]

2.4.1 Origin of color: Transmittance, absorption and reflectance

Three things are important in describing color: A light source, an object illuminated by the light source and a viewer that can either be a set of eyes (and a brain) or a photoresponsive detector.The different perception between the human eye and that of a photodetector is one of the reasons why the color spaces described later are used to standardize color description. [29, 30]

When light strikes a surface (e.g. an ECP coated PET foil) several things can occur that affects the color of the foil. By measuring the amount of light passing through the foil one gets the transmittance of the material T (%) = $(I/I_0) \times 100$, where I is the irradiance

transmitted through the foil and I_o is the irradiance emitted by the light source. The optical contrast described in section 2.3.1 is the difference in *transmittance*, T, between two redox states (at a given wavelength). If all the incoming light passes through the foil ($I = I_0$) it is said to be fully *transparent*; in Figure 2-5 it is shown that glass is 90% transparent while the transparency of PET is around 80%. By depositing an ECP onto the foil, certain wavelengths are absorbed by the polymer film and hence do not pass through the foil, thereby coloring the foil. The *absorption*, A, is related to transmittance by A = -log T. Transmittance is frequently used in ECP description, as it describes the amount of light passing through e.g. a window. The reason that foils or other objects can be colored without being (partly) transparent, is because of light scattering due to differences between the refractive index of particles and the surrounding media. If a large amount of light is scattered it is said to be *reflected* or *diffusely reflected* (different from *specular reflectance* caused by mirrors or other smooth surfaces). The color of such an *opaque* (i.e. non-transparent) object depends on which wavelengths are absorbed and which are reflected, while the color of a transparent foil depends on the wavelengths that are transmitted (or absorbed) through the foil. The "combination" of an opaque and a transparent foil, is a *translucent* that where some of the light is transmitted, some is reflected and some is absorbed. Figure 2-6 depicts the three situations. The ECDs fabricated and presented in this thesis are of the absorptive/transmissive types (described in 2.6.2), which means that their color depend on their absorption.

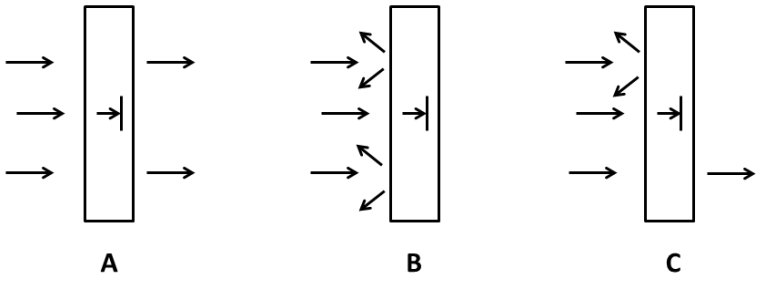

Figure 2-6: Light striking a material. (A) Light is transmitted through a transparent material that colors because some wavelengths are absorbed. (B) An opaque material reflects the light and colors as some wavelengths are absorbed. (A) A translucent material allows the transmittance of some wavelengths, while other wavelengths are absorbed or reflected.

2.4.2 How the eye perceives color

Without going into detail, the eye functions by light striking a lens that forms an image in the region of the eye called the retina, where two types of receptors are present: Rods that allow us to see in dim light and cones that respond to colors. Three types of cones are present, each one responding to different wavelengths of radiation. This means that the eye does not respond linearly to light i.e. some wavelengths have a larger impact than others, and the response between individuals may vary. Contrary to this, most spectrophotometers respond linearly to all wavelengths.

2.4.3 Color spaces and CIELAB

In trying to standardize the description of color, several methods have been proposed and are used depending on the circumstances.[31] Common to them is that they rely on a general description of color based on: *hue, lightness and saturation*. The hue of a color is what most closely resembles that gained from an absorption spectrum e.g. red, green, blue-green, yellow-orange etc. The hue is sometimes referred to as the dominant wavelength which is depicted in Figure 2-1. The lightness of a color refers to the amount of white or black mixed in that color, e.g. light-blue, dark-red etc. The saturation of the color refers to how much the color differs from grey or how colorful (how saturated) the color is. These three parameters form the basis for the Munsell color scale widely used in the color industry and shown in Figure 2-7.[32]

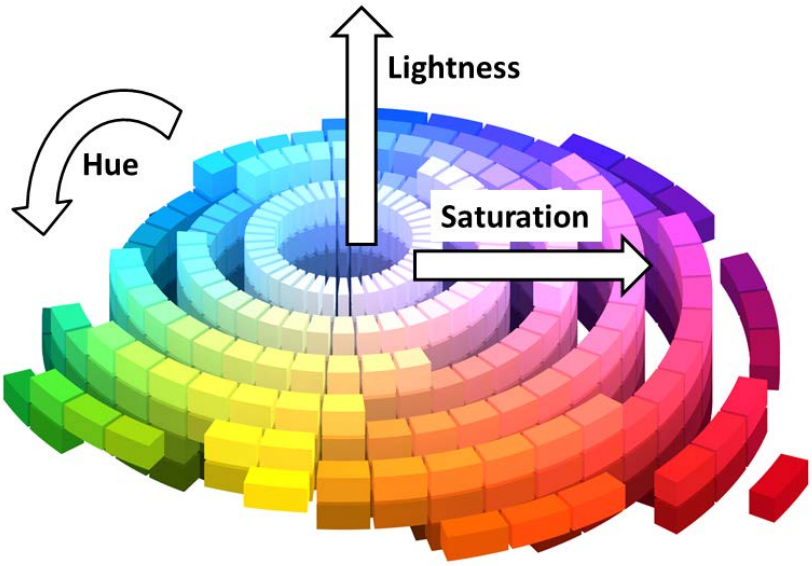

Figure 2-7: The Munsell system describing the hue, lightness and saturation. Permission of use granted under the terms of the GNU Free Documentation License.

The Munsell system is based on actual physical color samples, as opposed to the CIE system, that only incidentally resembles physical colors. This might seem a bit odd, but the CIE system does not aim at describing color but rather to determine if two colors are identical.[33, 33, 33-35] CIE is shorthand for Commision International de l'Eclairage (or International Commission on Illumination) and the system is based on that the brain perceives color due a stimulus provided by the combination of the spectral distribution of the light source, the transmittance (or reflectance) of an object and the spectral response of the eye as depicted in Figure 2-8.

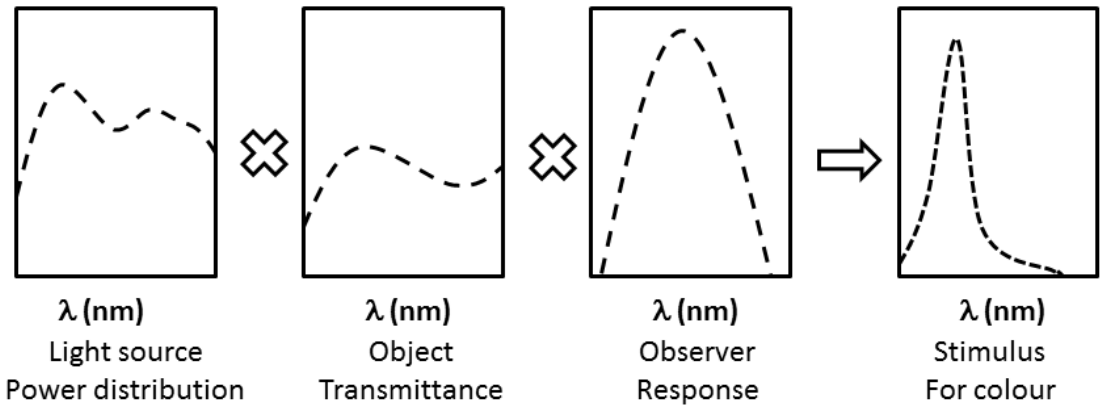

Figure 2-8: The stimulus perceived by the brain (or a photodetector) is made up by contributions from the spectral power distribution of the light source, the transmittance (or reflectance) of the object viewed and the spectral response of the eye (or instrument). The curves are imaginary approximations

The CIE system implies that a standard illuminant is used and that the object is seen by a standard observer.* Various light sources can be used to provide the spectral power distribution that resembles a standard illuminant, typically sources that resembles midday sun in the western or northern Europe (e.g. D65 or D50 illuminant).[23, 36] The response of an average person with normal color vision is categorized as a standard observer, and the response to three different colors is referred to as the tristimulus values. This means that the observer response in Figure 2-8 is divided into three and the color stimulus can be represented by three numbers; X,Y and Z. These tristimulus values can in the CIE system be converted into a two-dimensional chromaticity diagram, which to some extent represenst the hue and saturation.

* An illuminant is defined by a certain spectral distribution power. This distribution need not to be physically realizable i.e. a source (lamp) may not exist that that corresponds to a given illuminant.

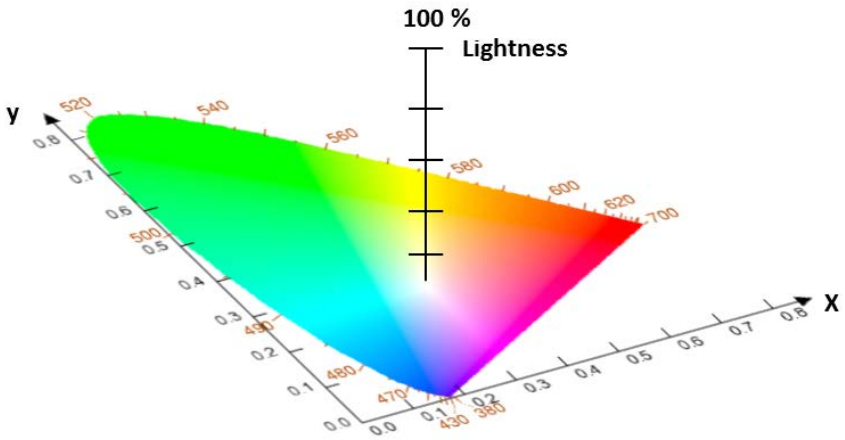

Figure 2-9: The CIE 1931 chromaticity diagram. The x and y values are calculated based on the tri-stimulus values X,Y and Z. The lightness (actually represented by capital Y) protrudes up from the two dimensional diagram. The numbers lining the diagram corresponds to approximate wavelengths.

In order improve the visual perception of the CIE color space it has been transformed into an opponent-type system which yield three new values L*, a* and b*. An opponent type system is based on how the signal observed by the eye gets coded on the way to the brain. In this way signals are categorized as light or dark, red or green and yellow or blue. Two opposing colors cannot constitute a signal e.g. a color cannot be red and green at the same time or blue and yellow. The redness or greenness are expressed by the number a*, the blueness or redness by b* and the lightness or darkness by L* as shown in Figure 2-10.

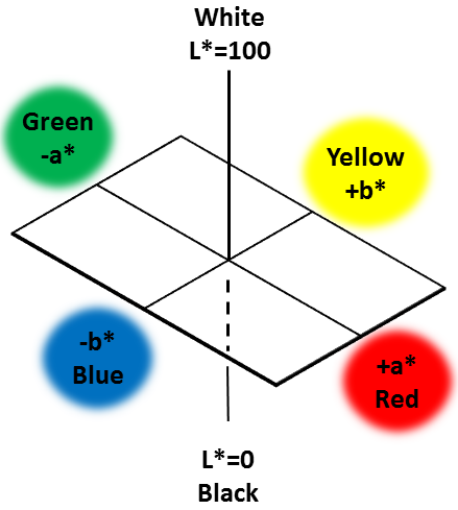

Figure 2-10: The CIE 1976 L*a*b* color space abbreviated CIELAB (CIE 1976). A given color can be categorized according to its redness-greenness (a*), yellowness-blueness (b*) and Lightness-darkness (L*).

2.4.4 Additive and subtractive color mixing

Readers familiar with the literature on electrochromics will know that color mixing is frequently referred to by many research groups when describing possible applications of ECPs,[37-40] but to the best of my knowledge there are currently not any ECDs that employ color mixing. The practical challenges associated with mixing and addressing different colored ECPs in devices will not be discussed here, but I find a brief review on color mixing theory appropriate.

Additive color mixing occurs when emissive light of different colors are mixed. An example could be green and red light emitted from two OLEDs that combines to give a yellow light. In this case the emission spectrum of the resulting (yellow) light is a combination of the green and red spectra. Televisions function by additive color mixing, but the lights are not mixed. Instead the pixels on a television screen are so close together that a red and a green pixel are perceived by the brain to be yellow. Mixing the three primaries red, blue and green will provide the largest amount of colors possible in additive mixing. If RGB primaries are mixed in the right proportions they add up to give white light, as shown in Figure 2-11.

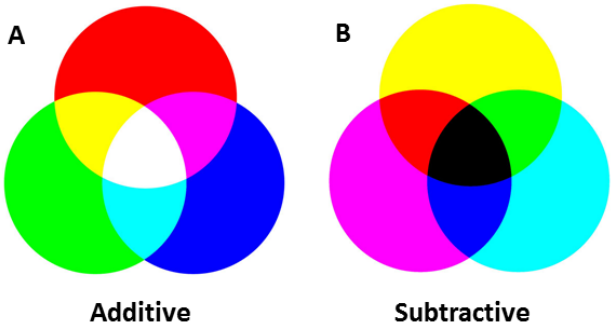

Figure 2-11: Color mixing. (A) Additive color mixing using red, green and blue (B) Subtractive color mixing using magenta, yellow and cyan. Permission of use granted under the terms of the GNU Free Documentation License.

Subtractive color mixing occurs when part of the light is subtracted from a light source by an object. Subtractive mixing is used in when developing photographs or when colors are mixed on a canvas or piece of paper. As electrochromic polymers are non-emissive they color due to light absorption, e.g. a PET sheet coated with ECP-magenta, absorbs (i.e. subtracts) roughly light of wavelengths between 500-600 nm. The light that is transmitted through the sheet will be magenta colored. By adding a layer of yellow ECP the resulting color will be red as shown in Figure 2-11 (B).[37] The three primaries commonly used for subtractive color mixing are magenta, cyan and yellow, which when all mixed will result in a black color.

2.5 Development of conjugated electrochromic polymers

To get sense of the progress within the field of electrochromic polymers; from the initial discovery to present day status, the next section reviews the development of ECPs using a historical-chronological approach. Reviewing can be done highlighting various aspects of a subject depending on interest, and since my background is that of an organic chemist the reader may find the following section having a slight synthetic bias. As it is beyond the scope of this dissertation to review every single polymer, the reader is directed to other good reviews on the subject.[2, 36, 38, 41]

2.5.1 From late 1980's to present day

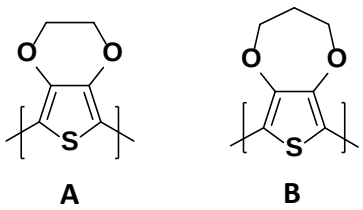

Figure 2-12: Structure of (A) poly(3,4-ethylene-dioxythiophene) (PEDOT) and (B) 3,4-propylene-diothiophene (ProDOT)

In the late 1980's and the beginning of the 1990's chemists at Bayer were trying to develop conducting polymers with increased stability compared to polyacetylene.[42-44] By fusing the alkylenedioxy bridge in 3,4-substituted alkoxythiophenes, poly(3,4-ethylenedioxythiophene) (PEDOT) was developed (Figure 2-12(A)), and this polymer showed increased stability in its oxidized state.[45, 46] Furthermore, the 3,4-substitution hindered α,β couplings (known to reduce conjugation length) during polymerization. The stabilizing effect of 3,4 alkyl substituents also lowered the oxidation potential leading to milder conditions during polymerization and consequently less risk of nucleophilic attack on the positive thiophene moiety. As poly(3,4-propylenedioxythiophene) (poly(ProDOT); Figure 2-12(B)), was found to be less conductive in the doped state than PEDOT it was not investigated to the same extent, but nevertheless, both polymers were found to undergo spectral changes in the visible region during electrochemical induced doping. PEDOT was found to switch from a deep blue neutral and insulating form to a transmissive sky blue form that was conducting when oxidized. Poly(ProDOT) was found to be purple in the neutral form, switching to reddish transmissive in the oxidized state.[45] While PEDOT was the subject of intense research for a variety of applications,[47-49] Reynolds and co-workers explored (during the mid-1990's) the use of alkyl substituted PEDOT for electrochromic applications.[50, 51] By attaching a tetradecyl chain to the ethylene bridge of the EDOT monomer oxidative polymerization was possible using ferric chloride in chloroform. The resulting polymer switched from purple to green, and while the molecular weight of the resulting polymer im-

posed some limitations on the solubility, Reynolds showed that large scale polymerizations of these compounds were possible, something that was not possible using electrochemical polymerization methods.[51]. Following this, various poly(3,4-alkylenedioxythiophenes) (PXDOTs) were synthesized and it was found that the electrochromic qualities of methyl substituted poly(ProDOTs) were more favorable than those of PEDOT, in that the near-infrared (NIR) absorption increased when oxidizing PEDOT, while it fell for poly(ProDOT-Me). The absence of NIR tailings resulted in clearer oxidized states for poly(ProDOT-Me).[52] Generally it was found that increasing the ring size and the size of the substituent resulted in better optical contrast and faster response time and this fact yielded the butyl derivative polyBuDOT as a superior compound (ΔT=63% vs 54% for polyProDOT and 45% for PEDOT), but since this polymer also showed NIR absorption in the oxidized state, it was polyProDOTs that was further researched. The propylene bridge in ProDOTs allowed for symmetric substitution of the C2 carbon and the dimethyl substituted derivative yielded an optical contrast of 78% at 578 nm and sub-second response times. These qualities was thought to originate from a more open morphology as the polymer chains cannot pack as efficiently due to the substituents. The more porous polymer structure should facilitate the ingress and ejection of ions. The disubstitution of the C2 propylene carbon required a change in the synthetic route, but was accomplished by the transetherification shown in Figure 2-13 where evaporation of methanol (distilled off or adsorbed onto molecular sieves) pushes the equilibrium to the right; a method repeatedly used in ProDOT synthesis.[52-54].

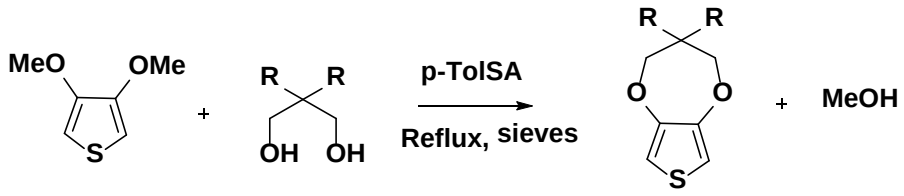

Figure 2-13: Transetherification of 3,4-dimethoxy thiophene using a diole and catalyzed by p-toluenesulfonic acid. The MeOH product is distilled of or trapped in molecular sieves. R= alkyl, alkoxy or halogen.

In the beginning of this millennium the dibutyl derivative of ProDOT was synthesized by a Grignard metathesis reaction and dropcast films of these polymers were compared to electrochemically polymerized films.[55] The latter still proved superior and showed a 75% optical contrast compared to the former. However, it was now possible to fully characterize the polymers and in 2004 Reynolds and co-workers managed to synthesize several soluble poly(ProDOT) derivatives that showed electrochromic film properties comparable to or better than electrochemical polymerized ECPs, when spray cast.[21] Figure 2-14 shows two routes to the 2-ethylhexyloxy derivative that switches between a magenta (hence the nickname ECP-magenta) neutral state (Abs$_{max}$=545 nm) and a transmissive oxidized state with an impressive 80% contrast in half a second. The monomer compound became an important building block and was used in several copolymers synthesized by the Reynolds group.

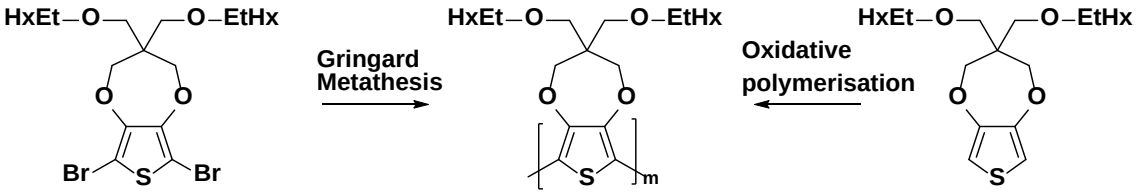

Figure 2-14: Two routes to poly(2,2-bis(2-ethylhexyloxymethyl)-propylene-1,3-dioxy)-3,4-thiophene-2,5-diyl (ECP-magenta). The Grignard route employs the dibromo monomer, which is not necessary in the oxidative route. Oxidative polymerization is done using $FeCl_3$.[56]

Around the same time Wudl and co-workers worked on another electrochromic system that employed thiophene substituted thienopyrazines. By having two well defined isolated conjugated systems, absorption of both red and blue light was achieved, which yielded the green polymer shown in Figure 2-15(A) by electrochemical polymerization. [40]

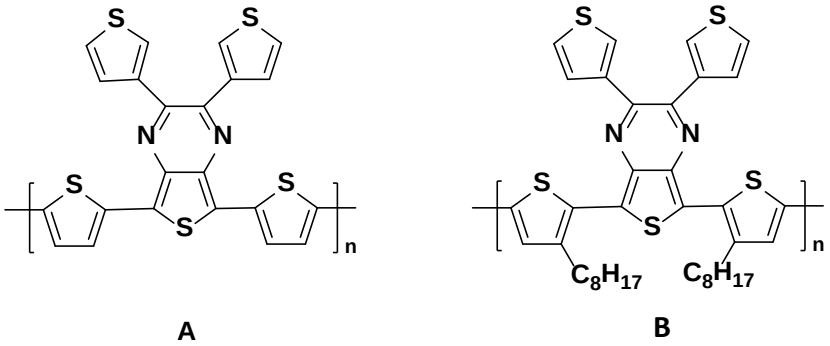

Figure 2-15: The polythienopyrazines developed by Wudl and co-workers. (A) poly(2,3-di(thien-3-yl)-5,7-di(thien-2yl)thieno[3,4*b*]pyrazine (PDDTP) and (B) poly(5,7-bis-(3-octyl-thiophen-2-yl)-2,3-dithiophen-3-yl-thieno[3,4*b*]pyrazine (PDODDTP)

In the neutral form the polymer showed dual band absorption at 410 nm and 670 nm, due to presence of an acceptor thienopyrazine group flanked by donor thiophene groups (the D-A approach is described further in section 2.5.3). Unfortunately the oxidized form of the polymer was a light brown color and not a colorless transmissive, but a solution processable derivative was achieved by attaching octyl groups to two of the thiophene groups as shown in Figure 2-15(B),[57]and the group aimed at making devices by additive color mixing of red, green and blue polymers, although it is unclear to me how additive color mixing can be realized using electrochromic compounds (see section 2.4.4).[58]

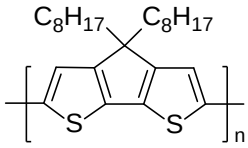

Figure 2-16: Polydioctylcyclopentadithiophene (PDOCPDT)

Yet another system showed promise, when Wu presented his groups work on polycyclopentadithiophenes (PCPDT) containing octyl side chains to induce solubility.[59, 60] The polydioctylcyclopentadithiophenes (PDOCPDT) depicted in Figure 2-16 was synthesized by oxidative polymerisation of the corresponding monomer using ferric chloride. The polymer showed an optical contrast of 60% at 580 nm, switching between a blue and a

transmissive state in less than a second. The polymer also possessed very high coloration efficiency, but lacked optical memory. Wu's group also aimed at completing the RBG primaries using the PCPDT structure, and succeeded in this by synthesizing copolymers with benzathothiadiazole, 3-octylthiophene and carbazole that yielded green, red and yellow ECPs, respectively. [3] These polymers were synthesized by Stille couplings of dioctylcyclopentadithiophene trimethyl-stannanes, but did not switch to transmissive when oxidized.

During the latter part of the 00's several ECPs were developed that relied on the donor-acceptor (D-A) approach (discussed in section 2.5.3). Particularly green polymers seemed to be the goal of several research groups. The difficulty in synthesizing green polymers lies in the fact that the polymer is required to absorb both red and blue light, and simultaneously switch these two absorptions to outside of the visible range. Two green soluble polymers were reported in 2008 that had a BTD group as the acceptor and various thiophene derivatives as donors.[61] The solubility was limited to 8 mg/ml and one of the polymers required hot dichlorobenzene to dissolve. The optical contrast ranges from 32-40%, and interestingly the authors showed how the hue could be tuned by varying the D-A ratio. Cihaner and co-workers likewise demonstrated color tuning by using benzoselenodiazole, benzothiodiazole and benzotriazole as acceptor groups to obtain various hues of blue and green, that switched to transmissive on oxidation.[62] Solubility was achieved by using alkyl bearing ProDOT as donor groups, and optical contrast values around 40% were reported. Even more difficult than green is the synthesis of black to transmissive polymers, as the ECP is required to absorb in the entire visible range and be able to switch all absorption bands to outside this region. Reynolds group accomplished this by oxidative polymerisation of a D-A-D trimer and the ProDOT-$(OEtHx)_2$ previously developed. The color was described as *"an intense ink like dark-blue color.*[63, 64] An improved synthesis was reported in 2010 where the tedious trimer synthesis had been replaced by a Stille coupling of three monomers. The color was likewise improved and the optical contrast was 40% on the average.[65] While the black to transmissive ECP was a major achievement, the devices that were constructed using MCCP (Minimally Color Changing Polymer, described in section 2.5.2) as

the charge balancing polymer were found to be light blue in the oxidized state and not completely colorless, underlining the challenge in device applications of ECPs. Another black polymer was presented in 2010 by the Cihaner group. The electrochemically synthesized co-polymer comprised ProDOT donor groups bearing long alkyl chain and benzotriazole and benzoselenodiazole as acceptor groups. The solubility was good in most common organic solvents, but the optical contrast was limited to 15%.[66]

2010 also saw a report on a blue D-A polymer utilizing BTD and ProDOT-$(OEtHx)_2$.[67] The synthesis of this polymer required an "inverse Suzuki" reaction where an electron poor BTD group acted as the nucleophile while electron rich thiophene derivate was the electrophilic counterpart. Furthermore blue ECPs bearing ester functionalities that could be saponified to insoluble carboxylic acids were also presented. This strategy of functionalizing ECP was similar to a previous report on ester substituted polyProDots that yielded alcohols on hydrolysis,[68] and was later expanded to yield water processable carboxylates.[56, 69]

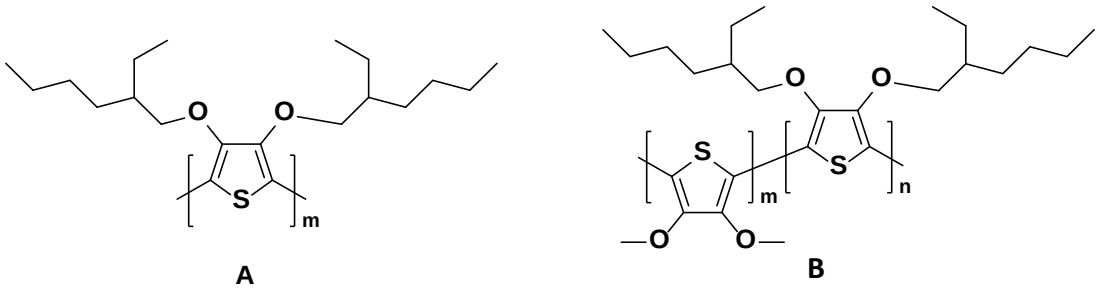

Figure 2-17:(A) Orange polymer; Poly(3,4-di(2-ethylhexyloxy)thiophene) (B) Red polymer; Poly(3,4-di(2-ethylhexyloxy)thiophene-co-3,4-di(methoxy)-thiophene).

The Toppare group also contributed to ECP development,[2] but as their focus is on electrochemically synthesized polymers my interest in these is quite limited as I see electropolymerization as a hindrance to efficient fabrication of large area polymer films. An example of their efforts is a blue D-A-D polymer comprising an alkylbenzotriazole flanked by EDOT groups that yields an optical contrast of 53%. The oxidized form is cyan colored, but the polymer is also n-dopable.[70] Another interesting electrochemically synthesized ECP reported by Bendikov in 2009 was PEDOS, a seleno derivative of PE-

DOT. An alkyl-PEDOS showed optical contrast of 89% and switched from blue to transmissive.[71]Even though the D-A approach seemed to be the method of choice in ECP synthesis during the late 2000's, color tuning due to conformational factors was also reported. Red and orange polymers were synthesized that employed open chain 3,4 dialkoxy thiophenes.[72] Though the alkoxy substituents stabilize the polymer, the steric effects of the large alkoxy substituents were found to force the polymer chain into a conformation that limits the conjugation length thereby increasing the band gap. The orange polymer in Figure 2-17(A) is an example of the latter, while the red polymer in (B) has randomly incorporated dimethoxythiophenes, which relaxes the chain, leading to a slight red shift in absorption. The most recent example of steric tuning, was the development of a cathodically coloring yellow polymer that employs alternating ProDOT-$(OEtHx)_2$ and phenylene moieties.[37] Even though an explanation for this is lacking, the polymer unquestionable switches efficiently (ΔT=73%) to a transmissive state when oxidized. Cathodically coloring yellow polymers are difficult to achieve as the high band gap (2.3 eV-2.7 eV) necessary to impose the yellow color, is required to shift into the NIR on oxidation.

2.5.2 Charge balancing polymers

The group of charge balancing polymers is more mixed, as several approaches to charge balancing are used. If the color complementary approach is used, the charge balancing species is an anodically coloring polymer. While polypyrroles (PPy) can be both anodically and cathodically coloring, it is the former property that has been most widely utilized in ECDs, since derivatives of PPy, can achieve high band gaps (up to 3.4 eV) and possess lower oxidation potentials compared to polythiophene derivatives.[73, 74] The higher band gap is (amongst other factors) obtained by N-alkylation of the pyrrole ring, whereby the effective conjugation length is reduced. Another polymer group using the color complementary approach is the poly(ProDOT-Cyanovinylenes), that were found to be both p- and n-dopable. Although they were developed for OPV applications, they could be used in ECDs as anodically coloring ECPs.[75]. A very different class of compounds is substituted aromatic polyamides exemplified with N,N,N',N'-

tetraphenyl-p-phenyldiamines that was employed as anodically coloring ECPs[76] Switching from colorless or pale yellowish to blue or green (dependent on the aromatic moiety), these polymers showed an optical contrast of around 60% and coloration efficiencies of 200-300 C^{-1} cm^2.

Instead of the color complementary approach, the recently published polypyrrole: poly(N-octadecyl-(propylene-1,3-dioxy)-3,4-pyrrole-2,5-diyl), nicknamed Minimally Color Changing Polymer (MCCP), lends limited absorption to the visible region in both its redox states. I made use of MCCP as a counter polymer in several ECDs, due to its good solubility and processing properties that allowed for a wide range of coating applications. While the fused poly(thieno[3,4-b]thiophene) reported by Sotzing is cathodically coloring, for practical applications it also lends limited absorbance in the visible spectrum in both redox states.[77, 78] Though transmissive sky blue in the oxidized state, the doping ratio was reported to be higher than both PEDOT and ProDOT-derivatives and hence a thinner layer was sufficient for efficient charge balance. ECDs utilizing poly(thiono[3,4-b]thiophene) as counter polymer was described by Sotzings group, and the differences in operational parameters between ECDs and ECPs was addressed.

2.5.3 Donor-acceptor approach and band gap engineering

First reported by Havinga in 1992/1993, the donor acceptor (D-A) approach to band gap engineering has become a valuable tool when designing conjugated polymers for optoelectrical purposes.[79, 80] The basic concept is that heterocyclic units can be either electron rich and act as (electron) donor units or they can be electron deficient and act as (electron) acceptor units. When donor and acceptor units are placed next to each other in a polymer chain, the difference in electronic distributions give rise to new electronic transitions, and hence optical transitions.

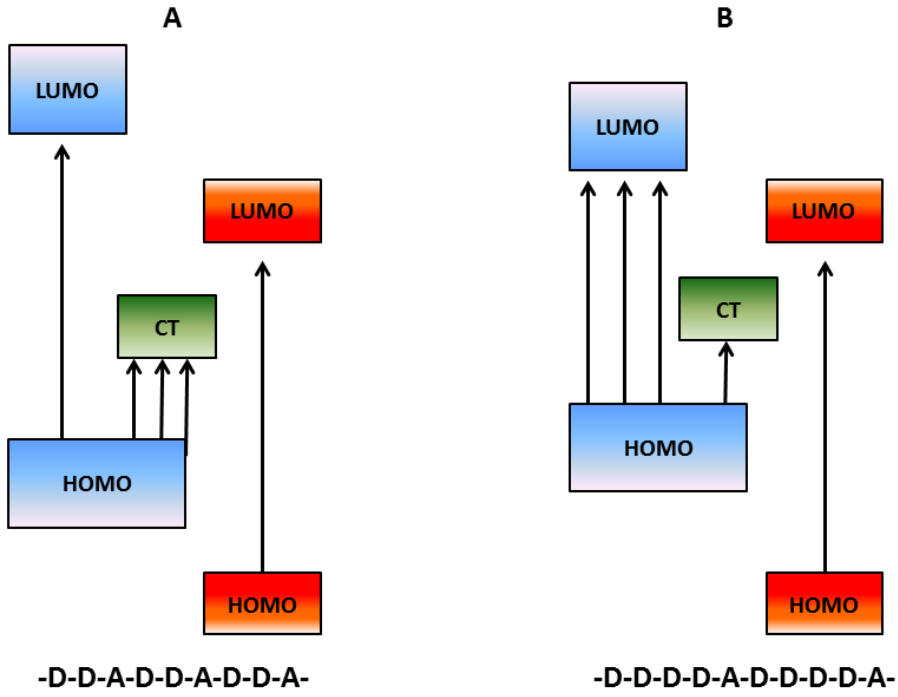

Figure 2-18: The D-A approach in the "the isolated dopants" representation. The blue MOs originate from the donor segments, the red from the acceptor "dopants", while the green Charge Transfer (CT) state is a result of D-A interactions. Beneath the MOs are shown a hypothetical D-A polymer. In going from situation (A) to situation (B), the amount of donor segments are increased, whereby the number of transitions from the donor HOMO to donor LUMO (blue) is increased while fewer transitions from donor HOMO to CT occur. Furthermore as the donor segments increase, the band gap is reduced. Adapted with permission from ref 81. Copyright (2010) American Chemical Society.

The D-A approach has been explained in several ways, but the "isolated dopants representation" presented here is the one I find most useful.[38, 81] In this representation the acceptor units are seen as "isolated dopants" whose interaction with the donor unit results in a low energy charge transfer (CT) state located between the HOMO and LUMO of the donor unit (as depicted in Figure 2-18 (A)). This low energy electronic transition from the HOMO of the donor to the CT gives rise to a second energy absorption band at long wavelengths. If the amount of donor units is increased compared to acceptor units, the short wavelength absorption (high energy transition) will increase in intensity and be red shifted since the donor-donor segments will increase.[7] Parallel to this, the intensity of absorption originating from the HOMO of the donor to the CT

states will diminish as these transitions become less populated (Figure 2-18 (B)), and the absorption blue shifts. Summarizing; as the D:A ratio increases the two peaks move towards an all-donor spectrum, as shown in Figure 2-19.

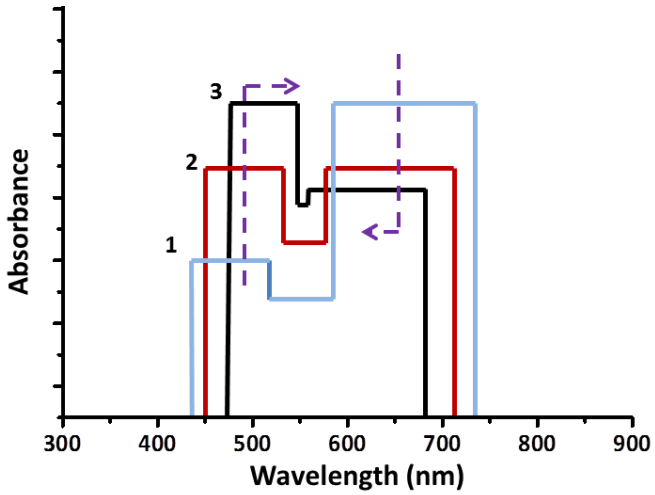

Figure 2-19: Evolution of D-A bands in the visible region. The D-A approach gives rise to short- and long wavelength absorptions bands. In going from 1 to 3 in a D-A polymer the amount of donor segments is increased, which redshifts the short wavelength absorption and blue shifts the long wavelength absorption. Adapted with permission from 81. Copyright (2010) American Chemical Society.

2.6 Electrochromic devices

2.6.1 Working principle

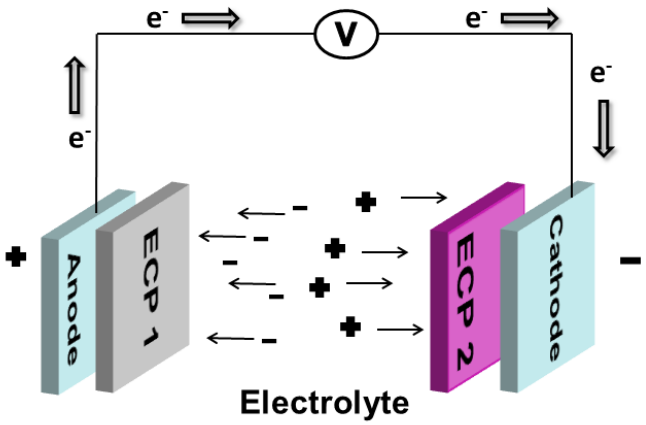

Figure 2-20: Working principle of an ECD. Reproduced from ref. 82 with permission from The Royal Society of Chemistry

The basic principle of an electrochromic device is the ability to change color by application of a suitable electric potential (shown in Figure 2-20). An ECD is fundamentally an electrochemical cell and by changing the potential across the electrodes, the polymer films can be oxidized if the electrode potential is higher (more positive) than the equilibrium potential of the cell or reduced/neutralized if the electrode potential is lower (more negative). Naturally the redox reaction at one electrode must complement the one at the other; so that one polymer is oxidized while the other is reduced/neutralized. During operation of the ECD an electric field is set up between the two electrodes. When subjected to this field, ions from the electrolyte layer move according to their charge and are injected into the polymer film, thereby doping the polymer and compensating for the developing charge (i.e. formation of polarons and bipolarons) in the polymer film.[20] The formation of polarons and bipolarons leads to a change in the electronic structure and a change in the band gap of the polymer. This changes the absorption profile of the polymer film, and is observed as a color change if it occurs in the visible region of the electromagnetic spectrum.

2.6.2 Device structure

While employing the same general working mechanism described above, the structure of an ECD depends on the utility of the device. Classically, ECDs are divided into absorptive/transmissive (A/T) or absorptive/reflective (A/R) based on function and structure. While the multi-layered device structure described below still accounts for the majority of polymer based ECDs, other ECD structures are currently explored in search of improving parameters such as response time, stability or processing; these state of the art ECDs are described at the end of this chapter.

2.6.3 Absorptive/transmissive devices

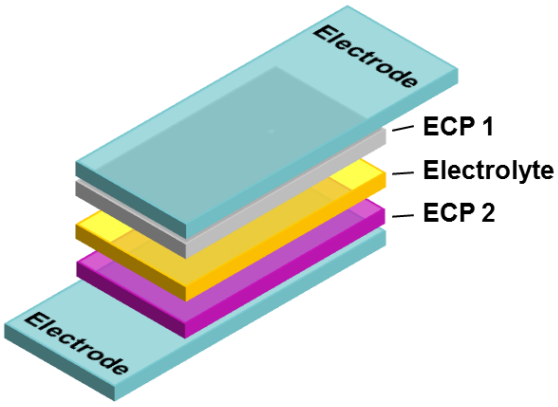

Figure 2-21: The general ECD structure for absorptive/transmissive devices. Both electrodes need to be transparent.

A typical absorptive/transmissive device structure is shown in Figure 2-21 and basically comprises two electrochromic polymers (ECP 1 and 2) and an electrolyte layer sandwiched between two transparent electrodes facing inwards. A/T devices are designed to switch between a highly absorptive and a highly transmissive state by application of a suitable potential. A/T devices are probably the ECDs most often encountered, as it represents switchable windows, goggles, spectacles and shutters. Since these applications require the viewer to see through the device in the transmissive state, both electrodes need to be transparent along the observable wavelengths. Two ECPs are used in

A/T devices; the primary ECP is the one responsible for the majority of the color change, while the secondary ECP functions as a charge balancing counter polymer. In fact the counter electrode does not need to contain a polymer as long as the species is electroactive and inorganic oxides have been used as the counter material in hybrid devices.[83-85] The secondary ECP can be a polymer with minimal absorbance in the potential region employed or it can switch complementary to the primary, which then implies that one ECP is cathodically coloring while the other is anodically coloring. While using a secondary ECP complementary to the primary ECP should enhance the optical density in the colored state, it has been found that the optical contrast is lowered by using two polymers in ECDs.[86] Another drawback using this approach is that is very difficult to find polymers that are exactly color complementary, which results in devices that have one color in the absorptive state and another color while being transmissive due to "tailings" from the secondary ECP.[87, 88] Using an approach where the secondary ECP is almost colorless and/or the color change in the potential region is minimal was achieved when the Minimally Color Changing Polymer (MCCP) was recently published, as described in section 2.5.2.[89]

2.6.4 Absorptive/reflective devices

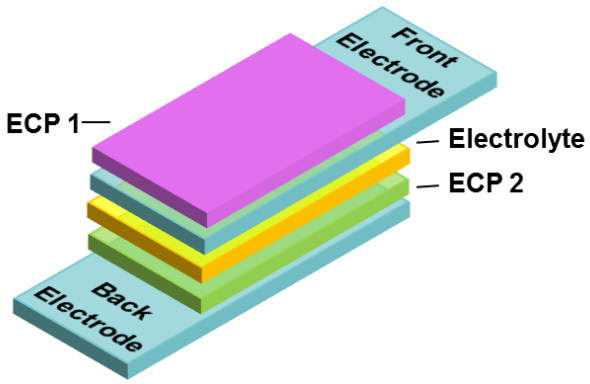

Figure 2-22: The general ECD structure for absorptive/reflective devices. Reproduced from ref. 82 with permission from The Royal Society of Chemistry

The structure of an absorptive/reflective type ECD is different than the A/T type devices, although most of the components are similar.[87, 90] The difference is mainly because an A/R device does not require the viewer to see through the device, since they attenuate reflection e.g. as a dimmable mirror. The primary ECP (ECP 1 in Figure 2-22) is coated onto the front electrode facing outwards. The front electrode is a specular reflecting conductive material, typically a porous metalized membrane that allows ion diffusion to ECP 1 when the device is operated. When ECP 1 is in the colored state, the membranes reflection is attenuated and the mirror is "off", and when the primary ECP is bleached the reflection from the membrane is unaltered and the mirror is "on". A/R devices have traditionally been used for mirrors and displays, but are not limited to the visible region, and near-infrared (NIR) modulation by A/R-devices has been suggested for optical telecommunication and thermal camouflage.[91-94] The operation mode of A/R ECDs alleviates constraints on device construction since the electrodes do not have to be transparent, and only the primary ECP and front electrode are visible. Since the counter polymer (ECP 2) is hidden from view, the optical properties do not affect the optical contrast of the device and consequently a wider range of electroactive species can be employed.

2.6.5 Electrolyte

The electrolyte layer in the ECD serves two purposes. The first being a source of moveable charge carriers (i.e. ions), which are able to counterbalance the induced charges on the ECPs during redox switching. The electrolyte layer typically constitutes an appropriate salt dissolved in an ion conducting solvent, and mixed into an electrically inert polymer matrix such as PMMA or PEO.[95-98] Propylene carbonate (PC), ethylene carbonate (EC) or acetonitrile are frequently used as the solvent. PC is a polar aprotic solvent that fulfills many of the requirements for an electrolyte solvent. The high polarity of PC allows it to dissolve the salt and its high relative permittivity introduces capacitance in the system allowing charge to build up on the ECPs. Additionally, its excellent properties as a plasticizer are used to modulate the plasticity of PMMA. The polymer matrix is used to gel the electrolyte to prevent leaking and deformation of the de-

vice,[95] though this is a trade off as the ionic mobility and hence the response time is increased by increasing viscosity.[99, 100] During the last 10 years, the use of ionic liquids (IL's) as electrolytes has become quite popular in ECDs.[101-103] IL's are useful as ECD electrolytes owing to their generally high ionic conductivity, low volatility and large electrochemical window in which they are stable to electrochemical reduction and oxidation. As IL's generally have low viscosities, they cannot solely be used as electrolyte, and are also gelled with electrically inert polymers; and as such they function both as a plasticizer and an ion source in ECD electrolytes, whereby high ionic concentrations are readily achieved. [102, 104-107] The secondary role of the electrolyte layer can be to function as an adhesive in joining the two substrates. Though many research groups use a separate adhesive (e.g. epoxy) for sealing ECDs,[10, 108-111] I have found that having adhesive properties in the electrolyte layer is advantageous as this simplifies the manufacture of devices. However, these properties have not yet been fine-tuned, and it is not unlikely that some sort of sealant is required in order to prevent solvents in the electrolyte layer from slowly evaporating. In summary, the challenge in developing suitable electrolyte layers for ECDs is balancing ionic conductivity with viscosity.

2.6.6 Electrode materials

The electrodes in ECDs serve the purpose of transporting electrons to and from the ECP layers as well as distributing an electrical field in which ions can move. In order for the electrodes to be usable in ECDs they need to as be transparent as possible. The optical transparency is dependent upon both electrode substrate and material as shown in Figure 2-5. ITO on glass or PET is commonly used as transparent electrodes in ECDs,[20, 112] which is problematic due to several factors: Thin ITO films are brittle and cracks can result if the films are bent, which increase the resistance.[113-116] From an operational point of view the low concentration of charge carriers in ITO gives rise to a large sheet resistance. It has been established that the electrode resistance has a marked effect on the response time and optical contrast of an ECD,[117] and high electrode resistance leads to a non-uniform potential across the electrode (ohmic loss), and a non-uniform current distribution in the electrolyte.[118]. When electrodes of mod-

erate conductivity are employed, increasing potentials are needed to achieve satisfactory response times and optical contrast, as the ionic mobility partially depends on the electric field between the two electrodes. High potentials conflict with the voltage limits of the device, and outside of this threshold side reactions are likely to occur due to the other chemical components or moisture.[119-121] Several alternatives to ITO as transparent electrode material exists,[122, 123] and I have explored the use of thin silver-based grids as one of way of replacing ITO in ECDs which is discussed in chapter 3.

2.7 State of the art ECDs

Though the structure of an ECD is usually like the one depicted in Figure 2-21 several research groups are seeking to improve one or more functionalities in ECDs such as addressability, optical contrast, stability, ease of processing etc. or exploring new ways of using ECPs.[124-129] The following two examples are by no means an adequate review of all new developments in ECD design, but were chosen as they seek to address some of the challenges I have encountered during my research. For a review of commercially available products that utilize electrochromic compound the reader is directed to ref. [20]

2.7.1 Addressable matrix displays

Displays with individual addressable pixels have been a long standing challenge in ECD technology, and one that is still largely unsolved. In order to address this challenge the group of Berggren proposed a method that utilizes *electronic paper*, which is a term that constitutes cellulose-based paper coated with polyethylene (PE) and further functionalized by deposition of ECPs and organic transistors.[130] The advantage of this approach is that well-known printing techniques using available equipment can be used, thereby keeping the manufacturing costs low. In their "smart pixel" design shown in Figure 2-23 the group exploits PEDOT:PSS having electrochromic and conductive properties (see section 2.5.1) , and that the latter can be electrochemically tuned, whereby PEDOT:PSS functions as a transistor.

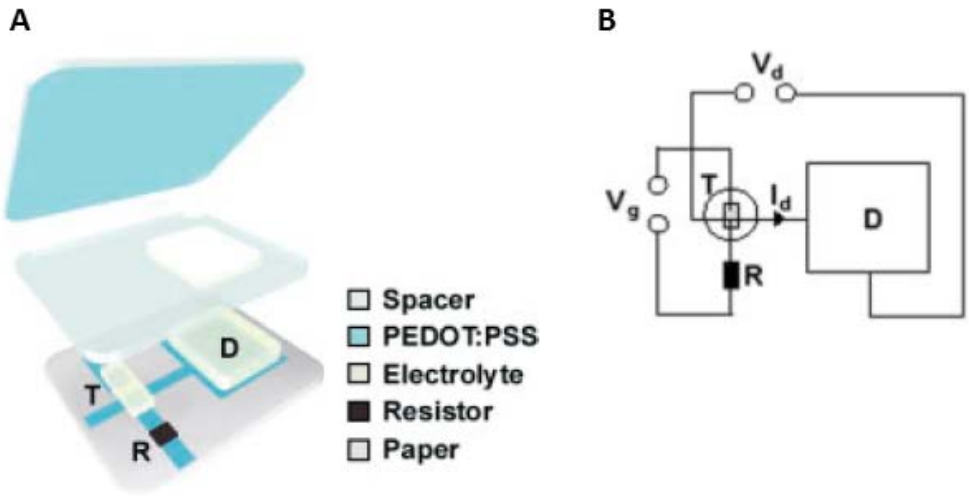

Figure 2-23: Smart pixel structure (A) that consists of a display cell (D) a resistor (R) and a transistor (T). The turquois color corresponds to PEDOT:PSS coatings and the cyan colored patches to electrolyte gel. (B) Electrical diagram representation of the smart pixel. The display cell voltage (V_d) and gate voltage (V_g) are supplied from two different power sources. The gate voltage controls the updating current I_d. Reproduced from ref. 130 Copyright © 2007 WILEY-VCH Verlag GmbH & Co. KGaA, Weinheim

Both the gate and display are operated between 0 V and +2 V, and the switch between the various redox states of PEDOT is reversible assuming that overoxidation does not occur. In that regard this design faces the same challenges as other ECDs. The response time of these smart pixels is dependent on the display cell area and was reported to be 5 seconds for a 13 x 30 mm^2 (95% switch). By using an electrolyte that comprised white opaque filler, the counter electrode was hidden and the reduced optical contrast usually encountered in symmetrical devices was avoided (see section 2.7.2);[8] this naturally prohibited any transparency in the device. By using PEDOT:PSS as a transistor material the on:off ratio should be 5000, meaning that the display voltage can be reduced by a factor 5000. In further developing the smart pixel a vertical structure was designed that increased the fill factor of the display (i.e. the ratio of switchable area versus total display area).[131] In addition to an increased fill factor a vertical structure reduces the response time due to shorter ionic drift. But as the top electrode (the one seen) is

larger than the counter electrode, a blooming effect analogously to the one described in section 3.6.1 as a consequence of lateral charge transport.

In a recent report on smart pixel design the transistor is an integrated part of the ECD in which the drain electrode in the transistor functions as the counter electrode in the ECD.[132] And while the prototypes from this new design show increased response times and limited optical contrast, the general design, manufacture and mode of operation show promise for addressable pixelated ECDs.

2.7.2 Single layer approach

As people familiar with organic electronics will recognize, depositing various functional layers on top of each other is not without complications, in the form of e.g. dewetting, insufficient interfacial contact, dissolution of previous layers etc. This also hold for ECDs, and especially for the semisolid electrolyte layer as previously discussed. One way of targeting this is to use only one layer sandwiched between two transparent electrodes as opposed to 3 (or more) layers as described in section 2.6.2. The single layer approach (sometimes referred to as the solid state approach) should amongst other things simplify the manufacturing process by reducing the number of deposition steps, avoid electrolyte leakage, reduce materials waste and overall increase the stability of the device. In a report from DuPont carbazole chromophores were grafted onto poly(epichlorohydrin-co-ethylene-oxide) chains, forming just one electrochromic layer.[133] Though not entirely convincing, the paper shows new ways of addressing this challenge, by integrating the electrochromic species in the solid electrolyte matrix. In another report the electrochromic species (here a viologen) was simply heated in thermoplastic poly(vinyl formal) (PVF) matrix and pressed into a self-supported film.[134] The simplicity in the approach is very attractive and the thermoplastic polymer PVF shows strong adhesive properties that increase the mechanical stability of the device.

Several strategies for the single layer approach rely on in-situ polymerization of the ECP inside the electrolyte matrix, whereby a semi-interpenetrating polymer network is formed (semi-IPN). It follows that such an approach employs just one ECP (in two separate films), that thus functions both as cathodically and anodically coloring ECP. A good

question would then be if there is any optical contrast in such a symmetrical device. The answer to this is yes and is depicted in Figure 2-24. The low transmittance/colored state is the one where one side of the device is fully reduced and the other is fully oxidized (Figure 2-24 (A)), the high transmittance/bleached state is the where the transmittance of both ECP films are at an intermediate state (equipotential state) (Figure 2-24(B)).

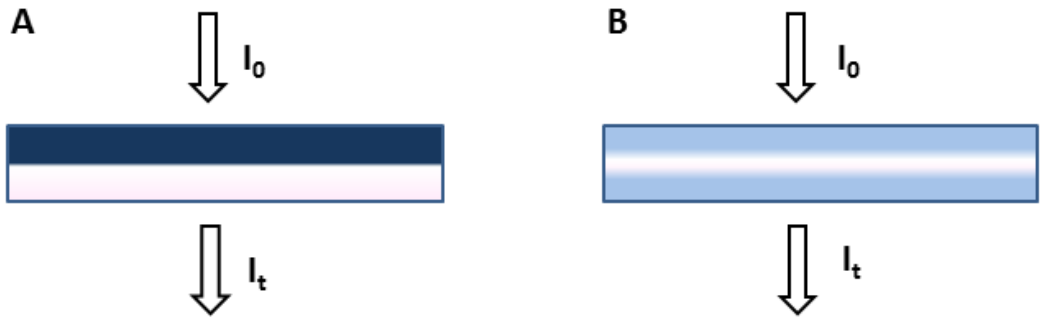

Figure 2-24: Schematic representation of a symmetrical ECD. (A) Depicts a situation where one layer is fully reduced (top layer) and the other is fully oxidized (bottom layer). This constitutes the colored form of the device. (B) Depicts a situation where both layer exhibits the same intermediate transmittance. The device is said to be in an equipotential state (ΔE=0).

The single layer approach has been elegantly demonstrated, in two reports by the Chevrot group where EDOT and ProDOT-Me_2 (3,4-(2,2-dimethyl propylenedioxy)thiophene were oxidatively polymerized in-situ inside a poly(ethylene glycol dimethacrylate)/poly(ethylene glycol methacrylate) matrix.[135, 136] By controlling the polymerization time and solvent composition it was possible to fabricate free standing electrochromic films where the ECPs were confined to the outer regions of the films, leaving the interior matrix ECP free and preventing the device from short circuiting. The optical contrast of these devices was around 30%, which is good compared to other symmetrical devices.[8] As expected the solid system shows increased response times ranging from 30 to 60 seconds depending on the direction of the switch, but neverthe-

less this method could prove to be useful, due to the facile fabrication process and because the ECP is intrinsically protected inside the polymer matrix.

References

1 A. L. Dyer, E. J. Thompson and J. R. Reynolds, *ACS Appl. Mater. Interfaces,* 2011, **3,** 1787-1795.

2 G. Gunbas and L. Toppare, *Chem. Commun.,* 2012, **48,** 1083-1101.

3 C. G. Wu, M. -I. Lu and P. -F. Tsai, *Macromol. Chem. Phys.,* 2009, **210,** 1851-1855.

4 J. Heinze, B. A. Frontana-Uribe and S. Ludwigs, *Chem. Rev.,* 2010, **110,** 4724-4771.

5 D. R. Gagnon, J. D. Capistran, F. E. Karasz, R. W. Lenz and S. Antoun, *Polymer,* 1987, **28,** 567-573.

6 Y. Li, Y. Cao, J. Gao, D. Wang, G. Yu and A. J. Heeger, *Synth Met,* 1999, **99,** 243-248.

7 M. Wohlgenannt, X. M. Jiang and Z. V. Vardeny, *Phys. Rev. B Condens. Matter Mater. Phys.,* 2004, **69,** 241204-1-241204-4.

8 D. Mecerreyes, R. Marcilla, E. Ochoteco, H. Grande, J. A. Pomposo, R. Vergaz and J. M. Sánchez Pena, *Electrochim. Acta,* 2004, **49,** 3555-3559.

9 A. A. Argun, A. Cirpan and J. R. Reynolds, *Adv Mater,* 2003, **15,** 1338-1341.

10 C. Ma, M. Taya and C. Xu, *Electrochim. Acta,* 2008, **54,** 598-605.

11 C. Pozo-Gonzalo, D. Mecerreyes, J. A. Pomposo, M. Salsamendi, R. Marcilla, H. Grande, R. Vergaz, D. Barrios and J. M. Sánchez-Pena, *Sol Energ Mater Sol Cells,* 2008, **92,** 101-106.

12 F. Miomandre, M. N. Bussac, E. Vieil and L. Zuppiroli, *Chem. Phys.,* 2000, **255,** 291-300.

13 C. K. Baker, Y. -l. Qiu and J. R. Reynolds, *Journal of Physical Chemistry,* 1991, **95,** 4446-4452.

14 S. Ramesh, C. -W. Liew and K. Ramesh, *J. Non Cryst. Solids,* 2011, **357,** 2132-2138.

15 J. Heinze, *Synth. Met.,* 1991, **43,** 2805-2823.

16 Q. Zhou, C. J. Kolaskie and L. L. Miller, *Journal of Electroanalytical Chemistry and Interfacial Electrochemistry,* 1987, **223,** 283-286.

17 A. R. Hillman, K. S. Ryder, V. C. Ferreira, C. J. Zaleski and E. Vieil, *Electrochim. Acta,* 2013, .

18 P. -H. Aubert, A. A. Argun, A. Cirpan, D. B. Tanner and J. R. Reynolds, *Chem. Mater.,* 2004, **16,** 2386-2393.

19 J. Jensen, H. F. Dam, J. R. Reynolds, A. L. Dyer and F. C. Krebs, *J. Polym. Sci. Part B,* 2012, **50,** 536-545.

20 P. M. S. Monk, R. J. Mortimer and D. R. Rosseinsky, *Electrochromism and Electrochromic Devices,* Chamebridge University Press, 2007.

21 B. D. Reeves, C. R. G. Grenier, A. A. Argun, A. Cirpan, T. D. McCarley and J. R. Reynolds, *Macromolecules,* 2004, **37,** 7559-7569.

22 C. L. Gaupp, D. M. Welsh, R. D. Rauh and J. R. Reynolds, *Chem. Mater.,* 2002, **14,** 3964-3970.

23 B. C. Thompson, P. Schottland, K. Zong and J. R. Reynolds, *Chem. Mater.,* 2000, **12,** 1563-1571.

24 J. L. Boehme, D. S. K. Mudigonda and J. P. Ferraris, *Chem. Mater.,* 2001, **13,** 4469-4472.

25 D. Witker and J. R. Reynolds, *Macromolecules,* 2005, **38,** 7636-7644.

26 S. S. Kalagi, S. S. Mali, D. S. Dalavi, A. I. Inamdar, H. Im and P. S. Patil, *Synth. Met.,* 2011, **161,** 1105-1112.

27 H. Shin, Y. Kim, T. Bhuvana, J. Lee, X. Yang, C. Park and E. Kim, *ACS Appl. Mater. Interfaces,* 2012, **4,** 185-191.

28 R. J. Mortimer and T. S. Varley, *Sol Energ Mater Sol Cells,* 2012, **99,** 213-220.

29 F. Carpi and D. De Rossi, *Opt. Laser Technol.,* 2006, **38,** 292-305.

30 J. Kawahara, P. A. Ersman, I. Engquist and M. Berggren, *Org. Electron. : Phys. Mater. Appl.,* 2012, **13,** 469-474.

31 F. W. Billmeyer, *Principles of Color Technology,* John Wiley & Sons, Troy, New York, 1981.

32 A. H. Munsell, *A Color Notation,* Munsell Color Co., Baltimore, Maryland, 1963.

33 CIE, 1931

34 CIE, 1971

35 CIE, 2103

36 C. M. Amb, A. L. Dyer and J. R. Reynolds, *Chem. Mater.,* 2011, **23,** 397-415.

37 C. M. Amb, J. A. Kerszulis, E. J. Thompson, A. L. Dyer and J. R. Reynolds, *Polym. Chem.,* 2011, **2,** 812-814.

38 P. M. Beaujuge and J. R. Reynolds, *Chem. Rev.,* 2010, **110,** 268-320.

39 L. -T. Huang, H. -J. Yen, C. -W. Chang and G. -S. Liou, *J. Polym. Sci. Part A,* 2010, **48,** 4747-4757.

40 G. Sonmez, C. K. F. Shen, Y. Rubin and F. Wudl, *Angew. Chem. Int. Ed.,* 2004, **43,** 1498-1502.

41 R. J. Mortimer, A. L. Dyer and J. R. Reynolds, *Disp,* 2006, **27,** 2-18.

42 C. B. Duke, A. Paton, W. R. Salaneck, H. R. Thomas, E. W. Plummer, A. J. Heeger and A. G. MacDiarmid, *Chemical Physics Letters,* 1978, **59,** 146-150.

43 C. K. Chiang, Y. W. Park, A. J. Heeger, H. Shirakawa, E. J. Louis and A. G. MacDiarmid, *J. Chem. Phys.,* 1978, **69,** 5098-5104.

44 P. J. Nigrey, A. G. MacDiarmid and A. J. Heeger, *Journal of the Chemical Society, Chemical Communications,* 1979, 594-595.

45 M. Dietrich, J. Heinze, G. Heywang and F. Jonas, *J Electroanal Chem,* 1994, **369,** 87-92.

46 G. Heywang and F. Jonas, *Adv Mater,* 1992, **4,** 116-118.

47 F. Louwet, L. Groenendaal, J. Dhaen, J. Manca, J. Van Luppen, E. Verdonck and L. Leenders, *Synth. Met.,* 2003, **135-136,** 115-117.

48 L. Groenendaal, F. Jonas, D. Freitag, H. Pielartzik and J. R. Reynolds, *Adv Mater,* 2000, **12,** 481-494.

49 A. Elschner, S. Kirchmeyer, W. Lövenich, U. Mercher and K. Reuter, 2011, .

50 G. A. Sotzing, J. R. Reynolds and P. J. Steel, *Chem. Mater.,* 1996, **8,** 882-889.

51 A. Kumar and J. R. Reynolds, *Macromolecules,* 1996, **29,** 7629-7630.

52 A. Kumar, D. M. Welsh, M. C. Morvant, F. Piroux, K. A. Abboud and J. R. Reynolds, *Chem. Mater.,* 1998, **10,** 896-902.

53 P. Wegener, M. Feldhues and H. Litterer, Aromatic and heterocyclic ether prodn. from halide|from alkoxy-thiophene(s) and alcohol(s) with acid catalysis; patent; PT: P; PN: EP328984-A1; DE3804522-A; AU8929788-A; NO8900585-A; PT89688-A; FI8900624-A; JP2003685-A; US4931568-A; CN1035291-A; EP328984-B1; DE58902312-G; ES2052786-T3; AE: HOECHST AG; UT: DI-IDW:1989242925

54 B. M. W. Langeveld-Voss, R. A. J. Janssen, M. P. T. Christiaans, S. C. J. Meskers, H. P. J. M. Dekkers and E. W. Meijer, *J. Am. Chem. Soc.,* 1996, **118,** 4908-4909.

55 D. M. Welsh, L. J. Kloeppner, L. Madrigal, M. R. Pinto, B. C. Thompson, K. S. Schanze, K. A. Abboud, D. Powell and J. R. Reynolds, *Macromolecules,* 2002, **35,** 6517-6525.

56 P. M. Beaujuge, C. M. Amb and J. R. Reynolds, *Adv Mater,* 2010, **22,** 5383-5387.

57 G. Sonmez, H. B. Sonmez, C. K. F. Shen, R. W. Jost, Y. Rubin and F. Wudl, *Macromolecules,* 2005, **38,** 669-675.

58 G. Sonmez, H. B. Sonmez, C. K. F. Shen and F. Wudl, *Adv Mater,* 2004, **16,** 1905-1908.

59 P. Coppo, D. C. Cupertino, S. G. Yeates and M. L. Turner, *Macromolecules,* 2003, **36,** 2705-2711.

60 C. -G. Wu, M. -I. Lu, S. -J. Chang and C. -S. Wei, *Adv. Funct. Mater.,* 2007, **17,** 1063-1070.

61 P. M. Beaujuge, S. Ellinger and J. R. Reynolds, *Adv Mater,* 2008, **20,** 2772-2776.

62 Merve Içli, M. Pamuk, F. Algi, A. M. Önal and A. Cihaner, *Chem. Mater.,* 2010, **22,** 4034-4044.

63 P. M. Beaujuge, S. Ellinger and J. R. Reynolds, *Nat. Mater.,* 2008, **7,** 795-799.

64 F. C. Krebs, *Nat. Mater.,* 2008, **7,** 766-767.

65 P. Shi, C. M. Amb, E. P. Knott, E. J. Thompson, D. Y. Liu, J. Mei, A. L. Dyer and J. R. Reynolds, *Adv Mater,* 2010, **22,** 4949-4953.

66 M. Içli, M. Pamuk, F. Algi, A. M. Önal and A. Cihaner, *Org. Electron. : Phys. Mater. Appl.,* 2010, **11,** 1255-1260.

67 C. M. Amb, P. M. Beaujuge and J. R. Reynolds, *Adv Mater,* 2010, **22,** 724-728.

68 B. D. Reeves, E. Unur, N. Ananthakrishnan and J. R. Reynolds, *Macromolecules,* 2007, **40,** 5344-5352.

69 P. Shi, C. M. Amb, A. L. Dyer and J. R. Reynolds, *ACS Appl. Mater. Interfaces,* 2012, **4,** 6512-6521.

70 A. Balan, G. Gunbas, A. Durmus and L. Toppare, *Chem. Mater.,* 2008, **20,** 7510-7513.

71 M. Li, A. Patra, Y. Sheynin and M. Bendikov, *Adv Mater,* 2009, **21,** 1707-1711.

72 A. L. Dyer, M. R. Craig, J. E. Babiarz, K. Kiyak and J. R. Reynolds, *Macromolecules,* 2010, **43,** 4460-4467.

73 R. M. Walczak and J. R. Reynolds, *Adv Mater,* 2006, **18,** 1121-1131.

74 R. M. Walczak, J. K. Leonard and J. R. Reynolds, *Macromolecules,* 2008, **41,** 691-700.

75 B. C. Thompson, Y. -. Kim, T. D. McCarley and J. R. Reynolds, *J. Am. Chem. Soc.,* 2006, **128,** 12714-12725.

76 G. -S. Liou and C. -W. Chang, *Macromolecules,* 2008, **41,** 1667-1674.

77 G. A. Sotzing and K. Lee, *Macromolecules,* 2002, **35,** 7281-7286.

78 M. A. Invernale, V. Seshadri, D. M. D. Mamangun, Y. Ding, J. Filloramo and G. A. Sotzing, *Chem. Mater.,* 2009, **21,** 3332-3336.

79 E. E. Havinga, W. ten Hoeve and H. Wynberg, *Polym. Bull.,* 1992, **29,** 119-126.

80 E. E. Havinga, W. ten Hoeve and H. Wynberg, *Synth. Met.,* 1993, **55,** 299-306.

81 P. M. Beaujuge, C. M. Amb and J. R. Reynolds, *Acc. Chem. Res.,* 2010, **43,** 1396-1407.

82 J. Jensen, M. V. Madsen and F. C. Krebs, *J. Mater. Chem. C,* 2013, **1,** 4826-4835.

83 V. K. Thakur, G. Ding, J. Ma, P. S. Lee and X. Lu, *Adv Mater,* 2012, **24,** 4071-4096.

84 C. O. Avellaneda, M. A. C. Berton and L. O. S. Bulhões, *Sol Energ Mater Sol Cells,* 2008, **92,** 240-244.

85 C. Kaneko, C. Xu, L. Liu, D. Ning and M. Taya, *Proc SPIE Int Soc Opt Eng,* 2005, **5759,** 518-524.

86 J. Padilla and T. F. Otero, *Electrochem. Commun.,* 2008, **10,** 1-6.

87 A. Cirpan, A. A. Argun, C. R. G. Grenier, B. D. Reeves and J. R. Reynolds, *J. Mater. Chem.,* 2003, **13,** 2422-2428.

88 S. A. Sapp, G. A. Sotzing and J. R. Reynolds, *Chem. Mater.,* 1998, **10,** 2101-2108.

89 E. P. Knott, M. R. Craig, D. Y. Liu, J. E. Babiarz, A. L. Dyer and J. R. Reynolds, *J. Mater. Chem.,* 2012, **22,** 4953-4962.

90 H. Pagès, P. Topart and D. Lemordant, *Electrochim. Acta,* 2001, **46,** 2137-2143.

91 A. L. Dyer, C. R. G. Grenier and J. R. Reynolds, *Adv. Funct. Mater.,* 2007, **17,** 1480-1486.

92 P. Chandrasekhar, B. J. Zay, T. McQueeney, A. Scara, D. Ross, G. C. Birur, S. Haapanen, L. Kauder, T. Swanson and D. Douglas, *Synth. Met.,* 2003, **135-136,** 23-24.

93 P. Chandrasekhar, B. J. Zay, T. McQueeney, G. C. Birur, V. Sitaram, R. Menon, M. Coviello and R. L. Elsenbaumer, *Synth. Met.,* 2005, **155,** 623-627.

94 I. Schwendeman, J. Hwang, D. M. Welsh, D. B. Tanner and J. R. Reynolds, *Adv Mater,* 2001, **13,** 634-637.

95 H. J. Byker, *Electrochim. Acta,* 2001, **46,** 2015-2022.

96 S. A. Agnihotry, P. Pradeep and S. S. Sekhon, *Electrochim. Acta,* 1999, **44,** 3121-3126.

97 T. Mani and J. R. Stevens, *Polymer,* 1992, **33,** 834-837.

98 S. Legenski, C. Xu, L. Liu, M. L. Guilly and M. Taya, *Proc SPIE Int Soc Opt Eng,* 2004, **5385,** 319-325.

99 S. -C. Wang and H. -K. Tsao, *Macromolecules,* 2003, **36,** 9128-9134.

100 A. B. McEwen, H. L. Ngo, K. LeCompte and J. L. Goldman, *J. Electrochem. Soc.,* 1999, **146,** 1687-1695.

101 W. Lu, A. G. Fadeev, B. Qi, E. Smela, B. R. Mattes, J. Ding, G. M. Spinks, J. Mazurkiewicz, D. Zhou, G. G. Wallace, D. R. MacFarlane, S. A. Forsyth and M. Forsyth, *Science,* 2002, **297,** 983-987.

102 S. Desai, R. L. Shepherd, P. C. Innis, P. Murphy, C. Hall, R. Fabretto and G. G. Wallace, *Electrochim. Acta,* 2011, **56,** 4408-4413.

103 M. Döbbelin, R. Marcilla, C. Pozo-Gonzalo and D. Mecerreyes, *J. Mater. Chem.,* 2010, **20,** 7613-7622.

104 M. A. B. H. Susan, T. Kaneko, A. Noda and M. Watanabe, *J. Am. Chem. Soc.,* 2005, **127,** 4976-4983.

105 A. Georg and A. Georg, *Sol Energ Mater Sol Cells,* 2009, **93,** 1329-1337.

106 O. Winther-Jensen, S. Desai, R. L. Shepherd, P. C. Innis, B. Winther-Jensen, M. Forsyth, G. G. Wallace and D. R. MacFarlane, *Electrochem. Commun.,* 2010, **12,** 1505-1508.

107 K. Matsumoto, B. Talukdar and T. Endo, *Polym. Bull.,* 2011, **66,** 771-778.

108 C. Xu, C. Ma, X. Kong and M. Taya, *Polym. Adv. Technol.,* 2009, **20,** 178-182.

109 M. Nikolou, A. L. Dyer, T. T. Steckler, E. P. Donoghue, Z. Wu, N. C. Heston, A. G. Rinzler, D. B. Tanner and J. R. Reynolds, *Chem. Mater.,* 2009, **21,** 5539-5547.

110 W. Lu, A. G. Fadeev, B. Qi and B. R. Mattes, *J. Electrochem. Soc.,* 2004, **151,** H33-H39.

111 C. Pozo-Gonzalo, M. Salsamendi, A. Viñuales, J. A. Pomposo and H. -. Grande, *Sol Energ Mater Sol Cells,* 2009, **93,** 2093-2097.

112 C. G. Granqvist, *Appl. Phys. A,* 1993, **57,** 19-24.

113 Y. Leterrier, L. Médico, F. Demarco, J. -. E. Månson, U. Betz, M. F. Escolà, M. K. Olsson and F. Atamny, *Thin Solid Films,* 2004, **460,** 156-166.

114 Y. C. Lin, W. Q. Shi and Z. Z. Chen, *Thin Solid Films,* 2009, **517,** 1701-1705.

115 Y. F. Lan, W. C. Peng, Y. H. Lo and J. L. He, *Org. Electron. : Phys. Mater. Appl.,* 2010, **11,** 670-676.

116 G. Gu, Z. Shen, P. E. Burrows and S. R. Forrest, *Adv Mater,* 1997, **9,** 725-728.

117 H. Kaneko and K. Miyake, *Appl. Phys. Lett.,* 1986, **49,** 112-114.

118 K. Ho, D. E. Singleton and C. B. Greenberg, *J. Electrochem. Soc.,* 1990, **137,** 3858-3864.

119 A. A. Pud, *Synth. Met.,* 1994, **66,** 1-18.

120 E. W. Tsai, S. Basak, J. P. Ruiz, J. R. Reynolds and K. Rajeshwar, *J. Electrochem. Soc.,* 1989, **136,** 3683-3689.

121 H. Harada, T. Fuchigami and T. Nonaka, *J Electroanal Chem,* 1991, **303,** 139-150.

122 K. Ellmer, *Nat. Photon.,* 2012, **6,** 809-817.

123 D. Angmo and F. C. Krebs, *J Appl Polym Sci,* 2013, **129,** 1-14.

124 S. I. Cho, W. J. Kwon, S. -. Choi, P. Kim, S. -. Park, J. Kim, S. J. Son, R. Xiao, S. -. Kim and S. B. Lee, *Adv Mater,* 2005, **17,** 171-175.

125 R. Sydam, M. Deepa and A. K. Srivastava, *RSC Adv.,* 2012, **2,** 9011-9021.

126 Y. Ding, M. A. Invernale, D. M. D. Mamangun, A. Kumar and G. A. Sotzing, *J. Mater. Chem.,* 2011, **21,** 11873-11878.

127 M. A. Invernale, Y. Ding and G. A. Sotzing, *ACS Appl. Mater. Interfaces,* 2010, **2,** 296-300.

128 L. -M. Huang, C. -P. Kung, C. -W. Hu, C. -Y. Peng and H. -C. Liu, *Sol Energ Mater Sol Cells,* 2012, **107,** 390-395.

129 A. L. Beresford, R. M. Brown, A. R. Hillman and J. W. Bond, *J. Forensic Sci.,* 2012, **57,** 93-102.

130 P. Andersson, D. Nilsson, P. -. Svensson, M. Chen, A. Malmström, T. Remonen, T. Kugler and M. Berggren, *Adv Mater,* 2002, **14,** 1460-1464.

131 P. Andersson, R. Forchheimer, P. Tehrani and M. Berggren, *Adv. Funct. Mater.,* 2007, **17,** 3074-3082.

132 J. Kawahara, P. Andersson Ersman, D. Nilsson, K. Katoh, Y. Nakata, M. Sandberg, M. Nilsson, G. Gustafsson and M. Berggren, *J. Polym. Sci. Part B,* 2013, **51,** 265-271.

133 S. Percec and S. Tilford, *J. Polym. Sci. Part A,* 2011, **49,** 361-368.

134 G. Chidichimo, M. De Benedittis, J. Lanzo, B. C. De Simone, D. Imbardelli, B. Gabriele, L. Veltri and G. Salerno, *Chem. Mater.,* 2007, **19,** 353-358.

135 F. Tran-Van, L. Beouch, F. Vidal, P. Yammine, D. Teyssié and C. Chevrot, *Electrochim Acta,* 2008, **53,** 4336-4343.

136 M. Mallouki, P. -H. Aubert, L. Beouch, F. Vidal and C. Chevrot, *Synth. Met.,* 2012, **162,** 1903-1911.

Chapter 3

3. Fabrication of electrochromic devices

3.1 Introduction

This chapter describes the processing of electrochromic polymers onto flexible substrates, and how electrochromic devices are fabricated from these. As my work has dealt with solution processable polymers (as opposed to electrochemically polymerized), these will be the focus of this chapter. The chapter begins with a review of various coating methods describing the strengths and weaknesses of each method. Both matrix displays and devices employing fully continuous conducting flexible substrates are covered, and the challenges in fabricating them are discussed. This is exemplified by showing possible uses for ECDs in the form of a simple device driven by organic polymeric photovoltaics (OPVs). Also included in this chapter is a discussion on how indium doped tin oxide (ITO) can be replaced as the transparent electrode in ECDs, and this is exemplified by operational devices.

In order to be processable from organic solvents, the polymer backbone needs to contain solubilizing alkyl or alkoxy side chains. This is based on the chemist's rule of thumb that "like dissolves like", hence apolar side chains are required in order to match the apolar solvents. Another contributing factor to the solubility is the mobility of the side chains. A substantial amount of work has already been carried out on these subjects, as described in chapter 2. Common to all solution-based deposition methods, is the dissolution of the polymer in an appropriate solvent and deposition onto a substrate. Following evaporation of the solvent, a thin polymer film (approximately 50-200 nm for the films described in this dissertation) is formed that is switchable between the various redox states.

Prior to my work, the majority of the reports on ECPs and ECDs were done using spin and spray coating of ECPs onto ITO-glass substrates, and as such, the use of roll coating methods for ECP deposition on flexible substrates constitutes the state of the art. The development of roll coating methods that ensures manufacture of uniform re-

producible electrochromic film and electrolyte layers is the first step towards full roll-to-roll manufacturing of ECDs. Commercialization of ECDs is a necessary and natural step in the development of this technology, and in order to successfully achieve this, efficient, robust manufacturing processes are needed. A major challenge in this regard is identification of a printable electrolyte system that balances several opposing properties.

The experimental work that forms the basis of this chapter was done from July to October 2011 at DTU with the assistance of Henrik Friis Dam (DTU) and Aubrey L. Dyer (Georgia Tech) who also co-authored the paper "Manufacture and Demonstration of Organic Photovoltaic-Powered Electrochromic Displays Using Roll Coating Methods and Printable Electrolytes" (appendix 3.1). An important part of this work was the fabrication of an OPV/ECD demonstrator, which was done at Mekoprint A/S with the kind assistance of Jan Fynbo. The work on ITO free devices were done from October 2012 to March 2013, with the assistance of Markus Hösel (DTU) who co-authored the paper "Fast switching ITO-free electrochromic devices" (appendix 3.2).

3.2 Processing of soluble polymers

While numerous methods exist for depositing polymers onto a substrate, cost considerations have to be acknowledged when developing devices for commercial purposes.[1] Employing energy demanding deposition methods increases production costs, and while all deposition methods require energy, the ones described in the following section are considered low in energy consumption. Common to them is that a wet film of the dissolved polymer is formed upon deposition, followed by evaporation of the solvent whereupon a thin polymer film is formed.

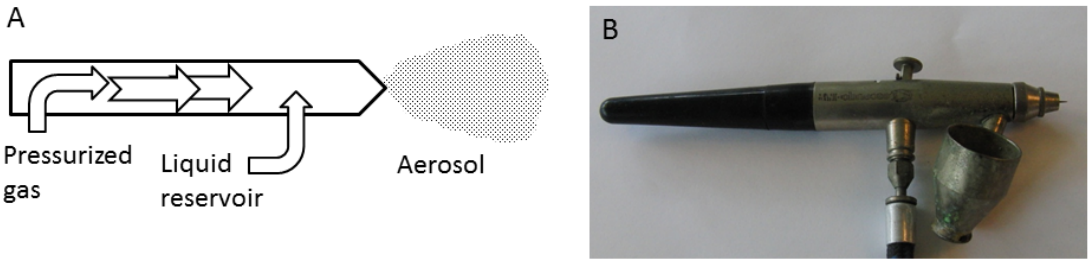

Figure 3-1: Airbrush. (A) Schematic of a simple spray gun. The polymer solution is supplied from a liquid reservoir and extruded through the nozzle as an aerosol by pressurized gas (typically N2 or Ar). (B) A picture of a simple spray gun. This type has the reservoir directly attached to the gun.

For laboratory scale trials, spin and spray coating are two established methods, which are both facile and have manageable requirements to equipment. For spray coating, only a simple airbrush and a connection to pressurized inert gas, usually nitrogen or argon is sufficient. More advanced forms of this coating method are available e.g. ultrasonic spraying,[2, 3] but the simple form works well for polymer deposition. Figure 3-1 shows a schematic (A) and a picture (B) of the airbrush used for my experiments. The polymer solution is supplied to a small nozzle where tiny aerosol droplets are formed when the pressurized gas is supplied. When vaporized, the increased area of the droplets will cause some solvent to evaporate prior to impact on the substrate. On impact, the droplets are shattered, and the remaining solvent evaporates leaving behind a thin polymer film. Manually spray coating takes some practice as it is difficult to get an even film, and it is preferable to use solvents of low vapor pressure. Using a dilute solution and continuously spraying within the same area should ensure an even film and prevent streaking. A low boiling solvent (e.g. chloroform or THF) increases the speed of evaporation, while using high boiling solvents (e.g. chloro-benzene or dichloro-benzene) increases the risk of uneven films due to streaks of solvents. Spray coating produced films with a rough surface as it consists of droplets that form clusters. A rough surface makes thickness determination difficult, but leads to an increased surface area and an open morphology that has been reported to increase the ion ingress into the polymer film.[4]

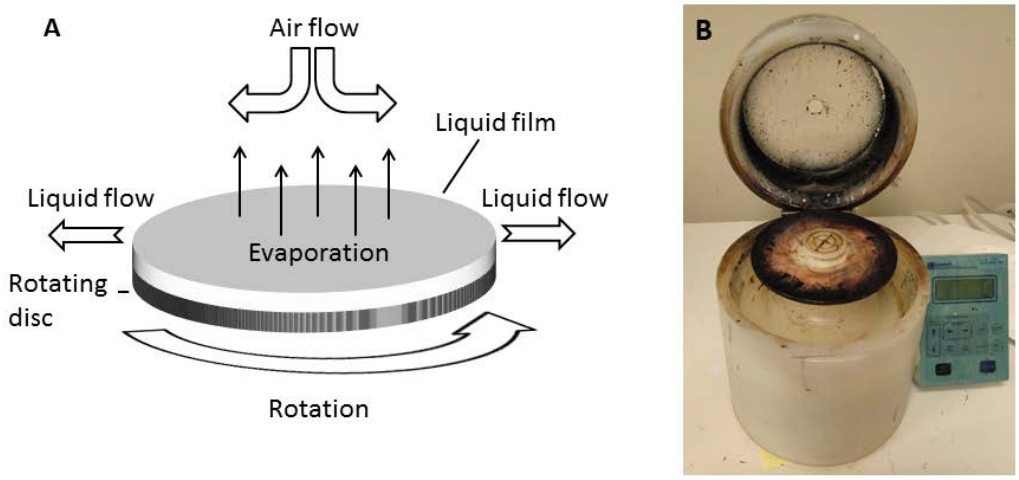

Figure 3-2: (A) Schematic of the spin coating process. The polymer solution is placed on the substrate prior to - or while spinning. By centrifugal forces the solution is forced from the center of the disc to the edges. Evaporation of the solvent produces a thin solid film. Adapted from ref. 5 with permission of The Royal Society of Chemistry. (B) Picture of a spincoater. The substrate is held in place by vacuum while spinning. The panel on the right controls the rotational velocity and enables simple programming of the spincoater.

Spin coating is another well-known technique that is fast, easy to use and requires relatively simple equipment.[5] Figure 3-2 (A) shows the spin coating process. The substrate is placed on the spincoater and held in place by a vacuum. Following this, the polymer solution is applied which can be done either while the substrate is spinning or prior to this. The solution is forced to the edges of the substrate by centrifugal forces, whereby a wet polymer film is formed. A thin *solid* film is formed by evaporation of the solvent. A further advantage of spin coating is that the results are highly reproducible, yielding films of identical thickness and morphology. These advantages make spin coating an excellent technique for small-scale laboratory experiments. The disadvantage is the large amount of material that is wasted in the process, which makes this method material inefficient and unsuitable for large-scale production. In addition, manually changing and cleaning the substrate is time consuming.

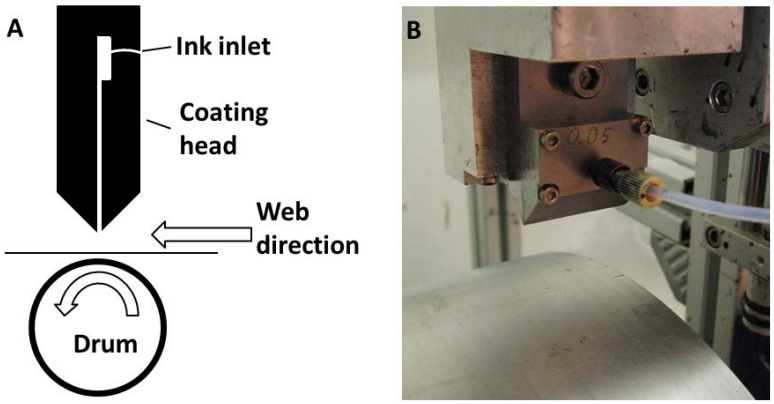

Figure 3-3: (A) Schematic of the slot-die coating technique showing the coating head above the substrate. From the inlet the solution is introduced into a small reservoir, from where it flows through a void and is dispersed onto the substrate. The substrate is carried forward by the rotating drum Adapted from ref. 1 Copyright (2009), with permission from Elsevier.(B) A picture of a slot die coating head with a tube attached to the ink inlet. Part of the rotating drum is seen at the bottom of the picture (no substrate attached).

While spin and spray coating are well suited for small-scale lab experiments, the large amount of manual work and the amount of wasted material make them unsuited for larger manufacturing tasks. Slot-die coating is ideally suited as it is a fast and robust technique that is roll-to-roll compatible. Figure 3-3 shows the slot-die coating process using a small-scale laboratory roll coater.[6] The ink is dispersed onto a substrate through a coating head by a syringe pump (not shown). The substrate is carried forward by a rotating drum. After solvent evaporation, a thin film is formed. The thickness of the film is controlled by ink concentration, rotational speed of the drum and the speed of deposition. Laboratory scale roll coaters limit the amount of ink necessary for coating, and are useful for optimizing procedures for large-scale roll-to-roll equipment

3.3 Matrix displays

3.3.1 Spray coating

As described in chapter 2, recent work on ECPs has addressed the challenges in regard to color availability and solubility. This work has resulted in a full color palette of solution processable polymers, not previously available.[7-10] However, little effort has

focused on utilizing these materials in manufacture of operational electrochromic devices. This has limited characterization to a standard laboratory setup, which commonly involves electrochemical and optical characterization of polymer films that is deposited on transparent indium-doped-tin oxide (ITO) electrode immersed in a cuvette. As most ECDs use glass substrates, very little effort has extended to use of roll coating and roll-to-roll coating methods for large areas, flexible devices or demonstrators. My work focused on bringing these polymers from the safe haven of the laboratory and into operational devices using roll coating methods (and in particular slot-die coating). This was done in order to develop commercially attractive applications such as those currently available in car mirrors or aircraft windows, as described in chapter 1. The work done on roll coated ECDs were stimulated by the success of using similar methods for manufacturing organic polymer photovoltaics. By exploring the use of flexible substrates and large area processing, efficient production methods that combine high output and reliability, at a low cost, are considered realistic.

The first step in this research was the development of addressable matrix displays for use as billboards, switchable price tags, etc. (e.g. a sort of device where one would be able to display simple letters and numbers). The ambition was to coat the individual layers onto transparent ITO/PET electrodes from opposite sides, followed by sealing the device using a UV curable binder. A key point in the roll-to-roll fabrication of a flexible ECD is development of a solid or semi-solid electrolyte system that enables sealing of the device while maintaining fast and robust switching. As described in chapter 2, a liquid electrolyte is incompatible with roll coating procedures and, among other challenges, requires meticulous sealing of the device.[11] The binder should be contained in the electrolyte layer, thus functioning both as an ion storage layer and as an adhesive. This procedure avoids epoxy or peripheral adhesives for sealing of the device, which is advantageous as, from a production point of view, the use of double-sided adhesive is challenging as it is not compatible with fast processing using batch methods. I examined two different electrolyte systems in order to explore the advantages and disadvantages of each one; one system was UV crosslinkable, and one was fully cured prior to coating. The former comprised of poly(methyl methacrylate)(PMMA; M_n 80.000

KDa) swelled in propylene carbonate (PC) as the matrix polymer and tetrabutylammonium-hexafluorophosphate ($TBAPF_6$) as the ionic component. The crosslinkable component was a commercially available UV-curable acrylate oligomer; Ebecryl 150® (2-Hydroxy-2-methyl-1-phenylpropan-1-one) in combination with Ebecryl P116® and Additol BCPK. Ebecryl P116® is a reactive amine-containing acrylate group used to increase the curing speed of UV-curable coatings. The structure of this compound is proprietary to the manufacturer and not known, but the structures of the other components in the UV curable system are depicted in Figure 3-4. Additol BCPK is a blend of Additol BP (benzophenone) and Additol CPK (1-hydroxy-cyclohexylphenyl-Ketone) and functions as a radical photoinitiator.

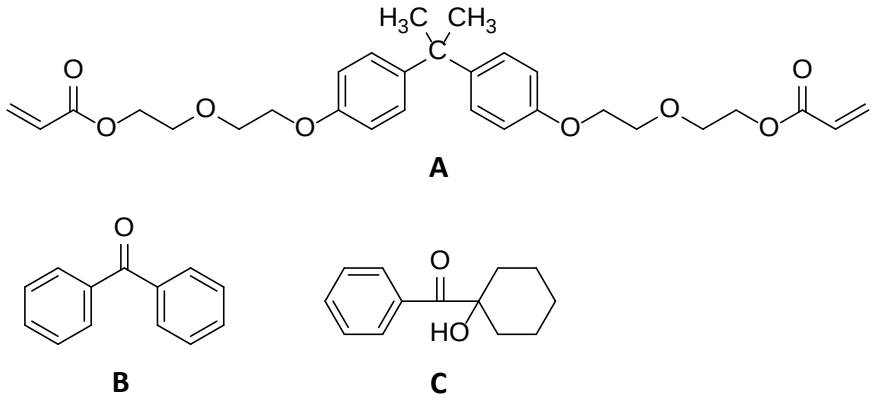

Figure 3-4: Structures of the components in the UV-curable electrolyte. (A) Ebecryl 150® (2-Hydroxy-2-methyl-1-phenylpropan-1-one). (B) Additol BP (benzophenone). (C) Additol CPK (1-hydroxy-cyclohexylphenyl-ketone)

Following coating, the electrolyte system was UV cured until a satisfactory adhesiveness was obtained. The second electrolyte system consisted of methyl methacrylate (MMA) polymerized in bulk to PMMA in the presence of an ionic liquid.[12-15]. The viscosity of this system was varied by changing the PMMA/Ionic liquid ratio, or by addition of a small amount of swelling agent (typically acetonitrile or PC). Details of the individual electrolyte systems can be found in the experimental section.

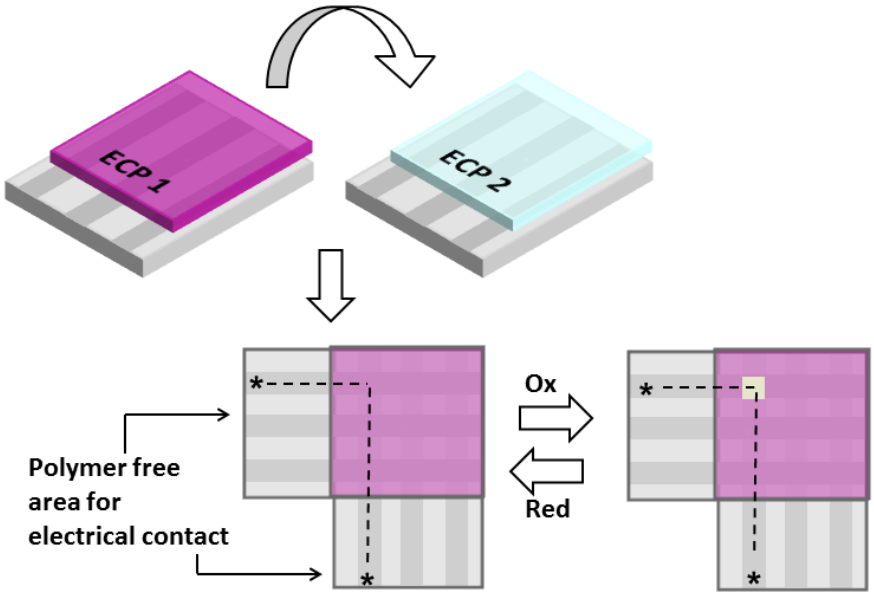

Figure 3-5: Electrochromic matrix display assembly and operation. ECP 1 is ECP-magenta while ECP 2 is MCCP. The color of ECP 2 has been modified for clarity. The two substrates are assembled perpendicular with the conducting side facing each other. The pixels are addressed by applying a potential over an ITO stripe on each foil (e.g. the asterisks-marked stripe on each substrate).

Fabrication of devices using the above procedure enables roll coating of the individual polymer layers using either spray or slot-die coating as film forming techniques, followed by printing of the electrolyte-binder layer onto the electrodes. This multilayer approach is not without its limitations, as the lamination of the devices has to be done manually. And although it is possible to use roll coating with this assembly method, the multilayer approach is a challenge for roll-to-roll manufacturing, as the coated surfaces of two electrodes are to be joined through a lamination step with an adhesive electrolyte. Figure 3-5 depicts the assembly and operation of an electrochromic matrix display. Two pieces of flexible foil containing stripes of ITO are coated with ECP 1 and 2, respectively. Following this, an electrolyte layer (not shown for clarity) is coated on both polymer films. The foils are assembled with the polymer films (and electrolyte layer) facing each other and with the ITO stripes on one foil perpendicular to those on the other foil. This creates a pixelated device as shown in the bottom of the figure. It is

important that the polymer films on both electrodes are coated with electrolyte solution, as coating on only one side results in uneven and slower switching. I did not explore the reason for this, but it may stem from a reduced contact at the interface between the electrolyte layer and the polymer film. If this is so, then charge balancing of the polaron states is limited, and this has been shown to compromise redox switching.[16] Following assembly, an area of the foil is made available for electrical contact by removing both electrolyte and polymer film using chloroform or toluene. The individual pixels can be addressed by applying a suitable potential across the device as marked by the asterisks in Figure 3-5. By doing so, a redox reaction occurs at the intersection of the two ITO stripes. When oxidizing the primary ECP (in these trials ECP magenta) the effect is a bleaching of the pixel as shown in bottom right of the figure. Reducing/neutralizing reverses the redox process and color is restored.

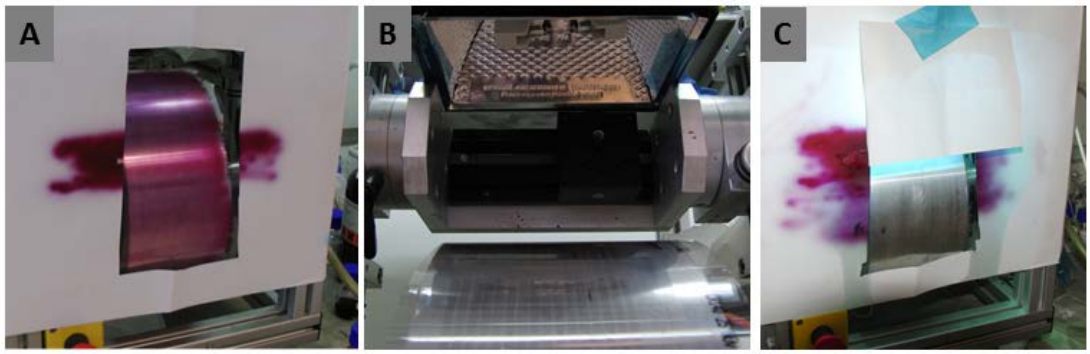

Figure 3-6: Spray coating and UV curing using a small scale roll coater. (A) Spray coating of ECP-magenta. (B) Mounting of UV the lamp above the substrate. (C) Curing of the electrolyte layer, while the drum is rotating. The lamp is screened for protection. The polymer film beneath the electrolyte layer is MCCP, which explains the colorless substrate.

The initial experiments involved spray coating PET substrates, having 0.4mm ITO stripes etched into the foil; while they were rotated on the small-scale roll coater (both ECPs and electrolyte/binder solutions were spray coated).[6] In Figure 3-6 (A) a coated substrate using a standard airbrush is shown. The substrate was coated by manually moving the airbrush back and forth in a horizontal direction as seen from residue polymer on the protection screen. Figure 3-6 (B) and (C) show the mounting of a UV lamp and curing of the electrolyte layer, respectively.

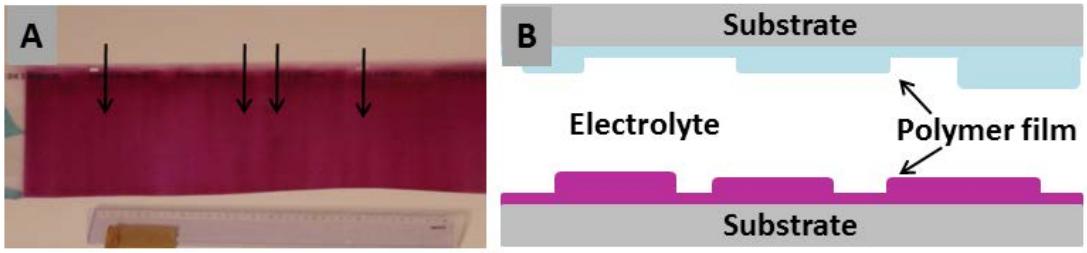

Figure 3-7: Uneven layers of polymer **film (ECP-magenta) using spray coated flexible substrate. (A) A section of the spray coated PET foil. The arrows indicate areas of increased film thickness. (B) Schematic showing a cross section of an ECD comprising two layers of spray coated substrate with an uneven ECP film thickness.**

As the spray coating was done manually, getting an even layer of polymer film on the substrate proved to be difficult. This resulted in areas of polymer film that based on increased absorption were found to be thicker than others, as shown in **Figure 3-7** (A). **Figure 3-7** (B) depicts a cross section of an ECD having uneven polymer films.

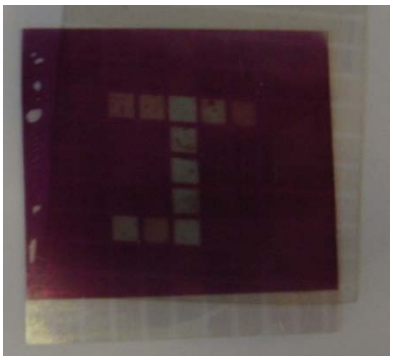

Figure 3-8: Spray coated matrix ECD display. The letter "J" was written by addressing the individual pixels.

After coating of the polymers ECP-magenta and MCCP, and curing of the electrolyte, the foils were cut and laminated. The resulting pixilated ECDs had (for the majority of the devices), individual addressable pixels as shown in Figure 3-8. Some areas of the device were observed to switch faster than others, and in general, the pixels (0.4 x 0.4 mm^2) switched between the two redox states in 10-20 seconds. The reason for the variation in response times is most likely due to the unevenness of the polymer films,

since the response time is increased by thicker increasing the film thickness, and unevenness in the polymer film leads to an inhomogeneous electrical field in the devices.

3.3.2 Slot-die coating

Following the spray coating experiments, slot-die coating was performed on ITO/PET substrates using the small-scale roll coater (see experimental section for more detail). Figure 3-9 show the small-scale roll coater with a PET foil, having 13 mm wide ITO stripes, attached to the drum. A 50 mm coating head is mounted, whereby three stripes were coated at a time. A tube connects the coating head to the syringe pump, which supplies the polymer solution (pump not shown).

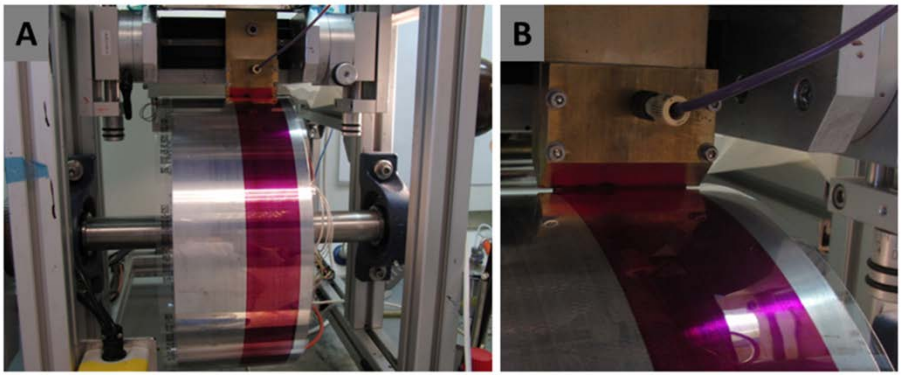

Figure 3-9: Slot-die coating of ECP-magenta on PET foil containing 13mm ITO stripes. (A) The small-scale roll coater including drum and rack (B) Enlargement showing a zoom in on the coating head, with the tube connected to the syringe pump (pump not shown).

Four slot-die coated devices were tested using spectroelectrochemistry at -3 V and +3V (tests done by Aubrey Dyer at the University of Florida, September 2011). The individual pixels were addressed as shown in Figure 3-10 and switched until no further optical response was recorded. The transmittance values for the reduced and oxidized states for all four devices are shown in Table 3-1. The table shows large variations for pixels within individual devices and also between each device. Looking at all four devices, the lowest and highest transmittance values for the reduced state is 5.4% (device 1, pixel F) and 28.6% (device 2, pixel G), respectively. These pixels also show the lowest (14.7% for 1-F) and highest (58.3% for 2-G) transmittance values in the oxidized state. As the average transmittance in both redox states is generally lower in device 1 than in the

other devices, and higher in device 2, this could indicate a variation in the film thickness of the primary ECP as discussed for spray coating in relation to **Figure 3-7**. The table also shows that pixel A-3, D-3 and G-3 were not capable of switching, while A-2 only showed very limited switching. The most plausible reason for this is that the two ITO stripes constituting the pixel have short-circuited. When short-circuited, current flows through the pixel without an electrochromic response. The absence of an electrochromic response in the polymer film is due to increased resistance in the film compared to the ITO substrate.

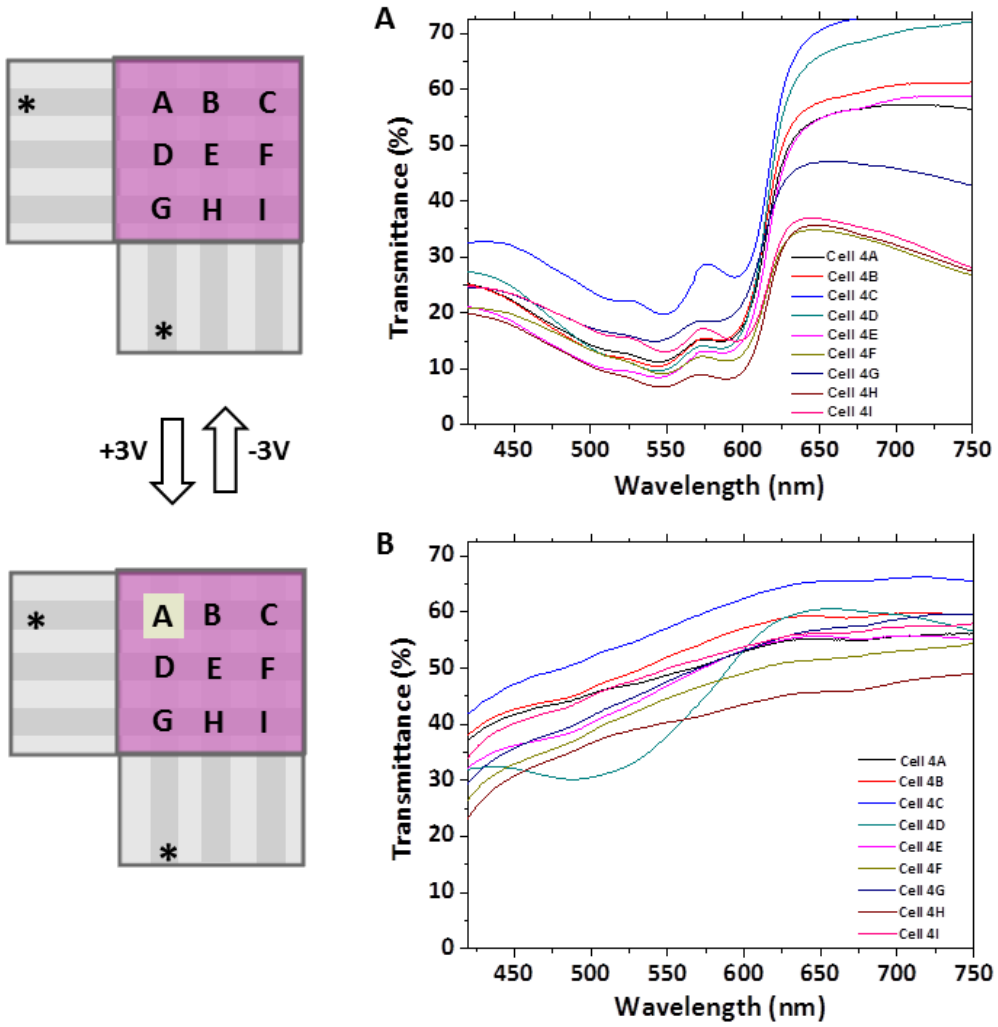

Figure 3-10: Spectroelectrochemistry of a 3x3 electrochromic matrix display (device #4). (A) Transmittance in the reduced state (-3V) for the pixels in device 4. (B) Transmittance in the oxidized state (+3V) for the pixels in device 4. The schematic to the left shows the relationship between the pixels and the legends in (A) and (B). The pixels were switched separately to obtain the spectra; here exemplified by addressing pixel A, which corresponds to the black line in graph (A) and (B).

In general, device 4 shows the most consistent switching with ΔT values between 30% and 40%, however variations in both redox states of around 10% between the individual pixels are also found for this device. The variations in the transmittance values could also arise from an inhomogeneously cured electrolyte layer as discussed in the following section.

Table 3-1: Transmittance for electrochromic matrix displays (3x3 pixels). The pixels were switched between a reduced colored state at -3V and an oxidized bleached state at +3V. N/A refers to un-switchable pixels.

	Device 1		Device 2		Device 3		Device 4	
Pixel	**%T (red)**	**%T (ox)**	**%T (red)**	**%T (ox)**	**%T (red)**	**%T (ox)**	**%T (red)**	**%T (ox)**
A	14.7	24.0	15.1	15.3	N/A	N/A	11.6	48.8
B	8.76	25.4	22.7	34.1	7.90	39.6	10.9	52.0
C	8.53	24.7	20.6	50.3	12.9	44.3	19.8	57.0
D	9.50	19.8	21.5	42.4	N/A	N/A	10.1	38.0
E	6.87	33.2	19.7	33.2	10.3	27.5	8.73	47.0
F	5.43	14.7	20.5	49.3	9.55	48.5	9.31	44.7
G	10.1	25.0	28.6	58.3	N/A	N/A	15.5	47.8
H	10.1	24.0	18.3	32.5	12.3	44.5	6.93	40.3
I	7.83	27.0	18.3	52.0	12.5	42.9	13.1	50.0

3.3.3 Electrolyte considerations

I experienced several challenges using the Ebecryl® based electrolyte/binder system. Adjusting the solubility by varying the PC/PMMA ratio to suit the deposition method was a relatively easy task, but obtaining an adhesive surface that would enable satisfactory lamination of the ECDs proved to be challenging. In order to explore this, I irradiated electrolyte coated PET substrates, whereby I found that approximately 1700 mJ/cm^2 of UV light dosage made the surface adhesive,and allowed sealing of the device upon lamination. In general, it was difficult to get reproducible results using this binder system. The first problem was inhomogeneous curing that resulted in areas of the electrolyte film being more cured than others. This reduced the adhesiveness in those areas and made lamination of the devices problematic as well as increasing the response time of the devices. From a manufacturing point of view, inhomogeneous curing is problematic as every foil has to be inspected during the curing process to

evaluate the degree of curing. The inhomogeneity also consisted of the surface tending to cure faster than the rest of the electrolyte film. A second obstacle in using this electrolyte system was that dewetting occurred when it was applied to the ECP-magenta film. I tried to solve both problems by varying the various components in the electrolyte system but these attempts proved largely unsuccessful. Finally, I discovered continued curing of the binder after lamination of the device. This discovery was made during outdoor operation of the OPV/ECD demonstrator (see section 3.5), and the continuing curing process made the electrolyte layer solid and brittle. As a consequence hereof, the response time was markedly increased, and ultimately the devices ceased to switch. The reduced switchability could also be attributed to the relatively large potentials (-/+3 V), whereby overoxidation or irreversible nucleophilic attack can occur. Delamination was also observed owing to the reduced adhesiveness of the binder.
The electrochromic response of a pixel (or ITO stripe between pixels) that is not addressed, known as crosstalk, was a general problem observed for all the pixelated devices. Crosstalk occurs since the electrical field extends beyond the cross section of the two perpendicular ITO stripes, and it was to some extent possible to minimize the effect be increasing the electrolyte viscosity, but at the expense of the response time, which became unsatisfactorily high. The crosstalk challenge is better solved by other approaches such as patterning (see chapter 4) or by a different device construction (see section 2.7.1).

The overall conclusion to the Ebecryl® based electrolyte/binder system was that it did not meet the requirements for en ECD electrolyte, and another electrolyte/binder solution was investigated that consisted of a PMMA matrix swollen with an ionic liquid (IL), described in the following section.

3.4 Fully covered ECDs

3.4.1 Spin coating

As continuing trials did not lead to satisfactory matrix displays, due to crosstalk and electrolyte curing following lamination, I decided to backtrack the manufacturing process and use spin coating of continuous (non-patterned) ITO-coated PET substrates.

Even though spin coating is not well suited for high through-put production, due to the amount of manual unit operations required, it is an effective laboratory technique that was frequently used to test new ideas. Using non patterned substrates for matrix displays requires a more complex multicomponent setup, since each pixel has to be individually connected to the power supply, but in addition to multicomponent matrix, full coverage devices can be used for light-management elements. A PMMA/IL electrolyte system was employed in these spin-coated devices and found to function satisfactorily, both as ion storage layer and as an adhesive**.** I made several ECDs by this procedure with switchable areas from 10 cm^2 to 56 cm^2. However, on prolonged storage of the devices partial delamination and leakage (and consequently reduced switchability) was observed. This was later found to originate from dewetting of the electrolyte layer, and addressed as described in section 3.6.2. The fully covered ECDs were found to switch at -2V to +2V, being substantially lower than the potentials required for switching of the matrix displays described in section 3.3. A reduction of the potential requirements is encouraging as irreversible side reactions are less likely to occur at the electrodes. The lower voltage requirements are ascribed to the IL based electrolyte, as the sheet resistance of the fully covered ITO sheets were equal to the ITO striped substrates.

3.4.2 Optical contrast and response time

The transmittance at 550nm (Abs_{max}) in these ECDs was measured to be 54.6% and 9.2%, for the oxidized and reduced state respectively, as shown in Figure 3-11. Subtracting these values amount to an optical contrast of 44% obtained without a reference sample i.e. the optical contrast as seen by the eye. If a bleached sample is taken as the reference, the optical contrast is 58%. This calculated value ignores absorption contributions from the PET substrates, ITO layer, and the electrolyte solution, and is thus solely a measure of the ECPs absorption at 550 nm at the applied potentials; even though it is intrinsically influenced by those same components. For comparison, an optical contrast of 80% (at Abs_{max}) has been reported for spray coated ECP-magenta films in a 0.1M PC/$TBAPF_6$ solution, while operational ECDs encompassing ECP-magenta and

MCCP spray coated onto ITO-sputtered glass slides were reported to have an optical contrast of 61% when measured against a blank device.

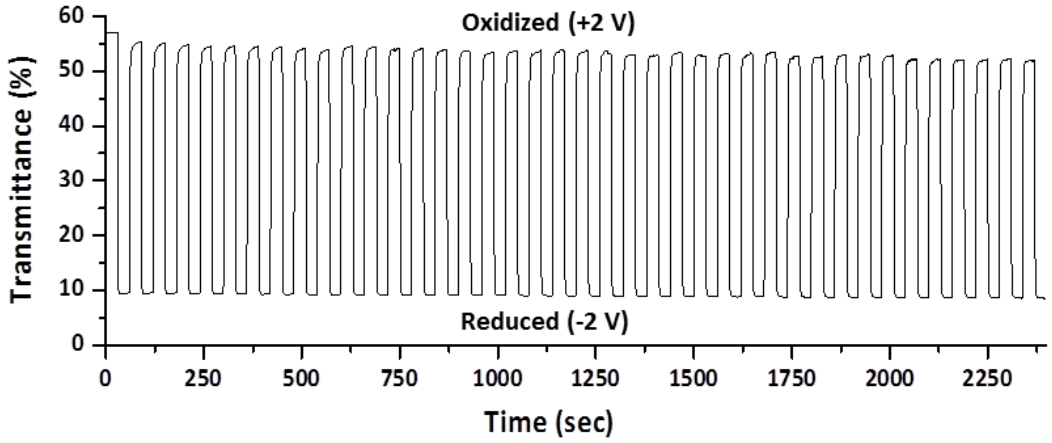

Figure 3-11: Transmittance for a 10 cm^2 ECD comprising ECP-magenta as the primary electrochromic polymer and MCCP as the secondary charge balancing electrochromic polymer. The electrolyte layer consisted of a PMMA/IL solution. The device was switched at -2 V and +2 V for 30 seconds at each potential.

[17, 18] No record was made of the transmittance observed by the eye, but the values are most likely slightly higher than the 44% measured for my devices due to the increased transmittance of glass compared to PET foils (see figure 2.5).By disregarding the other ECD components, the similar ΔT values of 58% for flexible ECDs and 61% for rigid glass based ECDs, shows that the spin coated flexible ECDs are comparable in optical contrast to the spray coated ECDs. The slot-die coated ECDs described in section 3.3.2 likewise show comparable transmittance values (e.g. ΔT= 41% for pixel E and G in in device 4, see Table 3-1). These devices were not measured against a blank reference, but since they comprise the same component it is fair to assume that by not taking those into account, the devices will show an optical contrast of approximately 55%. Comparing the optical contrast (disregarding contributions from device components) of spray, spin and slot-die coated ECDs to that of the ECP film switched in solution previously mentioned (ΔT= 80%), emphasizes the challenge in reproducing ECP properties in ECDs as discussed in chapter 2, if possible at all. Naturally, it is not possible to re-

move the absorbance due to substrate and electrolyte, but optimization of parameters such as film thickness could increase the optical contrast.[19-21]

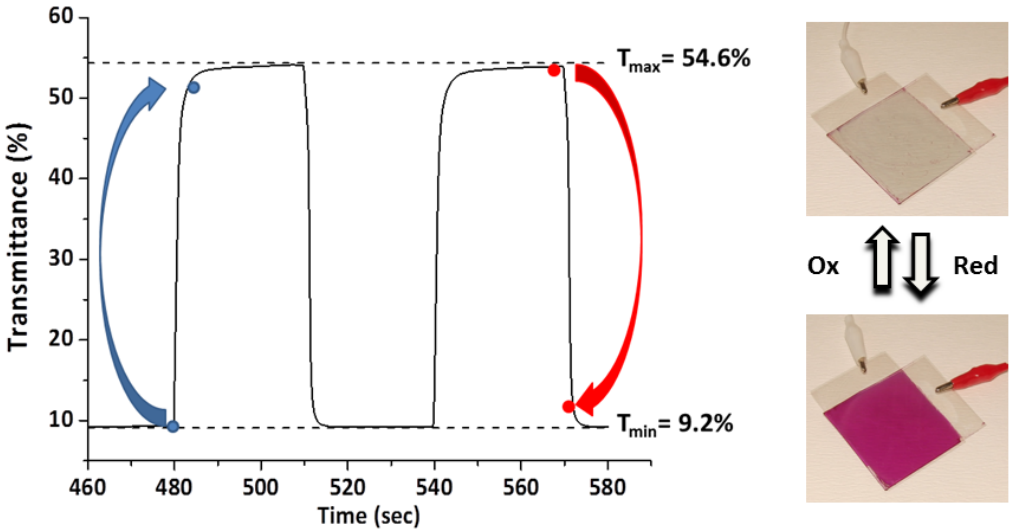

Figure 3-12: Transmittance (460-580 second range) of the ECD described in Figure 3-11. The blue arrow constitutes a 95% switch when oxidizing the device (from T_{min} to 52.3%). The red arrow constitutes a 95% switch when reducing the device (from T_{max} to 11.4%). The device was switched at -2 V (reduction) and +2 V (oxidation) for 30 seconds at each potential.

Since a common protocol on how to report response time has not been defined, I find it relevant to report a series of response times covering different levels of optical contrast. The fastest response times are linked to the smallest changes in optical contrast, but since the majority of the redox reactions (and hence color change) occur in the beginning of a switch, 90% of a full switch might occur in two seconds while the remaining 10% of the switch takes 10 seconds to complete. Secondly, the sensitivity of the human eye makes it unable to distinguish single digit changes in transmittance.[22] Figure 3-12 shows the transmittance in the 460-580 seconds range for the device described in relation to Figure 3-11. The blue and red arrow (and dots) indicating the transmittance for a 95% of a full switch when oxidizing or reducing respectively, i.e. 95% of the maximum achievable optical contrast). The figure shows that the time necessary to achieve a 100% switch is large compared to a 95% switch. This is shown more clearly in Table 3-2, where the

Table 3-2: Response time for a 10 cm^2 ECD switched between -2 V (bleach to colour) and +2 V (colour to bleach).

		Colour to bleach		Bleach to color	
% of full switch	**ΔT (%)**	**% T**	**t (sec)**	**%T**	**t (sec)**
100%	45.4	54.6	10	9.2	9.8
98%	44.5	53.7	6.2	10.1	6.8
95%	43.1	52.3	3.8	11.4	4.8
92%	41.2	51.0	2.7	12.8	4.2
90%	40.9	50.1	2.3	13.7	3.9

response time is given for a range of ΔT values. The table shows a relatively large difference in time required for a full switch compared to various degrees of switching and the corresponding small optical contrast between them Compared to the aforementioned devices employing similar polymers, these response times are significantly reduced, possibly because slightly higher potentials were applied or due to differences in electrolyte composition.[18]

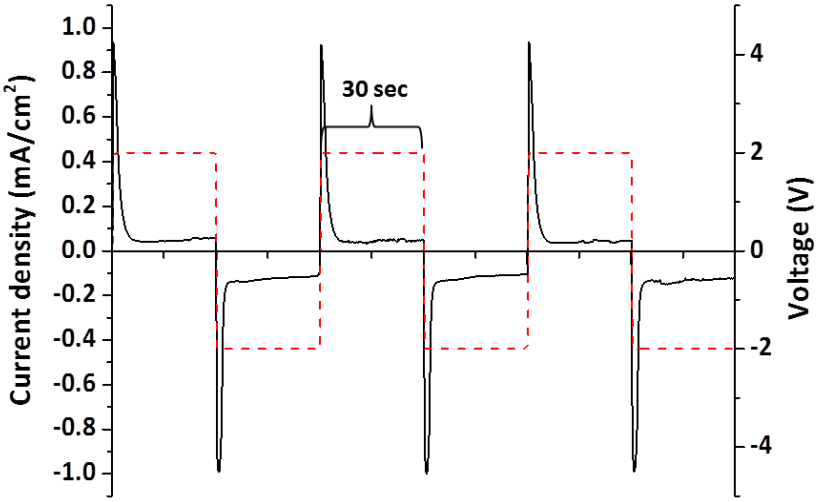

Figure 3-13: Current-voltage graph. The solid black line (left axis) displays the current-density for a 10 cm^2 device switched potentiostatically between -2 V and +2 V. The voltage is shown by the dashed red line (right axis). The potential is held for 30 seconds at each potential as shown by the bracket.

Figure 3-13 shows the current density in the device as a function of the applied potential when switched potentiostatically between -2 V and +2 V. The current spike of maximum 1 mA cm^{-2} denotes that a substantial portion of the redox reaction occurs in the beginning of each voltage switch, although electric double layer charging account for some of this.[23] Following the initial spike, the current-density rapidly decays into a background current of approximately 0.05 mA/cm^2, as a result of the redox reactions in the polymer film having gone to completion.

3.4.3 Coloration efficiency

As described in chapter 2 the coloration efficiency, η, describes the number of color centers formed as a function of the charge used to evoke this change. The coloration efficiency for ECP-magenta has been reported to be around 1200 C^{-1} cm^{-2} in standard cuvette tests employing a 0.1 M electrolyte solution.[17] This value is the maximum limit for ECP-magenta, and the equivalent device coloration efficiency for ECDs, η_d, is expected to be lower as the optical contrast is lower in the devices and more charge is needed for switching. The latter is due to an increased viscosity and a magnitude lower concentration of charge carriers in the device electrolyte. Table 3-3 shows the device

coloration efficiency, η_d, along with the charge, Q, passed for a 10 cm^2 ECD where the potentials are held for various switch lengths.

Table 3-3: Device coloration efficiency values for a 10 cm^2 ECD, where the potential is held for various switch length. The negative values obtained when oxidizing the device is due to the definition of coloration efficiency.

	Oxidizing (+2 V)			Reducing (-2 V)		
Switch length (sec)	**Q (mC)**	**Log (T_1/T_2)**	**η_d $C^{-1}cm^{-2}$**	**Q (mC)**	**Log (T_1/T_2)**	**η_d $C^{-1}cm^{-2}$**
1	0.81	-0.53	-654	0.94	0.06	63
2	0.94	-0.70	-744	1.59	0.6	377
5	1.68	-0.75	-446	2.1	0.76	361
10	1.98	-0.76	-384	2.73	0.76	278
30	2.62	-0.76	-290	4.97	0.76	153

The table shows that η_d drops as the switch length is increased, which is to be expected as most of the color change occurs in the beginning of a switch, where a relatively small amount of charge has a pronounced effect on the transmittance. As the optical contrast saturates (i.e. completion of the redox reactions), charge continues to pass through the device as background current, and possibly for electrochemical side reactions. Therefore, η_d values beyond the point of saturation (i.e. a 100% switch) are meaningless as these are not related to the generation of new color centers. Contrary to this this, η_d values for incomplete switches are relevant since they describe the color changing ability of the *device* at various stages in the redox process between a full switch and a near full switch. The point of saturation for the spin coated ECDs described in this section is approximately 10 seconds depending on the direction of the switch as seen from Table 3-2. The difference in η_d between oxidizing and reducing the device is difficult to explain, due to the complexity of an ECD. The difference is most pronounced at the beginning of a voltage pulse, where more charge is required to color than to bleach the device. A possible reason could be the difference in ion in-

gress and expulsion from the two polymer films i.e. or it could stem from differences in conductivity at the various levels of doping.

3.4.4 Memory effect

The memory effect is a property that distinguishes ECPs/ECDs from other display and light management applications in that it allows the ECD to remain in a redox state without continuous application of a bias. As an example of the contrary, commercially available liquid crystal based "shading elements" require a continuous bias of 110 volts to stay bleached, leading to high power requirements for such appliances.[24, 25] The stable state of the ECP-magenta/MCCP devices is the colored state (the reduced state of ECP-magenta), and as such the transmittance as a function of time (at open circuit) is a measure of the memory effect. For these devices, approximately 4 hours passed before they had reverted completely to the colored state (see appendix 3.1). If the bleached state is desired for extended periods of time, it needs to be refreshed every 30 minutes, which requires (18.7 mC x 2 V)/ 10 s = 3.7 mW; assuming that a 10 second voltage pulse is used to refresh the bleached states. This low power requirement is well matched by OPVs and lead to the development of an OPV/ECD demonstrator described in section 3.5.

3.4.5 Preliminary ECD stability

The photochemical stability is an important aspect of ECPs and ECDs, which is why a separate chapter is devoted to this subject. The small section on the subject in this chapter is included as it is relevant in relation to the development of the OPV/ECD demonstrator intended for outdoor use. In an initial attempt to assess the stability of the ECDs, the shelf life and photochemical stability were investigated (experiments done by Frederik C. Krebs, November 2011). The shelf life test proved to be encouraging as no decrease in absorbance or performance were observed after keeping the devices in the dark for 4 months.

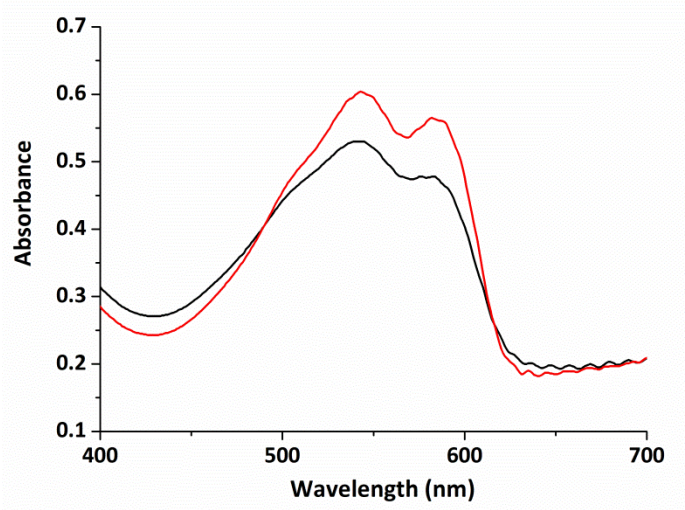

Figure 3-14: Photochemical stability of ECDs. The absorbance of a pristine ECD (red line), and after exposure to 100 hours of illumination (AM 1.5G, 1000 Wm^{-2}) (black line). The absorbance was measured for the reduced state of the ECD.

The devices were illuminated using a solar simulator (AM1.5G, 1000 W m^2, 45°C) continuously for 100 hours, which resulted in a 20% loss of absorbance (shown in Figure 3-14) which is fairly limited considering that the devices were not protected by any additional barrier foils, other than the substrate PET foil. The photobleaching was most pronounced around the edges of the devices and in areas where delamination had occurred, thereby allowing ingress of water and oxygen. A discussion on barrier foils and encapsulation is found in chapter 5. The effect on operational stability was also addressed and following 100 hours of exposure the transmittance in the bleached state was reduced from 71% to 63% (i.e. the device was unable to achieve the same level of transparency) while the transmission in colored state was increased from 28% to 32%. In short, the ability of the ECDs to both bleach and color was reduced as a consequence of solar exposure, whereby the optical contrast was reduced by 30%. These results lead to further investigation of the photochemical stability of ECPs and ECDs, which is the subject of chapter 5.

3.5 OPV powered electrochromic demonstrator

I ascribe the absence of focused (polymer) ECD development to be one of the primary reasons for the lack of commercially available polymer based ECDs. While most research has been directed towards achieving large optical contrasts and developing polymers; fabrication of stable ECDs has not experienced the same degree of interest. While achievements in polymer development are intrinsically important; the field of electrochromic polymers is now in a situation where these state of the art polymers, that show excellent properties in a laboratory setting, are not tested in devices outside the lab. As this dissertation points out, the key issues to address in that context are efficient processing, electrolyte composition and stability, but the primary objective in advancing polymeric ECDs is simply the fabrication of a working ECD; a gadget or device that “does something” using electrochromic polymers. Realistic examples of this could be an electrochromic business card, a simple billboard or a shading device, as long as it is something that shows how electrochromic polymers can be used. To target this objective an OPV powered EC display was developed. Using OPVs to power an ECD was a natural choice as our group is knowledgeable on many areas within OPV research and manufacture. But OPVs were also chosen as the power density is well matched to the ECD power requirements and bistability. Printed module devices, integrating both OPVs and ECD, where fabricated wherein one OPV powers a switch to the colored state and a second OPV powers a switch to the bleached state. In situations where constant lighting is not available, modules were constructed and demonstrated where a lithium battery stores the charge harvested by the OPV and further powers the ECD.

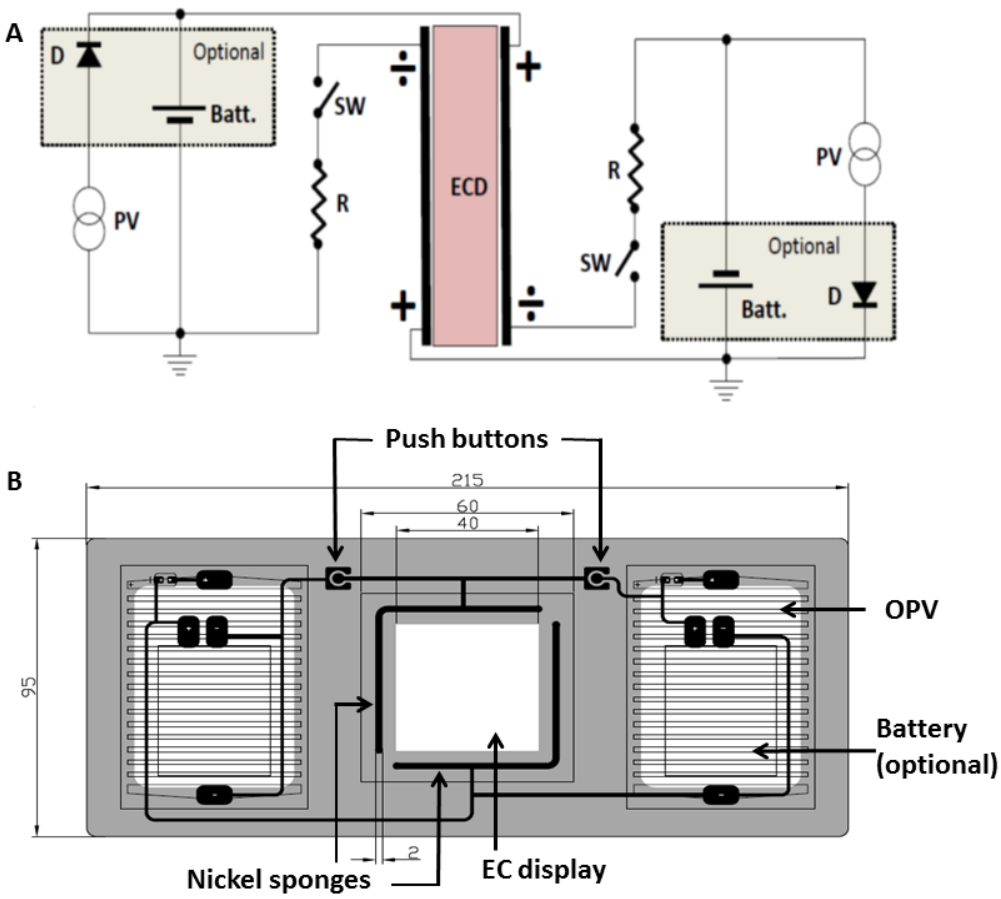

Figure 3-15: The electrical diagram (A) for the demonstrator. OPVs power two independent circuits that switch the ECD between the colored and transparent state. The switches are push buttons that are pressed alternately. The optional circuit element is a lithium battery that was included in some demonstrators. (B) A schematic illustrating the circuit diagrams for the demonstrator. Nickel sponges were used for electrical contact between the OPV and ECD. The dimensions are in mm. Reproduced from ref. 26 by permission of John Wiley & Sons Ltd.

The electrical and circuit diagrams for the demonstrator are depicted in Figure 3-15 and show a printed module device, integrating both OPVs and ECD. One OPV powers a switch to the colored state and a second OPV powers a switch to the bleached state. In situations where constant lighting is not available, modules were constructed where a lithium battery (3.7 V to 4.2 V depending on the state of charging) stores the charge harvested by the OPV and further powers the ECD. Electrical connection between the ECD and circuitry is ensured via nickel sponges. The dimension of the active ECD was 40 X 40 mm^2.

The demonstrator was prepared using printed electronic circuitry and assembly that was previously developed for an OPV/lithium-polymer battery powered flashlight. [27, 28] The OPV modules were prepared according to ProcessOne and typically presented a V_{OC} in the range of 7.5-8.5 V and an I_{SC} in the range of 10-15mA, and a fill factor of 30-35% under illumination with 1 sun (AM 1.5G; 1000 W m^{-2}).[29]

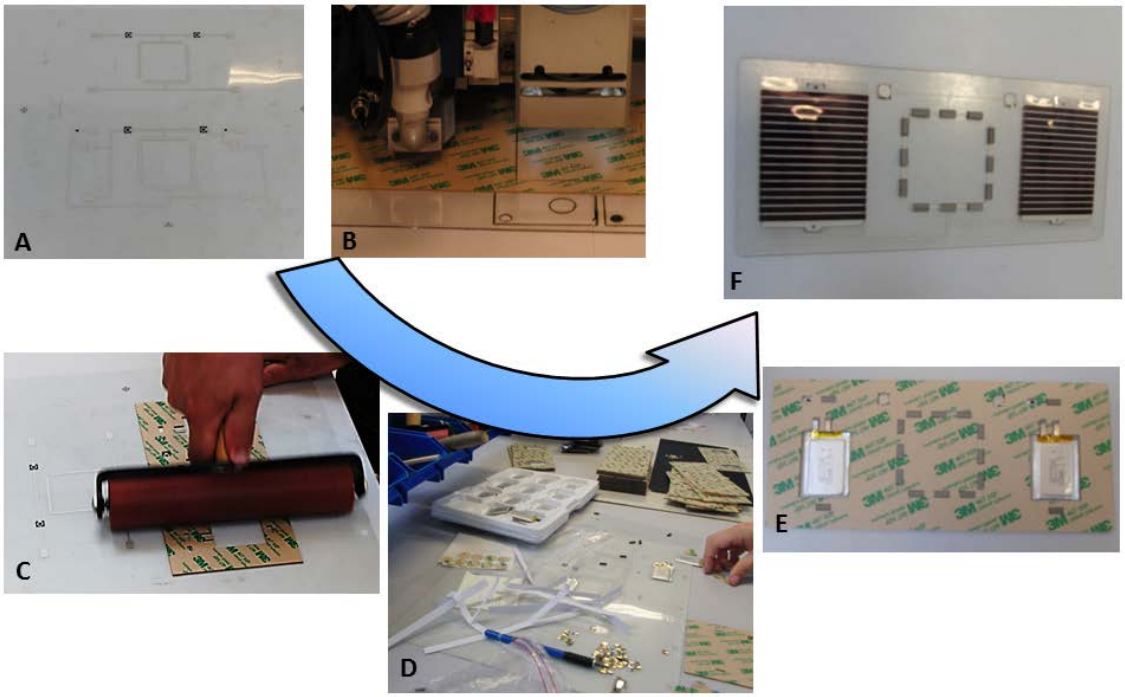

Figure 3-16: Fabrication of the OPV/ECD demonstrator. (A) Electronic circuitry consisting of silver lines printed onto a polyester foil. (B) Laser cutting of the polyester plate used for the device. (C) Lamination of electronic circuitry onto the polyester plate. (D) Manual assembly of device components – nickel sponges, push buttons and OPV modules. (E) Polyester plate with lithium batteries and nickel sponges. (F) Demonstrator with OPV modules, nickel sponges and push buttons (without ECD module).

The demonstrator was fabricated by the process shown in Figure 3-16 (with the assistance of Jan Fynbo at Mekoprint A/S, July 2011). Electronic circuitry was printed onto a polyester foil (Figure 3-16 (A)), following this a 2.5 mm thick polyester plate was prepared on each side with pressure sensitive adhesive. The polyester sheets carrying the adhesive were laser cut (Figure 3-16 (B)) into the desired shape of the

demonstrator by cutting holes for the batteries, discrete component (1N4148 blocking diode), switches and the nickel sponges. The adhesive liner was then removed at one side, and the printed circuit was applied to the adhesive (Figure 3-16 (C)). Nickel sponges and push buttons (and in some instances lithium-polymer batteries modules) were manually mounted (Figure 3-16 (D) and (E)). Finally the OPV modules were applied (Figure 3-16 (F)), and the electrochromic device mounted followed by a final lamination to complete the device (Figure 3-17). The demonstrator platform was used for both matrix displays and fully ITO covered displays. The former constituted a simple prototype where it was impossible to address the pixels individually, as each push button was connected to all the nickel sponges on one side by a bus bar made from copper tape (see Figure 3-15 (B) and Figure 3-17 (A) and (B)). It was nevertheless instructive to experience the challenges in ensuring good electrical connections to all the etched ITO stripes.

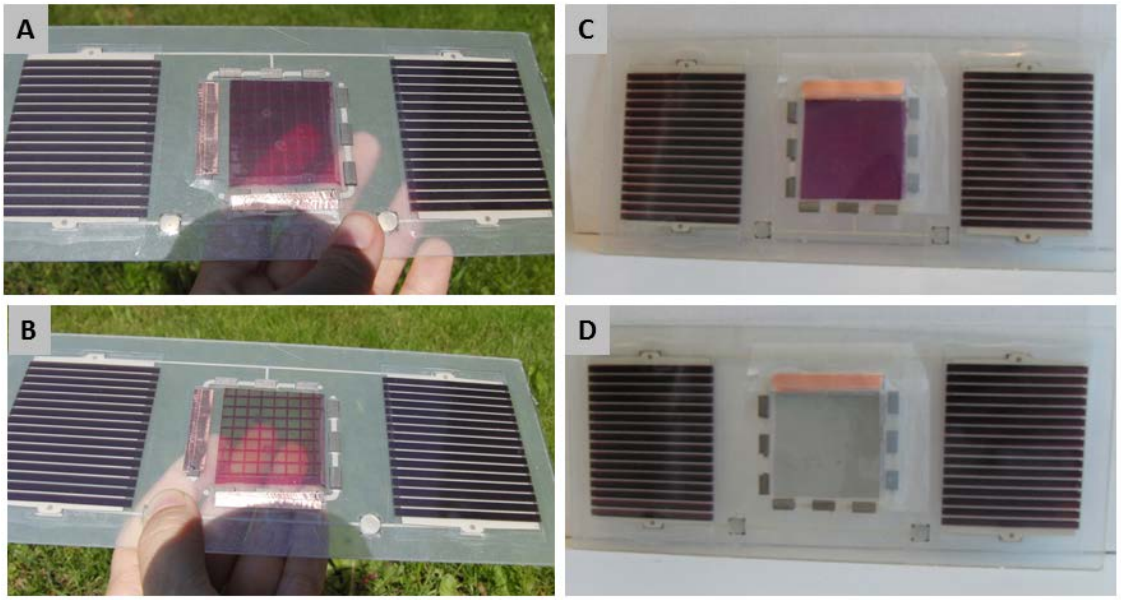

Figure 3-17: The OPV/ECD demonstrator. The devices are solely driven by OPVs and operated by push buttons, shown between the OPV modules and the EC display. Copper tape was used on one side to ensure connection due to the architecture of the ECD (see Figure 3-5). Figure (A) and (B) show the reduced and oxidized state, respectively for a matrix display, while (C) and (D) show the equivalent for a display employing full ITO covered ECD module. Reproduced from ref. 26 by permission of John Wiley & Sons Ltd.

The demonstrators were switched outside (6th July 2011, Støvring, Denmark) on a sunny day, and were found to switch with a response time in the same range as when operated by a power supply. For practical reasons it was not possible to determine the response time or optical contrast in more detail, as getting a 200 cm^2 demonstrator into a spectrophotometer and measuring absorbance while illuminating with a solar simulator is quite a challenge.

As mentioned in section 3.3.3 the Ebecryl based electrolyte was found to become hard and brittle on continuous operation of the device. It seems unlikely that this should be due to leakage or evaporation of the plasticizer (PC) as the vapor pressure of PC is high, and the devices were thoroughly encapsulated. I attribute the hardening of the electrolyte matrix to the continuing polymerization process, during illumination; an

quite unfortunate effect in a device powered by solar cells. I did not observe this effect when employing the ionic liquid based electrolyte.

3.6 ITO free devices

In order for new emerging technologies to be competitive they must show increased performance on parameters such as cost, efficiency, production speed, environmental impact etc. compared to existing solutions. Based on the experimental work that I have done on ECD development and the knowledge I have acquired during the preparation of this dissertation, I believe that electrochromic polymers have a potential as such an emerging technology since ECPs have several favorable properties. They have low power consumption, show a multitude of vibrant colors and can be efficiently processed onto flexible substrates. As there are still no commercial available products comprising ECPs, the question is whether if a focus on developing one of these specifically could advance this process. The redox processes responsible for the color change is very fast, and most ECPs show sub-second response times. However, the current development level of electrolyte gels limits the response times to several seconds, as the devices in this dissertation also show. This excludes ECD from several applications, especially mobile ones and raises the question if polymer based ECD should target applications where response time is not crucial, and instead focus on other parameters. Large area signs are one such application, where polymer based ECDs shows promise as the low power consumption is particular advantageous. Manufacturing cost is another parameter where ECP is competitive as the roll coating processes are devoid of high temperature, vacuum or other energy demanding steps. However, a main obstacle to low manufacturing costs is the use of ITO as the transparent electrode material. ITO is commonly used as electrode material in organic electronics, but due to the scarcity of indium substituting this material for a less expensive one would significantly reduce production costs of ECDs.[30-32] Another reason for the high cost of ITO substrates is the vast amount of energy consumed in the sputtering process when producing ITO covered substrates. By avoiding such an energy consuming process, the cost of ECDs but also the environmental impact would be significantly reduced.

3.6.1 Blooming effect in grid structures

The operational challenges associated with using ITO substrates are discussed in chapter 2, but nevertheless ITO is still used in ECDs even though reports on ITO free ECDs have been published.[33-35] The reason for the continual use of ITO shall probably be found in the optical limitations that these reports show, but also in the fact that production cost is not an issue as most published ECD is of rather limited size and not intended for production. A preliminary report on using thin metal grids as transparent electrode material for large area ECDs, showed promise in replacing ITO although issues of inhomogeneous switching and slow response times were unaddressed.[36]

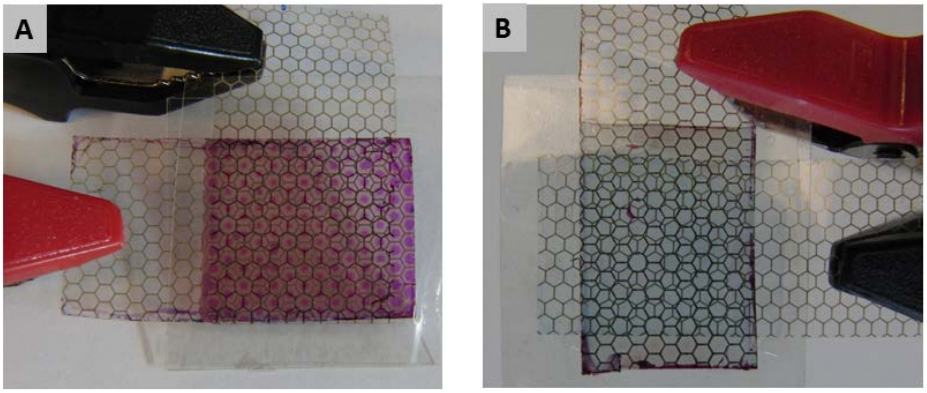

Figure 3-18: Inhomogeneous switching (blooming effect) of a device employing flexoprinted Ag grids as transparent electrodes and ECP-magenta/MCCP as ECPs.

The inhomogeneous switching was observed as a "blooming" where the areas closest to the grid lines changed color before the center of the hexagon. The blooming (shown in Figure 3-18 (A)) is due to the hexagonal grid structure, as the areas inside the hexagons are non-conductive. This requires lateral charge transport for complete switching to occur, which means that areas in close proximity to the metal grid lines respond faster compared to those in the center of a hexagon.[37] An increase in the conductivity of the areas inside the hexagons should result in an overall homogenization of the electrical field within a grid-based ECD hereby eliminating the blooming effect and reducing response times.[38] This was solved by coating a thin layer of a conductive

PEDOT:PSS formulation on top of the grid, effectively eliminating the blooming effect and significantly improving response times, as shown in Figure 3-18 (B) While both PEDOT and ECP-magenta are cathodically coloring polymers, the absorption that the PEDOT:PSS layer lends to the device is limited (ΔT=2% at 550nm), though a bluish hue is recognized in the bleached state of such a device (see appendix 3.2).

3.6.2 Dewetting

In addition to homogenizing the electrical field and functioning as a charge balancing polymer, PEDOT was also used as an intermediate layer to prevent dewetting of the electrolyte when coated on top of the ECP-magenta layer. Dewetting is a common challenge in layer-by-layer deposition and is caused by a difference in surface energy between two layers in contact with each other.[39]

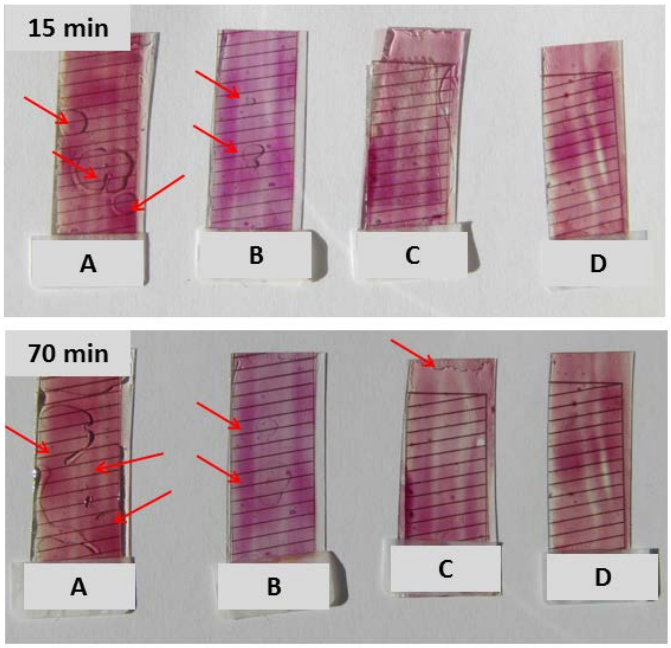

Figure 3-19: Dewetting of PMMA based electrolyte layer coated onto a solid film of ECP-magenta. The red arrows in (A), (B) and (C) indicates where the electrolyte has dewetted.

Several methods exist to prevent polymer layers from dewetting, but as many of these depend on subsequent formation of a solid phase by solvent evaporation, they are not particularly useful for depositing the semisolid electrolyte layer. I observed the

dewetting of the electrolyte layer by accident, as I left a sheet of slot-die coated foil in the laboratory overnight. The following day the electrolyte layer had dewetted the ECP-magenta film, which implies that this also occurs in laminated ECDs. This could explain the reduced function upon prolonged storage and usage (see section 3.4.1). Addressing dewetting is largely a learning-by-doing task, and I found that a very thin layer of PEDOT:PSS on top of ECP-magenta prevented dewetting even on prolonged storage as shown in Figure 3-19 that compares four slot-die coated samples of electrolyte on an ECP-magenta film. As seen, the amount of dewetting is increased in going from (D) to (A), and this becomes more pronounced in going from 15 min to 70 min. Substrate (D) does not show any dewetting, and this is attributed to the very thin layer of PEDOT coated on top of the ECP-magenta layer. The resulting device structure is depicted in Figure 3-20: ECD structure comprising an additional PEDOT:PSS layer

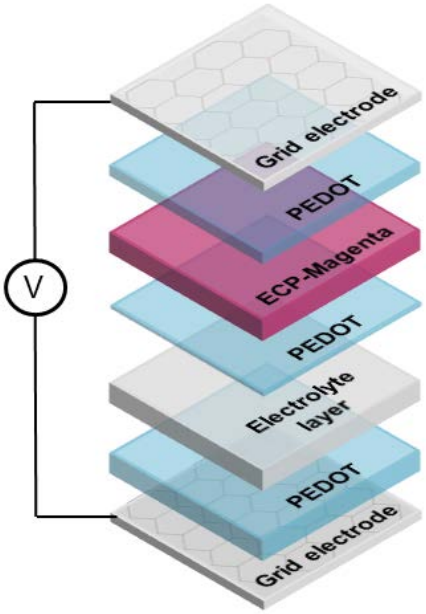

Figure 3-20: ECD structure comprising an additional PEDOT:PSS layer between ECP-magenta and the electrolyte layer in order to prevent dewetting of the latter. Reproduced from ref. 40 by permission of John Wiley & Sons Ltd.

3.6.3 Decomposition of organic material

In addition to increasing the overall conductivity of the substrate, PEDOT also replaced MCCP as the charge balancing polymer. This solved another problem that I en-

countered during the preliminary test of flexoprinted silver grids, as I noticed a discoloring of the devices. This reddening of the ECDs became more pronounced as the number of switches increased, in parallel to an increased response time until the devices ceased to switch. I initially attributed this to electrochemical decomposition of surfactants in the silver nanoparticle based ink used for printing the hexagonal grid structure, but as the discoloring was still observed on foils that had been post-treated using intensive pulsed light (photonic sintering of the silver),[41] the reason had to be found elsewhere. By carefully taking the device apart, the discoloring was found to reside on the electrode coated with MCCP, and the reddish taint was believed to originate from reactions of this polymer. As I have used MCCP on ITO in many ECDs without any discoloring, I gather that the MCCP might have irreversible reacted with the silver,[42-46] but as the problem was already solved by using PEDOT, I did not explore this phenomenon any further.

3.6.4 Flexoprinted vs. Embedded grid substrates

Figure 3-21 shows the redox switching of two ECDs comprising a flexoprinted (A) or embedded silver grid (B).[47-49] The fabrication of these grids is described in the experimental section, but as shown the dimensions of the two grid structures are vastly different. The two structures were chosen as each has certain advantages compared to the other. The dimensions and manufacturing speed of the flexoprinted grid is certainly beneficial when considering large area applications. 1 meter wide substrates are currently realizable, but wider substrates are not unrealistic as the width is only limited by the size of the printing machine; and the length of the flexoprinted Ag web is in theory infinite.

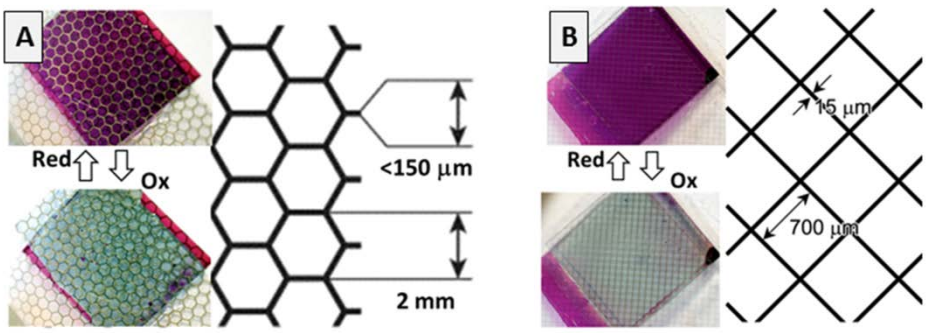

Figure 3-21: Redox switching of ECDs comprising (A) flexoprinted and (B) embedded Ag grid substrates. The dimension of the grid pattern is shown next to pictures. Reproduced from ref. 40 by permission of John Wiley & Sons Ltd.

The disadvantage of this structure is that the gridlines are noticeable upon close viewing (but unnoticeable when viewed from a few meters), which causes some optical distortion. Contrary to this, the line with of the embedded grid is 15 microns wide, and just noticeable as a slight blur. However, manufacturing the embedded grid is more complicated which accounts for two orders of magnitude price difference between the two.[48]

3.6.5 Response time of grid based ECDs

ECDs comprising the two silver grid structures were found to switch faster and at a lower potential than comparable devices that have ECP-magenta as the primary polymer (see section 3.4.2 and ref.[18]) Although the redox potential, at which a given polymer is reduced or oxidized, is property of that specific polymer, subjecting a polymer to similar potentials in difference device settings might affect the response. Therefore, discussing difference in switching potential for different device setting is only valid in connection with response times. The reduced optical contrast seen in grid based devices is not due to incomplete redox reaction, but rather stems from substrate absorption as shown in Figure 2.5 in chapter 2.

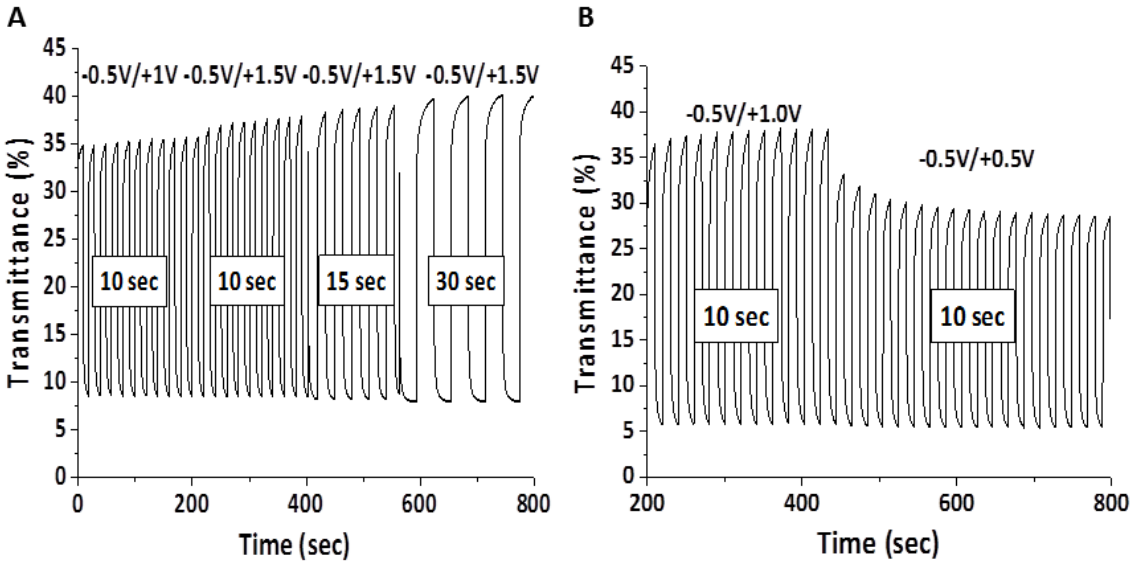

Figure 3-22: Response time of ECDs using (A) flexoprinted grid electrode (B) Embedded grid electrode. Transmittance was measured at 550 nm. Reproduced from ref. 40 by permission of John Wiley & Sons Ltd.

Figure 3-22 shows the response time of ECDs using flexoprinted Ag grid (A) and embedded grid (B) electrodes, and more detailed information is found in appendix 3.2. The maximum obtainable optical contrast (i.e. a full switch) is 33% with a response time of 44 seconds at -0.5 V/+1.5 V. But fully switching an ECD lowers the long term stability (due to electrochemically initiated side reactions), and the contrast gain is limited compared to e.g. a 95% switch as discussed in chapter 2. This is exemplified in that an optical contrast of 30% (at -0.5 V and +1.5 V) is obtained in 10 seconds, and 26% in 2 seconds. Low switching potentials is beneficial from a stability perspective as well as in relation to power consumption, and I found that reducing the switching potentials to -0.5 V and +1 V gave a 24% optical contrast in approximately 10 seconds, which is a reasonable response time for potentials at that level. Using the same low switching potentials (-0.5 V and +1 V) with the embedded grid as electrode substrate resulted in ECDs with an optical contrast of 32% in 10 seconds, which could be reduced to 0.8 seconds for an optical contrast of 31% and 0.3 seconds for an optical contrast of 29%. The sub-second response times were only observed when bleaching the device (i.e. oxidizing ECP- magenta). When coloring the device, the 29% optical contrast was ob-

tained in 2.5 seconds. The denser grid structure in the embedded grid might be responsible for the faster switching compared to the flexoprinted grid, but is not unlikely that the conductive PEDOT layers also influence the response time. Furthermore, the embedded grid devices showed a response time of 10 seconds for a 23% optical contrast at even lower potentials (-0.5 V and +0.5V).

3.7 Summary and perspectives

In this chapter, I have explored how large area electrochromic displays can be manufactured using three different coating techniques and two different electrolyte systems. All devices presented in this chapter, were made from flexible substrates since this is advantageous from a production point of view as well in the usage of such devices.

The initial trials using manual spray coating in combination with a small scale roll-coater resulted in matrix devices having the pixels that, to some extent, were individually addressable. The major problems with these devices were the crosstalk between the pixels and inhomogeneous switching. More homogenous switching was observed in devices made from slot-die coating films. The matrix displays encompassing these films showed an average optical contrast of 40% for the best device, but three out of the four devices tested did not switch satisfactorily and also suffered from crosstalk similar to that found in the spray coated devices. Devices made from fully ITO covered substrates was also investigated and exhibited a 44% optical contrast (58% vs a blank reference) when fully switched and response times of less than 5 seconds for a 95% switch. The power requirement for the devices were low with +/-2 V applied and maximal current density of less than 1 mA cm^{-2} (background current of 5 µA cm^{-2}), and paired well with the power output of a printed organic polymer photovoltaic module, allowing fabrication of a self-powered OPV/ECD demonstrator. Furthermore, two electrolyte systems were tested and the one employing MMA polymerized in ionic liquid proved to be the most efficient and stable. The replacement of ITO substrates was explored by using two different silver grid designs that showed good response times although the optical contrast was reduced due to increased substrate absorption.

Future work in ECD development should focus on the electrolyte layer as a way of increasing the mechanical and operational stability of the device. This might be done by crosslinking the electrolyte matrix and the ECP. In addition, the promising results on ITO free ECDs show that thin metal grids as viable electrode materials, and optimization on substrate absorbance will make this approach more interesting.

References

1 F. C. Krebs, *Sol Energ Mater Sol Cells,* 2009, **93,** 394-412.

2 K. X. Steirer, M. O. Reese, B. L. Rupert, N. Kopidakis, D. C. Olson, R. T. Collins and D. S. Ginley, *Sol Energ Mater Sol Cells,* 2009, **93,** 447-453.

3 Y. Kim, J. Lee, H. Kang, G. Kim, N. Kim and K. Lee, *Sol Energ Mater Sol Cells,* 2012, **98,** 39-45.

4 R. J. Mortimer, K. R. Graham, C. R. G. Grenier and J. R. Reynolds, *ACS Appl. Mater. Interfaces,* 2009, **1,** 2269-2276.

5 K. Norrman, A. Ghanbari-Siahkali and N. B. Larsen, *Annu. Rep. Progr. Chem. Sect. C,* 2005, **101,** 174-201.

6 H. F. Dam and F. C. Krebs, *Sol Energ Mater Sol Cells,* 2012, **97,** 191-196.

7 G. Gunbas and L. Toppare, *Chem. Commun.,* 2012, **48,** 1083-1101.

8 C. M. Amb, A. L. Dyer and J. R. Reynolds, *Chem. Mater.,* 2011, **23,** 397-415.

9 M. Sassi, M. M. Salamone, R. Ruffo, C. M. Mari, G. A. Pagani and L. Beverina, *Adv Mater,* 2012, **24,** 2004-2008.

10 A. L. Dyer, E. J. Thompson and J. R. Reynolds, *ACS Appl. Mater. Interfaces,* 2011, **3,** 1787-1795.

11 H. J. Byker, *Electrochim. Acta,* 2001, **46,** 2015-2022.

12 S. Desai, R. L. Shepherd, P. C. Innis, P. Murphy, C. Hall, R. Fabretto and G. G. Wallace, *Electrochim. Acta,* 2011, **56,** 4408-4413.

13 K. Matsumoto, B. Talukdar and T. Endo, *Polym. Bull.,* 2011, **66,** 771-778.

14 M. A. B. H. Susan, T. Kaneko, A. Noda and M. Watanabe, *J. Am. Chem. Soc.,* 2005, **127,** 4976-4983.

15 D. R. Macfarlane, M. Forsyth, P. C. Howlett, J. M. Pringle, J. Sun, G. Annat, W. Neil and E. I. Izgorodina, *Acc. Chem. Res.,* 2007, **40,** 1165-1173.

16 S. Sindhu, K. Narasimha Rao and E. S. R. Gopal, *Bull. Mater. Sci.,* 2008, **31,** 15-18.

17 B. D. Reeves, C. R. G. Grenier, A. A. Argun, A. Cirpan, T. D. McCarley and J. R. Reynolds, *Macromolecules,* 2004, **37,** 7559-7569.

18 E. P. Knott, M. R. Craig, D. Y. Liu, J. E. Babiarz, A. L. Dyer and J. R. Reynolds, *J. Mater. Chem.,* 2012, **22,** 4953-4962.

19 J. Y. Lim, H. C. Ko and H. Lee, *Synth Met,* 2005, **155,** 595-598.

20 J. Padilla, V. Seshadri, G. A. Sotzing and T. F. Otero, *Electrochem. Commun.,* 2007, **9,** 1931-1935.

21 J. Padilla and T. F. Otero, *Electrochem. Commun.,* 2008, **10,** 1-6.

22 P. G. J. Bartens, *Contrast Sensitivity of the Human Eye and its Effects on Image Quality,* SPIE PRESS BOOK, 1999.

23 D. Pletcher, R. Greff, R. Peat, L. M. Peter and J. Robinson, *Instrumental Methods in Electrochemistry,* Woodhead Publishing Limited, Philadelphia, USA, 2001.

24 DM display; www.dmdisplay.com; accessed October 2013, updated 2013

25 Media vision; www.media-vision.de; accessed October 2013, updated 2013

26 J. Jensen, H. F. Dam, J. R. Reynolds, A. L. Dyer and F. C. Krebs, *J. Polym. Sci. Part B,* 2012, **50,** 536-545.

27 F. C. Krebs, J. Fyenbo and M. Jørgensen, *J. Mater. Chem.,* 2010, **20,** 8994-9001.

28 F. C. Krebs, J. Fyenbo, D. M. Tanenbaum, S. A. Gevorgyan, R. Andriessen, B. Van Remoortere, Y. Galagan and M. Jørgensen, *Energy Environ. Sci.,* 2011, **4,** 4116-4123.

29 F. C. Krebs, S. A. Gevorgyan and J. Alstrup, *J. Mater. Chem.,* 2009, **19,** 5442-5451.

30 European Commission, Critical raw materials for the EU: Report of the Ad-hoc Working Group on defining critical raw materials; 2010.

31 R. L. Moss, E. Tzimas, H. Kara, P. Willis and J. Kooroshy, Critical Metals in Strategic Energy Technologies 2011, SETIS (JRC 65592)

32 C. J. M. Emmott, A. Urbina and J. Nelson, *Sol Energ Mater Sol Cells,* 2012, **97,** 14-21.

33 D. Mecerreyes, R. Marcilla, E. Ochoteco, H. Grande, J. A. Pomposo, R. Vergaz and J. M. Sánchez Pena, *Electrochim. Acta,* 2004, **49,** 3555-3559.

34 A. A. Argun, A. Cirpan and J. R. Reynolds, *Adv Mater,* 2003, **15,** 1338-1341.

35 J. Kawahara, P. Andersson Ersman, D. Nilsson, K. Katoh, Y. Nakata, M. Sandberg, M. Nilsson, G. Gustafsson and M. Berggren, *J. Polym. Sci. Part B,* 2013, **51,** 265-271.

36 R. R. Sondergaard, M. Hösel, M. Jørgensen and F. C. Krebs, *J. Polym. Sci. Part B,* 2013, **51,** 132-136.

37 P. Andersson, R. Forchheimer, P. Tehrani and M. Berggren, *Adv. Funct. Mater.,* 2007, **17,** 3074-3082.

38 F. Miomandre, M. N. Bussac, E. Vieil and L. Zuppiroli, *Chem. Phys.,* 2000, **255,** 291-300.

39 F. C. Krebs, J. Fyenbo and M. Jørgensen, *J. Mater. Chem.,* 2010, **20,** 8994-9001.

40 J. Jensen, M. Hösel, I. Kim, J. Yu, J. Jo and F. C. Krebs, *Advanced Funtional Materials,* 2013, accepted october, .

41 M. Hösel and F. C. Krebs, *J. Mater. Chem.,* 2012, **22,** 15683-15688.

42 N. L. Pickup, J. S. Shapiro and D. K. Y. Wong, *Anal. Chim. Acta,* 1998, **364,** 41-51.

43 C. Visy, E. Pintér, T. Flüei and R. Patakfalvi, *Synth. Met.,* 2005, **152,** 13-16.

44 K. Maksymiuk, *Electroanalysis,* 2006, **18,** 1537-1551.

45 Y. Tian, Z. Li, K. Shi and F. Yang, *Sep. Sci. Technol.,* 2008, **43,** 3891-3901.

46 J. Stejskal, *Chem. Pap.,* 2013, **67,** 814-848.

47 M. Hösel, R. R. Søndergaard, M. Jørgensen and F. C. Krebs, *Energy Technology,* 2013, **1,** 102-107.

48 J. -S. Yu, I. Kim, J. -S. Kim, J. Jo, T. T. Larsen-Olsen, R. R. Søndergaard, M. Hösel, D. Angmo, M. Jørgensen and F. C. Krebs, *Nanoscale,* 2012, **4,** 6032-6040.

49 I. Kim, J. -S. Yu, G. H. Jung, J. Jo, J. S. Kim, J. W. Kim, S. -W. Kwak, J. -L. Lee and D. Kim, *Sol Energ Mater Sol Cells,* 2013, **109,** 142-147.

Chapter 4

4. Photopatterning of electrochromic polymers

4.1 Introduction

This chapter describes the development of a novel photo-patternable electrochromic polymer. The chapter begins with a review of the patterning techniques applicable to ECPs and the state of the art within this field. For a comprehensive review on patterning in general, the reader is directed to reference 1-4. To reflect the experimental work, a large part of this chapter is devoted to characterizing the electrochromic properties of the new ECP and to explore any changes in its electrochromic properties due to crosslinking. The general mechanism of photopatterning is fairly simple: When a photo-patternable polymer is exposed to irradiation (typically of the shorter wavelengths), a chemical reaction is triggered that induces a solubility change. If the polymer is rendered insoluble, it is referred to as a *negative resist*, while it is a *positive resist* if the solubility is increased. Exposing a polymer coated substrate through a patterned photomask, leads to areas of different solubility. Upon exposure to organic solvents, the soluble areas dissolve, while the insoluble areas are unaffected and will reflect the pattern of the mask. Patterning can be used in the processing of ECPs as a method of converting 0 and 1 dimensional coating techniques into 2 dimensions i.e. a fully ECP coated surface can be covered with letters etc. Further, control of polymer solubility following coating can be exploited for orthogonal processing.

The main challenge when patterning ECPs by irradiation is to retain good electrochromic properties following exposure to light, and furthermore that the introduction of crosslinkable functionalities does not compromise the processability of the polymer. Looking ahead, I see photopatternable polymers as a step in the development of a new generation of ECPs that contain functionalities (in addition to electrochromism) that can be exploited in a post processing step.

The synthesis of the new patternable ECP was based on a polymer structure developed by the group of prof. John. R. Reynolds. Acrylate functionalities were incorporated in

the monomer, and a well-known photoinitiator was used for crosslinking upon light exposure. The properties of the new polymer were compared to the well characterized parent polymer, ECP-magenta. The experimental work that forms the basis of this chapter was done from January to May 2012 at Georgia Institute of Technology, where I spent 5 months working in the group of prof. John R. Reynolds. Several group members assisted me during my stay, most notably Aubrey L. Dyer and Eric Shen who also co-authored the paper "Direct Photopatterning of Electrochromic Polymers" (appendix 3.3).

4.2 Patterning techniques

Patterning of polymeric materials can be categorized based on a number of parameters e.g. as "bottom-up" or "top-down" techniques. The former constitutes deposition of material on a substrate to create a pattern while in the latter a pattern is created by removing material from a fully covered substrate. In general, printing techniques belong to the "bottom-up" category and photolithography belongs to the top-down category, but there are exceptions to this rule of thumb. While high resolution patterning is a very important parameter in the microelectronics industry, it is not of primary concern in macro-electronic systems such as large electrochromic displays and a resolution in the mm regime is satisfactory.

4.2.1 Printing techniques

Several techniques that rely on mechanical, non-chemical patterning are available. When describing the various techniques, it makes sense to differentiate between coating and printing techniques. Coating refers to contact free techniques where the ink flows onto a substrate, while printing techniques (with ink jet printing being an exception) are contact based and depends on ink being transferred to the substrate by a stamp, mold, pad, screen, etc. Two-dimensional patterning is possible with most printing techniques, while coating methods are limited to zero and one dimension (stripes). A few coating methods are described in chapter 3 and the following description shows some printing methods available for patterning large area ECDs. Although several

methods such as AFM, E-beam, nanoimprinting, etc are available I do not consider these techniques relevant for ECP patterning due to the limited areas these techniques cover in given time.

Microcontact printing (μCP) is an additive technique where a stamp is used to transfer ink to the substrate.[4, 4-6] The pre-patterned stamp features a bas-relief whereby a 2D pattern is created when brought into contact with the substrate. *Direct μCP* transfers polymers, while *indirect μCP* uses monomers or pre-polymers as inks that are subsequently polymerized.[7, 8] Indirect μCP can be used in combination with the Self-Assembled Monolayer approach (SAM). The SAM technique utilizes a patterned layer (usually an organothiol) on an electrode which hinders polymerization in the patterned area. The monomer is deposited on top and polymerization is done by radical initiation, light exposure or by electrochemical methods in the areas not covered by the SAM.[9-11] Using this approach for ECD, the electrochromic polymer is set-up for redox switching. The resolution of μCP ranges from 25-100 μm, and as this technique is R2R compatible it can be used for efficiently patterning of ECPs.

Screen printing (SC) is a method that is ideally suited for large area patterning of ECPs.[12] In *flat bed* screen printing, a woven mesh made of metal or synthetic fibers is stretched in a frame. By filling areas of the mesh with a substance impervious to the polymer ink, a pattern is created in the screen. When employing screen printing, the open mesh is filled with a polymer ink and brought into proximity of the substrate. A squeegee is drawn linearly across the screen pressing the ink filled mesh into contact with the substrate and at the same time forcing the ink through the mesh, whereby a pattern is created. High viscosity, low volatile ink is required, but ink waste is limited as leftover ink is recoverable. Screen printing is R2R compatible, both as *flat-bed* using rectangular screens or as *rotary* screen printing, where both ink and squeegee are placed inside a rotating cylinder.[13, 13, 14] Screen printing is already much used in the microelectronic industry for fabrication of printed circuit boards, organic light emitting diodes (OLEDs), organic field effect transistors (OFETs) and organic photovoltaics (OPVs).[15-18] Resolution ranges from 250-100 μm for flat-bed SC and from 100-80 for rotary SC, with processing speeds of 20-50 m/min, and 100-300m/min respectively.

Ink jet printing is a relatively new technique for patterning of conjugated polymers and differs from μCP and SC in that it is a non-contact printing method. An advantage in ink jet printing is probably that laboratory-scale experiments to some extent can be done using common house hold ink jet printers. In ink jet printing, a piezoelectric nozzle creates droplets of the polymer ink that are charged and directed onto the substrate by an electric field. A challenge in Ink Jet printing is ink formulation, as additives for printing can make up to 1% of the ink, and complex solvent compositions are necessary.[19, 19-21] A major advantage is that patterns can be created digitally without the need for a physical stamp or screen.

4.2.2 Lithographic techniques

Photopatterning or photolithography is one the most common patterning techniques within the optoelectronics and has been so for the last 30 years. Photolithography relies on materials (photoresists) which on exposure to light change functionality, such as photo induced crosslinking, polymerization, or degradation. The general process is shown Figure 4-1. Patterns are generated by depositing the resist material onto a substrate and exposing the surface to irradiation through a patterned mask. Irradiation triggers a chemical reaction in the exposed areas, while the unexposed areas are left unaffected. Following exposure, the pattern is developed by dissolution in an organic solvent. If the photoresist is rendered insoluble by light exposure it is a *negative resist* (or negative tone), while a photoresist that is rendered soluble is referred to as a *positive resist* (or positive tone). After resist development the “active material” (e.g. a conjugated polymer) is deposited onto the pattern and the resist material is removed by etching or peeling. For the majority of photolithographic techniques, the resist material is not the functional material, however in direct photopatterning the photoresist also doubles as such. This somewhat simplifies the patterning process, but increases the stability requirements to the active material. One of the challenges in patterning polymers is developing new procedures and materials for organic polymers to be used as resist material, solvents, etc. while being applicable to large area high throughput processing.

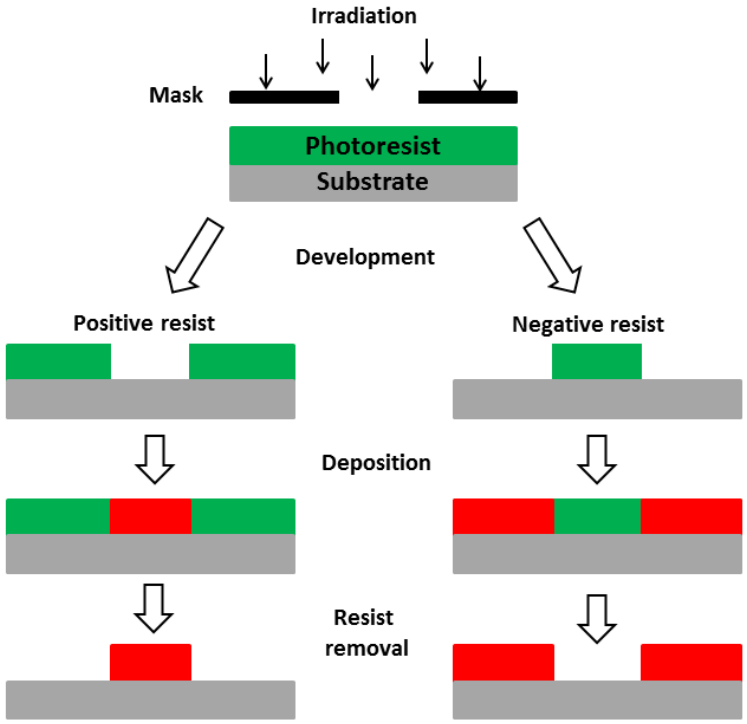

Figure 4-1: General photolithographic processes. A photoresist covered substrate is irradiated through a mask. Following development a pattern is created that depends on the resist material (positive or negative resist). The active material is deposited in the pattern, and finally the resist material is removed.

In order to avoid photodegradation of the conjugated polymer Chemically Amplified Photolithography (CAP) has been developed. The technique relies on photochemical reactions in a material (the amplifier) different from the resist material.[22] The two materials are formulated together, and irradiation triggers a chemical response (typically liberation of an acid or base) that induces a solubility change in the resist material. It should be noted that the word amplifier should not be taken literally as amplification infers that a signal is somehow being increased, which does not always occur in CAP. CAP was exploited by the use of N-(trifluoromethylsulfonyloxy)-1,8-naphthalimide as a photoacid generator (PAG) which upon exposure liberates trifluromethanesulfonic acid. When formulated with a tetrahydropyranyl protected polythiophene and irradiated, the photogenerated acid cleaves the THP group whereby the polymer becomes in-

soluble.[23] Other uses of PAG involves cationically promoted polymerization of oxetane functionalities to yield luminescent OLEDs,[24] and conversion of polyaniline (PANI) to an insoluble form through the use of onium salts.[25] While PAG is frequently employed in CAP procedures, photogenerated bases and radical initiators can also be employed.[26-29] It is debatable whether or not crosslinking reaction initiated by photoinitiator is CAP or Non Chemically Amplified Photolithography (NCAP), as the initial photochemical reaction occurs in the initiator species, yet crosslinking of unsaturated moieties can occur by irradiation.[1] In general, the irradiation used in the direct procedure approach (laser, UV lamp, etc.) generates free radicals, and using NCAP procedures increase the risk of damaging the polymer backbone by irreversible photobleaching, rendering the photoresist useless as an electroactive component.[30, 31] Patterning of poly(3-hexyl thiophene) (P3HT) has been done by laser irradiation, but the π-system was disrupted by this treatment, resulting in reduced conductivity under ambient conditions.[32, 33] By appending crosslinkable methacrylate groups and relying on residual Fe(III) salts as a initiator, polythiophenes was crosslinked without affecting the thiophene backbone.[34] Also relying on crosslinking of methacrylate groups, Kumar et. al. presented an elegant way of circumventing photooxidation of the thiophene backbone. By crosslinking the methacrylate groups prior to oxidative polymerization of the thiophenes, the harsh radiation procedures that potentially damage polymers π-system were avoided.[35]

4.3 Synthesis and crosslinking

My objective was to develop a simple patterning process that avoided tedious processing steps such as etching and peeling found in conventional photolithography. The idea of using direct photopatterning to generate negative toned electrochromic films, led to considerations of how to preserve the electronic and optical properties. Based on previous reports on photobleaching of polythiophenes described in section 4.2.2, I followed a strategy based on two guidelines (1) incorporation of a large amount of crosslinkable sites in the monomer species; (2) employment of a suitable UV induced radical initiator in combination with a crosslinker for photo crosslinking. By following these guidelines, I thought to minimize the irradiance necessary for crosslinking. The

first point was achieved by synthesizing the methacrylate containing ProDOT monomer (3,4-dihydro-2H-thieno[3,4-b][1,4]dioxepine-3,3-yl)bis(methylene)bis(2-methylacrylate) as shown in Figure 4-2

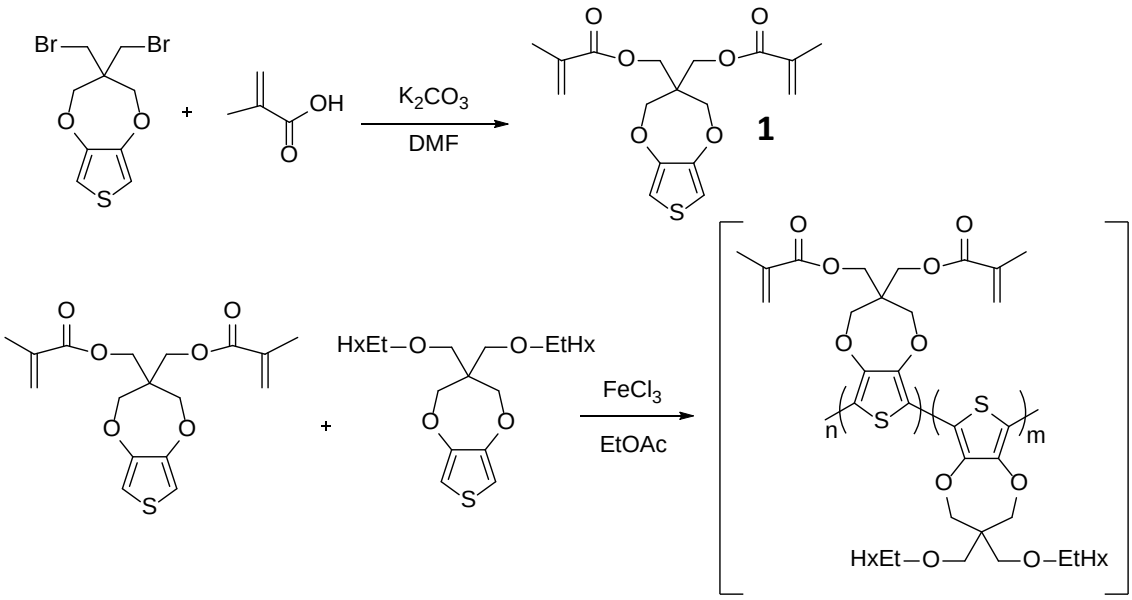

Figure 4-2: Synthesis of bis-methacrylate ProDot monomer (top) and bis-methacrylate containing co-polymer (bottom)

The available starting material 3,3-bis(bromomethyl)-3,4-dihydro-2H-thieno[3,4-b][1,4]dioxepine was reacted with methacrylic acid under basic conditions in dry DMF affording the bis-methacrylate thiophene, 1, in 45% yield after purification by dry column vacuum chromatograph (DCVC).[36] As described in chapter 2, the aliphatic groups in the 2-position on the ProDOT propylene bridge are central in controlling solubility and processability in poly(ProDOTs). I synthesized a homopolymer where the ethylhexyl groups were replaced with methacrylates groups, which turned out to be insoluble in common organic solvents (incl. boiling di-chlorobenzene). In order to increase the solubility of the polymer, I synthesized random copolymers comprising the ethylhexyl and bis-methacrylate monomer (see Figure 4-2). These copolymers contained from 6-60% of the bis-methacrylate monomer and were fully soluble in common organic solvents. The co-polymerization of the two monomers was carried out by oxidative coupling using ferric chloride in ethyl acetate while bubbling argon through the so-

lution. The polymerization gave poly(3,3-bis(((2-ethylhexyl)oxy)methyl)-3,4-dihydro-2H-thieno[3,4-][1,4]dioxepine)-co(3,4-di- hydro-2H-thieno[3,4-b][1,4]dioxepine-3,3-yl)bis(methylene)-bis(2-methylacrylate) as the product in 30-50% yield with an M_n of 10 to 20 kDa (detailed procedures are found in the experimental section).

Table 4: Polymer composition and molecular weight estimation by GPC. Reproduced from ref.37 with permission from WILEY-VCH

Monomer 1 in reaction	Monomer 1 In polymer[a]	Yield	M_n [Da]	M_w [Da]	PDI
10%	6%	36%	10500	22000	2
20%	12%	50%	15700	33500	2.1
50%	30%	31%	16900	31700	1.9
80%	60%	30%	7300[b]	15400	2.1

a/ Determined by ^{1}H-NMR
b/ Crosslinking of the polymer was observed during analysis, which might cause a lower Mn to be detected.

Table 4 shows the composition and molecular weight estimation of the various copolymers synthesized. The copolymers were estimated to have a slightly lower M_n compared to the homopolymer (ECP-Magenta) of the ethyl-hexyl monomer (M_n of 35000 Da) when polymerized following the same procedure. This is possibly due to steric hindrance imposed by the acrylate groups during polymerization. By comparing the first two columns in Table 4, it is seen that this polymerization favors incorporation of the ethylhexyl monomer, since the bis-methacrylate monomer content found in the polymer ranges from 60-75% of that in the reaction mixture. The composition of the copolymers was determined using ^{1}H-NMR and supported by FT-IR.

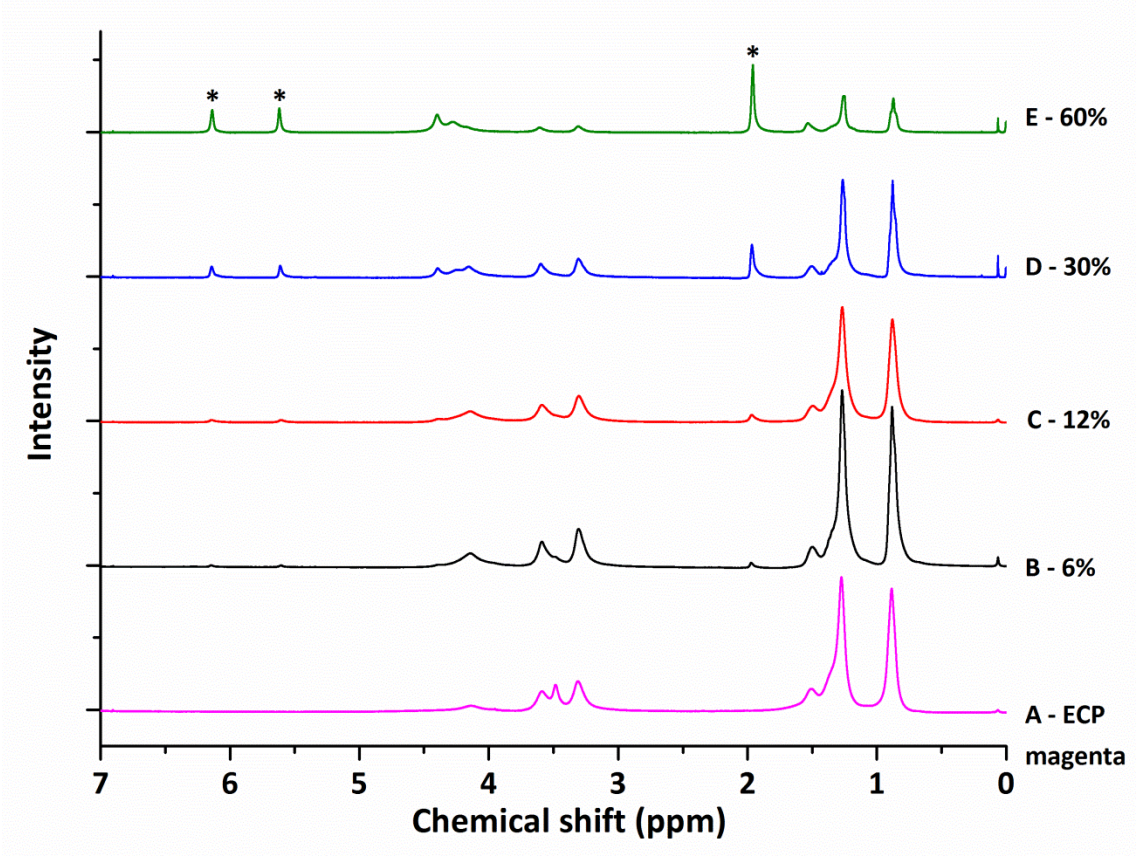

Figure 4-3: NMR spectra of homopolymer ECP-magenta (A) and for copolymers with varying content of bis-methacrylate monomer (B-E). The asterisks at 6.14, 5.61 and 1.97 ppm mark the alkene and methyl group protons (respectively) found in the methacrylate. Reproduced from ref. 37 with permission from WILEY-VCH

Figure 4-3 shows the ^{1}H NMR spectra of homopolymer ECP-magenta (A) and of the methacrylate containing copolymers (B-E). The difference in polymer composition between the homopolymer of ECP-magenta and the copolymers is shown by the three peaks marked by asterisks (shown only for E), which is due to the methacrylate group. The peak at 1.97 ppm is due to the methyl group protons and the two peaks at 6.14 and 5.61 ppm originates from protons on the alkene group. The intensity of these peaks increases in correspondence to the increasing content of bis-methacrylate monomer in the copolymer, which was determined by integration to range from 6-60%. The copolymers are named according to their bis-methacrylate content e.g. a copolymer containing 30% bis-methacrylate monomer is named copolymer 30.

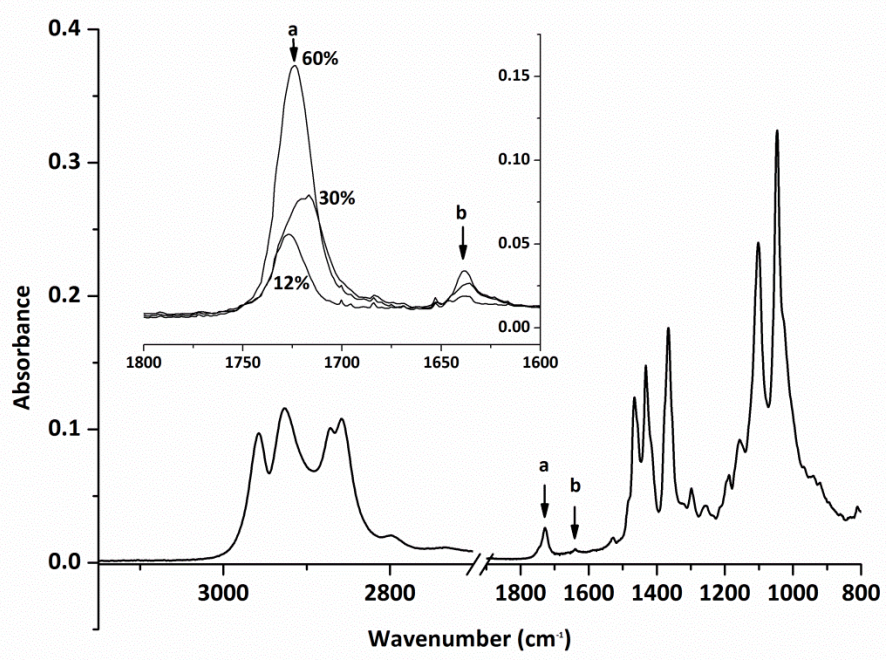

Figure 4-4: FT-IR absorption spectrum for copolymer 6 determined by FT-IR. The insert shows the 1800-1600 cm^{-1} region for copolymer 12%, 30% and 60%. Reproduced from ref 37 with permission from WILEY-VCH

Figure 4-4 shows the FT-IR absorption spectrum obtained from a spincoated film of copolymer 6. When comparing Figure 4-4 with the corresponding absorption spectra of the bis-methacrylate monomer (found in the appendix 3.3), it is found that the bands at 3103 cm^{-1} assigned to C-H stretches in the 2- and 5-positions on the thiophene ring are absent in the polymer film, which indicates a successful polymerization. Of further interest is the intense sharp band at 1712 cm^{-1} from the C=O stretch of the ester and the less intense band at 1643 cm^{-1} from the C=C stretch in the acrylate (marked a and b respectively in Figure 4-4). These bands support the proposed copolymer structure as they are not found in the IR spectra of the homopolymer ECP-magenta, and preservation of the C=C stretches confirms the stability of the acrylate groups to the polymerization conditions. Further support for the successful incorporation of methacrylate groups is the band at 2974 cm^{-1} originating from the C-H stretch in the methyl group of the methacrylate. Due to bands from other aliphatic groups, this band is obscured in Figure 4-4, but it is visible in the spectrum of the 100% bis-

methacrylate homopolymer (found in appendix 3.3). The inset in Figure 4-4 shows the increasing absorption of the C=O and C=C bands as a result of increasing the bis-methacrylate monomer content in the feed. As the intensity of absorption bands is directly proportional to the content of the group resonating at that wavelength, the FT-IR and NMR data presented support each other satisfactorily.

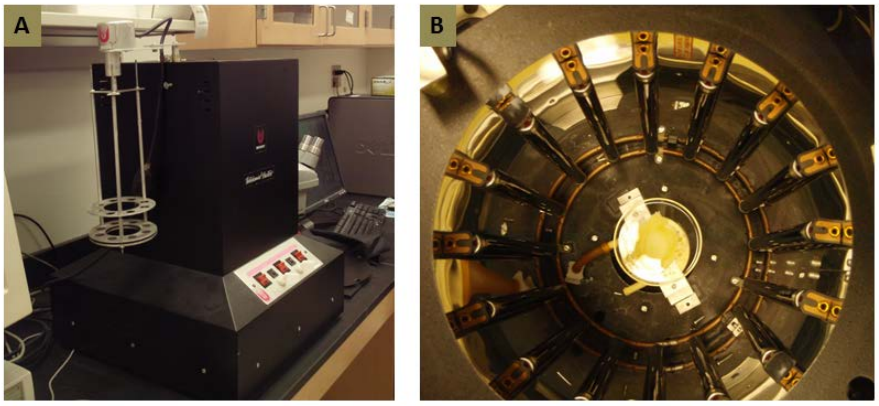

Figure 4-5: (A) The Rayonet RPR-100, photoreactor used for crosslinking. (B) A view looking down into the reactor. The reactor is equipped with sixteen RPR-3500 light bulbs (the spectrum is found as appendix 2.

In order for crosslinking to occur without degradation of the polymer film, mild reaction conditions in terms of irradiance and temperature exposure were employed. I attempted to crosslink the methacrylate groups without a photoinitiator, as reported by Lowe and Holdcroft,[34], but was unsuccessful in doing so. They did, however, use a considerably longer irradiation period, which I found incompatible with efficient processing of the polymer films. To reduce reaction time, I employed azobisisobutyronitrile (AIBN), which was found to be reliable as a photoinitiator and soluble in the organic solvents used in formulating the polymer solutions. AIBN is a well-known azo-radical initiator that decomposes upon irradiation at wavelengths of 300-360 nm, yielding the 2-cyanoprop-2-yl radicals responsible for initiating the polymerization of the methacrylate groups. An additional product of the reaction is gaseous nitrogen, which was expected to evaporate from the polymer film. In addition, ethyleneglycol dimethacrylate (EGDMA) was added to induce crosslinking, in order to make the poly-

mer more insoluble. The crosslinking process was monitored by FT-IR during irradiation of thin polymer films that were spin-cast onto freshly pressed KBr pellets.

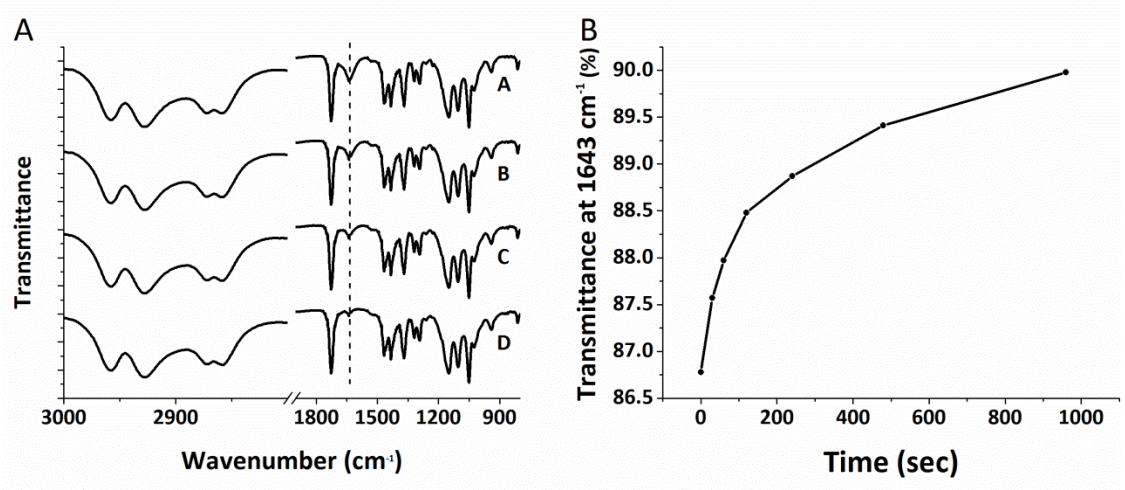

Figure 4-6: FT-IR time study of photo crosslinking. Graph A shows the transmittance of copolymer 30 during light exposure: (A) 0 sec; (B) 60 sec; (C) 240 sec and (D) 960 sec. Graph B shows the transmittance at 1643 cm^{-1} corresponding to the C=C stretch in the acrylate group.

Figure 4-6 (A) shows the resulting transmission spectra for copolymer 30 obtained from 0 to 960 seconds. Comparing spectra (A) and (D), an increase in transmittance is observed for the band at 1643 cm^{-1}, which corresponds to a depletion of the acrylate double bonds. It is noteworthy that no other changes in the spectra are observed during light exposure (especially the bands originating from the ester functionality), and this shows that crosslinking proceeds exclusively through the carbon-carbon double bonds of the acrylate, without disrupting the ester/C=O (band at 1712 cm^{-1}) nor the ProDOT backbone. Figure 4-6 (B) shows the transmittance at 1643 cm^{-1} as a function of exposure time, where the derivative of the curve represents the reaction speed. It can be seen from the time progression that the majority of the crosslinking occurs within the first 200 seconds of exposure, which is also where the reaction is fastest. It should be noted that longer exposure does not deplete the band 1643 cm^{-1} altogether. A likely explanation is that while the exposed surface of the polymer film is relatively uniform, the surface of the KBr pellet (on which the film is cast) is rough. This might cause non-uniformity in crosslinking through the thickness of the polymer film.

The effect of crosslinking on the solubility was determined by comparing the absorption spectra of an as-cast film to that of an exposed one after being submerged in stirring toluene for one minute. Films of the ethyl-hexyl homopolymer (ECP-Magenta) were fully dissolved in less than 10 seconds, and as similar behavior was observed for copolymer 6 and 12, they were not further studied.

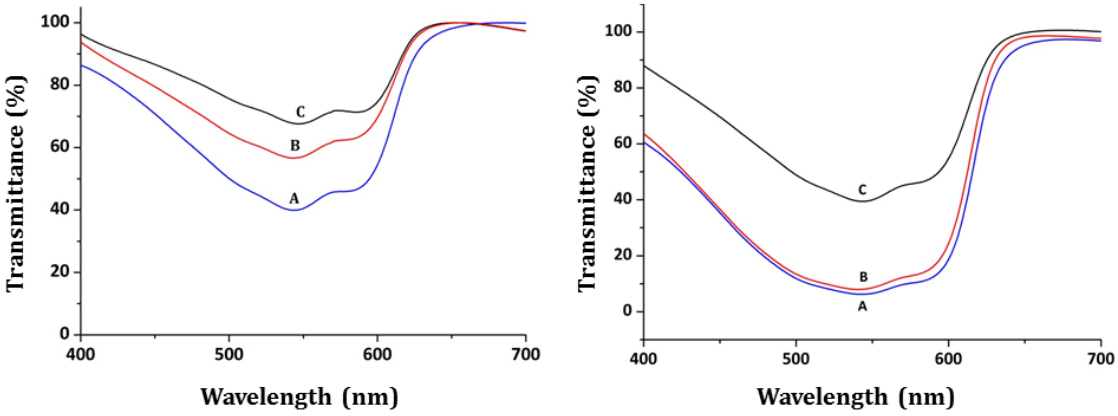

Figure 4-7: Solubility studies. Transmission profiles for copolymer 30 (left) and copolymer 60 (right). The (A) traces show the transmittance of the as-cast films, while the (B) traces show the transmittance after 600 seconds of light exposure followed by toluene rinsing. The C traces show the transmittance for non-exposed films after toluene rinsing. Reproduced from ref. 37 with permission from WILEY-VCH

Figure 4-7 show the difference in transmittance between non-irradiated and irradiated films for copolymer 30 (left) and copolymer 60 (right). The effect of irradiation on the solubility of the polymer films can be seen by comparing the B traces, which show the transmittance following 600 seconds of irradiation and immersion in stirring toluene for 60 seconds, with the C traces that show the transmittances of the as-cast films following toluene rinsing, but without prior irradiance. The A traces, which show the transmittances of the as-cast films, are included for comparison. The difference between B and C are 10% for copolymer 30 and 30% for copolymer 60 at $\lambda_{max.}$ These observations seem reasonable as the latter polymer contains twice as many acrylate functionalities, thus increasing the extent of crosslinking compared to the former. The C traces also show that even though the polymer films are not exposed to irradiation, there is still polymer residues left after toluene rinsing. These residues might be cross-

linked species due to radiation from the fluorescent tubes in the laboratory or they could be species that was adsorbed due to the polarity of the acrylate functionalities. Further work on crosslinking and tuning solubility, could involve substituting EGDMA for crosslinker species with different structure or increased functionalities (e.g. tetra-ethyleneglycoldiacrylate or pentaerythritol triacrylate).

4.4 Electrochemistry

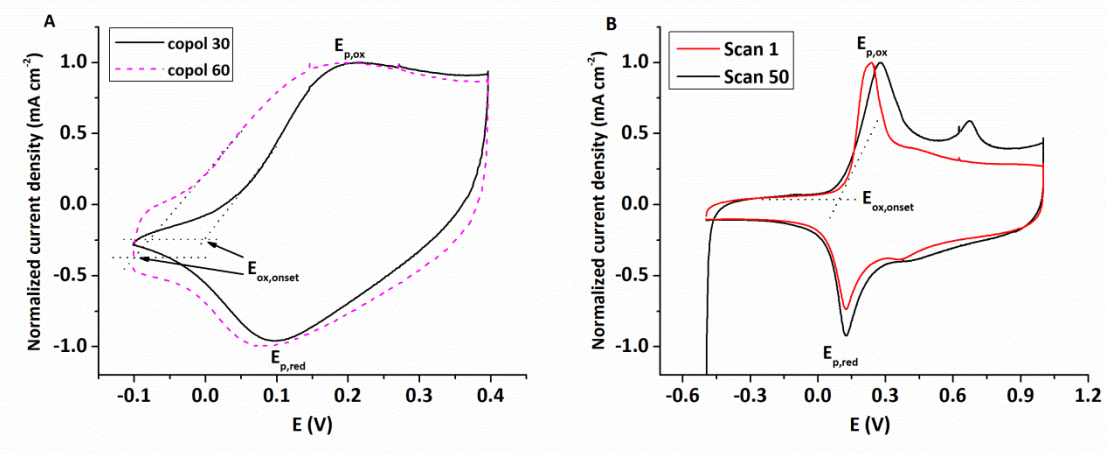

Figure 4-8: Cyclic voltammetry analysis of ECP films. (A) CV of copolymer 30 (solid black line) and co-polymer 60 (dashed pink line) prior to crosslinking (B) CV of ECP-magenta showing the 1st and 50th scan. Potentials are relative to Ag/Ag^{+}. Reproduced from ref. 37 with permission from WILEY-VCH

The electrochemical behavior of the polymer films was investigated by use of cyclic voltammetry, as shown in Figure 4-8 and detailed in the experimental section. In particular, interest was directed towards differences in redox activity due to the replacement of the ethyl-hexyl-oxy groups with methacrylate groups at the C2 carbon of the propylene bridge, and upon photo crosslinking of polymer films. Figure 4-8 (A) shows the CV scans for the 50th cycle for the non-crosslinked copolymer 30 and 60 and Figure 4-8 (B) that of the 1st and 50th scan of homopolymer ECP-Magenta. While there are several similarities in the current-voltage profiles between these three polymers, there are several differences that can be ascribed to the acrylate functionality. The redox switching windows were similar for all three polymers with the onset of oxidation, E_{ox},

observed to be 0V and -0.1V for the copolymer 30 and 60 respectively, while E_{ox} was 0.1V for ECP-Magenta. A broader redox process and higher level of charging current during cycling is observed for copolymer 30 and 60, due to the acrylate functionality that can lightly crosslink under ambient conditions. The broad redox process for the acrylate-functionalized polymers is similar to that seen for the 1st CV scan of the alkyloxy homopolymer in Figure 4-8 (B). A common trait for ECPs including ECP-magenta is "electrochemical annealing", wherein the polymers chains adopt a more ordered conformation during the first oxidation-reduction cycle.[38, 39] This cause a slight shift in the visible absorption spectra and also results in sharper redox peaks for the following scans. However, in the acrylate-functionalized polymers, a low level of crosslinking causes the polymer chains to lock in their conformation and not reorder on redox switching. This semi-locked conformation can also lead to a larger component of the current resulting from diffusional-dependent double-layer charging as the solvated counter ions are more restricted in their ability to diffuse through the polymer film. This is supported by the higher background charging current observed in copolymer 60 than in copolymer 30, where copolymer 60 has a higher density of acrylate functionality and, hence, a larger amount of ambient crosslinking occurring. Any differences between the copolymers and homopolymer being due to electrochemical crosslinking are excluded as there is an absence of additional redox peaks within the potential window scanned, and it is therefore concluded that no electrochemical polymerization of the acrylate functionality occurs. This relates well to the observation that insolubilisation was not observed during cycling and indicates that the acrylate functionality is stable within the potential window scanned.

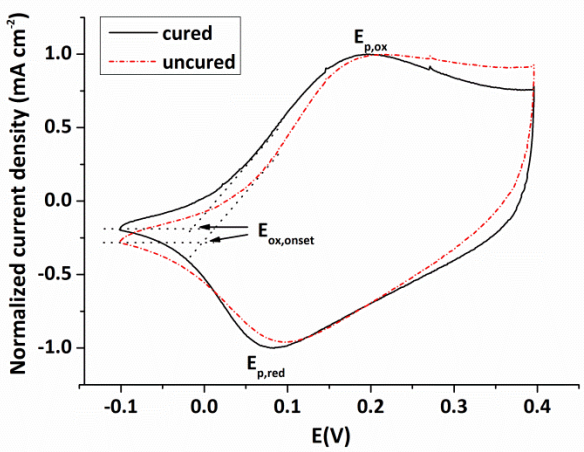

Figure 4-9: Cyclic voltammetry of cured (solid black line) and uncured (dashed red line) copolymer 30. Potential are relative to Ag/Ag^+. Reproduced from ref.37 with permission from WILEY-VCH

In utilizing crosslinkable functionalities, the retention of electroactivity in the polymer films after photo-induced crosslinking, is essential. Figure 4-9 shows a CV scan of a pristine copolymer 30 film overlaid with that of a crosslinked polymer film following 600 seconds of light exposure. The similarities of the two CVs demonstrate that the polymer electroactivity is preserved in the crosslinked film, and the absence of change in the redox peaks indicates that there are no detrimental side reactions on UV exposure.

4.5 Spectroelectrochemistry and colorimetry

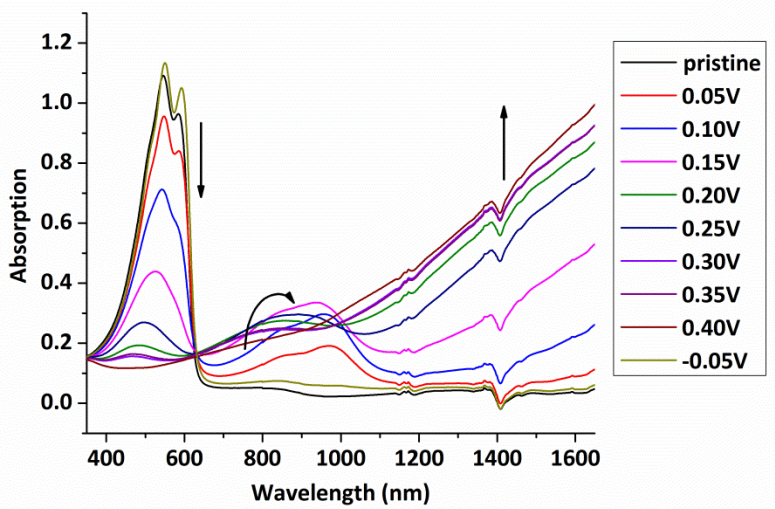

Figure 4-10: Spectroelectrochemistry for a spray cast film of copolymer 30. The absorption was recorded for 50mV increments between -0.05V and 0.4V. Potentials are relative to Ag/Ag^+.

I employed spectroelectrochemistry to correlate the applied potential with the optical absorption profile. This was done in-situ by measuring the absorbance spectrum from -0.05 V to 0.4 V with the potential stepped in increasing increments of 50mV as shown in Figure 4-10 for copolymer 30. The neutral polymer film absorbs in the 400 to 620 nm range and has Abs_{max} = 548nm. On increasing the potential (oxidation), the absorbance in the visible region decreases due to depletion of the π-π^* transition while absorptions at longer wavelengths begin to appear due to the introduction of lower energy electronic transitions (polarons and bipolarons). Upon full oxidation at 0.4V, the polymer has little absorption in the visible region as nearly all of the absorption is now occurring in the near infrared (NIR), with little tailing into the visible region, as is also seen for the alkoxy-substituted homopolymer. Photo-crosslinking copolymer 30 does not affect the absorption profile, and there is no loss of electrochromic switching on UV exposure as the copolymer retains a high level of optical contrast before and after crosslinking.

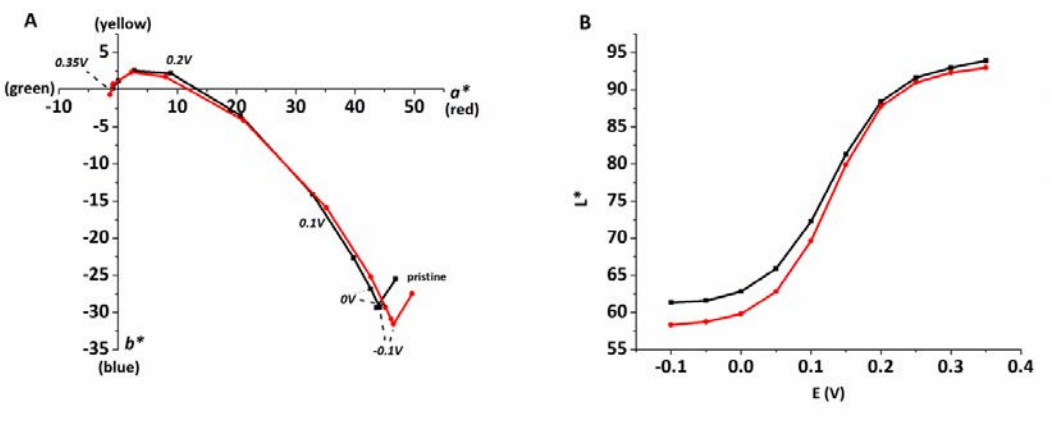

Figure 4-11: Colorimetry measurements of cured and uncured copolymer 30. (A) Development of a* and b* at potentials from -0.1V to 0.35V. (B) Lightness (L*) as a function of applied potential. Potentials are relative to Ag/Ag+. Reproduced from ref. 37 with permission from WILEY-VCH

Since the human eye perceives color differently than a spectrophotometer, the color of the electrochromic films was quantitatively described by colorimetry, using a Minolta colorimeter and a standard background illumination as detailed in the experimental section. The 1976 CIE LAB (L*a*b*) method was utilized to represent colors measured in situ from the fully neutral/reduced state (-0.1 V) to the fully oxidized state (0.35 V) as shown in Figure 4-11. The (a*, b*) values are (46,-32) at -0.1V, corresponding to a color with a blue-red component as expected for a magenta colored film. As the potential was progressively stepped from fully neutralized to fully oxidized at 0.35 V, the (a*, b*) values changed to (-1,-1) indicating a highly achromatic film at that potential. These values are very similar to those previously reported for the ECP-Magenta homopolymer. The lightness, or L*, is a measure of the weighted response of the eye to light intensity variations (whereas transmittance is a linear response of a photodetector) and was simultaneously measured as a function of applied voltage as shown in Figure 4-11 (B). In the fully neutralized state at -0.1V, the polymer is in a colored, absorptive state, transitioning to a near colorless, high lightness state between 0.1V to 0.2V until fully oxidized 0.35V when the L* value maximizes at 93. Similarly with the a* and b* values there is negligible difference in the L* values between the films before and after photo-crosslinking, except for a slightly higher L* value in the neutral state. This can be ascribed to a slight loss of non-crosslinked material in the film after crosslinking and

rinsing, as was also observed in the absorption spectra (see Figure 4-7). This minimal difference in the L*a*b* values of the pristine- compared to the crosslinked films, supports the analysis that crosslinking does not affect the colorimetric properties of the polymer films in either the neutral or oxidized states.

4.6 Patterning and orthogonal processing

If photopatterning is to compete with efficient printing techniques such as screen printing, it should be facile and compatible with roll-to-roll coating procedures. The ability to print a soluble material using roll-to-roll methods, followed by photolithographic patterning will allow for large area processing with small feature patterning as desired for e.g. large area signs.

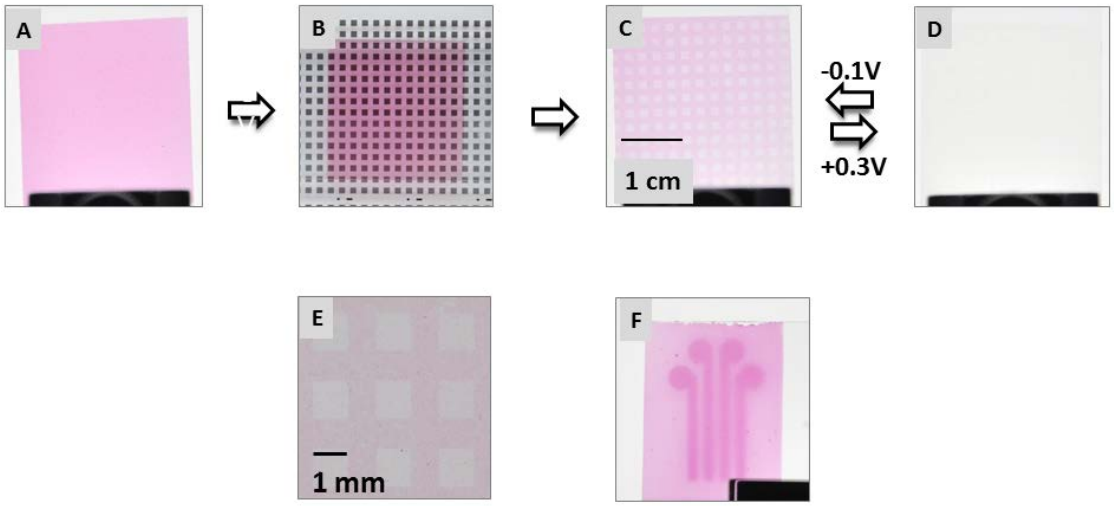

Figure 4-12: Direct photopatterning. (A) ITO covered glass substrate coated with copolymer 30 (3 x 3 cm^2). (B) Irradiation through a photomask. (C) Removal of photomask and dissolution of non-exposed polymer (D) Oxidized state of the patterned area (E) Optical enlargement of pattern in picture (C). (F) Example of another pattern.

This method was demonstrated as shown in Figure 4-12. Figure 4-12 (A) shows an ITO covered glass substrate spray coated with copolymer 30. The substrate is covered with a photomask shown in Figure 4-12 (B) and irradiated for 600 seconds. Figure 4-12 (C) shows the patterned surface with dimensions in the order of 1 mm following removal

of the mask and development by dissolution in toluene. After drying, the electrochromic film was switched at -0.1 V and + 0.35 in an electrolyte solution as shown in Figure 4-12 (D).

As with other polymer and organic electronic devices, most electrochromic devices consist of several successively deposited organic layers. The deposition of multiple layers can be challenging, as the layers are often soluble in the same common solvents. Several strategies have been explored that rely on post-processing steps whereby the coated layer is made insoluble in the following processing solvent.[40-44] For ECPs, ester substituted poly(ProDots) where soapofied to yield insoluble diols, or water soluble carboxylates.[45-47] Such methods, commonly known as *orthogonal processing,* could enable the fabrication of devices from the bottom-up, a further step towards complete roll-to-roll processing of ECPs. To that end, the copolymers presented here show promise where both the 30 and 60% copolymer are rendered insoluble in toluene after crosslinking.

4.7 Summery and perspectives

This chapter described the successful synthesis and characterization of a new conjugated electroactive polymer that doubles as a negative photoresist. By synthesizing a copolymer based on an alkoxy-substituted ProDOT and a methacrylate-substituted ProDOT, the resulting polymer was soluble in common organic solvents. Thin films of the polymer were cast along with a common photoinitiator and a crosslinking agent, and during irradiation the methacrylate functionality was crosslinked to render the film insoluble, while maintaining electrochemical, spectroscopic, and colorimetric properties. The patterns thus created were in the millimeter range, which is satisfactory for large area signage. As the photolithographic patterning was performed under standard laboratory conditions, light crosslinking of the masked areas occurred. It is expected that the resolution can be improved under rigorous lithographic conditions such as appropriate UV light filters; to selectively block UV emission from typical laboratory fluorescent lamps as the irradiation from room lighting can initiate crosslinking. Using a different photoinitiator is another thing that could be explored. While AIBN was found

stable under ambient conditions, the relatively low decomposition temperature (65^{o}C) does pose a challenge upon selective irradiation as the substrate material and photomask may reach temperatures approaching that of AIBN decomposition. An increase in the pattern resolution would open the way for applications such as smart-cards, and smaller information displays, but as discussed in section 4.2, the resolution and speed of techniques such as screen printing is such that it is currently hard to imagine photopatterning being competitive. However, the work presented in this chapter is an initial assessment of photo crosslinking as a patterning technique for ECD development. There are several issues that can be explored including crosslinkable groups such as azides, oxetanes and epoxides. Also of interest are the crosslinker additive, that can be varied, and the choice of initiator.

The idea of using the photo crosslinkable for ECP orthogonal processing started out as a secondary objective of this research, but could turn out being very advantageous during processing. More generally, this chapter shows an ECP that facilitate a post processing step without compromising the electrochromic properties.

References

1 Y. Xu, F. Zhang and X. Feng, *Small,* 2011, **7,** 1338-1360.

2 S. Holdcroft, *Adv Mater,* 2001, **13,** 1753-1765.

3 Z. Nie and E. Kumacheva, *Nat. Mater.,* 2008, **7,** 277-290.

4 E. Menard, M. A. Meitl, Y. Sun, J. -U. Park, D. J. -L. Shir, Y. -S. Nam, S. Jeon and J. A. Rogers, *Chem. Rev.,* 2007, **107,** 1117-1160.

5 M. Geissler and Y. Xia, *Adv Mater,* 2004, **16,** 1249-1269.

6 A. Kumar and G. M. Whitesides, *Appl. Phys. Lett.,* 1993, **63,** 2002-2004.

7 T. Granlund, T. Nyberg, L. S. Roman, M. Svensson and O. Inganäs, *Adv Mater,* 2000, **12,** 269-273.

8 D. Li and L. J. Guo, *Appl. Phys. Lett.,* 2006, **88,** .

9 Y. Xia and G. M. Whitesides, *Angew. Chem. Int. Ed.,* 1998, **37,** 550-575.

10 R. R. Shah, D. Merreceyes, M. Husemann, I. Rees, N. L. Abbott, C. J. Hawker and J. L. Hedrick, *Macromolecules,* 2000, **33,** 597-605.

11 S. Brittain, K. Paul, X. -M. Zhao and G. Whitesides, *Phys. World,* 1998, **11,** 31-36.

12 F. C. Krebs, *Sol Energ Mater Sol Cells,* 2009, **93,** 394-412.

13 F. C. Krebs, J. Fyenbo and M. Jørgensen, *J. Mater. Chem.,* 2010, **20,** 8994-9001.

14 F. C. Krebs, M. Jørgensen, K. Norrman, O. Hagemann, J. Alstrup, T. D. Nielsen, J. Fyenbo, K. Larsen and J. Kristensen, *Sol Energ Mater Sol Cells,* 2009, **93,** 422-441.

15 F. Garnier, R. Hajlaoui, A. Yassar and P. Srivastava, *Science,* 1994, **265,** 1684-1686.

16 C. Gray, J. Wang, G. Duthaler, A. Ritenour and P. Drzaic, *Proc SPIE Int Soc Opt Eng,* 2001, **4466,** 89-94.

17 N. S. Lee, D. S. Chung, I. T. Han, J. H. Kang, Y. S. Choi, H. Y. Kim, S. H. Park, Y. W. Jin, W. K. Yi, M. J. Yun, J. E. Jung, C. J. Lee, J. H. You, S. H. Jo, C. G. Lee and J. M. Kim, *Diamond Relat. Mat.,* 2001, **10,** 265-270.

18 D. -H. Lee, J. S. Choi, H. Chae, C. -H. Chung and S. M. Cho, *Disp,* 2008, **29,** 436-439.

19 C. N. Hoth, S. A. Choulis, P. Schilinsky and C. J. Brabec, *Adv Mater,* 2007, **19,** 3973-3978.

20 A. Lange, M. Wegener, C. Boeffel, B. Fischer, A. Wedel and D. Neher, *Sol Energ Mater Sol Cells,* 2010, **94,** 1816-1821.

21 S. H. Eom, S. Senthilarasu, P. Uthirakumar, S. C. Yoon, J. Lim, C. Lee, H. S. Lim, J. Lee and S. -H. Lee, *Org. Electron. : Phys. Mater. Appl.,* 2009, **10,** 536-542.

22 H. Ito, *Adv. Polym. Sci.,* 2005, **172,** 37-245.

23 J. Yu, M. Abley, C. Yang and S. Holdcroft, *Chem. Commun.,* 1998, 1503-1504.

24 C. D. Müller, A. Falcou, N. Reckefuss, M. Rojahn, V. Wiederhirn, P. Rudati, H. Frohne, O. Nuyken, H. Becker and K. Meerholz, *Nature,* 2003, **421,** 829-833.

25 M. Angelopoulos, J. M. Shaw, R. D. Kaplan and S. Perreault, *J. Vac. Sci. Technol. B,* 1989, **7,** 1519.

26 S. K. Lee, B. -J. Jung, T. Ahn, I. Song and H. -K. Shim, *Macromolecules,* 2003, **36,** 9252-9256.

27 S. H. Kang, K. S. Jang, P. Theato, R. Zentel and J. Y. Chang, *Macromolecules,* 2007, **40,** 8349-8354.

28 K. S. Schanze, T. S. Bergstedt and B. T. Hauser, *Adv Mater,* 1996, **8,** 531-534.

29 E. Scheler and P. Strohriegl, *J. Mater. Chem.,* 2009, **19,** 3207-3212.

30 J. Kim, J. You, B. Kim, T. Park and E. Kim, *Adv Mater,* 2011, **23,** 4168-4173.

31 J. Kim, J. You and E. Kim, *Macromolecules,* 2010, **43,** 2322-2327.

32 M. S. A. Abdou, G. A. Diaz-Guijada, M. I. Arroyo and S. Holdcroft, *Chemistry of Materials,* 1991, **3,** 1003-1006.

33 M. S. A. Abdou, Z. W. Xie, A. M. Leung and S. Holdcroft, *Synth. Met.,* 1992, **52,** 159-170.

34 J. Lowe and S. Holdcroft, *Macromolecules,* 1995, **28,** 4608-4616.

35 A. Kumar, S. -Y. Jang, J. Padilla, T. F. Otero and G. A. Sotzing, *Polymer,* 2008, **49,** 3686-3692.

36 D. S. Pedersen and C. Rosenbohm, *Synthesis,* 2001, 2431-2434.

37 J. Jensen, A. L. Dyer, D. E. Shen, F. C. Krebs and J. R. Reynolds, *Advanced Functional Materials,* 2013, **23,** 3728-3737.

38 S. Hellström, T. Cai, O. Inganäs and M. R. Andersson, *Electrochim Acta,* 2011, **56,** 3454-3459.

39 D. M. Welsh, L. J. Kloeppner, L. Madrigal, M. R. Pinto, B. C. Thompson, K. S. Schanze, K. A. Abboud, D. Powell and J. R. Reynolds, *Macromolecules,* 2002, **35,** 6517-6525.

40 T. T. Larsen-Olsen, B. Andreasen, T. R. Andersen, A. P. L. Böttiger, E. Bundgaard, K. Norrman, J. W. Andreasen, M. Jørgensen and F. C. Krebs, *Sol Energ Mater Sol Cells,* 2012, **97,** 22-27.

41 J. Liu, E. N. Kadnikova, Y. Liu, M. D. McGehee and J. M. J. Fréchet, *J. Am. Chem. Soc.,* 2004, **126,** 9486-9487.

42 M. Manceau, M. Helgesen and F. C. Krebs, *Polym Degradation Stab,* 2010, **95,** 2666-2669.

43 M. Helgesen and F. C. Krebs, *Macromolecules,* 2010, **43,** 1253-1260.

44 M. Helgesen, M. V. Madsen, B. Andreasen, T. Tromholt, J. W. Andreasen and F. C. Krebs, *Polym. Chem.,* 2011, **2,** 2536-2542.

45 B. D. Reeves, E. Unur, N. Ananthakrishnan and J. R. Reynolds, *Macromolecules,* 2007, **40,** 5344-5352.

46 P. M. Beaujuge, C. M. Amb and J. R. Reynolds, *Adv Mater,* 2010, **22,** 5383-5387.

47 C. M. Amb, P. M. Beaujuge and J. R. Reynolds, *Adv Mater,* 2010, **22,** 724-728.

Chapter 5

5. Photochemical stability of electrochromic polymers

5.1 Introduction

This chapter explores how electrochromic polymers react to solar exposure. As all organic material at large are degraded by sunlight at ambient conditions, it is not so much a question of if, but rather *how much* or *how fast*, and as the chapter shows, the chemical composition of the polymers affect the photochemical breakdown.

The chapter starts with a review on the photochemical stability of conjugated polymers mainly used in OPVs (in particular poly-3-hexylthiophene (P3HT)). This serves as the background on which to compare the resulted obtained for the ECPs. Several aspects of photodegradation in ECPs are described beginning with an establishment of the degradation rate based on chemical composition and thicknesses of the polymer films. Since a working ECD constitutes several components, the effect of electrolyte and barrier film are addressed in a layer by layer approach, as a way of extending ECD lifetime. The chapter ends with an evaluation of the effect of solar exposure on the operational parameters response time and optical contrast.

In general, the energy in solar irradiation triggers chemical reactions in the polymer chain. These are typically oxidation reactions which are increased by exposure to oxygen. The difference in photochemical stability between different compounds is due to differences in the electronic structure that arises from the various chemical groups. From a commercial and development point of view, stability is a key factor, and as such it is rather odd that photochemical stability has been largely ignored for ECPs. This can to a large extent be attributed to the fact that so far, photochemical stability has not been the limiting factor for the stability of ECDs.

The article “Photochemical stability of electrochromic polymers and devices” on which this chapter is based, constitutes the state of the art for photochemical stability of ECPs,[1] and is to the best of my knowledge the only thorough study on this subject.

However, similar investigations on polymers for OPVs that are also valid for ECPs has been carried out by our and other groups.[2-4] This led to a rule of thumb for photochemical stability for a large range of donor-acceptor polymers where alkyl side chains, quaternary sites and C-N/C-O bonds were found to reduce the photochemical stability while aromatic polycyclic units stabilized these polymers.[5]Furthermore the use of solar concentrators and interlaboratory outdoor testing also constitutes important advances within analysis of photo stability for conjugated polymers.[6, 7]

My objective was to expose a large range of ECPs to simulated sunlight (AM 1.5 G) in order to establish how chemical composition affects the photochemical stability, and how to extend the lifetime of these polymer films. These investigations on "static" properties were supplemented by the effect of solar exposure on the two operational parameters; response time and optical contrast. This required the synthesis and subsequently degradation of 11 published ECPs. The experimental work that forms the basis of this chapter was done from August 2012 to March 2013 at RisøDTU with the assistance of Morten Vestager Madsen (DTU) who also co-authored the paper "Photochemical Stability of Electrochromic Polymers and Devices", appended as appendix 3.4.

5.2 Photochemical degradation of conjugated polymers

It is well known that the combination of oxygen, moisture and light are responsible for the photochemical breakdown of polymers,[8-13]; a subject which is discussed further in chapter 6 for non-conjugated polymer substrates such as PET and PE. For conjugated polymers, a linear relation between irradiation time and decrease in optical density was found by analyzing poly(3-hexylthiophene) in oxygen saturated solutions.[14] This decrease was seen as an indication of a reduced number of conjugated π-electrons. The absorbance maximum was also slightly shifted, and this was attributed to a decrease in the average conjugation length. Oxygen concentration, solvent and the wavelength of the light was identified as the three main components affecting the photo degradation process. Further studies identified photobleaching and photolytic chain scission as two separate mechanisms of photodegradation in solution.[15] It was concluded that singlet oxygen was responsible for the majority of photobleaching by ring

opening of the thienyl residue through a 1,4-Diels-Alder addition. A free radical pathway of chain scission was proposed, in which residual transition metal salts from the polymerization reactions (mainly Fe^{3+}) were photolyzed to radicals. These were believed to initiate proton abstraction from the alkyl side chain, leading to addition of ground state oxygen and subsequently chain scission through multiple pathways.

Whereas singlet oxygen was found be the cause of degradation in solution, the degradation mechanism in the solid state is different.[16]. Photobleaching of P3HT thin film differs from solution, in that crosslinking (due to alkoxy radicals) instead of chain scission reactions is observed.[17, 18]. The involvement of singlet oxygen in the degradation of P3HT films has been ruled out, and instead photobleaching is attributed to oxidation of the alkyl side chains, while oxidation of the thiophene ring is responsible for backbone oxidation and chain scission that leads to loss of conjugation and bleaching of the sample.[19, 20] Both pathways involve radical chain mechanisms where the α-protons on the side chains play a significant role in the degradation, and observations that shorter wavelengths lead to an increase in the photooxidation supports this.[21] Other studies propose that the polymer is mainly attacked at the terminal thiophene rings and at points of broken conjugation.[4, 22] This observation supports the radical chain mechanism driven by photogeneration of radicals by the photolysis of precursors absorbing in the ultraviolet region.

5.2.1 ECP considerations

In order to give a broad overview of the photochemical degradation in ECPs, I synthesized 11 different ECPs encompassing as wide a range of structural motifs as possible.[23-30] Although the synthesis and characterization of these polymers have already been published, the synthesis required a substantial amount of work, and the synthetic procedures of these polymers are described in appendix 1.1, while a general discussion of ECP development is found in chapter 2.

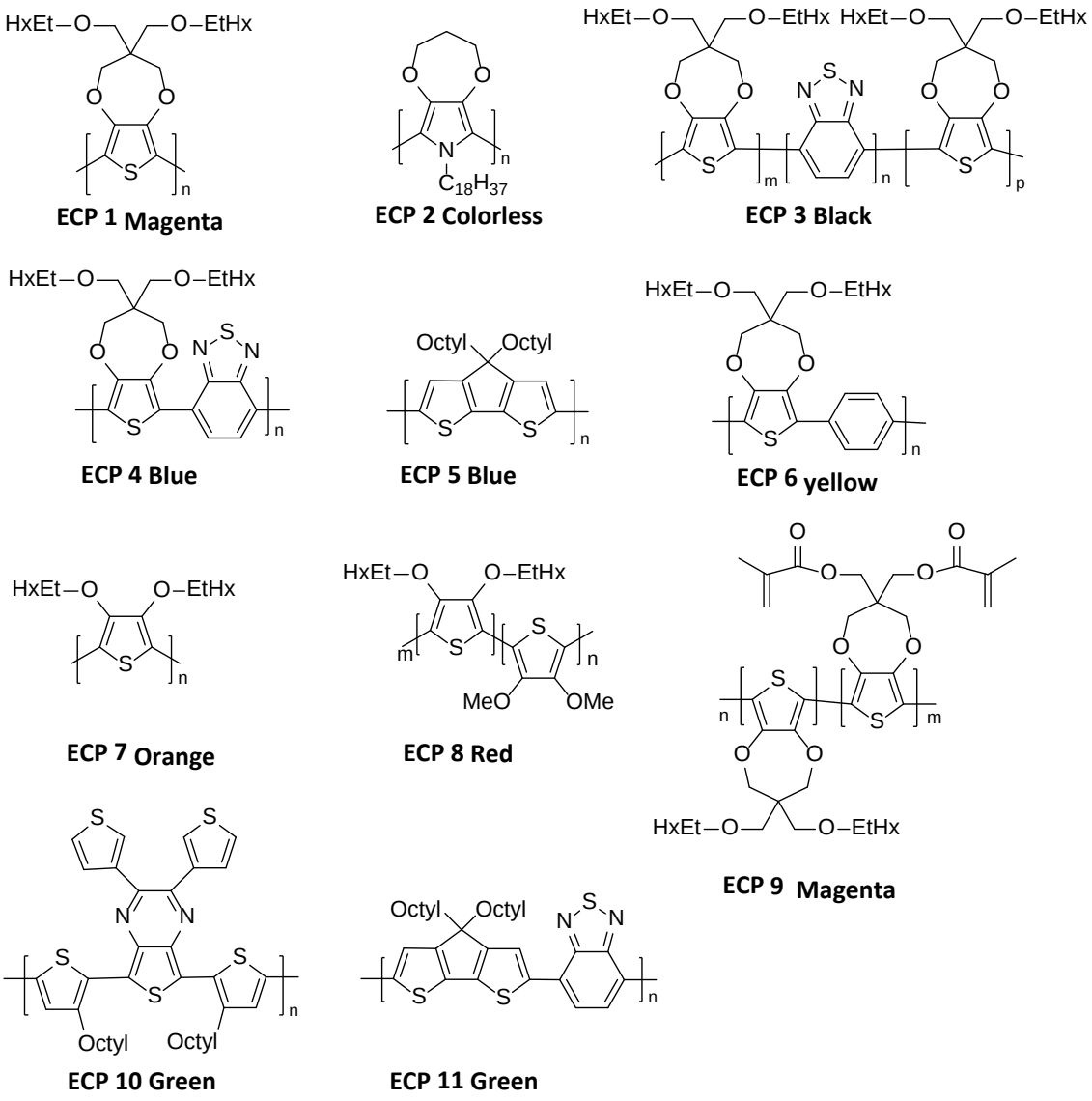

Figure 5-1: The electrochromic polymers synthesized and investigated for photochemical stability. Reproduced from ref. 1 with permission from The Royal Society of Chemistry

Owing to the fact that many p-dopable ECPs are polythiophenes, this structural motif is repeated in several of the polymers as seen in Figure 5-1. An important requirement was that the polymers should be solution processable, as this is necessary for roll coating. Further, the polymers were chosen to represent a wide range of colours as shown in Figure 5-2 in order to cover for the requirements in signs, displays, windows etc.

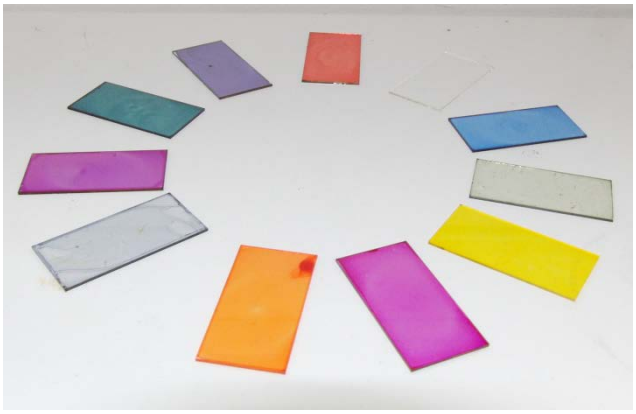

Figure 5-2: Picture of the ECPs synthesized and studied. Starting at 12 o'clock and going clockwise is ECP 8, 2, 4, 6, 10, 6, 1, 7, 3, 9, 11 and 5. Reproduced from ref. 1 with permission from The Royal Society of Chemistry

ECP 1 and ECP 9 are both magenta colored in the neutral state. ECP 1 has been extensively studied over the last decade and is a key polymer since the structure is part of several of the other copolymers.[25] The analogue ECP 9 is capable of network formation, and I thought that this might affect the photochemical stability.[31] ECP 3 is a random copolymer, with a structure that produces several absorption peaks in the visible spectrum. The result is a black colored polymer which is interesting since this is the only ECP capable of switching between black and clear. This has the potential of being useful in particular for e-paper, but also for shading and black/white displays.[27, 32] ECP 4 and ECP 5 are both blue in their neutral state and are interesting since they comprise different chemical motifs.[23, 33] The blue color in ECP 4 is a result of the donor-acceptor approach, having ProDot(OEtHx)$_2$ and benzothiodiazole as the donor moiety and acceptor moiety respectively.[34] The steric effect of the phenyl ring in ECP 6 is another approach by which to alter absorption of ECPs. By a combination of steric and acceptor properties, the absorption is blue shifted compared to ECP 1, and therefore ECP 6 appear yellow in the neutral state.[26] ECP 7 and ECP 8 both have non-bridging substituents in the 3 and 4 positions. ECP 7 is orange in the neutral state and possesses a higher band gap than ECP 8 that has methoxy substituted thiophenes randomly incorporated. These substituents relax the steric repulsion between the substituents and lower the band gap to 2.0 eV, which redshift the absorption to 525 nm producing a red poly-

mer.[24] Two green polymers are included; ECP 10 that was selected based on the different chemical motif compared to the other polymers,[30] and ECP 11 which comprises a BTD acceptor group that confer an additional absorption peak compared to ECP 5, typical of donor-acceptor polymers.[29, 33, 34] ECP 2 is an almost colorless polymer in both redox states (MCCP, see chapter 2), which is advantageous in electrochromic devices, where it can be employed as a charge balancing polymer with minimal effect on the optical contrast.[28]

5.2.2 Degradation of ECPs

As a first step in investigating the photochemical degradation, I correlated film thickness with absorption in the UV-visible range, as film thickness influences the observed degradation rate. Even so, the comparison of degradation rates for different polymers of equal thickness can be challenging (due to differences in extension coefficients), and reports have shown an order of magnitude of difference in the degradation of P3HT.[22, 35, 36] Using the absorption maximum (Abs_{max}) has been suggested as a better alternative, which was why the degradation experiments were conducted for several thicknesses of each polymer. It should be noted that it was not possible to obtain the exact same thicknesses for all polymers. However, initial absorption values as close to 0.5 as possible have been used for comparing the degradation rate of the polymers (see appendix 3.4). The polymers were then spincoated onto ITO sputtered glass and exposed to irradiation in a fully automated custom made set-up employing a solar simulator (AM 1.5G) and a spectrophotometer, previously developed by our group and described in the experimental section.[2] During the first five hours of solar irradiation, a marked decrease in the visible absorbance is observed for the majority of the polymers as shown in Figure 5-3. The graph shows the degradation state, which is the percentage of absorbance at Abs_{max} relative to the pritine film, as a function of exposure time. Three polymers (ECP 4, 10 and 11) show a distinct difference in photochemical stability compared to the others, and the polymers could be tentative grouped based on this. However, on closer inspection, the degradation behavior can more accurately described by including the degradation mechanism. This is not obvious when looking at

Figure 5-3, but by expanding the time scale, the difference between the two degradation modes becomes more pronounced, as shown in Figure 5-4(A).

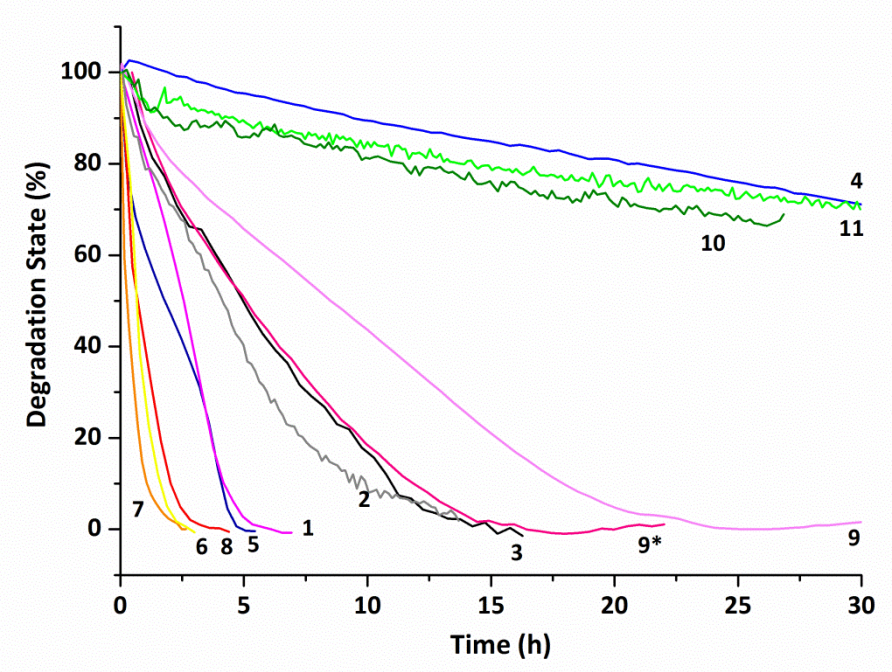

Figure 5-3: Degradation of ECPs as a function of irradiation time. The degradation state describes the percentage of Abs_{max} relative to the pristine film. The numbers of the traces corresponds to the numbering in Figure 5-1, while the colors correspond roughly to those of the polymer films. Two traces are seen for ECP 9. The asterisk marked trace corresponds to a film containing ethyleneglycol dimethacrylate (EGDMA) and AIBN photoinitiator.

The difference in degradation behavior is exemplified by ECP 1 and EC 7 and shown in Figure 5-4(A). This divides the polymers into two groups based on their degradation rate and degradation mode. Group 1 constitutes ECP 1, 2, 3, 4, 10 and 11 which exhibit a linear decline of absorption during exposure, while group 2 constitutes ECP 5, 6, 7 and 8 which exhibit an exponential decay. The grouping of the polymers is indicative of the underlying mechanism governing the photochemical degradation of the polymers. The two mechanisms are depicted in Figure 5-4(B) and are considered as follows: The linear degradation behavior exhibited by group 1 can be explained by the hypothesis that if the polymers of this group solely degrade by a mechanism wherein the terminal

positions on the polymer chain are targeted, the degradation would be linear since the number of reaction sites will remain constant.

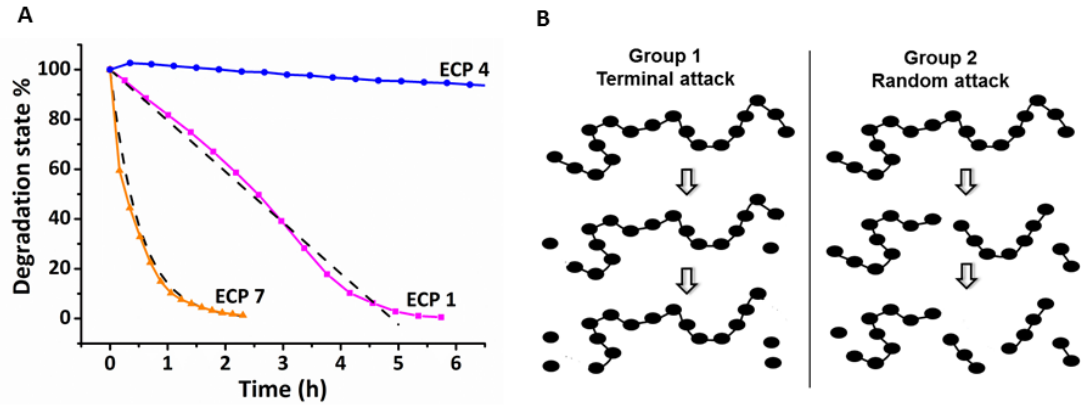

Figure 5-4: Degradation state as a function of exposure time for ECP 1 and ECP 7 (orange and magenta trace) along with the fitted curves (dashed traces) showing the difference in degradation rate. ECP 4 is included to show the large difference in degradation rate for this polymer. Reproduced from Ref. [1] with permission from The Royal Society of Chemistry

Contrary to this is a mechanism where there is no preferred attack point on the polymer; the degradation rate would decelerate since the number of reaction sites diminishes, as seen for group 2. If it is assumed that the degradation is not oxygen limited or limited by light shielding, the only rate-determining factor is the number of attack points.[4] The rate will be given by the recurrence equation f(n+1)=(1-a)f(n), where n represents numbered time intervals and a is the percentage loss of attack points per time iteration. The solution to this equation can be written on the form f(n)=c(1-a)n. By letting f(1)=100 and optimizing to the degradation state values, this function can be fitted to the experimental data. I found that all polymers in group 2 can be described with an r-squared value better than R^2=0.98, which is a strong indication that the degradation mechanism is targeting random positions on the polymer chain. Finally, a mixed state where the polymer is degraded at both terminal positions and intermediate points would result in accelerating degradation rate, but this is not observed for any of the groups. However, this depends on the respective rates of the two degradation mechanisms.

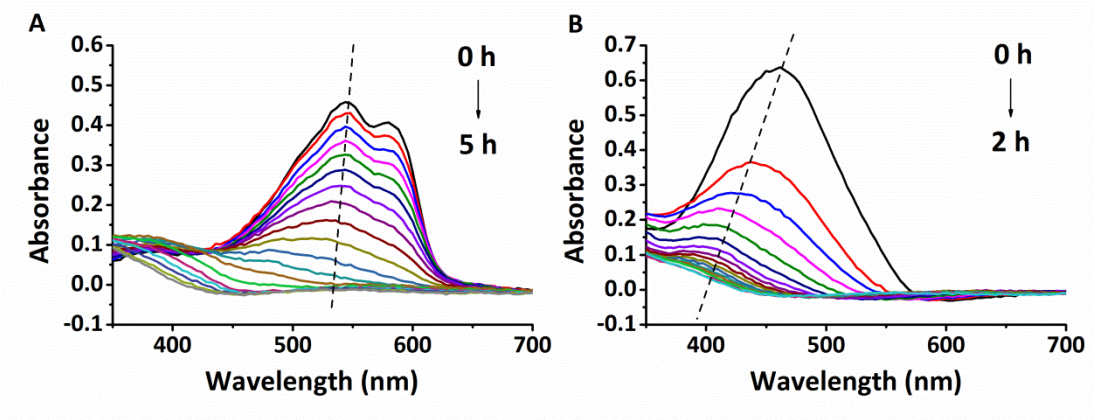

Figure 5-5: Spectral development for ECP 1 magenta (A) and ECP 7 orange (B) during irradiation for 5 and 2 hours respectively. The dashed lines show the position of the maximum absorbing peak.

The terminal attack point hypothesis infers that the conjugation must be preserved for the majority of the degradation period; this means that the absorption peak position must remain near constant for the major part of the degradation.[37] When looking at the peak position at Abs_{max} during irradiation, shown in Figure 5-5 , it is evident that the peak at Abs_{max} changes position faster for ECP 7 than for ECP 1. This lead to the establishment of a new parameter for the polymers: *the peakshift rate,* which intrinsically depends on the specific polymer, but also encompasses wavelength and intensity of light along with film thickness and other processing dependent characteristics. Table 5 shows a review of peakshift values and degradation rates for the various polymers during irradiation. As is evident, group 1 polymers exhibit a slower peak shift than group 2 polymers; an observation consistent with the proposed hypothesis since the conjugation length would change faster in the random attack mode.

Table 5 Degradation and Peakshift rate for ECPs during irradiation (AM 1.5G). (a) Peakshift rate cannot be determined as the spectrum does not contain any distinct peaks. (b) The polymer film comprised ethylenglycol dimethacrylate (EGDMA) and AIBN. Adapted from ref. 1 with permission from The Royal Society of Chemistry

Polymer	Abs_{max} (nm)	Degradation rate (%/h)	Peakshift rate (nm/%)	Group
ECP 11 Green	670	0.44	0.10	1
ECP 4 Blue	645	1.17	0.39	1
ECP 10 Green	717	1.58	0.49	1
ECP 9 Magenta	544	3.85	0.10	1
ECP 3 Black	539	7.32	0.37	1
ECP 2 Colorless[a]	302	7.93	-	1
ECP 9 Magenta[b]	545	8.48	0.15	1
ECP 1 Magenta	546	16.95	0.26	1
ECP 5 Blue	584	34.91	1.41	2
ECP 6 Yellow	445	43.49	0.75	2
ECP 7 Orange	460	81.48	0.62	2
ECP 8 Red	504	81.70	0.72	2

Furthermore, it can be seen that group 1 polymers have a lower degradation rate than group 2 polymers, thus group 1 polymers are more photochemically stable than group 2 polymers. As an example ECP 11, the most photostable polymer, is 200 times more stable than ECP 8, the least photostable polymer.

The hypothesis is a starting point for a more fully understanding of the degradation mechanism and several questions are at present unanswered. Primarily, the factors governing the preferred mode of attack are unknown. If we assume the reactive spe-

cies have a substantial amount of energy (e.g. a radical species), the difference in bond strength between a mid-chain position and terminal position cannot account for any preferences. In addition, the connection between peakshift rate and degradation mode assumes that all the polymers have the same effective conjugation length, which is not necessarily so.

Even though the presented hypothesis has unanswered questions, a common feature for the two most photochemically stable polymers ECP 11 and ECP 4 is a benzothiadiazole (BTD) group. Being an electron-deficient (i.e. an acceptor) group, the incorporation of the BTD group is expected to lower the oxidation potential of the polymer, due to a relative lower lying HOMO level of the resulting polymer.[35, 35, 38] This could explain the increase in photochemical stability observed for the ECP 4 and 11 compared to the homopolymers ECP 1 and ECP 5 that have similar chemical motifs but do not comprise BTD groups. One should be careful to base conclusions on just two examples, but the 80 and 14 times increase in stability seen for these polymers is pronounced, which is consistent with another report from our group wherein BTD groups were found to increase the photochemical stability of conjugated polymers.[5] The third most photo-stable polymer was the thienopyrazine, ECP 10 which is in good accordance with previously published results. [5, 39] While the electrochemical stability of conjugated polymers depends on the electrode potentials (and consequently HOMO/LUMO levels), the photon energy from sunlight is so high that other reactions such as radical initiated side-chain scission contribute to the degradation of conjugated polymers. This explains why the position of the HOMO is not necessarily correlated with photochemical stability. Another interesting difference between to similar polymers is the stability difference between the magenta coloured polymers ECP 1 and ECP 9, where the latter show a four-fold increase compared to the former. As the difference between the two is the presence of methacrylate groups in ECP 9, a likely explanation is that these groups absorb some of the irradiation that would otherwise degrade the polymer. I did not examine if this leads to crosslinking of the polymer chain, but when developing ECP 9 and characterizing thin films for photopatterning during my stay at Georgia Tech, I found it necessary to include EGDMA and AIBN for photo initiated

crosslinking to occur. For these photostability studies I also examined a film that comprised EGDMA and AIBN and found that the increase in photo stability was half that of films without these agents. This indicates that crosslinking does somehow postpone degradation, and since films without crosslinking agents require more energy (i.e. irradiation) than those comprising these agents, they show increased photochemical stability compared to the latter. Another explanation is that without additives, ECP 9 is incapable of crosslinking, and the thus preserved acrylate groups absorb more irradiation than the ester groups found in the crosslinked films.

5.2.3 Analysis using infrared spectroscopy

I used Infrared spectroscopy to support the results obtained using UV-vis spectroscopy. My objective was to correlate changes in the IR range to specific functional groups and compare these to changes in the UV-vis range. When examining conjugated polymers by UV-vis spectroscopy, one relies on absorption originating from π-π^* transitions, charge transfer transitions and macromolecular features such as regioregularity of the polymer chain and conjugation length. Since a certain conjugation length is required for UV-vis absorption to be detected, the “window of observation” is restricted compared to IR analysis and is one reason why IR is so useful in studying degradation of conjugated polymers.

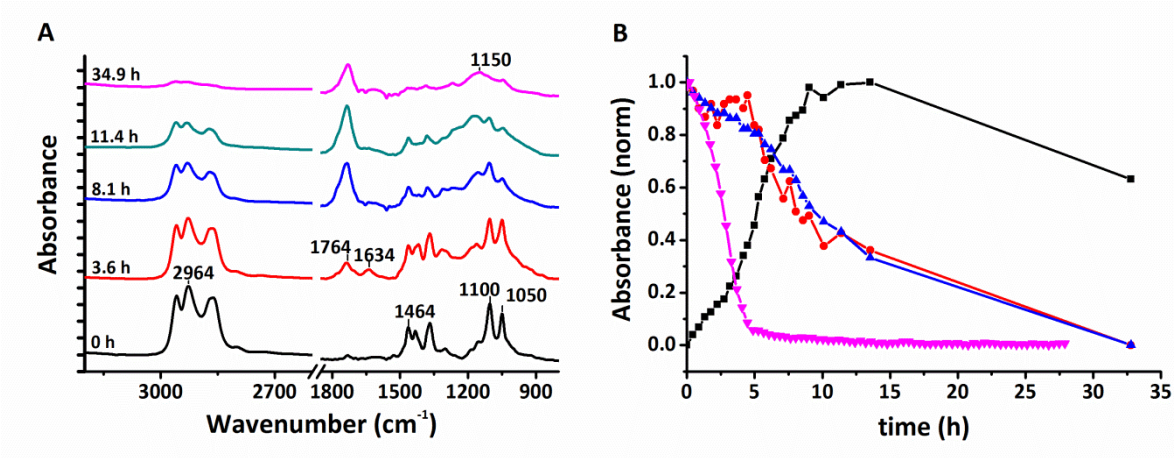

Figure 5-6: (A) Infrared spectra of ECP 1 obtained during irradiation. (B) Peak development during photochemical degradation. The absorbance has been normalized to allow for comparison of the signals. ● 1464 cm^{-1}; C=C stretching in thiophene rings ▲2964 cm^{-1}; C-H stretching in alkyl groups at; ■ 1734 cm^{-1}; C=O stretching from carbonyl moiety ; ▼ absorbance measured at 545 nm. Reproduced from ref. 1 with permission from The Royal Society of Chemistry

As all the polymers were quite similar (if not actual polythiophenes, they contained a thiophene rings in some form), this reflected in similar IR spectral features. Figure 5-6(A) shows the assignment of the major peaks and spectral development of ECP 1 during solar exposure. The IR spectra for the remaining polymers are found in appendix 3.4. The peaks from 2960 cm^{-1} to 2860 cm^{-1} are assigned to C-H stretching mainly from the aliphatic side chains. The intensity of these peaks progressively decreased during irradiation as a result of photolytic scission of the aliphatic side chains. The peaks from 1500 cm^{-1} to 1434 cm^{-1} are assigned to symmetric and asymmetric C=C stretching in the thiophene rings. These signals disappear during exposure which is ascribed to changes in the ring structure and conjugation. The decrease in the intensity of these peaks was found in accordance with the UV-visible absorption spectra. The peaks at 1100 cm^{-1} to 1050 cm^{-1} likewise decreased during irradiation of the film. These peaks are assigned to the C-O-C stretch from the ether groups. During exposure, two bands appeared in the carbonyl region at 1764 cm^{-1} and 1634 cm^{-1}. The appearance and increase in these peaks is a strong indication of C=O formation. The intensity of the former band increased up to a certain point where after it decreased slowly.

This band has, under similar conditions, previously been assigned to anhydride species. The latter band can be assigned to an aromatic ketone that is photochemically unstable, which is in accordance with the disappearance of this band on continuous irradiation. A broad band centered at 1150 cm^{-1} also appeared during exposure, which previously has been assigned to sulphur-oxygen oxidation products such as sulfinic acids or esters i.e. a breakdown/opening of the thiophene ring.[19] In the hydroxyl region, a broad signal between 3200 and 3700 cm^{-1} increased during progressive irradiation. The appearance of bands in this region indicates formation of hydroxyl or peroxy adducts. Figure 5-6(B) shows the (normalized) development in the intensity of various bands in the infrared spectrum of ECP 1 as a function of irradiation time alongside the absorption at 545nm. As IR spectroscopy relies on molecular vibrations in the thiophene ring, which are detectable long after the electronic transitions observable using UV-vis spectroscopy. This is observed for the signals corresponding to aliphatic side chains (2964 cm^{-1}) and the thiophene ring (1464 cm^{-1}) which decrease in intensity at the same rate, while the visible absorbance at 545 nm decreased at a rate four times as fast during the first 5 hours, before reaching a minimum. The carbonyl signal at 1734 cm^{-1} show the opposite development. The signals increase during the first eleven 11 hours, where after the intensity slightly decreases; suggesting formation of a carbonyl containing oxidation product that subsequently decompose. The occurrence and development of the signals during irradiation show trends much alike those obtained for P3HT, which implies that the ECPs degrade via similar intermediates.[19]

5.2.4 Long term stability

The requirements to photochemical stability and thus lifetime of ECDs may vary depending on the application, but it is clear that the limited photochemical stability of the ECP films under ambient conditions described in section 5.2.2 excludes extended use in ECDs. I addressed this problem by employing barrier foils capable of protecting the ECP films from atmospheric oxygen and UV irradiation, as shown in Figure 5-7. The barrier foils were applied directly onto ECP films coated on flexible PET substrates, and being equally flexible, this was done without compromising the flexibility of the sam-

ples. The oxygen barrier comprised a polyethylene terephthalate (PET) multi-layered foil and a pressure sensitive adhesive (PSA) that facilitated encapsulation of the sample. The encapsulation was done under ambient conditions, and though small amounts of oxygen were intrinsically trapped inside the samples, the effects were considered limited. Following encapsulation, the samples were irradiated and the degradation state was monitored weekly by measuring absorbance.

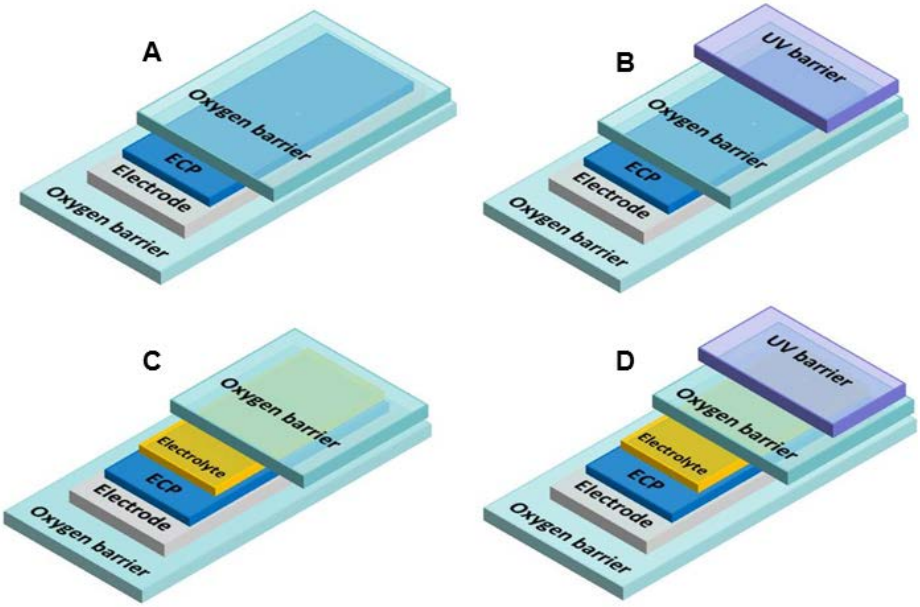

Figure 5-7: ECP samples for long term stability tests. All samples consist of ECPs coated onto ITO/PET substrates. Sample (A) is encapsulated in an oxygen barrier foil while (B) have half the samples additionally covered in a UV barrier foil. (C) and (D) corresponds to (A) and (B) respectively but furthermore comprise the PMMA/ionic liquid electrolyte gel. Adapted from ref. 1 with permission from The Royal Society of Chemistry

After 2200 hours of continuous illumination the average level of degradation for group 1 polymers was so limited that it was immeasurable, while the group 2 polymers showed a degradation rate of 0.027 % pr. hour on average. Comparing this to the degradation rates shown in Table 5, a drastic 1300-3300 fold increase in lifetime for group 2 polymers was observed. In parallel experiments the effect of the PMMA electrolyte was investigated.[40] These experiments showed that the PMMA based gel did not enhance degradation, and a slight increase in stability was observed for some samples.

The UV barrier foil did not seem to have any direct effect on the stability of the ECPs, as the oxygen barrier already conferred some UV protection, but the additional UV barrier did protect the oxygen barrier from UV induced decomposition, thereby extending device lifetime. To put the protection conferred by the barrier foils into perspective, northern latitudes (ex. Copenhagen) have a yearly average of 2.8 sun peak hours pr. day while subtropical latitudes (ex. Miami) have 4.9 sun peak hours pr. day; This means that the 2200 hours during which the protected substrates were exposed to solar irradiation (AM 1.5G, 1000 W m^{-2}) amount to more than two years at northern latitudes and a year and half for southern latitudes.

5.2.5 Operational stability

The results presented in section 5.2.2 and 5.2.4 represent a “static” description of the photochemically induced degradation, and it does not describe how irradiation affects the operation of an ECD. I studied this by irradiating samples of ECP-magenta for various amounts of time and using them as primary ECPs in ECDs comprising MCCP and PMMA/IL. The ECDs were switched between the two redox states while transmittance and response time were monitored. I tried to minimize electrochemical induced degradation by keeping the switching potential to -0.6 V and + 1.5 V. This was a trade off since the optical contrast and response time were compromised, but as these experiments were designed to explore the differences between exposed and non-exposed ECDs, I found this trade off acceptable.

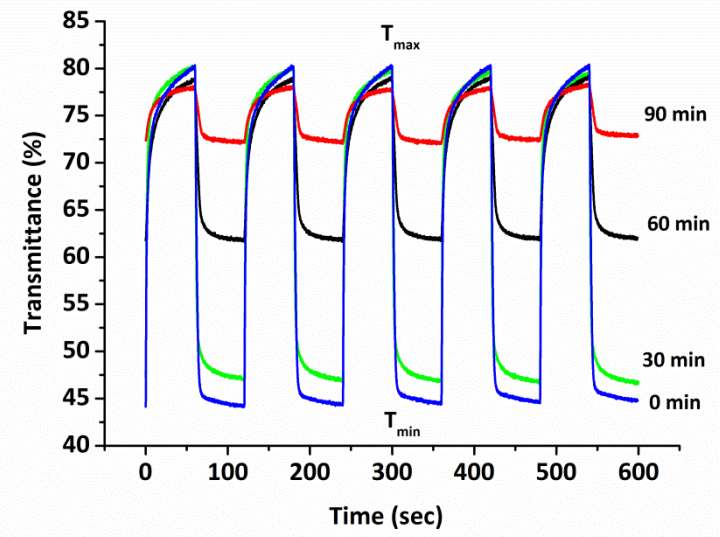

Figure 5-8: Response time and optical contrast of irradiated electrochromic devices switched potentiostatically from -0.6V to +1.5V with 60 seconds hold at each potential. The transmittance was measured at 545 nm. Reproduced from ref. 1 with permission from The Royal Society of Chemistry

Figure 5-8 shows the optical contrast (ΔT) and response time of photo exposed ECDs potentiostatically switched between - 0.6V and +1.5V. The figure shows that exposure to irradiation (AM 1.5 G) affects both redox states of the device with the most pronounced effect on the colored state of the devices. After 30 minutes of exposure the minimum transmittance obtainable (T_{min}) increased from 45% (non-exposed) to 47% (30min), 62% (60 min) and following 90 minutes of irradiation T_{min} was 73%. Irradiation had a less pronounced effect on the bleached state, which is expected as photodegradation involves oxidation of the film. The difference in maximum transmission (T_{max}) between the non-exposed and the film exposed for 90 minutes was just 3%. The effects on T_{min} and T_{max} lead to a decrease in optical contrast from 35% in the non-exposed device to 33% (30 min), 17% (60 min) and 6% (90 min).

Table 6: Response time for ECDs where the primary ECP has been exposed to various amounts of solar irradiation (AM 1.5G). The response time is given for 90%, 95% and 98% of a full switch. The optical contrast of a 100% switch is given in parentheses. Reproduced from ref. 1 with permission from The Royal Society of Chemistry

% of full switch	Colored to bleached (+1.5 V) Exposure time				Bleached to colored (-0.6 V) Exposure time			
	0 min	30 min	60 min	90 min	0 min	30 min	60 min	90 min
90%	19.6s	14.1s	19.4s	25.6s	4.0s	5.7s	10.5s	9.4s
95%	34.7s	30.8s	40.3s	34.5s	6.1s	14.0s	18.2s	12.4s
98%	48.8s	43.3s	49.0s	45.2s	11.2s	28.0s	31.2s	19.4s
100%	58.8s (35.9%)	59.2s (33.0%)	59.1s (17.2%)	51.8s (5.8%)	49.3s (35.7%)	55.3s (33.1%)	59.9s (17.3%)	55.1s (5.5%)

Table 6 lists the response times and optical contrast values for the exposed ECDs. Going from left to right in the "Colored to bleached" columns, a slight decrease in response time is observed between the non-exposed samples and those exposed for 30 min. This faster switching is probably caused by the reduced optical contrast of the exposed samples, hence less chemical reactions need to occur for the switch to be complete. The increased response time seen for films exposed for 60 and 90 minutes is attributed to widespread degradation of the polymer chains, not yet occurring in the 30 min. exposed film. It is also worth stressing that while similar response times are found for the non- and 90-minute exposed samples at 95% of a full switch, the optical contrast of the former is roughly six times that of the latter; meaning that more chemical reactions occur during the same time interval. Finally, though the polymer films respond faster to reduction than to oxidation (a discrepancy commonly encountered for p-dopable ECPs), this reaction is slowed relatively more by irradiation than the corresponding oxidation reactions. An explanation to this would be that the oxidized functional groups caused by exposure impede delocalization of π-electrons, which affects reduction more than oxidation since they are already oxidized.

5.3 Summary and perspectives

This chapter explored several aspects of photochemical degradation of ECPs and established that the majority of 11 ECPs degraded within 5 hours of irradiation. I hypothesized that ECPs can be divided into two groups, depending on the degradation mechanism and stability. Group 1 polymers were believed to degrade by a mechanism where the polymer chains are attacked at terminal positions only, which lead to a linear loss of absorption. For Group 2 polymers, the polymer chains are believed to be attacked at random positions during irradiation, with a logarithmic decrease in the degradation rate as a consequence. Even though the hypothesis is backed up by mathematical models that fit the experimental data well, the hypothesis does not address the reason for the assumed difference in degradation behavior. The relative short lifetime under ambient conditions is insufficient if ECDs are to gain significant commercial importance, and this was addressed by encapsulating the ECPs in oxygen and UV barrier foils. These foils drastically improved the stability, by increasing the lifetime 1300 to 3300 times for group 2 polymers, while degradation was immeasurable for group 1 polymers. It is my belief that the results presented in this chapter are very important for the development of ECDs employing conjugated polymers, as stability issues are commonly explored electrochemically. Future work should address the effects of processing methods and film morphology on photostability.

References

1 J. Jensen, M. V. Madsen and F. C. Krebs, *J. Mater. Chem. C,* 2013, **1,** 4826-4835.

2 T. Tromholt, M. V. Madsen, J. E. Carlé, M. Helgesen and F. C. Krebs, *J. Mater. Chem.,* 2012, **22,** 7592-7601.

3 M. Manceau, J. Gaume, A. Rivaton, J. -L. Gardette, G. Monier and L. Bideux, *Thin Solid Films,* 2010, **518,** 7113-7118.

4 M. V. Madsen, T. Tromholt, A. Böttiger, J. W. Andreasen, K. Norrman and F. C. Krebs, *Polym Degradation Stab,* 2012, **97,** 2412-2417.

5 M. Manceau, E. Bundgaard, J. E. Carlé, O. Hagemann, M. Helgesen, R. Søndergaard, M. Jørgensen and F. C. Krebs, *J. Mater. Chem.,* 2011, **21,** 4132-4141.

6 M. V. Madsen, T. Tromholt, K. Norrman and F. C. Krebs, *Adv. Energy Mater.,* 2013, **3,** 424-427.

7 S. A. Gevorgyan, M. V. Madsen, H. F. Dam, M. Jørgensen, C. J. Fell, K. F. Anderson, B. C. Duck, A. Mescheloff, E. A. Katz, A. Elschner, R. Roesch, H. Hoppe, M. Hermenau, M. Riede and F. C. Krebs, *Sol Energ Mater Sol Cells,* 2013, **116,** 187-196.

8 D. Kockott, *Polym Degradation Stab,* 1989, **25,** 181-208.

9 P. Gijsman, G. Meijers and G. Vitarelli, *Polym. Degrad. Stab.,* 1999, **65,** 433-441.

10 S. H. Hamid and M. B. Amin, *J Appl Polym Sci,* 1995, **55,** 1385-1394.

11 D. E. Duvall, *Polym. Plast. Technol. Eng.,* 1995, **34,** 227-242.

12 J. V. Gulmine, P. R. Janissek, H. M. Heise and L. Akcelrud, *Polym Degradation Stab,* 2003, **79,** 385-397.

5.4 13 M. Day and D. M. Wiles, *J Appl Polym Sci* , 1972, **16**, 191–202,

14 S. Holdcroft, *Macromolecules,* 1991, **24,** 4834-4838.

15 M. S. A. Abdou and S. Holdcroft, *Macromolecules,* 1993, **26,** 2954-2962.

16 M. Koch, R. Nicolaescu and P. V. Kamat, *J. Phys. Chem. C,* 2009, **113,** 11507-11513.

17 M. S. A. Abdou, Z. W. Xie, A. M. Leung and S. Holdcroft, *Synth. Met.,* 1992, **52,** 159-170.

18 M. S. A. Abdou, G. A. Diaz-Guijada, M. I. Arroyo and S. Holdcroft, *Chemistry of Materials,* 1991, **3,** 1003-1006.

19 M. Manceau, A. Rivaton, J. -. Gardette, S. Guillerez and N. Lemaître, *Polym Degradation Stab,* 2009, **94,** 898-907.

20 M. Manceau, A. Rivaton and J. -. Gardette, *Macromol. Rapid Commun.,* 2008, **29,** 1823-1827.

21 H. Hintz, H. -J. Egelhaaf, L. Lüer, J. Hauch, H. Peisert and T. Chassé, *Chem. Mater.,* 2011, **23,** 145-154.

22 H. Hintz, H. -J. Egelhaaf, H. Peisert and T. Chassé, *Polym Degradation Stab,* 2010, **95,** 818-825.

23 C. M. Amb, P. M. Beaujuge and J. R. Reynolds, *Adv Mater,* 2010, **22,** 724-728.

24 A. L. Dyer, M. R. Craig, J. E. Babiarz, K. Kiyak and J. R. Reynolds, *Macromolecules,* 2010, **43,** 4460-4467.

25 B. D. Reeves, C. R. G. Grenier, A. A. Argun, A. Cirpan, T. D. McCarley and J. R. Reynolds, *Macromolecules,* 2004, **37,** 7559-7569.

26 C. M. Amb, J. A. Kerszulis, E. J. Thompson, A. L. Dyer and J. R. Reynolds, *Polym. Chem.,* 2011, **2,** 812-814.

27 P. Shi, C. M. Amb, E. P. Knott, E. J. Thompson, D. Y. Liu, J. Mei, A. L. Dyer and J. R. Reynolds, *Adv Mater,* 2010, **22,** 4949-4953.

28 E. P. Knott, M. R. Craig, D. Y. Liu, J. E. Babiarz, A. L. Dyer and J. R. Reynolds, *J. Mater. Chem.,* 2012, **22,** 4953-4962.

29 C. -G. Wu, M. -I. Lu and P. -F. Tsai, *Macromol. Chem. Phys.,* 2009, **210,** 1851-1855.

30 G. Sonmez, H. B. Sonmez, C. K. F. Shen, R. W. Jost, Y. Rubin and F. Wudl, *Macromolecules,* 2005, **38,** 669-675.

31 J. Jensen, A. L. Dyer, D. E. Shen, F. C. Krebs and J. R. Reynolds, *Advanced Functional Materials,* 2013, **23,** 3728-3737.

32 P. M. Beaujuge, S. Ellinger and J. R. Reynolds, *Nat. Mater.,* 2008, **7,** 795-799.

33 C. -G. Wu, M. -I. Lu, S. -J. Chang and C. -S. Wei, *Adv. Funct. Mater.,* 2007, **17,** 1063-1070.

34 P. M. Beaujuge, C. M. Amb and J. R. Reynolds, *Acc. Chem. Res.,* 2010, **43,** 1396-1407.

35 N. Blouin, A. Michaud, D. Gendron, S. Wakim, E. Blair, R. Neagu-Plesu, M. Belletête, G. Durocher, Y. Tao and M. Leclerc, *J. Am. Chem. Soc.,* 2008, **130,** 732-742.

36 S. Schuller, P. Schilinsky, J. Hauch and C. J. Brabec, *Appl. Phys. A,* 2004, **79,** 37-40.

37 M. Wohlgenannt, X. M. Jiang and Z. V. Vardeny, *Phys. Rev. B Condens. Matter Mater. Phys.,* 2004, **69,** 241204-1-241204-4.

38 Y. Liang and L. Yu, *Acc. Chem. Res.,* 2010, **43,** 1227-1236.

39 J. C. Bijleveld, M. Shahid, J. Gilot, M. M. Wienk and R. A. J. Janssen, *Adv. Funct. Mater.,* 2009, **19,** 3262-3270.

40 Y. Fu and F. Tsai, *Organic Electronics,* 2011, **12,** 179-184.

Chapter 6

6. Photocatalytic conversion of carbon dioxide

6.1 Introduction

This chapter describes the development of a photocatalytic system that utilizes titanium dioxide nanoparticles, coated onto flexible PET foils or glass substrates, for the reduction of carbon dioxide (CO_2). Developing such a system was quite challenging, and this chapter is just as much about the pitfalls encountered in photocatalysis when using flexible foils as carrier substrates, as it is about the reduction of carbon dioxide.
Photocatalysis is a very interesting research subject since it is targeting one of mankind's greatest challenges, namely reducing the carbon dioxide levels in the atmosband of a semiconductor to its conducting band such that it becomes available for reduction of carbon dioxide. By doing so one would be able to produce an energy rich carrier e.g. methane or carbon monoxide and at the same time lower carbon dioxide levels. Traditionally, titanium dioxide has been utilized as the photocatalytic species due to its photochemical stability, ease of synthesis and non-toxicity, but as the wide band gap limits does not match the solar spectrum very well other photocatalyst are gaining importance as well as doping with metal and metal salts.

The experimental work that forms the basis of this chapter was done from August 2010 to May 2010 at DTU with the assistance of Mette Mikkelsen (DTU) who also co-authored the paper "Flexible substrates as basis for carbon dioxide reduction" (appendix 3.5).

6.2 Thermodynamical considerations

The carbon dioxide molecule is linear and has two polar bonds between the electrophilic carbon and the nucleophilic oxygen atoms. Being in its most oxidized state, CO_2 is a rather unreactive molecule, which is mirrored in the large standard enthalpy of formation which is -393 kJ mol^{-1}, see reaction [1].

$C + O_2 \rightarrow O=C=O$ **[1]** **$\Delta H_f^{\theta} = -393\ kJ\ mol^{-1}$**

The stability of the CO_2 molecule requires that a large amount of energy is supplied in order for transformations to occur. The energy requirements for CO_2 reduction vary, depending on the product, as shown for carbon monoxide and methane:

$$CO_2 \rightarrow CO + \tfrac{1}{2} O_2 \quad [2] \qquad \Delta H^o = 283\ kJ \bullet mol^{-1};\ \Delta G^o = 257\ kJ\ mol^{-1}$$

$$CO_2 + H_2O \rightarrow CH_4 + 2O_2 \quad [3] \qquad \Delta H^o = 285\ kJ \bullet mol^{-1};\ \Delta G^o = 237\ kJ\ mol^{-1}$$

For the reaction [2] to occur thermochemically, it needs to be carried out at a minimum of 3075°C ($\Delta G = 0$),[1], and to be energetically viable, the energy should come from a renewable source, such as concentrated solar irradiation.[2]However, such high temperatures are not compatible with the flexile substrate approach that I used, for which only low temperatures (<100°C) are viable. Photocatalysis using transition metal oxide semiconductors is one way of achieving this.

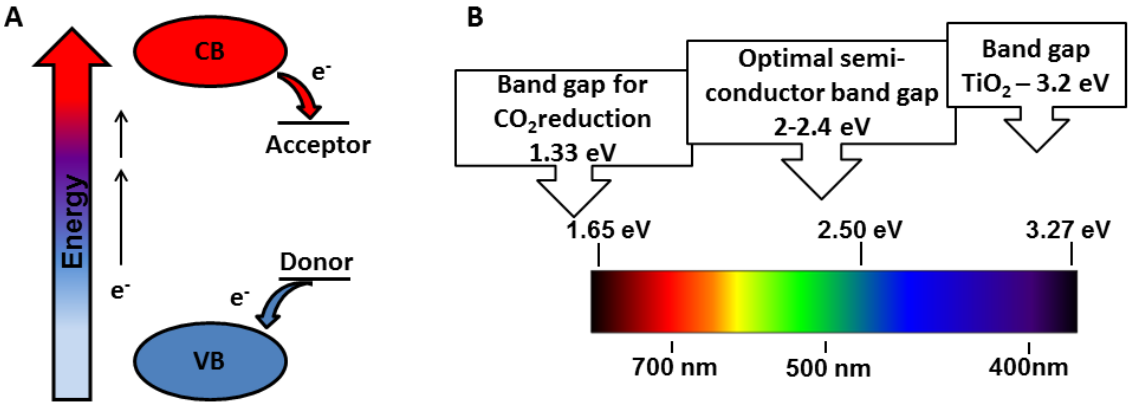

Figure 6-1: Energy levels necessary for photocatalytic reduction (A) Upon solar irradiation an electron is excited from the valence band (VB) to the conducting band (CB), from where it is accessible for reduction of an acceptor molecule (e.g. CO_2). The excitation creates an electron deficiency or "hole" in semiconductor. Simultaneously a donor molecule (e.g. water) donates an electron to the hole completing the catalytic circle. (B) The visible part of the electromagnetic spectrum, showing the wavelength below and photon energies above. The arrows indicate the reduction potential of CO_2, the optimal band gap for practical purposes, and the band gap of TiO_2, respectively.

6.3 Band gap and photocatalytic properties

In carbon dioxide conversion, CO_2 is the acceptor molecule, while compounds such as hydrogen or water act as donor molecules. If reaction [2] is to occur by photocatalysis, the band gap of the photocatalyst should be at least 1.33 eV (per photon), which corresponds to wavelengths below 930 nm (E(eV) = 1240 eV / λ (nm)). Due to entropy changes and other losses associated with reduction of CO_2, the optimal energy required per photon ranges from 2 to 2.4 eV, see Figure 6-1 (B)[3] Of the semiconductors commonly used, titanium dioxide is by far the most well studied. TiO_2 is found in several crystal forms, with anatase and rutile being the forms usually employed for photocatalysis. Due to differences in lattice structures and electronic densities, anatase and rutile have band gaps of 3.20 eV and 3.02 eV, respectively. This corresponds to absorption thresholds of 384 and 410 nm.[4] It is still debated whether or not the band edges of TiO_2 are such that photocatalysis can occur without doping the catalyst, but I found that photocatalytic reduction of CO_2 was possible using unmodified TiO_2.[4-9]

6.4 Carbon dioxide conversion reactors

In order to convert CO_2 into useful products, a suitable reactor needs to be developed. Ideally, the source of CO_2 would come from the atmosphere, but since the amount of CO_2 in the atmosphere is approximately 0.04 %, the available CO_2 for conversion is low. Moreover, the conversion system risks being polluted by other atmospheric compounds. All in all purification of CO_2 must be accomplished before conversion. The carbon capture and sequestration technology commonly used for CO_2 capture today is characterized by high energy consumption for desorption of CO_2, which makes using these technologies for purification of CO_2 in connection with photocatalytic reduction questionable. However, by using CO_2 diffusion selective membranes, extraction from the atmosphere would be possible using a minimum amount of energy.[10, 11]Another solution is to use the Direct Air Capture (DAC) system, where air is cycled through solid alkali sorbents that binds the weak acid CO_2. The concentrated CO_2 becomes available by replacement with water at low temperatures (40-45^{o}C).[12] A schematic for a purification system in combination with a photocatalyst is shown in

Figure 6-2. In Figure 6-2 (A) the conversion agent is coated onto a membrane that selectively allows CO_2 to permeate into the reaction chamber. The other side of the chamber consists of a window that allows sunlight to pass. The energy for conversion is supplied by solar irradiation, and products are recovered as liquid/gaseous energy carriers. A slightly different conversion unit is depicted in Figure 6-2 (B), where CO_2 in a similar way is separated from the atmosphere by a membrane, but differs in that the photocatalyst is coated onto a flexible substrate that also functions as the reactor window.

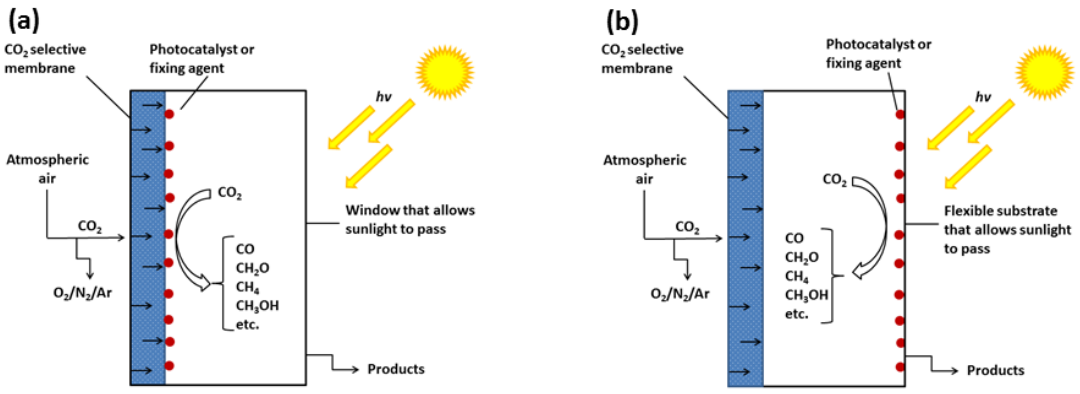

Figure 6-2: Two examples of CO_2 conversion units, that functions by extraction of atmospheric CO_2 using a selective membrane. In (a) the conversion reagent is coated onto the membrane, whereas in (b) it is coated onto a flexible substrate that functions as the reactor window.

In order to convert such a unit into an operational device I addressed the following issues:

- Stability of window substrate
- Photocatalytic efficiency
- Analysis of products

This was done by designing the reactor depicted in Figure 6-3, which comprised a lathed aluminum chamber with a demountable top.[9, 13, 14] Introduction of gaseous components and flushing of the chamber is done through Swagelock™ valves, and variation of the chamber volume was possible using blocks of lathed aluminum (see Figure 6-3 (D). The chamber construction allowed for two modes of usage corresponding

to the situation (a) and (b) in Figure 6-2. By having a coated substrate inside the reactor facing out, and using a window material that allows passage of solar irradiation, conditions like those in Figure 6-2 **(**A) are established. I also tried a more unconventional operational mode, like that schematized in Figure 6-2 (B), by coating the photocatalyst onto a PET foil, that functioned as the front window (photocatalyst facing inwards) (Figure 6-3 (C).

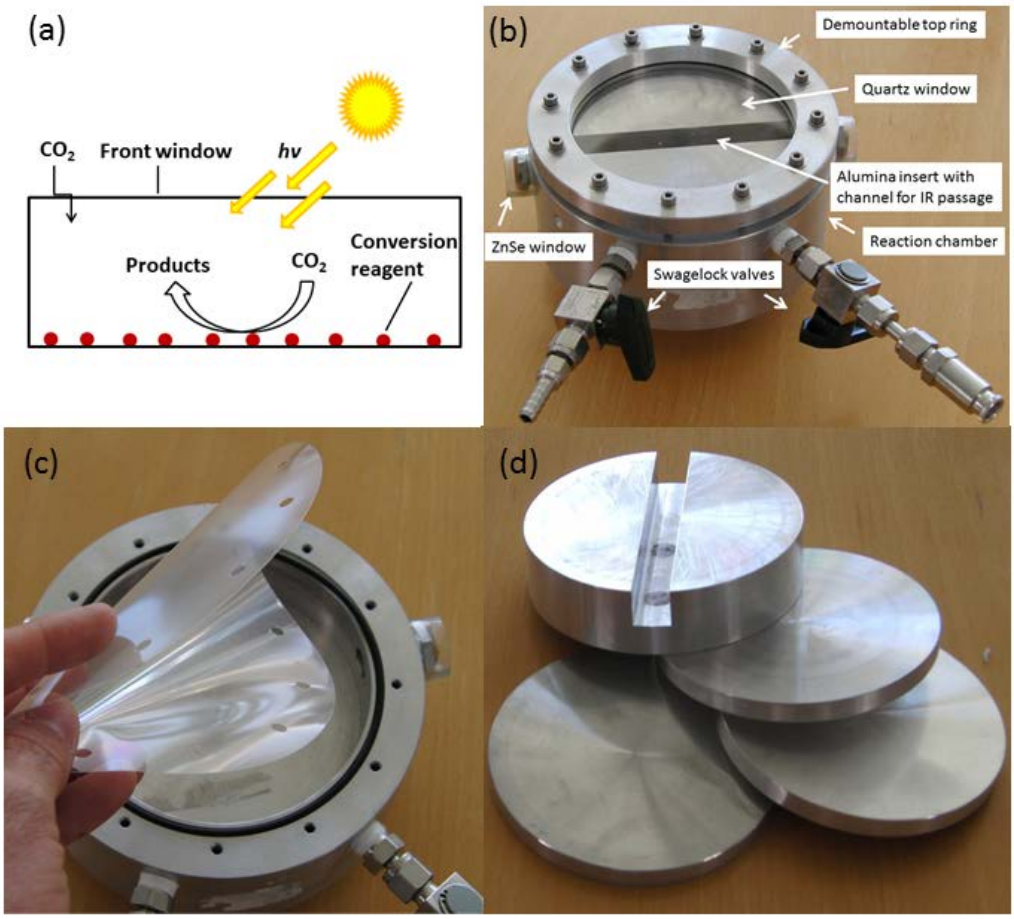

Figure 6-3: (a) Schematic of simple prototype conversion unit. (b) An operational conversion reactor equipped with a quartz window. (c) PET foil to be used as reactor window (d) Alumina inserts allowing variations in reactor volume.

6.4.1 Infrared spectroscopy

Since the reaction products of photocatalytic CO_2 reduction using the reactor are generally gasses, they are detectable by either GC-MS or infrared spectroscopy.[15-17]. I used

the latter, and the reactor design allowed me to do in-situ infrared spectroscopy during irradiation, as the reactor was equipped with zink-selenide windows (see Figure 6-3 (B)). I found IR spectroscopy particularly useful, as it is a non-destructive method that combines chemical fingerprinting with a reasonable sensitivity. As the products of photocatalytic CO_2 reduction are simple molecules like CO, CH_4 and CH_3OH, the identification by IR is straightforward, and I quantified the yields by making standard calibration curves of methane and carbon monoxide (the detection limit of CO was approximately 0.01 % by volume). Table 6-1 shows the major bands of some simple carbon volatiles.[17-22]

Table 6-1: Major infrared bands for simple carbon volatiles. For additional spectral information, the reader is directed to the National Institute of Standards and Technology's Chemistry Webbook.

Compound	Major bands (cm-1)
CO_2	2349
CO	2143
CHO	2850, 2785, 1750, 1485, 1250
CH_3OH	3337, 2934, 2822, 1029, 655
CH_4	3020, 1534, 1305

As will become apparent in the following section, CO_2 and its precursors are widely present, which severely complicates product analysis. In order to verify product composition, I used isotopically labeled $^{13}CO_2$ to distinguish between reaction products originating from introduced carbon dioxide or products due to carbon dioxide from sources such as the flexible substrate, surfactants, catalyst precursor etc.[23, 24] The difference in isotopes results in different IR spectra that can be determined using the harmonic equation. [23] The difference in the IR spectrum due to isotopically substitution for carbon monoxide is shown in Figure 6-4. Spectrum (A) displays the infrared spectrum of ^{12}CO, where the C-O stretching is centered at 2143 cm^{-1}. This vibration has

moved to 2096 cm^{-1} in spectrum (B) that displays ^{13}CO. Spectrum C is a mixture of the two isotopes.[9, 17, 19]

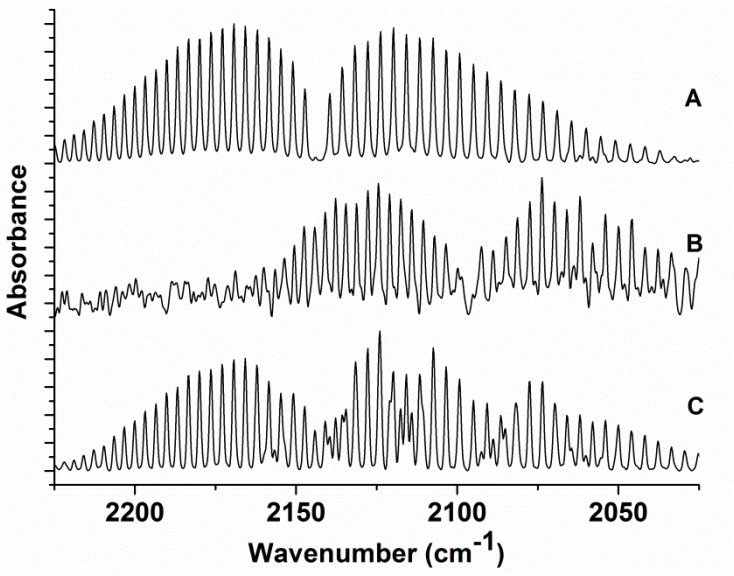

Figure 6-4: infrared absorbance spectra of gaseous carbon monoxide isotopes in argon (1 cm^{-1} resolution). (A) ^{12}CO (B) ^{13}CO (C) A mixture of ^{12}CO and ^{13}CO. Reprinted from ref. 9 Copyright (2011), with permission from Elsevier.

6.5 Flexible substrates as carrier foils

By employing roll-to-roll coating of the photocatalyst onto flexible substrates, large area photocatalytic surfaces can be achieved at high production rates.[25] Standard choices for roll-to-roll substrates are foils made of poly(ethylene terephthalate) (PET), poly(ethylene napthalate) (PEN) and poly(ethylene) (PE); the structures of these three polymer substrates are depicted in Figure 6-5**.**

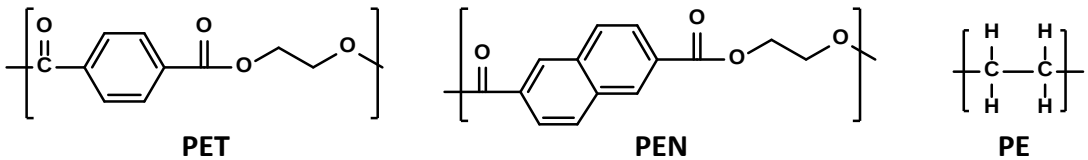

Figure 6-5: Structure of poly(ethylene terephthalate) (PET), poly(ethylene napthalate) (PEN) and poly(ethylene) (PE). The figure shows the repeating unit of the polymeric structure.

While employing flexible substrates is advantageous for large-scale manufacture and processing, there are questions that need to be addressed in order to use these as carrier foils for photochemical conversion of carbon dioxide. An obvious challenge is that polymeric films degrade when exposed to solar irradiation, oxygen and moisture i.e. conditions that are found outdoors where the photocatalytic system is to operate.[26-31] Moreover, as the oxidative degradation products include volatiles such as carbon dioxide and carbon monoxide, employing polymeric substrates for photo conversion of CO_2 could seem like Sisyphus' work.[32-35] In spite of this, polymeric substrates foils remain interesting as carrier foils since it is the total amount of carbon dioxide converted that matter i.e. the amount of reduced carbon dioxide should exceed that of oxidized carbon species released during substrate decomposition. Two other factors support this: (1) Coating of absorbing nanoparticle can in some instances protect the substrate material from solar irradiation. (2) Construction of a system that eliminates the access to atmospheric oxygen. To assess the viability of polymeric substrates and aid in designing reactors for such, I have included a short review of the fundamental degradation processes.

It has been found that photodegradation of polymer substrates is a combination of two reactions; photocatalytic oxidation and photolysis.[32, 35-42] Photolysis is the "direct" cleavage, whereby photo initiated radicals generated in the polymeric substrate lead to cleavage by e.g. a Norrish type I reaction pathway as depicted in Figure 6-7**.** Photooxidation is likewise initiated by radicals generated in the polymer, but differs in that addition of oxygen generate hydroperoxide species that decompose as shown in Figure 6-6 and Figure 6-8 for PE and PET, respectively. Since photooxidation involves molecular oxygen, it should be possible to negate this reaction by employing an oxygen-free atmosphere. However, oxidation of the substrate has been found to occur even when oxygen-free conditions were employed.[13] This puzzling observation was attributed to reduction of TiO_2 or residual substrate oxygen or carbon dioxide, but do in any instance testify to the complexity of these chemical systems and the care that must be taken when evaluating results hereof.

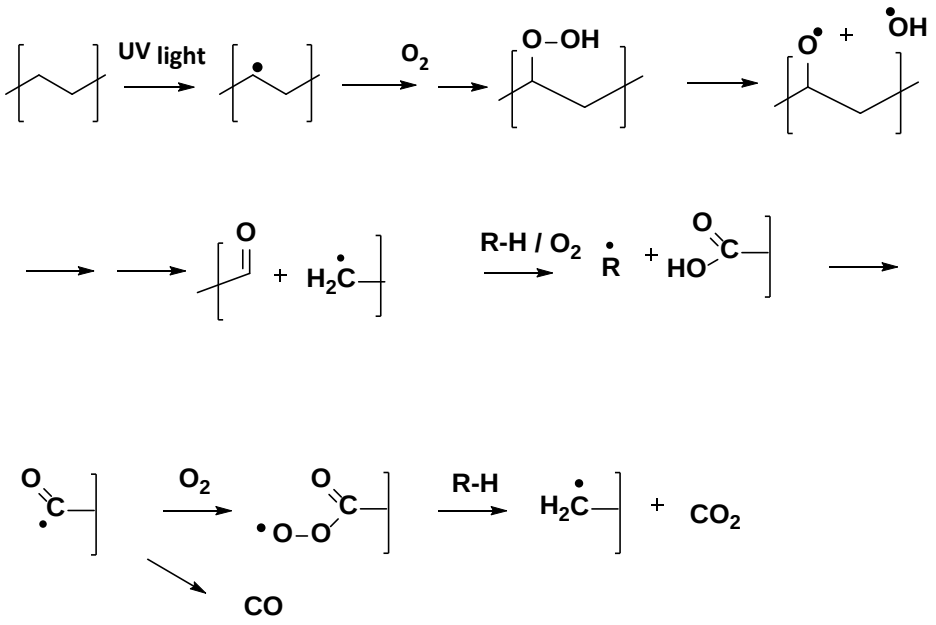

Figure 6-6: Photo oxidation of polyolefins. Reactive intermediates are generated on the surface of the substrate by UV irradiation. This is followed by addition of oxygen and proton abstraction to yield hydroperoxide species that decompose to carbonyl compounds and alkyl radicals. The alkyl radicals react further with oxygen to generate carbonyl radicals that decompose to CO or CO_2 via another sequence of oxygen addition and proton abstraction.

Due to the difference in chemical composition of polyolefins (PE, PP etc.) and polyesters (PET, PBT etc.), the predominant degradation mechanism differs. Though multiple pathways might occur simultaneously, the predominant reaction for irradiated polyolefins in an oxygen-containing atmosphere is photocatalytic oxidation. This is due to the absence of chromophoric groups capable of absorbing energy from terrestrial sunlight (>290nm), which results in insufficient energy for direct bond cleavage. However, light absorbing chromophores are found to develop in the films during processing and storage of polyolefins, which could generate of active intermediates on the surface. These react with oxygen and decompose as shown in Figure 6-6.[38] Since PET and related polyesters contain chromophoric groups as part of their molecular structure (aromatic and ester groups), they are capable of absorbing high energy irradiation, which make them susceptible to direct photolytic cleavage that can proceed via Norrish type I or II pathways as illustrated in Figure 6-7.[29, 32, 35-37]

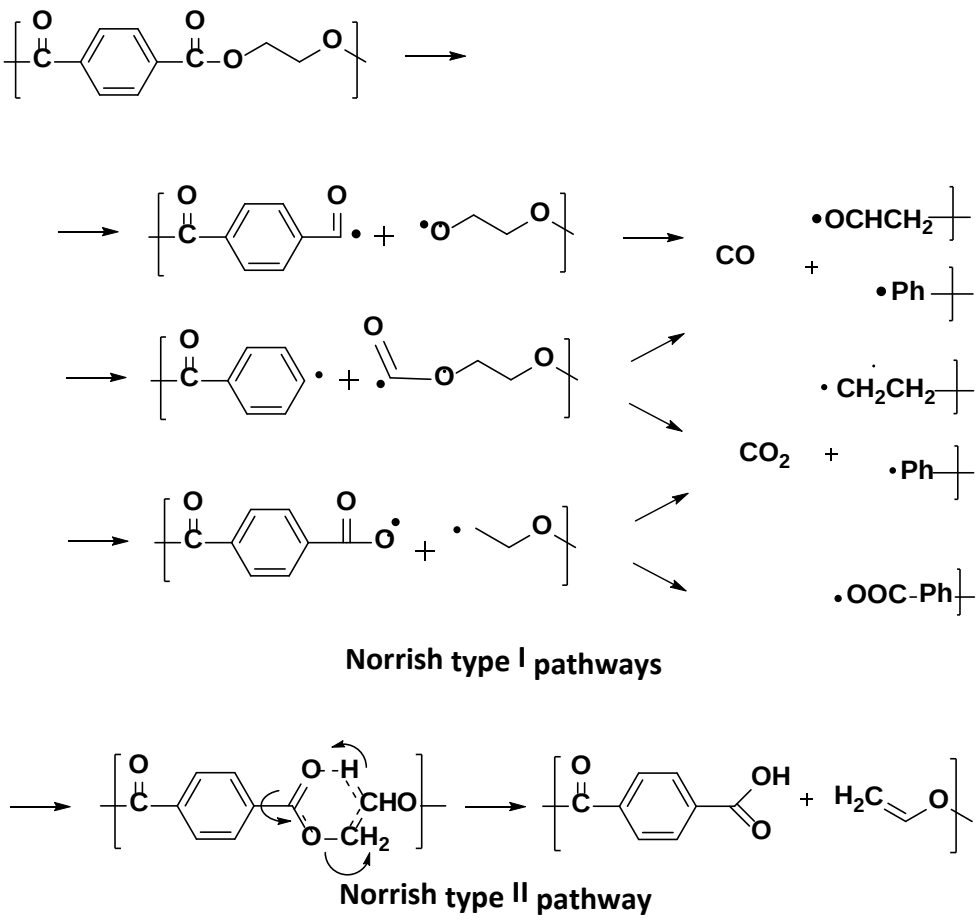

Figure 6-7: Photolytic pathways for PET and related polyester substrates.

While the photolytic cleavage is the predominant mechanism in PET and related polyesters, photooxidative decomposition is also observed analogous to that seen for polyolefins. Radical species, capable of reaction with oxygen, are produced in the surface by irradiation. This yields hydroperoxide species that decompose to various products including carbon dioxide as shown in Figure 6-8.[13, 35, 43, 44]

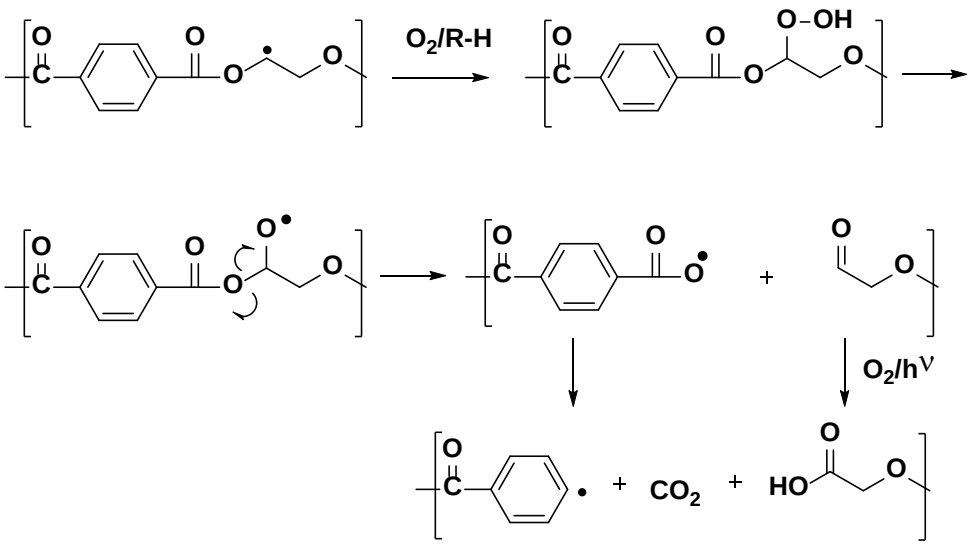

Figure 6-8: Photocatalytic oxidation mechanism of PET and related polyesters

6.6 Effect of TiO_2 coatings

Chemical species on the substrate surface have been found to alter the photo and thermal stability, albeit the results of such coatings are ambiguous. On one hand, TiO_2 can attenuate decomposition and protect the substrate by scattering and absorbing UV irradiation. On the other hand, TiO_2 has been exploited in environmental management such as wastewater treatment and self-cleaning surfaces where it functions by photooxidizing organic molecules; a process that could enhance degradation in the substrate.[45-48] The former situation is depicted in Figure 6-9 (A), the latter in Figure 6-9 (B).

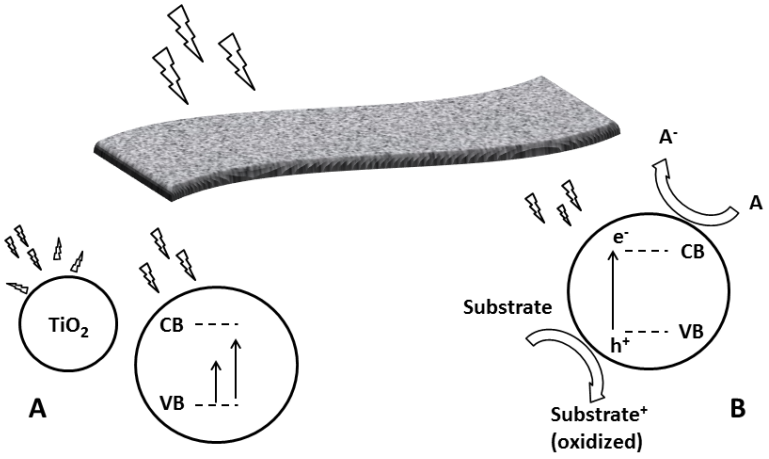

Figure 6-9: Effect of TiO_2 nanoparticles on flexible substrates during irradiation. When flexible substrates are subjected to irradiation (top), the coated particles can affect the substrate in two ways: (A) Protect the substrate by scattering the irradiation or absorb irradiation without electron excitation. (B) Enhance photooxidation whereby the substrate donates electrons to the acceptor photocatalyst.

The effect of TiO_2 has been studied in some detail for paint (where TiO_2 is used as a filler/pigment) and films containing TiO_2. Results from these studies show that the effect depends on the crystal form of the oxide. Rutile TiO_2 contain stable OH groups on the surface and hence stabilize the substrate, whereas the anatase form of TiO_2 is reactive and consequently enhance photooxidation.[13, 49-51] Adding to the complexity, commercially available flexible substrates contain various stabilizers, additives and surfactants that might interact with TiO_2 and either enhance photooxidation or protection. Whether one or the other will prevail must be determined experimentally.

In order to successfully convert small-scale laboratory experiments into large-scale photocatalytic systems, the atmosphere composition must be taken into account. Prior to operation, the amount of evolved CO_2 must be measured if flexible substrates are used as carrier foils. This is best done under CO_2-free conditions to be as reliable as possible, but at the same time, the atmosphere should mimic the operational conditions as closely as possible. The operational conditions depend on the reactor, and the concentration of CO_2 employed. But factors such as temperature and pressure are also of importance as described.

6.7 Adsorption of carbon containing volatiles

Using all quartz reactors is possible for small-scale reactors, but scaling these quickly becomes problematic, which is why most photocatalysis reactors consist of a metal chamber with a window. What might not be so obvious is that the gaseous components have the ability to adsorb onto the chamber surface and herby complicate the analysis of the products, when desorbing at a later stage. I observed this as isotopically labeled $^{13}CO_2$ and ^{13}CO were detected in the reaction chamber that was devoid of any catalyst and after flushing with pure hydrogen gas and subsequent UV illumination. As $^{13}CO_2$ was not introduced, I believe that it stems from earlier experiments performed in the reaction chamber. As the chamber is made of aluminum, a likely explanation is that alumina and aluminum hydroxides were formed on the reactor surface due to the reaction conditions (water vapor, oxygen and light), and that these adsorbed CO_2 and CO for later desorption.[13, 52-55] The complete desorption of carbon dioxide from alumina has been shown to take place at around 200^{o}C for mesoporous alumina and γ-alumina.[56-58] To prevent unwanted carbon-oxygen species on the chamber surface, I used a prolonged flushing procedure that consisted of heating the chamber to 65^{o}C for 60 min, flushing with hydrogen for 10 minutes and followed by evaporation at reduced pressure; and repeating the procedure twice.

6.8 Surfactants and carbonaceous residues

Inorganic photocatalysts usually require organic surfactants in order to meet the solubility requirement solution processing. In addition the surfactants ensure the correct growth of the metal oxide nanoparticles and suppress aggregation, agglomeration and precipitation.[59-61] The list of surfactants is extensive, but a few examples are given in figure 4.[62-64]

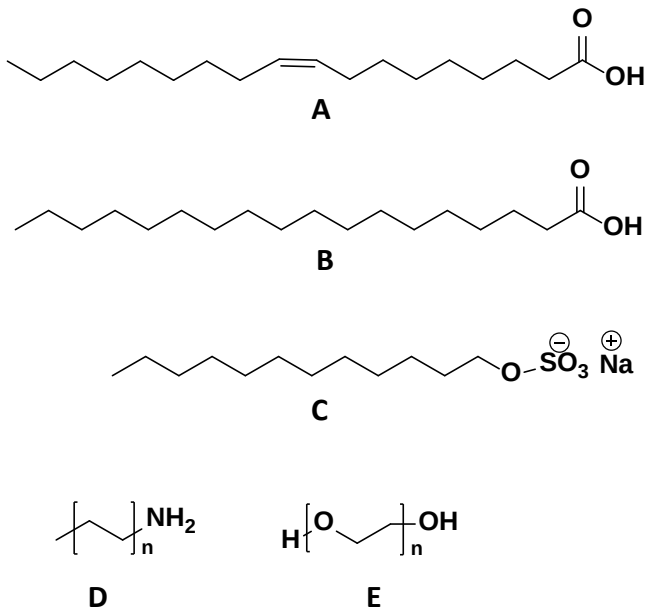

Figure 6-10 - Surfactants used for stabilization of photocatalyst nanoparticles. (A) Oleic acid (B) Stearic acid (C) Sodium dodecyl sulfate (D) Primary alkyl amines (E) Polyethylene glycol

Of particular interest when working with flexible substrates, is the removal of surfactants at low temperatures. As I used oleic acid as surfactant during synthesis of TiO_2 nanorods, I explored if the photo oxidative abilities of TiO_2 could be used to decompose oleic acid.[47, 65-68] This was done by subjecting oleic acid capped TiO_2 nanoparticles to UV irradiation while monitoring the photooxidative process by IR. Figure 6-11 shows the infrared spectra of TiO_2 nanoparticles in a KBr pellet during irradiation (1200 Wm^{-1}). The characteristic bands of oleic acid capped TiO_2 at 2924, 2852, 1523 and 1433 cm^{-1} are shown in spectrum A. Spectra B, C, and D show the IR spectra after 60, 120 and 360 minutes of UV light, respectively. As seen from Figure 6-11, the removal of oleic acid by UV light at low temperatures is a viable process. The disappearance of the characteristic bands after a relatively short while (~60 min), leaves a broad band centered at 3433 cm^{-1} and one at 1626 cm^{-1}. The former is attributed to water adsorbed on titanium or hydroxyl-groups on titanium; the latter is attributed to adsorbed water onto KBr.[69, 70]

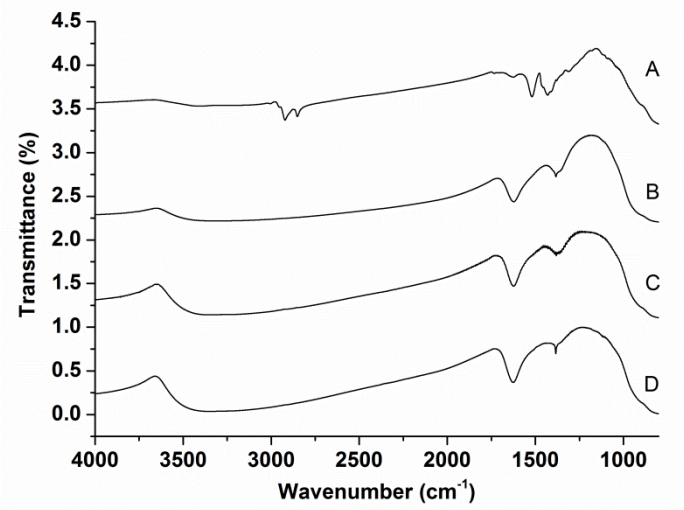

Figure 6-11: Infrared **analysis of the removal of oleic acid by UV-light. (A) Oleic acid capped TiO_2 particles prior to irradiation. (B-D)Sample following 60, 120 and 360 min of irradiation respectively. Reprinted from ref. 9 Copyright (2011), with permission from Elsevier.**

Whether thermal or photocatalytic procedures are employed to decompose the surfactant group, it is important to realize the presence of carbonaceous residues on the catalyst surface following surfactant decomposition.[71] For oleic acid thermally decomposed in air, infrared analysis show absorption bands in the carbonyl region (2200 cm^{-1}, 2259 cm^{-1} and 2330 cm^{-1}), suggesting that the leftover residues are CO_x complexes.[72] In addition to the oxygen containing species, amorphous carbon/graphite residues are formed when the decomposition takes place in an argon atmosphere, and alkane residues are believed to adsorb on the metal oxide surface beneath this graphite shell. The presence of carbon containing species should be noted as they contribute to the complexity in analyzing the product mixture.

6.9 Photocatalytic efficiency

Although the initial plan was to use flexible foils as carrier substrates, the photocatalytic efficiency was assessed in a set-up similar to Figure 6-2 (A). TiO_2 catalyst was coated onto laboratory glass slides and irradiated through a quartz window (a detailed description is found in the experimental section). Prior to irradiation, a reference experiment was conducted in the dark that did not show any conversion of $^{13}CO_2$ and only a

slight increase in $^{12}CO_2$, but no trace of ^{12}CO.The catalytic performance was monitored by measuring the increasing absorbance of isotopically labeled carbon species formed (notably ^{13}CO).

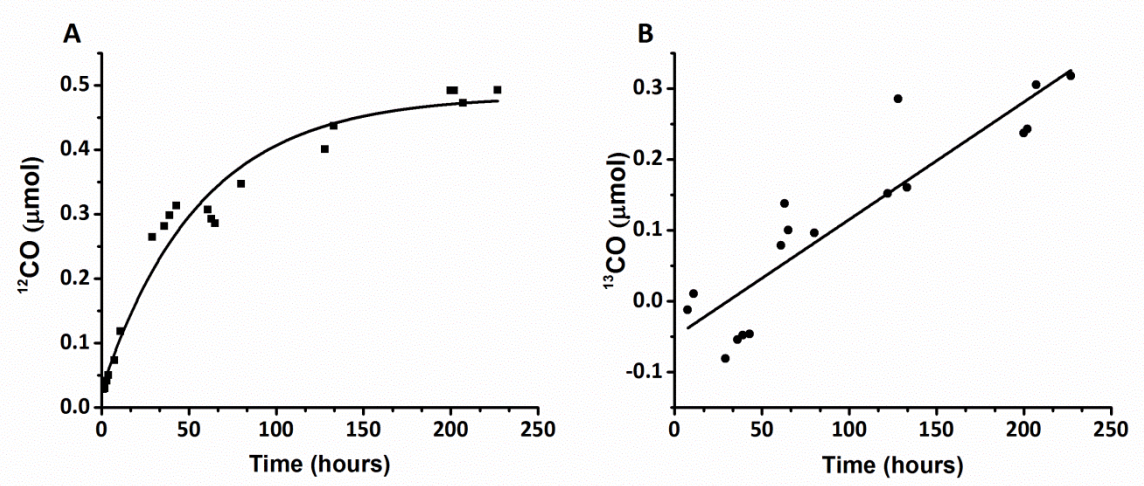

Figure 6-12: Photocatalytic conversion measured by IR spectroscopy. (A) ^{12}CO content in the photo reactor during irradiation (fitted line R^2=0.96). (B) ^{13}CO content in the photo reactor during irradiation. The observed values are based on standard curves. Reprinted from ref. 9 Copyright (2011), with permission from Elsevier.

Figure 6-12 shows the development of the ^{12}CO (A) and ^{13}CO (B) content in the chamber during irradiation of the photocatalyst. Following 0.5 hour of illumination, a band corresponding to $^{12}CO_2$ was observed (2361 cm^{-1}) with only minor fluctuations in the concentration throughout the experiment. After 1 hour of illumination, the formation of gaseous ^{12}CO was observed (2183 cm^{-1}), and both of these observations are interesting as no $^{12}CO_2$ was introduced into the reaction vessel. After 130 hours of illumination, the peak height at 2183 cm^{-1} corresponded to approximately 0,074 % (0.19 µmole) of the chamber volume being ^{12}CO.

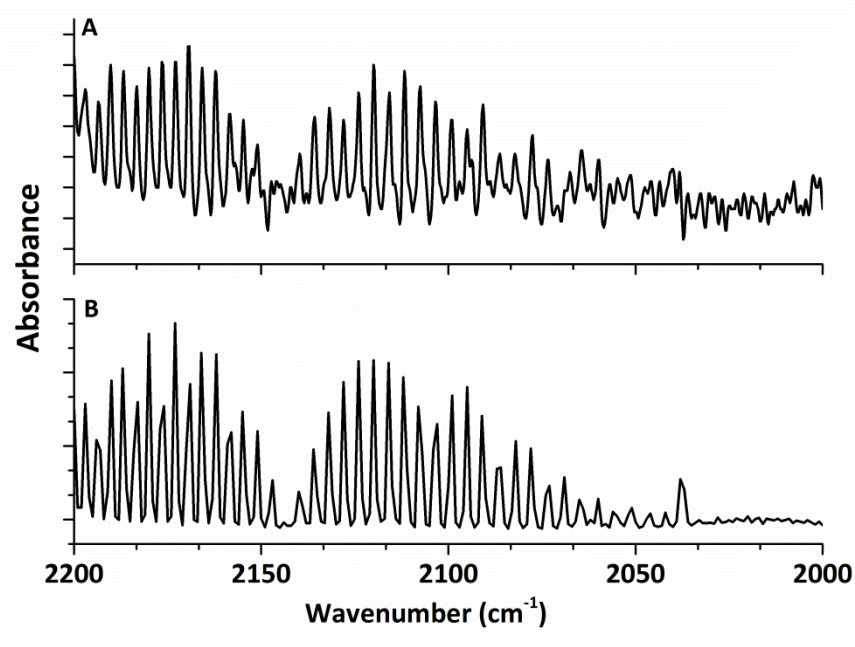

Figure 6-13: IR spectra of the 2200-2000 cm^{-1} region following (A) 2 hours and (B) 63 hours of irradiation.

After 2 hours, the formation of ^{13}CO is vaguely visible in the spectrum as indicated by the IR pattern, which becomes clearly visible further on in the experiment (compare Figure 6-13 (A) and Figure 6-4 (C)). The amount of ^{13}CO was found to increase during the first 11 hours of illumination, after which the characteristic ^{12}CO-^{13}CO motif disappears. This situation was observed for 50 hours, after which ^{13}CO was observed again as shown in Figure 6-13 (B). These observations might be caused by several simultaneously occurring reactions. A hypothesis is that during the first hours of illumination, two reactions could take place simultaneously – the photocatalytic reduction of $^{13}CO_2$ and the UV induced release of $^{12}CO_2$ due to carbonaceous residues on the catalyst, which is subsequently photocatalytically converted to ^{12}CO. This would explain the occurrence and development of peaks in the IR spectrum during the first hours of irradiation. After 11 hours a third reaction is presumed to take place. This is the release of carbon-oxygen containing species from deeper within the catalyst, which is activated due to the prolonged UV exposure. This saturates the catalyst surface, thereby excluding $^{13}CO_2$ from the catalytic sites and henceforth photocatalytic reduction. As the concentration of ^{12}CO increased, it obscures the detection of the small amount of the ^{13}C

isotope. After this amount of $^{12}CO_2$ has been converted, the catalyst returns to an equilibrium state, converting both $^{12}CO_2$ and $^{13}CO_2$. The content of ^{13}CO was found to increase with time at a rate of 0.0019 μmol h^{-1} during the experiment, but due to large fluctuations in the observed concentration it is not clear if the increase is linear or exponential. The catalytic efficiency for converting $^{13}CO_2$ into ^{13}CO was found to be 0.0013 μmol h^{-1} g^{-1}(catalyst).

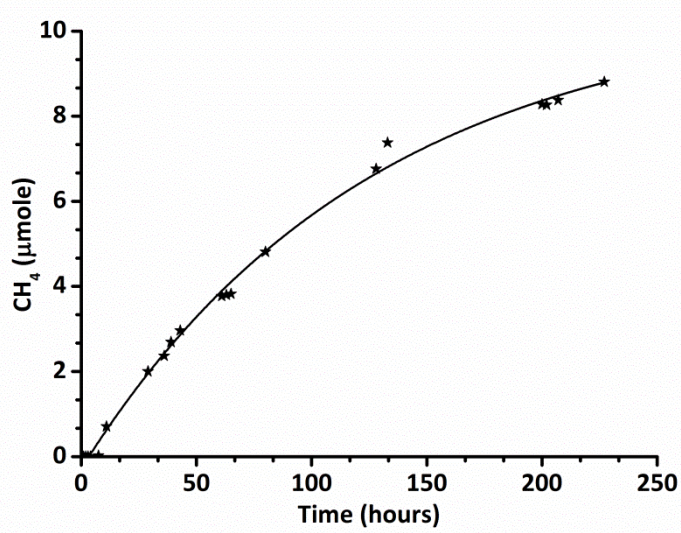

Figure 6-14: $^{12}CH_4$ content in the photo reactor during irradiation. The line is a fitted exponential function (R^2 = 0.99). Reprinted from ref. 9 Copyright (2011), with permission from Elsevier.

Figure 6-14 shows the formation of methane which was observed after 4 hours of illumination. By comparing the peak heights at 3017 and 1306 with standard curves for methane in the chamber, the concentration of methane was found to be 2.6%, which equals 6.7 μmole following 130 hours of irradiation, corresponding to a catalytic efficiency of 0.36 μmole h^{-1} g^{-1} catalyst. It should be noted that the peaks centered around 3017 and 1306 cm^{-1} correspond to $^{12}CH_4$. This implies that the methane cannot be a product of $^{13}CO_2$, and it is therefore likely a product other of carbon-oxygen species in the reaction chamber.

As seen from Figure 6-12, the ratio of ^{12}CO to ^{13}CO in the reaction chamber is approximately 2:1, which corresponds well with the detection of ^{12}CO and ^{13}CO after 1 and 2 hours respectively. The difference in ratio might be that ^{12}CO is the reduction product

of carbon containing species already adsorbed on the catalyst surface, which might favor their reduction compared to the gaseous $^{13}CO_2$. Yang et al. suggests that the observed CO species are the products of a reverse Bourdard reaction (eq. [4]) and a water induced photocatalytic surface carbon gasification (eq. [5]), with the latter being the predominant, as seen from a 1:6 ratio of ^{13}CO to ^{12}CO in that study.[23]

$^{13}CO_2$ + "^{12}C" → ^{13}CO + ^{12}CO **[4]**

H_2O + "^{12}C" → ^{12}CO + H_2 **[5]**

It cannot be ruled out that these reactions influenced my product composition, but as the observed ratio between the two CO isotopes is different (1:2 compared to 1:6), these are not the only reactions. As hydrogen gas is part of the reactant mixture, the gasification reaction might be suppressed by counteracting the disturbed equilibrium. The presence of H_2 in the reaction chamber makes the formation of methane achievable, though it is puzzling that solely $^{12}CH_4$ is observed as both isotopes were present. Methane must then be formed via other reaction pathways that does not include desorption/adsorption of gaseous CO_2 or CO.

6.9.1 Energy considerations and area requirements

In order to put photocatalysis into perspective, I have investigated the energy and area requirements necessary to address the challenges associated with the increased emission of CO_2. This is done in relation to equation [6] ($\Delta H_f^{\theta}(CO)$ = -110.53 kJ mol^{-1}; $\Delta H_f^{\theta}(CO_2)$ = -393.52 kJ mol^{-1}).

$CO_2 \rightarrow CO + ½\ O_2$ **[6]** **$\Delta H = 282.99 kJ\ mol^{-1}$**

The solar energy available at the surface of the earth is around 1000 W m^{-2} (AM 1.5G), which is 3600 kJ m^{-2} h^{-1}. If the solar energy impinging on a 1 square meter surface solely went into reaction [6], it would convert 12.72 mole carbon dioxide pr. hour equal of 560 g CO_2 pr. hour. As the amount of solar irradiation ranges from 1000-2000 hours pr.

year depending on local conditions, a conversion rate between 560 and 1120 kg m^{-2} $year^{-1}$ should be expected. If 2000 hours of sunlight pr. year is assumed, the required area is 21.4 x 10^9 m^2 = 21400 km^2 in order to match the annual man-made emissions of 24 gigaton (24 x 10^{12} kg). This is a large but manageable area (Denmark is approximately 43000 km^2). With catalytic performance of 0.1-1 %, the required area would be correspondingly larger, but compared to the globally available land mass of 1.5 x 10^8 km² with 20-30% being estimated as desserts, it is not an unrealistic scenario.

For the system presented in this chapter (looking solely at the photocatalytic conversion of $^{13}CO_2$ and assuming 2000 h of sunlight pr. year) the conversion rate of CO_2 to CO is 0.34 μmol m^{-2} h^{-1} or 680 μmol m^{-2} $year^{-1}$. These numbers are based on an irradiance of 500 W m^{-2} for wavelengths below 320 nm (the catalyst only absorbs wave length below 320 nm), but as natural sunlight is intended to supply the energy, the difference in spectral distribution has to be taken into account. The irradiance from natural sunlight below 320 nm is 1.56 W m^{-2}, which is a 320 fold reduction compared to the UV lamp. This means that under natural sunlight, the conversion of CO_2 to CO can be done at a rate of 2.1 μmol m^{-2} $year^{-1}$. If this energy is recovered by combustion of CO, one would be able to generate 0.6 J m^{-2} $year^{-1}$.

6.10 Summary and perspectives

The considerations in the preceding section highlight that even though photocatalytic reduction of CO_2 is a promising way of fighting the increasing content of atmospheric carbon dioxide, several issues must be addressed that relate to the challenges associated with going from the laboratory to the industrial scale.

The photocatalyst must be abundant, cheap and chemically stable. These qualities are found in TiO_2, possibly modified with dopants. But catalyst preparation is an issue that receives limited attention in connection with energy usage. Most catalytic species requires annealing at high temperatures for several hours to form an active crystal phase – an energy costly process that has to be repaid by catalytic action or carried out by using renewable energy e.g. concentrated sunlight in solar ovens. The price of manufacturing catalysts on a very large scale is also challenging, especially if doping with

expensive metals such as platinum is required. Construction of huge photocatalytic reactors is yet another challenge. Most reports are on laboratory-size reactors, but this is very far from what is needed as are the conditions under which tests are made. Depositing photocatalytic species onto large areas is an issue that is connected to the reactor size. In this chapter I have outlined the possibilities and difficulties in using flexible substrates as a solution. Flexible substrates can be coated with photocatalyst at a considerable rate and show promise to be compatible with membranes for carbon dioxide extraction. Unfortunately, both CO and CO_2 are formed in varying concentrations during the UV degradation of the flexible films in quantities that for now exceed the capability of the catalytic system. These findings suggest that the foils need to be protected from photolytic degradation.

As this chapter illustrates, the adsorption-desorption of CO_2 from reactor surfaces, porous catalysts, foils etc. complicates the interpretation of experimental results and elucidation of the mechanism. By using isotopically labeled gasses, the photocatalytic reduction of introduced CO_2 (by some referred to as true photocatalysis) can be distinguished from reactions where the carbon source originates from adsorbed gasses or carbon containing precursors,[23] although it can be argued that any converted species is proof of photocatalysis. Finally, the photocatalytic efficiency has to be increased, and to broaden the catalyst absorption into the visible region of the electromagnetic spectrum seems like a viable approach if catalysts are to achieve conversion factors that, as a start, match the energy input used for their manufacture.

References

1 L. R. Martin, *Sol. Energy,* 1980, **24,** 271-277.

2 A. J. Traynor and R. J. Jensen, *Ind Eng Chem Res,* 2002, **41,** 1935-1939.

3 O. K. Varghese and C. A. Grimes, *Sol Energ Mater Sol Cells,* 2008, **92,** 374-384.

4 O. Carp, C. L. Huisman and A. Reller, *Prog Solid State Chem,* 2004, **32,** 33-177.

5 C. -C. Lo, C. -H. Hung, C. -S. Yuan and J. -F. Wu, *Sol Energ Mater Sol Cells,* 2007, **91,** 1765-1774.

6 S. C. Roy, O. K. Varghese, M. Paulose and C. A. Grimes, *Acs Nano,* 2010, **4,** 1259-1278.

7 T. -V. Nguyen and J. C. S. Wu, *Sol Energ Mater Sol Cells,* 2008, **92,** 864-872.

8 A. L. Linsebigler, G. Q. Lu and J. T. Yates, *Chem. Rev.,* 1995, **95,** 735-758.

9 J. Jensen, M. Mikkelsen and F. C. Krebs, *Sol Energ Mater Sol Cells,* 2011, **95,** 2949-2958.

10 L. Deng and M. -B. Hägg, *J. Membr. Sci.,* 2010, **363,** 295-301.

11 A. Nishimura, N. Komatsu, G. Mitsui, M. Hirota and E. Hu, *Catal Today,* 2009, **148,** 341-349.

12 R. K. Derichter, T. Ming and S. Caillol, *Renewable Sustainable Energy Rev,* 2013, **19,** 82-106.

13 C. Jin, P. A. Christensen, T. A. Egerton, E. J. Lawson and J. R. White, *Polym Degradation Stab,* 2006, **91,** 1086-1096.

14 A. J. Robinson, J. R. Searle and D. A. Worsley, *Mater. Sci. Technol.,* 2004, **20,** 1041-1048.

15 J. Hong, W. Zhang, J. Ren and R. Xu, *Anal. Methods,* 2013, **5,** 1086-1097.

16 W. Su, X. Fu, K. Wei, H. Zhang, H. Lin, X. Wang and D. Li, *Guang Pu Xue Yu Guang Pu Fen Xi,* 2001, **21,** 34.

17 N. Ulagappan and H. Frei, *Journal of Physical Chemistry a,* 2000, **104,** 7834-7839.

18 L. Fredin, B. Nelander and G. Ribbegård, *J. Mol. Spectrosc.,* 1974, **53,** 410-416.

19 J. Mascetti and M. Tranquille, *J. Phys. Chem.,* 1988, **92,** 2177-2184.

20 D. E. Burch and D. Williams, *Applied Optics,* 1962, **1,** 587-594.

21 M. Falk and E. Whalley, *J. Chem. Phys.,* 1961, **34,** 1554-1568.

22 B. Nelander, *J. Chem. Phys.,* 1980, **72,** 77-84.

23 C. -C. Yang, Y. -H. Yu, B. Van Der Linden, J. C. S. Wu and G. Mul, *J. Am. Chem. Soc.,* 2010, **132,** 8398-8406.

24 W. Lin, H. Han and H. Frei, *J Phys Chem B,* 2004, **108,** 18269-18273.

25 F. C. Krebs, S. A. Gevorgyan and J. Alstrup, *J. Mater. Chem.,* 2009, **19,** 5442-5451.

26 P. Gijsman, G. Meijers and G. Vitarelli, *Polym. Degrad. Stab.,* 1999, **65,** 433-441.

27 J. V. Gulmine, P. R. Janissek, H. M. Heise and L. Akcelrud, *Polym Degradation Stab,* 2003, **79,** 385-397.

28 S. H. Hamid and M. B. Amin, *J Appl Polym Sci,* 1995, **55,** 1385-1394.

29 M. Day and D. M. Wiles, 1972, *J Appl Polym Sci,* 1972, **16**, 191–202

30 M. Day and D. M. Wiles, 1972, *J Appl Polym Sci,* 1972, **16**, 175-189

31 D. Kockott, *Polym Degradation Stab,* 1989, **25,** 181-208.

32 M. Day and D. M. Wiles, 1972, .

33 J. -L. Philippart, F. Posada and J. -L. Gardette, *Polym Degradation Stab,* 1995, **49,** 285-290.

34 S. S. Fernando, P. A. Christensen, T. A. Egerton, R. Eveson, S. M. Martins-Franchetti, D. Voisin and J. R. White, *Mater. Sci. Technol.,* 2009, **25,** 549-555.

35 T. Grossetete, A. Rivaton, J. L. Gardette, C. E. Hoyle, M. Ziemer, D. R. Fagerburg and H. Clauberg, *Polymer,* 2000, **41,** 3541-3554.

36 G. J. M. Fechine, R. M. Souto-Maior and M. S. Rabello, *J Appl Polym Sci,* 2007, **104,** 51-57.

37 C. R. Hurley and G. J. Leggett, *ACS Appl Mater Interfaces,* 2009, **1,** 1688-1697.

38 C. H. Chew, L. M. Gan and G. Scott, *Eur Polym J,* 1977, **13,** 361-364.

39 P. Gijsman and A. Dozeman, *Polym Degradation Stab,* 1996, **53,** 45-50.

40 L. Costa, M. P. Luda and L. Trossarelli, *Polym Degradation Stab,* 1997, **58,** 41-54.

41 J. Lacoste, Y. Deslandes, P. Black and D. J. Carlsson, *Polym Degradation Stab,* 1995, **49,** 21-28.

42 R. Arnaud, J. -Y. Moisan and J. Lemaire, *Macromolecules,* 1984, **17,** 332-336.

43 A. Rivaton, *Polym Degradation Stab,* 1993, **41,** 297-310.

44 A. Rivaton, *Polym Degradation Stab,* 1993, **41,** 283-296.

45 M. N. Chong, B. Jin, C. W. K. Chow and C. Saint, *Water Res.,* 2010, **44,** 2997-3027.

46 A. Fujishima, X. Zhang and D. A. Tryk, *Surf Sci Rep,* 2008, **63,** 515-582.

47 I. P. Parkin and R. G. Palgrave, *J. Mater. Chem.,* 2005, **15,** 1689-1695.

48 D. Hufschmidt, L. Liu, V. Selzer and D. Bahnemann, *Water Sci. Technol.,* 2004, **49,** 135-140.

49 N. S. Allen, M. Edge, T. Corrales and F. Catalina, *Polym Degradation Stab,* 1998, **61,** 139-149.

50 G. J. M. Fechine, M. S. Rabello and R. M. Souto-Maior, *Polym Degradation Stab,* 2002, **75,** 153-159.

51 N. S. Allen, H. Khatami and F. Thompson, *Eur Polym J,* 1992, **28,** 817-822.

52 N. D. Parkyns, *Journal of the Chemical Society A: Inorganic, Physical, and Theoretical Chemistry,* 1967, 1910-1913.

53 C. -F. Mao and M. A. s. Vannice, *Appl. Catal. A Gen.,* 1994, **111,** 151-173.

54 K. L. I. Kobayashi, Y. Shiraki and Y. Katayama, *Surf. Sci.,* 1978, **77,** 449-457.

55 Y. Shiraki, K. L. I. Kobayashi and Y. Katayama, *Surf. Sci.,* 1978, **77,** 458-464.

56 C. Chen and W. -S. Ahn, *Chem. Eng. J.,* 2011, **166,** 646-651.

57 C. Morterra and G. Magnacca, *Catal Today,* 1996, **27,** 497-532.

58 Z. Zhou, T. Zeng, Z. Cheng and W. Yuan, *Ind Eng Chem Res,* 2011, **50,** 883-890.

59 P. D. Cozzoli, A. Kornowski and H. Weller, *J. Am. Chem. Soc.,* 2003, **125,** 14539-14548.

60 J. Kehres, J. W. Andreasen, F. C. Krebs, A. M. Molenbroek, I. Chorkendorff and T. Vegge, *Journal of Applied Crystallography,* 2010, **43,** 1400.

61 L. M. Bronstein, X. Huang, J. Retrum, A. Schmucker, M. Pink, B. D. Stein and B. Dragnea, *Chem. Mater.,* 2007, **19,** 3624-3632.

62 Z. Li and Y. Zhu, *Appl. Surf. Sci.,* 2003, **211,** 315-320.

63 X. Shi, R. Rosa and A. Lazzeri, *Langmuir,* 2010, **26,** 8474-8482.

64 A. L. Willis, N. J. Turro and S. O'Brien, *Chem. Mater.,* 2005, **17,** 5970-5975.

65 M. Gohin, E. Allain, N. Chemin, I. Maurin, T. Gacoin and J. -. Boilot, *J. Photochem. Photobiol. A Chem.,* 2010, **216,** 142-148.

66 Q. Kuai, H. -Q. Ye and Y. Gao, *Fenmo Yejin Cailiao Kexue Yu Gongcheng,* 2010, **15,** 283-287.

67 J. Rathouský, V. Kalousek, M. Kolář, J. Jirkovský and P. Barták, *Catal Today,* 2011, **161,** 202-208.

68 H. J. Harwood, *Chem. Rev.,* 1962, **62,** 99-154.

69 K. S. Kang, Y. Chen, K. H. Yoo, N. Jyoti and J. Kim, *Journal of Physical Chemistry C,* 2009, **113,** 19753-19755.

70 B. Hao, Y. Li and S. Wang, *Adv. Mater. Res.,* 2010, **129-131,** 154-158.

71 A. R. Pradhan, J. F. Wu, S. J. Jong, T. C. Tsai and S. B. Liu, *Appl Catal A Gen,* 1997, **165,** 489-497.

72 P. Roonasi and A. Holmgren, *Appl. Surf. Sci.,* 2009, **255,** 5891-5895.

Chapter 7

7. Photocatalytic water splitting

7.1 Introduction

This chapter describes the concept of photocatalytic water splitting (PWS) and the experiments I have conducted in order initiate this field of research in the Solar Energy section. As I did not did succeed in splitting water by photocatalysis it can be debated whether my trials should be present in a Ph.D. dissertation. However, I feel that even though positive results are currently lacking, this chapter serve to illustrate my thoughts on how to proceed from this stage and as such the chapter is a window on work in progress.

Photocatalytic water splitting is similar to photocatalytic carbon dioxide reduction in that the energy in solar radiation is transferred through a catalyst to a water molecule whereby it is reduced and oxidized to hydrogen and oxygen respectively. The differences between water splitting and CO_2 reduction has been outlined in chapter 1, but one also note that in water splitting, water serves as both donor and acceptor species. The main challenge in PWS as well as in CO_2 reduction is developing a photocatalyst that absorbs a substantial amount of the solar radiation while being able to produce the required potential. In addition the catalyst should be cheap and show extended stability. Currently, covering as much of the solar spectrum as possible are being pursued using Fe based photocatast's and dye- sensitized solar cells; in effect a sensitized-dye-sensitized solar cell[1-3]**.** As these devices are series-connected the voltage requirements to each photon harvesting system is lowered as it is the sum of applied potentials that drives the electrolytic reaction. Another approach to achieve a better correlation between solar irradiation and catalyst absorption was through by controlled combustion of TiO_2, whereby carbon substituted some of the lattice oxygen atoms which extended the absorption.[4]

My approach to photocatalytic water splitting was through synthesis of hematite (α-Fe_2O_3) a cheap abundant photocatalyst that has been shown to possess the right properties for PWS.[5] To compensate for the shortcomings of this photocatalyst with regards to band alignment and overpotentials, an OPV module were supposed to be connected to the photocatalytic system and thus provide the voltage sufficient for PWS.

7.2 Thermodynamic considerations

Water is split electrolytically by the simultaneous reduction of H^+ and oxidation of OH^- following reaction scheme [1]:

$2H_2O \rightarrow 2\ H_2 + O_2$ **[1]**

Reaction [1] is the sum of the two half cells reactions [2] and [3] (here balanced by acid). In reaction [2] electrons from the negatively charged cathode reacts with hydronium ions and hydrogen gas (H_2) is produced. In reaction [3] oxidation of water produces electrons and oxygen gas, as electrons are supplied to the anode:

$2\ H_3O^+ + 2\ e^- \rightarrow 2H_2O + H_2$ [2] – reduction $E^o_{red} = 0.0$ V

$6\ H_2O \rightarrow O_2 + 4\ H_3O^+ + 4\ e^-$ [3] – oxidation $E^o_{ox} = -1.23$ V

If the half reactions are balanced by base the reactions are:

$4\ H_2O + 4\ e^- \rightarrow 2\ H_2 + 4\ OH^-$ [4] - reduction

$4\ OH^- \rightarrow O_2 + 2\ H_2O + 4\ e^-$ [5] - oxidation

The cell potential for watersplitting is given by $E_{cell} = E^o_{ox} + E^o_{red} = -1.23$ V**.** As $\Delta G^o = -n\ F\ E^o_{cell}$ (n = moles of electrons, F = Faraday constant) a negative cell potential means the Gibbs free energy is positive, and hence the reaction is thermodynamically unfavorable, and energy has to be supplied in order for the reaction to occur. Although 1.23 V is the thermodynamical requirements for water splitting, in practice 1.5 to 2 V are used, where the difference in potential is due to overpotentials.[6]

7.2.1 Half-cell potentials and dependence of pH

As the cell potential is given by $E_{cell} = E^{o}_{ox} + E^{o}_{red}$ it is appropriate to review how these are calculated and how pH differences in the half cells affects the cell potential.

The half-cell potential is given by:

$E_{halfcell} = E^{o}_{halfcell} - RT/nF \ln Q$

Where R is the gas constant, T the temperature and Q the reaction coeffecient = $p(H_2)/([H_3O^+]^2$; n is moles of electrons in the redox process = 2. This can be written as:

$E_{halfcell} = E^{o}_{halfcell} - (0.0059\ V/n) \log Q \Leftrightarrow E_{halfcell} = E^{o}_{halfcell} + (0.0059\ V/2) \log 1/Q \Leftrightarrow$

$E_{halfcell} = E^{o}_{halfcell} + (0.0059\ V/2) \log [H_3O^+]^2 \Leftrightarrow E_{halfcell} = E^{o}_{halfcell} + (0.0059\ V/2) \log [H_3O^+]^2$

$\Leftrightarrow E_{halfcell} = E^{0}_{halfcell} + (0.0059\ V/n)\ 2 \log [H_3O^+]$

$E_{halfcell} = E^{o}_{halfcell} + (0.0059\ V/2)\ 2\ (-pH) \Leftrightarrow$

$E_{halfcell} = E^{o}_{halfcell} - 0.0059\ V\ pH$

For the two half-cell reactions in water splitting:

$E_{H3O+/H2} = 0\ V - 0.059\ V\ pH$

$E_{O2/H20} = 1.23\ V - 0.059\ V\ pH$ (for reduction)

This implies that increasing the pH value favors the oxidation of water and formation of oxygen (O_2), while lowering the pH favors reduction of water and formation hydrogen (H_2). The total cell potential is not changed if the two compartments have the same pH value. The cell potential can be increased by a chemical bias in two separate half cells each with a high and low pH value, and while this would increase the cell potential, maintaining a pH difference requires continuous supplying of acids and bases, which require energy to manufacture.[7, 8]

7.3 Reactor design

The configuration of a photocatalytic water splitting system naturally depends on the materials that are used.[8] Additional voltage is usually required if a single photosystem configuration is employed, to compensate for overpotentials and band edges that does not cover the water splitting potentials. This extra bias can be externally supplied (i.e. from the grid) or it can come from an internal source such as a photovoltaic module or a dye-sensitized solar cell (DSSC).

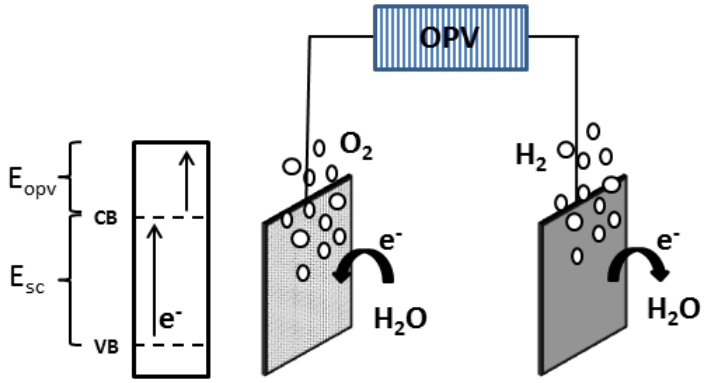

Figure 7-1: A photocatalytic system comprising a n-type photocatalyst in combination with an OPV. The energy diagram to the left depicts the energy provided by the semiconductor (E_{sc}) and the energy provided by the OPV (E_{opv}) required for water splitting.

Figure 7-1 depicts the approach that my experiments were based on: An n-type semiconductor is connected in series to an OPV module that supplies the extra bias required for watersplitting. For optimal efficiency in a photovoltaic-photo electrode system it is required that maximum current density is found for the device and not by maximizing the OPV and photo electrode system.[3]

The photoreactor that was used for these experiments are depicted in Figure 7-2, and is an example of an H type reactor. The reactor comprised of two vertical stainless steel tubes connected by a horizontal Teflon tube. The stainless steel tubes contain outlets for gas sampling when the reactor is sealed. Sealing the reactor is done by screwing a quartz glass against a gasket in the housing. It is noted that the some hydrogen gas and oxygen gas will dissolve in the aqueous electrolyte. The photo electrode and the counter platinum electrode are clamped to electrode connector and connection to the electrodes on the inside of the reactor is done via a ceramic bushing. This setup is not the most efficient concerning light harvesting, as a configuration where each photosystem is placed on top of each other will result in a higher solar to hydrogen (STH) or applied bias photon-to-current (ABPE) efficiency due to the smaller area when employing such a tandem set-up.[3, 7]

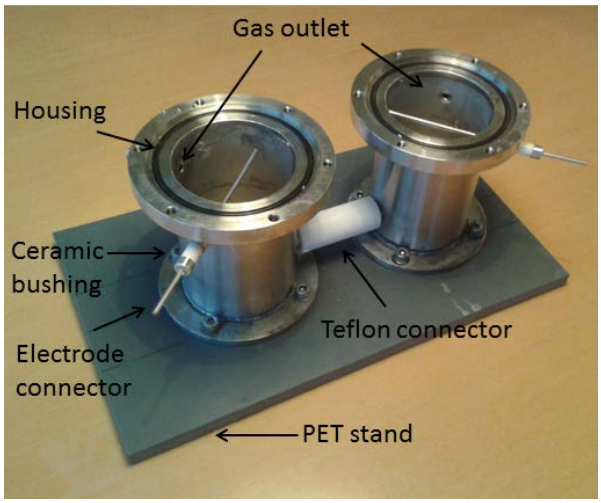

Figure 7-2: H-type photoreactor. The two chambers a made of stainless steel connected by a Teflon tube. The reactor can be sealed by screwing quartz glass against a gasket in the housing (glass not shown).

7.4 Hematite synthesis

As a starting point for a suitable photocatalyst I choose to explore hematite, the α-phase of Fe_2O_3, as this several favorable qualities. Primarily it has a narrow band gap (2.1 eV, see figure 1.3 chapter 1) which means that it absorbs wavelength of 590 nm, and below. Secondly it is abundant and hence cheap. The one thing that discourages the use of hematite is the position of the CB, which is slightly lower in energy than the reduction potential of the H_2/H_2O couple. This means that using hematite as photo-catalyst requires additional voltage or doping with other species to for a photocatalytic effect.[9, 10] Fe_2O_3 nanoparticles can be prepared by a multitude of methods relying on the thermal decomposition of iron containing precursors.[11-14] I explored two solution-based methods were $FeCl_3$ was used as the precursor, as shown by equation [1] [7, 11, 15, 16]

$$FeCl_3 + H_2O \rightarrow FeOOH \rightarrow Fe_2O_3 \qquad [1]$$

Hydrolyzing $FeCl_3$ produces iron oxyhydroxide, which on annealing undergoes a phase transformation to α-Fe_2O_3. Of the two crystal phases of Fe_2O_3, the α-phase is the one

found to be photocatalytic active, while the γ-phase amongst other things are used in ferrofluids, for gas sensors and color imaging.[17]

Unmodified α-Fe_2O_3 was chosen as the target compound, even though reports show that doping shows a substantial effect on the photocurrent. But as I wanted to familiarize myself with the synthesis and characterization of α-Fe_2O_3 nanoparticles, I thought it wiser to begin with a system that was as simple as possible. The limited efficiency of undoped α-Fe_2O_3 photoanodes has been the short diffusion length of charge carriers, which means that only the holes generated in close proximity to the electrolyte interface can oxidize water.[10, 18, 19]) This is problematic since the light penetration depth in α-Fe_2O_3 is in the order of 100 nm.[20]

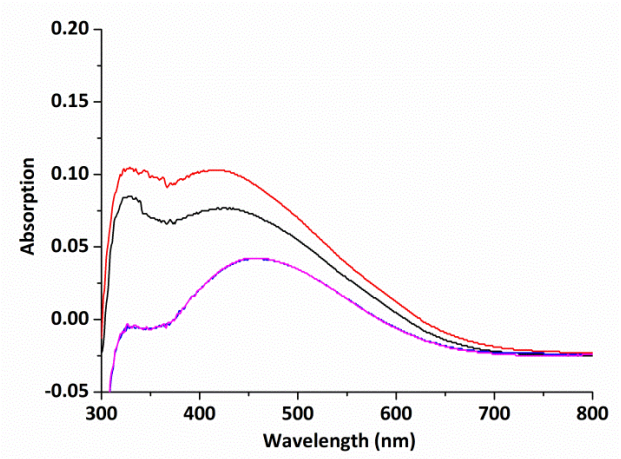

Figure 7-3: UV-vis spectra of hematite on ITO glass. The hematite was grown onto ITO from an ethanol/$FeCl_3$ solution.

In the first synthesis Fe_2O were grown on ITO glass by heating the substrate in a solution of $FeCl_3$ in ethanol at 100° for 24 hours followed by annealing of the rinsed substrates at 500°C for 3.5 hours.[15] Prior to annealing, the substrate was a faint yellow color, which changed to a more pronounced yellow-orange after annealing. The spectra in Figure 7-3 corresponds well with literature spectra, although the absorption is low. However it turned out that the substrate was non-conductive following this process, even though the ITO substrates had been positioned in the capped flask such that it was not entirely covered. The cause of this remains elusive, but optical microscopy suggested that the ITO layer was covered.

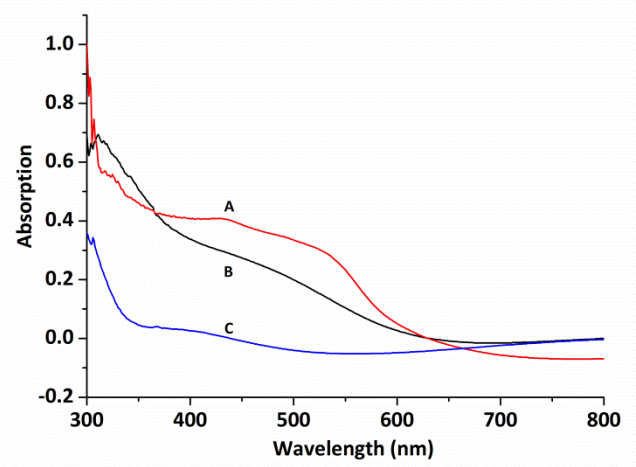

Figure 7-4: UV-vis spectra of hematite on ITO glass. The hematite was deposited onto ITO by succeeding deposition-annealing cycles from an ethanol/$FeCl_3$ solution, which is shown in (B). Spectrum (A) shows the absorption following final annealing at 500°C. Trace (C) shows the absorption of ITO glass following annealing.

The second synthetic method involved deposition of a $FeCl_3$/ethanol solution onto an ITO substrate followed by annealing on a hot plate (300°C).[16] This procedure was repeated for 10-15 times, where by the thickness of the oxide layer could be controlled. Following deposition the substrate was annealed at 500°C. The samples show increased absorption as seen in Figure 7-4, and as the conductivity was maintained the samples were made in photo electrodes by connecting a wire to the substrate using silver paste and sealing the connection with epoxy as shown

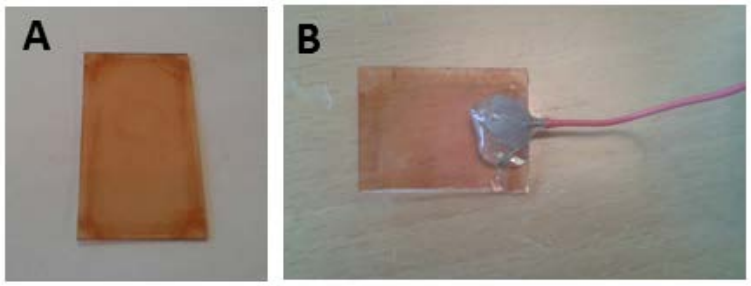

Figure 7-5: Hematite photo electrodes. (A) Shows the ITO substrate covered by 10 deposition-annealing steps and final annealing at 500°C. (B) Shows a photo electrode (2.25 cm^2) made from (A). The wire is connected by a silver paste and the connection sealed with epoxy.

The photo electrodes (15 in total) were tested in the reactor shown in Figure 7-2, in a 1 M NaOH solution with a platinum cathode. The potential range from -1 V to 4 V was scanned in the dark and following the experiment was repeated with the reactor placed under the solar simulator (AM 1.5 G). However exposure to solar radiation did not affect any changes in I-V profile. The reason for this is currently unknown, but two issues should be addressed: The UV-vis spectra indicate that Fe_2O_3 is formed, but the crystal phase has not been determined. This should be done by X-ray powder diffraction. Another important issue is the particle size, which should be established by scanning electron microscopy (SEM).

7.5 Summary and perspectives

This chapter shows that although PWS is conceptually simple, the practical employment of photo electrodes is not trivial. I chose Fe_2O_3 as a catalyst due to the apparent simplicity of its synthesis, the band gap, abundance, and stability. Although these initial trials did result in photocatalytic water splitting, I gained practical experience in synthesis and deposition of Fe_2O_3. The next step in the process is to determine crustal phase and size of the Fe_2O_3 particles. When photocatalytic action is obtained, the long term stability of the catalyst should be to address and furthermore monolithic device comprising an OPV could be explored.

References

1 J. H. Park and A. J. Bard, *Electrochem Solid State Letters,* 2006, **9,** E5-E8.

2 M. Grätzel, *Nature,* 2001, **414,** 338-344.

3 M. S. Prévot and K. Sivula, *J. Phys. Chem. C,* 2013, **117,** 17879-17893.

4 S. U. M. Khan, M. Al-Shahry and W. B. Ingler Jr., *Science,* 2002, **297,** 2243-2245.

5 J. A. Glasscock, P. R. F. Barnes, I. C. Plumb, A. Bendavid and P. J. Martin, *Proceedings of SPIE - the International Society for Optical Engineering,* 2006, **6340,** .

6 S. Dutta, D. L. Block and R. L. Port, *Int J Hydrogen Energy,* 1990, **15,** 387-395.

7 Z. Chen, T. F. Jaramillo, T. G. Deutsch, A. Kleiman-Shwarsctein, A. J. Forman, N. Gaillard, R. Garland, K. Takanabe, C. Heske, M. Sunkara, E. W. McFarland, K. Domen, E. L. Milled and H. N. Dinh, *J. Mater. Res.,* 2010, **25,** 3-16.

8 L. J. Minggu, W. R. Wan Daud and M. B. Kassim, *Int J Hydrogen Energy,* 2010, **35,** 5233-5244.

9 C. X. Kronawitter, S. S. Mao and B. R. Antoun, *Appl. Phys. Lett.,* 2011, **98,** .

10 S. Shen, J. Jiang, P. Guo, C. X. Kronawitter, S. S. Mao and L. Guo, *Nano Energy,* 2012, **1,** 732-741.

11 G. Wu, X. Tan, G. Li and C. Hu, *J Alloys Compd,* 2010, **504,** 371-376.

12 L. Vayssieres, N. Beermann, S. -. Lindquist and A. Hagfeldt, *Chem. Mater.,* 2001, **13,** 233-235.

13 K. Deshpande, A. Mukasyan and A. Varma, *Chem. Mater.,* 2004, **16,** 4896-4904.

14 S. U. M. Khan and J. Akikusa, *J Phys Chem B,* 1999, **103,** 7184-7189.

15 S. Shen, J. Jiang, P. Guo and L. Guo, *Int. J. Photoenergy,* 2013, **2013,** .

16 G. Wang, Y. Ling, D. A. Wheeler, K. E. N. George, K. Horsley, C. Heske, J. Z. Zhang and Y. Li, *Nano Lett.,* 2011, **11,** 3503-3509.

17 L. C. Varanda, M. Jafelicci Jr. and G. F. Goya, *J Magn Magn Mater,* 2001, **226-230,** 1933-1935.

18 A. Kay, I. Cesar and M. Grätzel, *J. Am. Chem. Soc.,* 2006, **128,** 15714-15721.

19 O. Khaselev and J. A. Turner, *Science,* 1998, **280,** 425-427.

20 R. F. G. Gardner, F. Sweett and D. W. Tanner, *J Phys Chem Solids,* 1963, **24,** 1183-1186,IN1-IN2,1187-1196.

Chapter 8

8. Experimental

8.1 Instrumentation

^{1}H and ^{13}C NMR spectra were recorded on a Gemini 300 FT-NMR or on a BRÜKER 250 or 500 MHz.

IR spectroscopy was performed on an IRAffinity-1 from Shimadzu or a Spectrum One from Perkin-Elmer. The IR spectra were obtained using either Attenuated Total Reflectance (ATR) technique on the pure solids or transmission/a IR on polymer films spin-cast onto KBr pellets.

UV-vis spectroscopy was done using a Pharma Spec UV-1700 from Shimadzu or a Cary 5000 model UV-Vis-NIR from Agilent

Film thickness was measured on a Dektak 3030 from Veeco Instruments Inc. scanning 500 μm with a stylus force of 0.05mN.

Slot-die coating was performed on a small-scale roll coater.[1]

Spray coating was done using an airbrush Badger Crescendo 175

Spin coating was performed on a Laurell WS-400-6NPP spin-coater

Electrochemical analysis was performed using a Princeton Applied Research (PAR) model 273A Potentiostat/Galvanostat

Colorimetry studies were performed using a Minolta Chromameter CS-100 colorimeter with a GraphicLite LiteGuard II standard D50 light source illuminating the sample from behind. The light source and the sample to be measured were placed in a color viewing booth. The interior of the light booth is coated with a standard gray neutral 8 (GTI Graphic Technology Inc.) matte latex enamel (equivalent to Munsell N8) to allow for accurate assessment of color of the sample during measurement. These values were subsequently used to calculate L*a*b* values

A Keithley 2440 Sourcemeter were used for switching the devices, and custom made software was used for logging data.

8.2 Experimental - chapter 3

The electrochromic materials were the conjugated electroactive polymers, poly((2,2-bis(2-ethylhexyloxymethyl)-propylene-1,3-dioxy)-3,4-thiophene-2,5-diyl) (PProDOT-$(CH_2OEtHx)_2$; *ECP-magenta,* 76 kDa) and poly(N-octadecyl-(propylene-1,3-dioxy)-3,4-pyrrole-2,5-diyl) (PProDOP-N-$C_{18}H_{37;}$ *MCCP*, 56 kDa).

Chloroform solutions of 5 mg/ml and 20 mg/ml were used for spray coating and spin coating respectively, whereas the concentration used for slot-die coating varied between 20-40 mg/ml. All the inks had a tetrabutylammonium-hexafluorophosphate content of 4 % (wt).

Electrolyte solutions: *Solution A* was a mixture of PMMA (4,4g; M_n 80 kDa), tetrabutylammonium-hexafluorophosphate ($TBAPF_6$) (2 g) and propylene carbonate (40 ml). The suspension was stirred at 100^o until the PMMA was completely dissolved (3-4 hours). To this was added a UV curable binder mixture comprising of Ebecryl® 150 (44 g), Ebecryl® 116 (3,5 g), BCPK (2,5 g) and Zonyl-100 (1,5 g). A typical electrolyte:binder solution was a 2:1 mixture, which was mixed well and sonicated before use.

The electrolyte was partly cured using a UV lamp ((Osram, HTT 150-211). The temperature under the lamp was 35 ± 5^{o}C.

Solution B was a slight modification of the procedure described elsewhere.[2] Methyl methacrylate (MMA) and ethylglycol dimethacrylate (EGDMA) were purified by distillation and degassed before use. Benzoylperoxide was recrystalised from chloroform/methanol before use. MMA (0,02 mol), EGDTA (2 mol%) and 1-ethyl-2-methyl-imidazolium-bis(triflourumethane sulfonyl)imide (EMITFSI) (0,02 mol) were mixed in a round bottomed flask and BPO (0,5 mol%) was added. A condenser was added, and the solution stirred at 85^{o}C for 4 hours, after which acetonitrile (10 ml) was

added. Further stirring (12 hours) at 85^{0}C yielded a slight yellow viscous solution that was used without further purification.

Foils for slot die coating:

The foil came prepared with a 175 µm sputtered ITO layer, etched into stripes of 4 or 13 mm with a nominal sheet resistivity of 100 Ω sq^{-1}. The foils were cleaned with isopropanol prior to coating and lengths of 1 m were coated at a time and with a coating width of 50 mm.

Foils for spincoating

The substrate PET foils came fully covered with a sputtered ITO with a nominal sheet resistivity of 30 Ω sq^{-1}. To ensure even films, the flexible substrate was attached to a glass microscope slide prior to spinning.

ECD assembly: The ECDs were assembled manually due to the adhesiveness of the electrolyte. After coating of the various layers, 1 cm of ITO was carefully made available for electrical contact by removing the polymer and electrolyte layer with isopropanol. The two films were assembled perpendicular to each other. After assembly, the device was run through a laminator effectively sealing the device.

Demonstrator assembly: The demonstrator circuitry was prepared by printing silver lines using sheet fed screen printing of a silver paste (Dupont 5007E) onto an optically clear polyester foil with a thickness of 130 microns that was cured at 140^{o}C for 10 min. A graphite paste was subsequently printed over the areas of the switch, and the material again cured at 140^{o}C for 10 min. MP467 from 3M was used as the pressure sensitive adhesive.

Indoor testing was done using a Steuernagel solar simulator with an Osram 1200 W metal halide arc lamp providing an approximate AM1.5G spectrum with an intensity of 1000 W m^{-2}.

8.3 Experimental - chapter 4

Monomer synthesis:

(3,4-dihydro-2H-thieno[3,4-b][1,4]dioxepine-3,3-yl)bis(methylene)bis(2-methyl-acrylate) :

A dry 250 ml round-bottomed flask was charged with anhydrous DMF (100 ml) in which ProDOT(CH_2Br_2) (5.0g; 14,6 mmol) was dissolved. To this solution was added methacrylic acid (3.75g; 43.8 mmol) and K_2CO_3 (7.3g; 52.8 mmol). A condenser was attached, and the frothing solution was stirred under argon at 100^oC for 21 hours, by which TLC (10% EtOAc in hexane) confirmed conversion of starting material. The solution was allowed to cool and water (150 ml) was added. The solution was extracted with DCM (3 x 100 ml), and the combined organic phases were washed with brine (2 x 100 ml). The organic phase was dried using $MgSO_4$ and concentrated in vacuo yielding a yellow-brownish oil. The crude compound was purified by Dry Column Vacuum Chromatography (DCVC) using EtOAc in hexane as the eluent (0 to 50%) in 50ml fractions.[3] The pure compound appeared as a white solid with a blue hue. Yield 2.35g (45%): mp 49-50^oC ^1H NMR (300 MHz, $CDCl_3$): δ ppm 6.46 (s, 2H); 6.09 (s, 2H); 5.58 (s, 2H); 4.28 (s, 4H); 4.06 (s, 4H); 1.93 (s, 6H). ^{13}C NMR (300 MHz, DMSO-d_6): 166.6, 149.5, 136.9, 127.9, 106.7, 72.6, 63.0, 46.2, 18.4; EIMS (*m/z* (%)): 352.1 (80) [M^+], 353.1 (20) [M^+ + H], 83 (40); calc.: 352.098; found: 352.097.

Polymer synthesis:

Poly(3,3-bis(((2-ethylhexyl)oxy)methyl)-3,4-dihydro-2H-thieno[3,4-][1,4]dioxepine) - co(3,4-dihydro-2H-thieno[3,4-b][1,4]dioxepine-3,3-yl)bis(methylene)bis(2-methylacrylate)

Copolymers with various amounts of bis-methacrylate monomer were synthesized by varying the amount of individual monomers in the reaction mixture. In a typical synthesis, a total of 2.8 mmol of monomers were added to a 50 ml round bottomed flask and dissolved in ethyl acetate (15ml). The solution was bubbled thoroughly with argon for 60 min while stirred. The flask was placed in a water bath (20^oC). $FeCl_3$ (anhydrous) (14 mmol, 2.2g, 5eq) was added to a small beaker of ethyl acetate (5ml) and bubbled with argon for 1 min. The resulting yellow solution was added by syringe in one portion to the monomer solution resulting in an immediate color change to dark green/blue. The reaction flask was covered in foil and the water bath removed after 5 min. During the polymerization the reaction mixture was continuously bubbled with

argon and stirred. The reaction was considered complete when the mixture was black and almost solid (around 3h). The viscous dark mixture was poured into MeOH (200ml) and stirred for 60 min. Hereafter, it was filtered and the residue washed with MeOH until the filtrate was clear. The solid was dissolved in toluene (200ml) and reduced with hydrazine (THF solution) until the resulting solution became bright purple (around 0.25ml). The mixture was transferred to a separatory funnel and washed twice with water (2 x 200ml). The organic phase was concentrated in vacuo, precipitated in MeOH (200ml) while stirred and filtered. The precipitate was Soxhlet extracted with MeOH (24h), hexanes (24h) and $CHCl_3$ (24h). The $CHCl_3$ fraction was concentrated in vacuo and reprecipitated in MeOH (200ml). The solution was filtered and the solid dried under vacuum for 24 hours yielding a magenta colored solid. For yield and composition see Table 1.

Gel-Permeation Chromatography (GPC) was performed at 35 °C in THF to determine molecular weight(s). A combination of a Waters HPLC pump 1515, UV-Vis Detector 2487, and a Refractive Index Detector 2414 were used. A Waters column (4.6 mm × 300mm; Styragel HR 5E) and polystyrene standards from Fluka were used. The polymer solution (1 mg/mL in THF) was prepared and filtered through a Mini-UniPrep PTFE vial with a 0.45 µm filter. 20 µL of each polymer solution was injected and molecular weights were calculated using Waters Breeze II software.

Film formation: For solubility studies, films were spin-coated from 20mg ml^{-1} solutions of toluene or $CHCl_3$. In addition, films subject to irradiation contained 6mg/mL AIBN and 2 drops mL^{-1} ethyleneglycoldimethacrylate (EGDMA, 1 drop ~ 21mg). The films were cast onto ITO-coated float glass (1"x1"; Delta Technologies, R_s<20 ohms/sq.) at an angular velocity of 800 rpm. For cyclic voltametry, films were drop-cast onto a Pt-button electrode from a 0.5mg ml^{-1} toluene solution and allowed to evaporate leaving a thin film. Irradiated films contained 0.25 mg mL^{-1} AIBN and 0.1 drop mL^{-1} EGDMA. For spectroelectrochemical measurements and direct photopatterning, thin films were spray-cast from a 2mg/mL toluene onto ITO-covered glass (Delta Technologies, CG-50IN-10V, R_s=5-10 Ohmns). Irradiated films contained 1mg mL^{-1} AIBN and 0.3 drops mL^{-1} EGDMA

Crosslinking: The polymer films were crosslinked using a Rayonet RPR-100 Photoreactor equipped with RPR-3500 lamps. The total irradiance were measured to be 12mW cm^{-2} using a Thorlabs PM100 and individual wavelengths were measured using a Newport Optical Power Meter 1830C employing a 818-UV detector (SN2009). The irradiance at 350 nm was determined to be 0.7 mW cm^{-2}.

Solubility studies was done on films spin cast onto ITO covered glass as described above. The absorbance of the individual slides was measured prior to irradiation. The samples were then irradiated for 0-600 seconds and the absorbance measured again. The slides when then emerged into a solution of stirring toluene at room temperature for 60 seconds. After drying, the absorbance was measured a third time and the spectra plotted. In some instances, the temperature of the toluene solution was raised to 100^{o}C.

Spectroelectrochemical and colorimetric analysis: Films were spray-cast as described above onto cuvette size ITO-covered glass, and used as the working electrode (WE). The WE was emerged in a solution of 0.5 M tertrabutylammonium hexafluorophophate ($TBAPF_6$) in acetonitrile in a cuvette. A standard Ag/Ag^+ (10 mM $AgNO_3$ in 0.5 M $TBAPF_6$/acetonitrile) was used as a reference electrode and a Pt flag was used as the counter electrode. The absorption spectrum was taken of the pristine film prior to any electrochemical switching. The films were electrochemically cycled between -0.1 and 0.4V until a stable voltammetric response was obtained (typically 5 cycles), to allow incorporation of electrolyte into the polymer film. Potentiostatic experiments were then performed between 0 and 0.4V and the absorbance spectra recorded at each potential. The same setup and procedure were used for colorimetric analysis. The ITO-covered glass was sprayed so that the absorbance was between 0.79 and 0.84. After the initial break-in of the films, potentiostatic experiments were performed and the Y, x and y valued measured using the setting described in section 1.1.

8.4 Experimental - chapter 5

Polymer synthesis: The polymers were synthesized according to the literature as described in appendix 1.1

Film formation was done by spin-coating from 20 mg ml^{-1} solutions of toluene or chlorobenzene (ECP 5 and ECP 6). The ECP 9 solution additionally contained 6 mg mL^{-1} AIBN and 2 drops per millilitre ethyleneglycoldimethacrylate (EGDMA, 1 drop ~ 21mg). Films were cast onto ITO-coated glass (2.5 cm x 5 cm; Rs~20 ohms/sq.) or onto ITO covered PET foil (2.5 cm x 5 cm; Rs~30 ohms/sq.) at angular velocities from 500-1400 rpm.

Film degradation were performed using a fully automated, high-throughput photo-chemical degradation setup as previously described.[4] The setup utilizes a Steuernagel solar simulator with an Osram 1200 W metal halide arc lamp providing an approximate AM1.5G spectrum with an intensity of 1000 W m^{-2}. The sample exchanger has a capacity of 22 samples and a UV-vis spectroscopic probe based on an optical fiber-based CCD spectrometer (Avantes AvaSpec 1024), and a halogen/deuterium light source (Avantes AvaLight-DHc) was used to measure the evolution in the absorbance of the samples.

Long term stability measurements: Samples were constructed by spincoating the ECPs onto ITO coated PET followed by encapsulation in a PET multilayer foil comprising a PSA adhesive (3M, MP467, cut-off 320nm) that functioned as an oxygen barrier foil. Half the sample was further covered with a UV barrier foil (Amcor, thickness 72μm, cut-off 400 nm). A second set of samples were constructed that in addition contained a PMMA based electrolyte previously employed in ECDs.[5] Samples were irradiated for 2200 hours using a solar simulator as described above. Absorption spectra were measured at weekly intervals, relative to an appropriate reference that was similarly exposed. It should be noted that blisters in the protective foil (following 500 hours of illumination) might cause reflections different from the reference.

Response time was measured from functional electrochromic devices that were constructed by spincoating. ECP 1 and ECP 2 onto ITO/PET substrates (1.5 cm x 3 cm;Rs~80 ohms/sq.) as previously reported. Prior to assembly, the ECP 1 coated

substrates were irradiated (AM 1.5G, 1000 W m^{-2}) for 0, 30, 60 and 90 minutes respectively. Potential square wave absorptiometry experiments were done from -0.6 V to + 1.5 V with a 60-second hold at each of the two potentials. After an initial "break in" of 35 double switches, the response time was obtained.

8.5 Experimental - chapter 6

Materials: Titaniumtetraisopropoxide (Ti(OPr^i)) 97%, oleic acid ($C_{18}H_{33}CO_2H$ or OLEA, 90%), carbon-^{13}C dioxide (99 atom % ^{13}C, 3 atom % ^{18}O) and carbon-^{13}C monoxide (99 atom % ^{13}C, <5 atom % ^{18}O) were used as received without further purification.

Nanorods synthesis: TiO_2 nanorods were synthesized according to a procedure by Cozzolli et al.,[6] with the minor modification that the nanoparticles were dissolved in chlorobenzene. The particles were coated onto laboratory glass slides using two methods:

Method A: The nanoparticles were deposited by spray coating, creating a semitransparent film. Hereafter, the substrates were annealed at 500^{o}C for 4 hours with an initial heating ramp of 10^{o}C/min. After cooling to room temperature, the glass slides were placed in the reaction chamber.

Method B: The nanoparticles were precipitated from the chlorobenzene solution by adding EtOH. The resulting precipitate was washed and isolated by centrifugation. This procedure was repeated 3 times to remove any unbound surfactant residues. The resulting solid was dried at 100^{o}C for 1 hour yielding a light yellow solid that was annealed using the above conditions. A small sample of the resulting white powder was analyzed by FT-IR, to confirm removal of the surfactant groups.. The remaining part was pestled in a mortar and dispersed in EtOH yielding a thick paste. This was coated onto laboratory glass slides by the doctor-blade technique, creating an opaque layer of TiO_2. Hereafter, the procedure was similar to the spraycoated slides.

8.6 Experimental - chapter 7

Hematite synthethis 1:[7] 4 ITO coated glass substrates was placed in a flask containg an 0.05M aqueous solution of $FeCl_3$. The flask was capped an heatted in an oven at 100^oC for 24 hours. The substrates was rinsed in demineralized water and dried with a heat gun. Following this the substrates were annealed at 500^oC for 3.5 hours, whereby the color changed from a faint yeloow to red-orange. Conductivity was measured using a Keithley 2440 Sourcemeter, but as the samples were nonconductive the were not further studied.

Hematite synthethis 2:[8] A 10 mM solution of $FeCl_3$ in ethanol was spin-coated on ITO coated glass substrates which were subsequently heated at 300^oC for 5 minutes on a hotplate. This procedure was repeated 10 times, and resulted in transparent yellow substrates. These were annealed at 500^oC for 4 hours. The now red-orange substrates were cut so that the area was 2.25 cm^2. Photoelectrodes were fabricated by connecting a copper wire to the coated glass substrates using heat curable silver paste. The connecting was selaed with epoxy.

Water splitting experiments were performed in the reactor depicted in figure 7.2. The cathode was platinum foil of a similar size as the photoanode (app. 2 cm^2). The Photocatalytic system was scanned from -1 to 3 V using a Keithley 2440 Sourcemeter. There was no observable difference between illuminating (AM 1.5 G) or not illuminating the system.

References

1 H. F. Dam and F. C. Krebs, *Sol Energ Mater Sol Cells,* 2012, **97,** 191-196.

2 M. A. B. H. Susan, T. Kaneko, A. Noda and M. Watanabe, *J. Am. Chem. Soc.,* 2005, **127,** 4976-4983.

3 D. S. Pedersen and C. Rosenbohm, *Synthesis,* 2001, 2431-2434.

4 T. Tromholt, M. V. Madsen, J. E. Carlé, M. Helgesen and F. C. Krebs, *J. Mater. Chem.,* 2012, **22,** 7592-7601.

5 J. Jensen, H. F. Dam, J. R. Reynolds, A. L. Dyer and F. C. Krebs, *J. Polym. Sci. Part B,* 2012, **50,** 536-545.

6 P. D. Cozzoli, A. Kornowski and H. Weller, *J. Am. Chem. Soc.,* 2003, **125,** 14539-14548.

7 S. Shen, J. Jiang, P. Guo and L. Guo, *Int. J. Photoenergy,* 2013, **2013,** .

8 G. Wang, Y. Ling, D. A. Wheeler, K. E. N. George, K. Horsley, C. Heske, J. Z. Zhang and Y. Li, *Nano Lett.,* 2011, **11,** 3503-3509.

9. Conclusion

This dissertation has addressed the development of electrochromic devices using conjugated polymers coated on flexible substrates. It is shown that electrochromic devices with high contrast and relatively fast response times can be achieved using electrochromic polymers in combination with a printed and cured adhesive electrolyte. The devices were prepared by using roll-coating methods on flexible substrates followed by lamination. The devices exhibited an optical contrast of 44% when fully switched in 10 seconds and 40% in less than 3 seconds. The low power requirements (+/-2V applied and <100μA/cm^2 max current density) of the electrochromic devices paired well with the power output of a printed polymer photovoltaic device and a self-powered OPV/ECD demonstrator was fabricated as an example of the possible appliance of polymer based electrochromic devices. ITO was successfully substituted by a highly conducting printed silver grid as electrode material when coated with PEDOT:PSS. PEDOT:PSS served both a stable charge balancing polymer and to homogenize the electric field in the devices was. Devices employing embedded silver grid electrodes these showed sub-second with an optical contrast of 30%. A solution processable conjugated electroactive copolymer based on an alkoxy-substituted ProDOT and an acrylate-substituted ProDOT was synthesized. Photo-crosslinking rendered the film insoluble, and a patterned surface with millimeter-sized dimensions was demonstrated as a utility of this polymer. Importantly it was shown that electrochemical, spectroscopic, and colorimetric properties were unaffected by the crosslinking process. The photochemical stability of 11 electrochromic polymers was established of which the majority degraded within 1-5 hours of solar radiation. Two proposed mechanisms of degradation based on fitted models were shown to match the experimental data. In order to extend the lifetime of the electrochromic polymers, such that they can be employed in commercially attractive devices, oxygen and UV barrier foils were applied and this considerably increased the lifetime.

A system for photocatalytic reduction of CO_2 was designed and evaluated. FT-IR analysis showed that reduction of carbon dioxide occurred in the presence of a titani-

um dioxide catalyst during solar exposure. Currently the photocatalytic efficiency of the system is limited, and unable to match the levels of carbon dioxide resulting from degradation of the flexible substrates used as carrier foils. The use of isotopically labeled $^{13}CO_2$ was found to be a facile way of determining the source of carbon in the product composition, which contained ^{13}CO, ^{12}CO and $^{12}CH_4$. Based on these findings carbonaceous residues are thought to reside on the chamber or catalyst surface, which possibly interferes with “true photocatalysis”, and hence makes determination of photocatalytic efficiency difficult. Photocatalytic water splitting experiments were performed using hematite deposited on ITO electrodes, but no photocatalytic action was observed during solar exposure for reasons that are currently being investigated

10. Appendices

Appendix 1	Polymer synthesis
Appendix 2	Rayonet lamp spectrum
Appendix 3.1	"Manufacture and demonstration of organic photovoltaic-powered electrochromic displays using roll coating techniques and printable electrolytes"
Appendix 3.2	"Fast switching ITO-free electrochromic devices"
Appendix 3.3	"Direct photopatterning of electrochromic polymers"
Appendix 3.4	"Photostability of electrochromic polymers and devices"
Appendix 3.5	"Flexible Substrates as Basis for photocatalytic reduction of carbon dioxide"

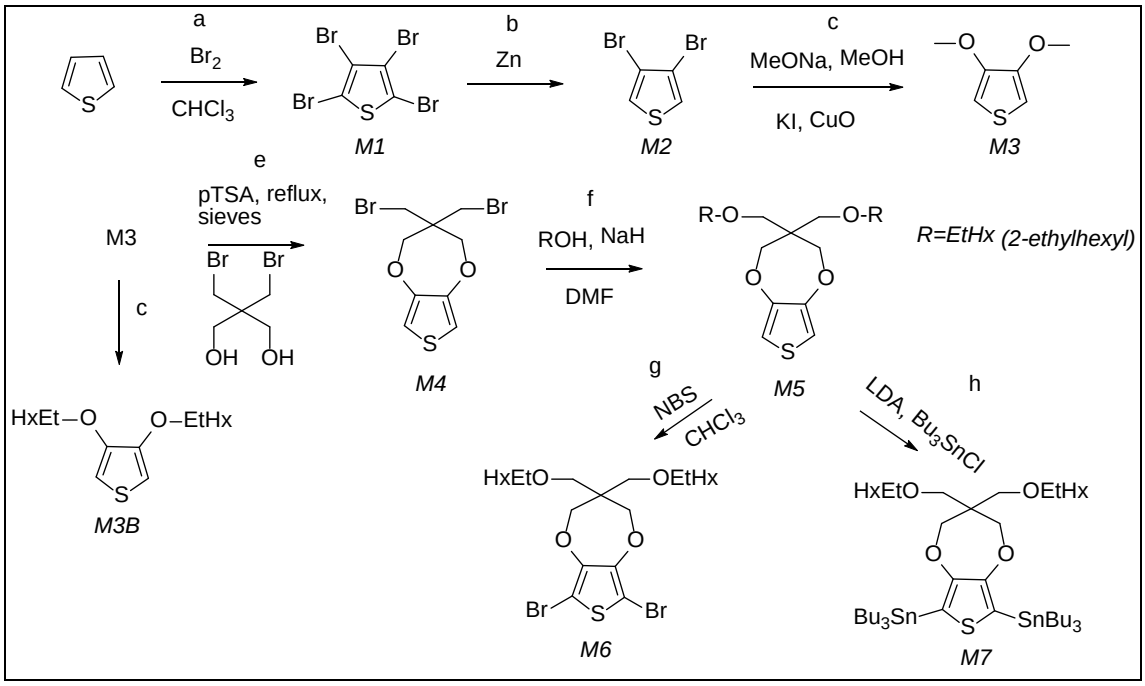

Scheme 1: ProDOT Monomer synthesis

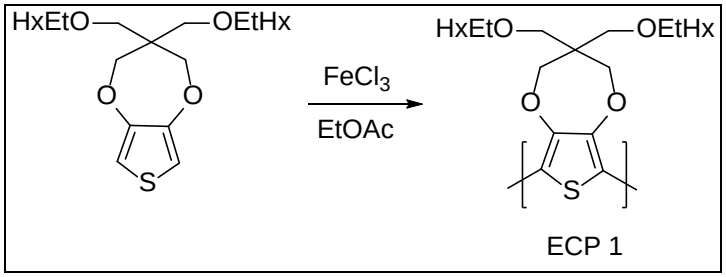

Scheme 2: Oxidative polymerization of ECP 1

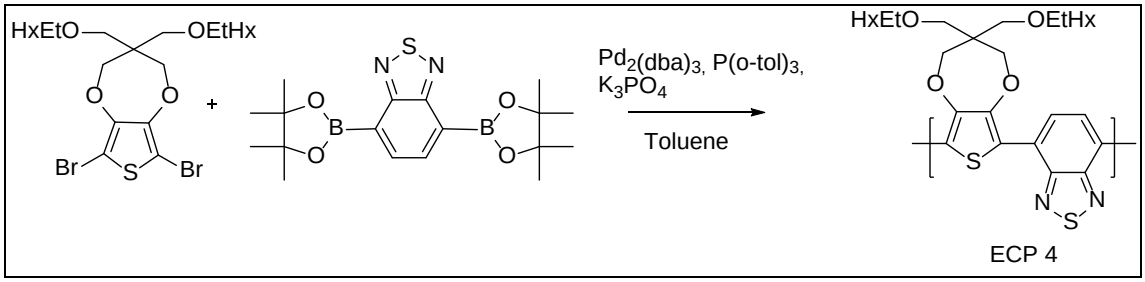

Scheme 3: Suzuki polymerization of ECP 4

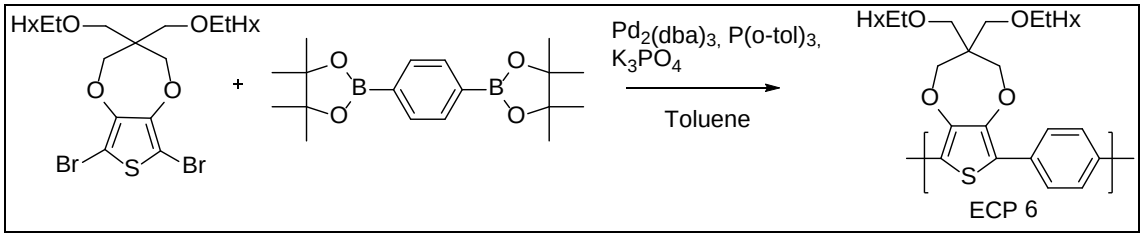

Scheme 4: Suzuki polymerization of ECP 6

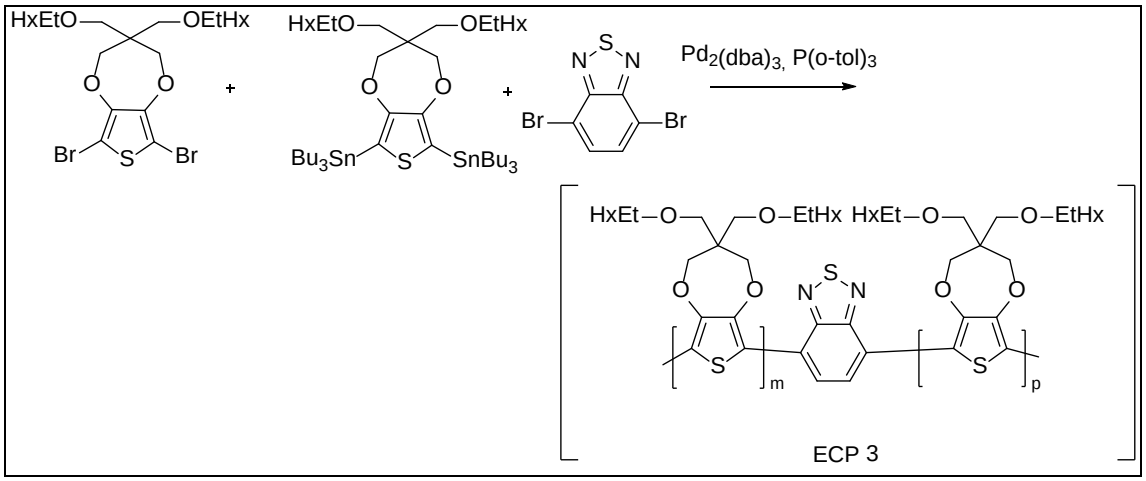

Scheme 5: Stille polymerization of ECP 3

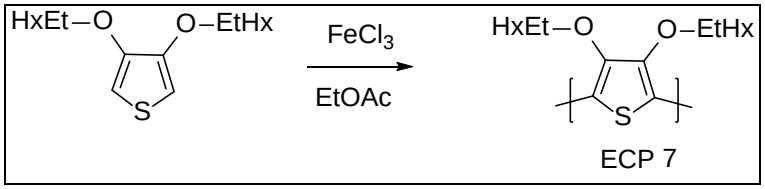

Scheme 6: Oxidative polymerization of ECP 7

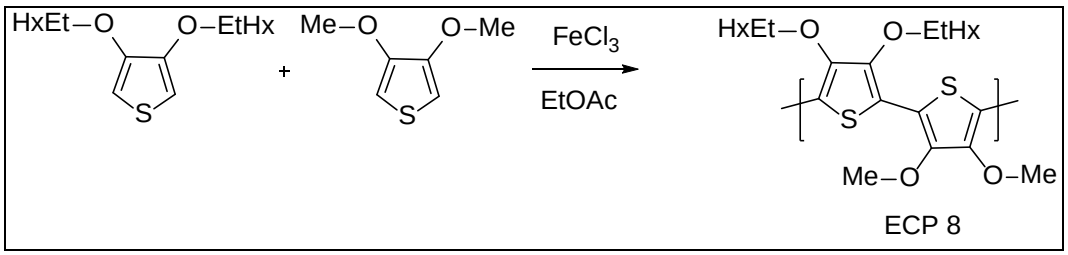

Scheme 7: Oxidative polymerization of ECP 8

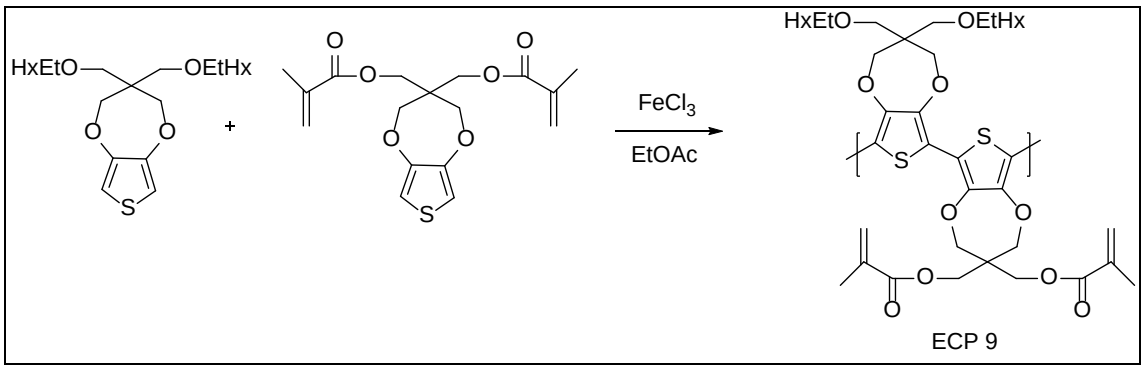

Scheme 8: Oxidative polymerization of ECP 9

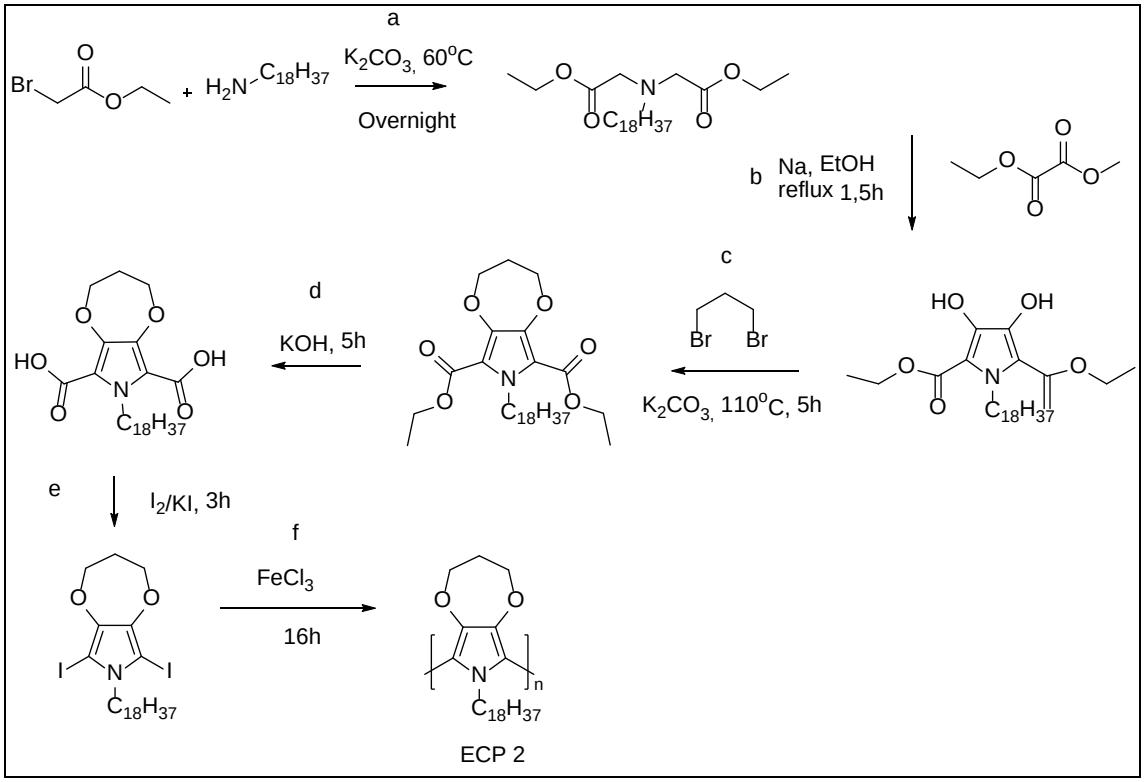

Scheme 9: MCCP synthesis; ECP 2

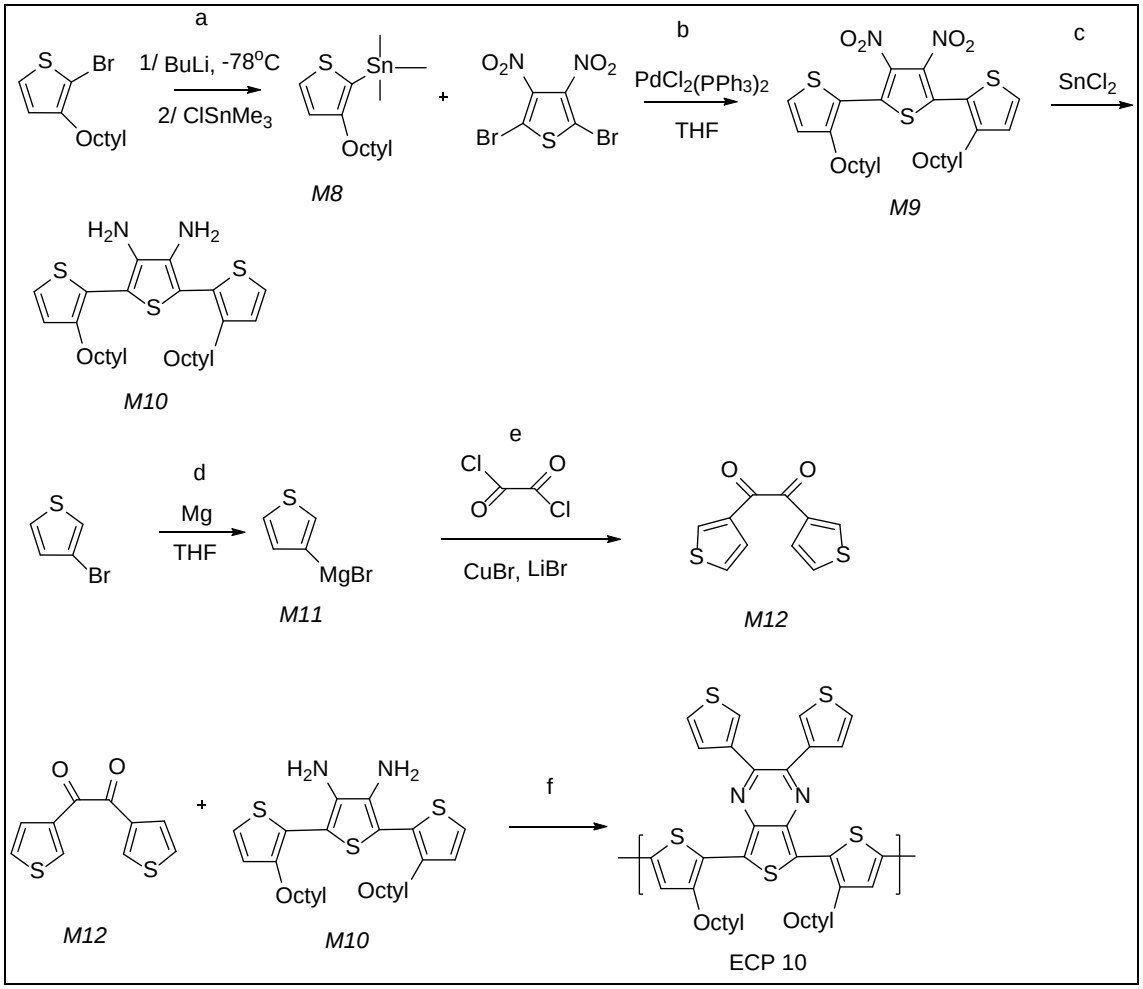

Scheme 10: Thionopyrazine synthesis; ECP 10

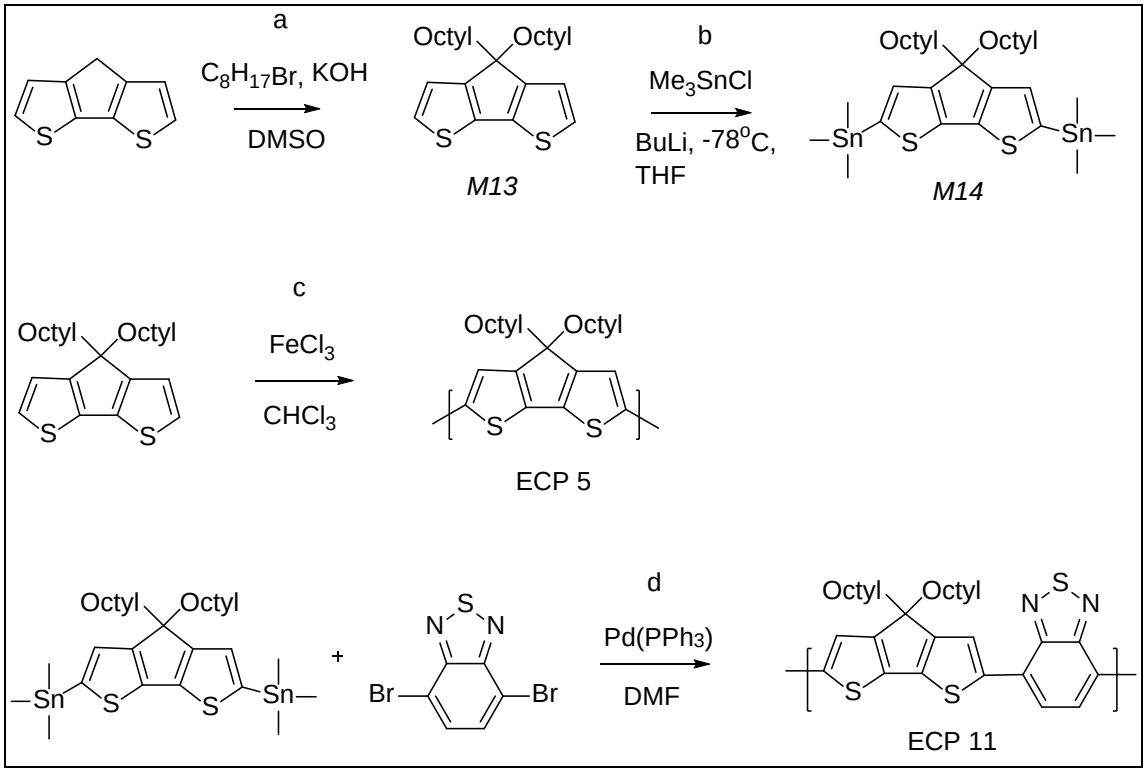

Scheme 11: **Synthesis of cyclopentadithiophene monomers and polymers; ECP 5 and ECP 11**

Synthetic procedures

Scheme 1:

Reaction 1a: Bromination

Thiophene (60 g, 0.7 mol, 1 eq)) was dissolved in $CHCl_3$ (30 ml) and bromine (503.4 g, 3.15 mol, 4.5 eq) was added via addition funnel under N_2 during 2 hours. Solution stirred overnight at RT. To the now solid reaction mixture was added more $CHCl_3$ and the solution was refluxed for 2 hours and allowed to cool to RT. KOH (70 g) in ethanol (400 ml) was added and the mixture was further refluxed for 4 hours, where after it was poured into 800 ml ice-water and extracted with $CHCl_3$ (3 x 300 ml). The organic phase was concentrated in vacuo and recrystallized from hot ethanol (2 L). The precipitate was filtered and washed with cold ethanol.

Yield (*M1)*: 140 g (0.35 mol; 50%); tetrabromothiophene

Reaction 1b: Reduction

Tetrabromothiophene (10 g, 25 mmol, 1eq) was dissolved in a acetic acid:water mixture (15 ml, 1:2). Zink dust (5.2 g, 80 mmol) was added in small potions to the stirred solution. The solution was stirred for 1 h at RT followed by 3 hours of reflux. The solution was then filtered through a pad of celite, which was washed with water and then ether. The aqueous filtrate was extracted with diethyl ether (3 x 40 ml), which was dried with Na_2SO_4, filtered and concentrated in vacuo. The crude product was distilled under vacuum yielding a clear colorless viscous liquid.

Yield (*M2*): 2.69 g (11 mmol, 44%); 3,4-dibromothiophene; ^{1}H-NMR (250 MHz, $CDCl_3$) δ= 7.40 (s, 2H)

Reaction 1c: Substitution of bromine

To a flame dried flask was added MeOH (75 ml), KI (10 mg, 0.066 mmol), CuO (5.09 g, 64.02 mmol), followed by solid Na (7.4 g, 325 mmol, 4.9 eq) in small portions while the solution was cooled in an water/ice bath. When all the Na was dissolved (app. 2.5 hours) 3,4-dibromothiophene (9 g, 37 mmol, 1 eq) was added and the reaction was stirred for 3 days. To the viscous dark solution was added MeOH (100 ml) and the mixture was filtered and concentrated in vacuo. The crude product was purified by DCVC in 10 fractions of 50 ml eluted with EtOAc (0 to 20%) in heptane to give a clear colorless liquid.

Yield (*M3*): 4.97 g (34 mmol, 93%); 3,4-dimethoxythiophene; ^{1}H-NMR (250 MHz, $CDCl_3$) δ= 6.18 (s, 2H); 3.85 (s, 6H)

Reaction 1d: Re-etherification

3,4-dimethoxythiophene (4.9g, 33.9 mmol, 1 eq), 2-ethylhexanol (11.5 g; 88.4 mmol, 2.6 eq) and p-toluene sulfonic acid (0.65 g; 3.3 mmol, 0.1 eq) were added to toluene (130 ml) in a flask equipped with a distillation head. The flask was heated to 90^{o}C for 15 hours in an oil bath whereby a clear liquid distilled of. The crude product further purified by vacuum distillation to give a clear viscous liquid.

Yield (*M3B*): 9.07 g (26.6 mmol, 78%); 3,4-bis((2-ethylhexyl)oxy)thiophene, ^{1}H-NMR (500 MHz, $CDCl_3$) δ = 5.87 (s, 2H); 3.88 (d, 4H, J=5.3 Hz); 1.77 (m, 2H); 1.54-1.27 (m, 16H); 0.93 (m, 12H)

Reaction 1e: Re-etherification

3,4-dimethoxythiophene (14 g, 97 mmol, 1 eq), 2,2-bis(bromomethyl)-1,3-propanediol (50.8 g, 194 mmol, 2 eq) and p-toluene sulfonic acid (1.8 g; 9.7 mmol, 0.1 eq) were added to toluene (600 ml) in a flask equipped with Soxleth condenser where the cotton thimble was filled with 4Å sieves. The reaction mixture was refluxed for 20 hours whereafter TLC (EtOAc:Hep 3:7) indicated full conversion. The solution was cooled, washed with water (500 ml) and brine (300 ml) and concentrated in vacou to a dark semisolid oil. The crude product was purified by DCVC in 15 fractions of 100 ml eluted with EtOAC (0-30%) in heptane to give a white solid.

Yield (*M4*): 8.77 g (25.5 mmol, 67%); 3,3-bis(bromomethyl)-3,4-dihydro-2H-thieno[3,4-b][1,4]dioxepine, ^{1}H-NMR (500 MHz, $CDCl_3$) δ = 6.51 (s, 2H); 4.12 (s, 4H); 3.63 (s, 4H)

Reaction 1f: Etherification

2-ethylhexanol (0.95g, 7.25 mmol, 5 eq) and NaH (1.16 g, 29 mmol, 10 eq, 60% dispersion) were mixed in DMF (50 ml) and cooled in a flask, where after the mixture was allowed to warm up to RT. 3,3-bis(bromomethyl)-3,4-dihydro-2H-thieno[3,4-b][1,4]dioxepine (0.5g, 1.45 mmol, 1 eq) and NaI (0.22 g, 1.45 mmol, 1 eq) were added and the reaction mixture was stirred at 110^{o}C for 2.5 hours, where TLC (EtOAc:Hep 8:2) showed full conversion. The mixture was cooled, poured into brine (150 ml) and extracted with diethyl ether (3 x 50 ml). The ether phases were subsequently washed with water (3 x 50 ml) and dried with $MgSO_4$. The crude product was purified by DCVC in 10 fractions of 25 ml eluted with EtOAC 0-10% in heptane to give a clear liquid

Yield (*M5*): 0.41 g (0.93 mmol, 65%); 3,3-bis(((2-ethylhexyl)oxy)methyl)-3,4-dihydro-2H-thieno[3,4-b][1,4]dioxepine; ^{1}H-NMR (250 MHz, $CDCl_3$) δ = 6.44 (s, 2H); 4.01 (s, 4H); 3.47 (s, 4H); 3.28 (d, 2H, J = 5.6 Hz); 1.53-1.20 (m, 16H), 0.88 (m, 12H)

Reaction 1g: Bromination

3,3-bis(((2-ethylhexyl)oxy)methyl)-3,4-dihydro-2H-thieno[3,4-b][1,4]dioxepine (2.6 g; 5.9 mmol, 1eq) and N-bromosuccinimide (3.15 g, 17.7 mmol, 3 eq) were dissolved in $CHCl_3$ and stirred overnight at RT in a covered flask. TLC (1:9 EtOAc:Hep) shows full conversion. The solution was concentrated in vacou and purfified by DCVC in 20 fractions of 50 ml eluted with CH_2Cl_2 (0-40%) in heptane.

Yield (*M6*): 2.8 g (4.6 mmol, 79%); 6,8-dibromo-3,3-bis(((2-ethylhexyl)oxy)methyl)-3,4-dihydro-2H-thieno[3,4-b][1,4]dioxepine; ^{1}H-NMR (500 MHz, $CDCl_3$) δ = 5.87 (s, 2H); 3.88 (d, 4H); 1.77 (m, 2H); 1.54-1.27 (m, 16H); 0.93-0.83 (m, 12H)

Reaction 1h: Stannylation

3,3-bis(((2-ethylhexyl)oxy)methyl)-3,4-dihydro-2H-thieno[3,4-b][1,4]dioxepine (0.7 g, 1.58mmol, 1 eq) was dissolved in anhydrous THF (10 ml) and cooled to -78^{o}C. A 2.5 M hexane solution of BuLi (2 ml, 5.0 mmol, 3 eq) was added by syringe during 30 minutes. The solution was then stirred at -78^{o}C for additional 30 minutes and allowed to reach RT (app. 1.5 hours). The soltion was then cooled to 0^{o}C and Me_3SnCl (1.20 g, 6.0 mmol, 4 eq) was added and the solution was stirred for 2 hours by which the absence of thiophene protons was shown by ^{1}H-NMR. Ether (200 ml) was added and the solution was washed with brine (6 x 50 ml), and run through a short silica pad pretreated with Et_3N (20% in heptane). Dried and concentrated in vacuo using an oil pump.

Yield (*M7*): 0.79g (1.0 mmol, 68%); (3,3-bis(((2-ethylhexyl)oxy)methyl)-3,4-dihydro-2H-thieno[3,4-b][1,4]dioxepine-6,8-diyl)bis(trimethylstannane); ^{1}H-NMR (250 MHz, $CDCl_3$) δ = 3.92 (s, 4H); 3,47 (s, 4H); 3.28 (d, 2H, J = 4.6 Hz) 1.54-1.27 (m, 16H); 0.93-0.83 (m, 12H); 0.31 (s, 18H)

Scheme 2 – Oxidative polymerization of ECP 1[1, 2]

3,3-bis(((2-ethylhexyl)oxy)methyl)-3,4-dihydro-2H-thieno[3,4-b][1,4]dioxepine (3 g, 6.7 mmol, 1 eq) was dissolved in EtOAc (80 ml) which was degassed with argon for 1 hour. A solution of $FeCl_3$ (5.5 g, 34 mmol, 5 eq) in EtOAc (20 ml) was added while keeping the

reaction flask in a water/ice bath. The reaction mixture was stirred 4 hours, while bubbling argon through the solution, until it was dark green and very viscous. The solution was poured into MeOH (200 ml) and stirred for 30 min, where after it was filtered and washed with MeOH until the filtrate was colorless. The solid was dissolved in $CHCl_3$ (250 ml) and hydrazine hydrate (0.5 ml, 30% in water) was added, which made the solution a bright purple. The solution was washed with water (300 ml) and brine (2 x 200 ml), where after it was concentrated in vacuo to a viscous liquid. The concentrated liquid was poured into MeOH (200 ml) affecting precipitation. The Precipitate was filtered and washed with MeOH, followed by Soxleth purification (MeOH 1 day, hexane 1 day, $CHCl_3$ 1 day). The $CHCl_3$ phase was precipitated in MeOH and the precipitate filtered of and dried in a vacuum oven overnight.

Yield: 1.3g (2.95 mmol, 44%); poly((2,2-bis(2-ethylhexyloxymethyl)-propylene-1,3-dioxy)-3,4-thiophene-2,5-diyl (ECP 1)

Scheme 3 – Suzuki polymerization of ECP 4[3]

Toluene (19 ml) and water (7 ml) were mixed in flask and purged with argon for 2 hours. 6,8-dibromo-3,3-bis(((2-ethylhexyl)oxy)methyl)-3,4-dihydro-2H-thieno[3,4-b][1,4]dioxepine (0.5 g, 0.83 mmol, 1 eq), 4,7-bis(4,4,5,5-tetramethyl-1,3,2-dioxaborolan-2-yl)-2H-1l4,3l4-benzo[d][1,3,2]dithiazole (0.32 g, 0.83 mmol, 1 eq), K_2CO_3 (13.28 mmol, 16 eq), Pd_2dba_3 (15.1 mg, 16.6 μmol), $P(o\text{-}tol)_3$ (79.7 mg, 66.4 μmol) and a few drops of aliquat 336 were mixed in a flask that was then filled with argon and evaporated. This procedure was repeated 6 times, before the water/toluene mixture were added, the reaction flask sealed and the resulting solution were degassed with argon for 10 minutes. The temperature was then raised to 85^{o}C and the reaction stirred overnight. The next day fresh Pd_2dba_3 (15 mg) and $P(o\text{-}tol)_3$ (80 mg) were added under argon and the solution was stirred for additionally 2 days at 85^{o}C. The solution was then precipitated in 20% water in MeOH solution and filtered directly through a cotton thimble. The polymer was purified by Soxleth extraction (MeOH 1 day, $CHCl_3$ 1 day). The $CHCl_3$ phase was concentrated in vacuo and precipitated in MEOH (200 ml), filtered and washed before drying in a vacuum oven for 24 hours.

Yield: 0.43g (0.75mmol, 90%); Poly(4-(3,3-bis(((2-ethylhexyl)oxy)methyl)-3,4-dihydro-2H-thieno[3,4-b][1,4]dioxepin-6-yl)benzo[c][1,2,5]thiadiazole) (ECP 4); ^{1}H-NMR (250 MHz, $CDCl_3$) δ = 8.45 (2H); 4.35 (4H); 3.67 (4H); 3.37 (4H); 1.49-0.6 (30H)

Scheme 4 – Suzuki polymerization of ECP 6[4]

A solution of toluene (15 ml) and water (5 ml) was degassed with argon for 20 minutes before adding 6,8-dibromo-3,3-bis(((2-ethylhexyl)oxy)methyl)-3,4-dihydro-2H-thieno[3,4-b][1,4]dioxepine (0.72 g, 1.21 mmol, 1 eq), 1,4-bis(4,4,5,5-tetramethyl-1,3,2-dioxaborolan-2-yl)benzene (0.49 g, 1.21 mmol, 1 eq), Pd_2dba_3 (11 mg, 3mol%), P(o-tol)$_3$ (11 mg, 3 mol%), K_3PO_4 (3.2 g, eq 3 M) and a few drops of Aliquat 336. The flask was sealed and the solution stirred for 3 days at 90^{o}C. The solution was poured into MeOH (200 ml) and washed and filtered. The precipitate was Soxleth extracted (MeOH 2 days, hexane 1 day and $CHCl_3$ 1/2 day) and the $CHCl_3$ concentrated in vacuo and precipitated in MeOH (200 ml). The precipitate was filtered and dried in an vacuum oven.

Yield: 422 mg (0.71 mmol, 58%); Poly(3,3-bis(((2-ethylhexyl)oxy)methyl)-6-phenyl-3,4-dihydro-2H-thieno[3,4-b][1,4]dioxepine)

Scheme 5 – Stille polymerization of ECP 3[5]

(3,3-bis(((2-ethylhexyl)oxy)methyl)-3,4-dihydro-2H-thieno[3,4-b][1,4]dioxepine-6,8-diyl)bis(trimethylstannane) (0.79g, 1.03 mmol, 1 eq), 6,8-dibromo-3,3-bis(((2-ethylhexyl)oxy)methyl)-3,4-dihydro-2H-thieno[3,4-b][1,4]dioxepine (0.43g, 0.7 mmol, 0.75 eq) and 4,7-dibromobenzo[c][1,2,5]thiadiazole (60 mg, 0.2 mmol, 0.25 eq) were dissolved in anhydrous toluene (15 ml) and degassed with argon for 1 hours prior to addition of Pd_2dba_3 (15 mg, 0.022mmol) and P(o-tol)$_3$ (22 mg, 0.09 mmol). The reaction flask was sealed and the reaction stirred at 110^{o}C for 48 hours. The reaction mixture were then filtered directly through a cotton thimble and Soxleth extracted for 4 days with MeOH, before it was dissolved in $CHCl_3$ and re-precipitated in MeOH, filtered and dried in a vacuum oven.

Yield: 55 mg

Scheme 6 – Oxidative polymerization of ECP 7[6]

3,4-bis((2-ethylhexyl)oxy)thiophene (2.84 g, 8.3 mmol, 1 eq) were dissolved in EtOAc (30 ml) and degassed with argon for 30 minutes. $FeCl_3$ (4.06 g, 25 mmol, 4 eq) was dissolved in EtOAc (10 ml) degassed with argon for 2 minutes and added to the other solution. The reaction mixture was stirred for 24 hours, concentrated slightly in vacuo and precipitated in MeOH (100 ml). The precipitate was dissolved in $CHCl_3$ (130 ml) and added hydrazine hydrate) (2 ml, 30% in water). The solution was washed with water (2 x 50 ml) and the phases were separated. The organic phase was concentrated in vacuo and precipitated in MeOH (100 ml). The resulting solid was dried in vacuum oven.

Yield: 0.69 g (2.02 mmol, 24%); Poly{3,4-di(2-ethylhexyloxy)thiophene; ^{1}H-NMR (500 MHz, $CDCl_3$) δ = 3.95 (4H); 1.72 (2H); 1.57-1.30 (16H); 0.89 (12H)

Scheme 7 – Oxidative polymerization of ECP 8[6]

3,4-bis((2-ethylhexyl)oxy)thiophene (1.4 g, 4.15 mmol, 1 eq) and 3,4-dimethoxythiophene (0.59g, 4.15 mmol, 1 eq) were dissolved in EtOAc (20 ml) and degassed with argon for 30 minutes. $FeCl_3$ (4.06 g, 25 mmol, 4 eq) was dissolved in EtOAc (10 ml) degassed with argon for 2 minutes and added to the other solution. The reaction mixture was stirred for 24 hours, concentrated slightly in vacuo and precipitated in MeOH (150 ml). The precipitate was dissolved in $CHCl_3$ (150 ml) and added hydrazine hydrate) (1.5 ml, 30% in water). The solution was washed with water (2 x 100 ml) and the phases were separated. The organic phase was concentrated in vacuo and precipitated in MeOH (100 ml). The resulting solid was dried in vacuum oven.

Yield: 0.46 g (1.0 mmol, 21%); Poly{3,4-di(2-ethylhexyloxy)thiophene-co-3,4-di(methoxy) ^{1}H-NMR (500 MHz, $CDCl_3$) δ = 3.95 (10H); 1.79 (2H); 1.57-1.23 (16H); 0.89 (12H)

Scheme 8 – Oxidative polymerization of ECP 9[7]

3,4-dihydro-2H-thieno[3,4-b][1,4]dioxepine-3,3-yl)bis(methylene)bis(2-methylacrylate)

(0.34 g, 0.95 mmol, 1 eq) and 3,3-bis(((2-ethylhexyl)oxy)methyl)-3,4-dihydro-2H-thieno[3,4-b][1,4]dioxepine (0.42 g, 0.95 mmol, 1 eq) were dissolved in ethyl acetate (20ml). The solution was bubbled thoroughly with argon for 60 min while stirred. The flask was placed in a water bath (20^{o}C). $FeCl_3$ (1.5 g, 9.5 mmol, 5 eq) was added to a small beaker of ethyl acetate (5ml) and bubbled with argon for 1 min. The resulting yellow solution was added by syringe in one portion to the monomer solution. During the polymerization the reaction mixture was continuously bubbled with argon and stirred. The reaction was considered complete when the mixture was black and almost solid (around 3 h). The viscous dark mixture was transferred to a solution of MeOH (200ml) and stirred for 60 min. Hereafter, it was filtered and the residue washed with MeOH until the filtrate became clear. The solid was dissolved in toluene (200ml) and reduced with hydrazine (0.25 ml, THF solution) until the resulting solution became bright purple. The mixture was washed with water (2 x 200ml), and the organic phase was concentrated in vacuo and precipitated in MeOH (200ml). The precipitate was transferred to a cotton thimble and Soxhlet extracted (MeOH 1day, hexanes 1 day and $CHCl_3$ 1 day). The $CHCl_3$ fraction was concentrated in vacuo and re-precipitated in MeOH (200ml). The solution was filtered and the solid dried under vacuum for 24 hours yielding a magenta colored solid.

Yield: 0.39 g (0.49 mmol, 50%); Poly(3,3-bis(((2-ethylhexyl)oxy)methyl)-3,4-dihydro-2H-thieno[3,4-][1,4]dioxepine)-co(3,4-dihydro-2H-thieno[3,4-b][1,4]dioxe-pine-3,3yl)bis-(methylene)bis(2-methylacrylate), ^{1}H-NMR (250 MHz, $CDCl_3$) $\delta = 6.15$ (1H); 5.62 (1H); 4.18 (12H); 3.36 (4H); 3.32 (44H); 2.14 (1H); 1.98 (2H); 1.64-1.05 (36H); 0.89 (22H)

Scheme 9 – MCCP synthesis[8-10]

Reaction 9a: Alkylation

Octadecylamine (40.42 g, 0.15 mol, 1 eq) and anhydrous K_2CO_3 (51.83 g, 0.375 mol, 2.5 eq) were suspended in anhydrous DMF (220 ml). Ethyl bromoacetate (45.18 g, 0.329 mol, 2.2 eq) was added and the solution was stirred under argon at 60^{o} for 19 hours, where after it was allowed to cool. The solution was poured into diethyl ether (250 ml) and filtered under reduced pressure to remove any solid. The filtrate was extracted

with water (2 x 250 ml) and brine (200 ml) although this was challenging due to poor phase separation. The organic phase was dried with $MgSO_4$ and concentrated in vacuo. The crude product was purified by vacuum distillation yielding a clear oil that precipitated when cooled.

Yield: 41.66 g (0.1 mol, 63%); Diethyl N-(2-octadecyl)iminodiacetate; ^{1}H-NMR (250 MHz, $CDCl_3$) δ = 4.04 (q, 4H, J=7.6 Hz); 3.43 (s, 4H); 2.56 (t, 2H, J=7.2Hz); 1.39-1.07 (M, 40H); 0.84 (t, 3H, J=8.1 Hz)

Reaction 9b: Hinsberg condensation

To a flame flask was added ethanol (99.9 %, 100 ml) followed by solid Na (5.6 g, 33.9 mmol, 3 eq) in small portion. The solution was stirred until all Na had dissolved. Diethyl oxalate (11.8 g, 80.9 mmol, 1 eq) and Diethyl N-(2-octadecyl)iminodiacetate (35.75 g, 80.9 mmol, 1 eq) was added and the reaction mixture was refluxed for 2 hours. The now semisolid reaction mixture was filtered and the solid washed with several times with ethanol (in total 1 L). The solid was then suspended in water (600 ml) and the pH was adjusted to approximately 4.5 by addition of glacial acetic acid (10ml). The solution was extracted with ether (600 ml) and the ether phase was washed with brine (200 ml) and allowed to evaporate. The crude product was recrystallized from hot ethanol (2 L) and the resulting solid was dried in a vacuum oven.

Yield: 16 g (32 mmol, 40%); 2-ethyl-5-methyl-3,4-dihydroxy-1-octadecyl-1H-pyrrole-2,5-di-carboxylate; ^{1}H-NMR (500 MHz, $CDCl_3$) δ = 7.71 (s, 2H); 4.43 (q, 6H, J=6.9 Hz); 1.63 (m, 4H); 1.43 (t, 6H, J=7.5 Hz); 1.34-1.23 (m, 30H); 0.90 (t, 3H, J=7.5 Hz)

Reaction 9c: Alkylation

2-ethyl-5-methyl-3,4-dihydroxy-1-octadecyl-1H-pyrrole-2,5-di-carboxylate (10 g, 20.1 mmol, 1eq), 1,3-dibromopropane (5.65 g, 28.0 mmol, 1.4 eq) and anhydrous K_2CO_3 (14g, 101 mmol, 5 eq) were mixed in anhydrous DMF (150 ml) and heated to 110^{o}C for 24 hours, by which TLC (2:8 EtOAc:heptane) shows conversion. Solution was allowed to cool and water (300 ml) and diethyl ether (250 ml) were added. The phases were separated and the aqueous phase was extracted with ether (200 ml). The combined organic

phases were washed with brine (2 x 200 ml), dried with $MgSO_4$ and concentrated in vacuo to a yellow oil. After 3 days the oil has crystalized to a brownish-yellow solid. The product was not purified further as the ^{1}H-NMR was identical to previously recrystallized sample.

Yield: 9.47 g (18.1 mmol, 90%); diethyl 7-octadecyl-3,4-dihydro-2H,7H-[1,4]dioxepino[2,3-c]pyrrole-6,8-dicarboxylate; ^{1}H-NMR (500 MHz, $CDCl_3$) $\delta = 4.59$ (2H); 4.36 (4H); 4.1 (4H); 2.26 (2H); 1.67 (2H); 1.39 (6H); 1.28 (25H); 0.91 (34H). Due to instrument malfunction it was not possible to determine peak splitting and coupling constants

Reaction 9d: Hydrolysis

Diethyl 7-octadecyl-3,4-dihydro-2H,7H-[1,4]dioxepino[2,3-c]pyrrole-6,8-dicarboxylate (9.4 g, 17.5 mmol, 1 eq) and NaOH (4.8 g, 115 mmol, 3 .2 eq) was dissolved in acetone:water (1:1, 140 ml) and bubbled with argon for 1 hour and then refluxed. After 4 hours TLC (2:8 EtOAc:heptane) shows complete conversion of starting material and he solution was allowed to cool. The acetone was removed in vacuo and ice (app. 150 ml) was added to the aqueous solution. pH was adjusted to app. 6 using sulfuric acid, which affected precipitation. The precipitate was filtered using a vacuum pump and washed with water (5 x 50 ml), where after it was dried overnight in a vacuum oven. The following day it turned out that the would-be solid was an emulsion and the product was a watery slurry. Extraction by $CHCl_3$ failed and both phases were concentrated in vacuo. The resulting greasy solid was recrystallized from hot ethanol, and put in the freezer to precipitate. The precipitate (2.8 g) was found to impure on ^{1}H-NMR and was combined again with remnant (5 g) that also contained product. The combined phases were purified by DCVC in 15 fractions eluted with 0-20% acetonitrile in toluene.

Fraction 3 and 4 (total 1.88 g) contained solely product and were used for further synthesis. Fraction 5-11 (total 4.3 g) contained product, but also other compounds (NMR indicates mono-hydrolyzed product).

Yield: 1.88g (3.9 mmol, 22%); 7-octadecyl-3,4-dihydro-2H,7H-[1,4]dioxepino[2,3-c]pyrrole-6,8-dicarboxylic acid; ^{1}H-NMR (500 MHz, $CDCl_3$) $\delta =$ 6.18 (s, 2H); 3.98 (t, 4H

J=5.1 Hz); 3.62 (t, 2H, J=7.1Hz); 2.13 (M, 2H); 1.67 (t, 2H; 8.1 Hz); 1.26 (s, 30H); 0.88 (t, 3H, J=7.0 Hz).

Reaction 9e: Iodination and oxidative polymerization

7-octadecyl-3,4-dihydro-2H,7H-[1,4]dioxepino[2,3-c]pyrrole-6,8-dicarboxylic acid (1.8 g, 3.7 mmol, 1eq) was dispensed in aqueous K_2CO_3 (1.1M, 35ml) and degassed with argon for 2 hours. I_2 (1.9 g, 7.5 mmol) was dissolved in aqueous KI (16ml) and likewise degassed for 2 hours, after which it was added the reaction mixture during 40 min, while argon was bubbled through the solution. After addition the solution was stirred for 20 minutes and CH_2Cl_2 (50 ml) was added. $Na_2S_2O_5$ (0.5 g, 2.6 mmol) was added to reduce excess I_3^-. The phases were separated and the aqueous phase washed with CH_2Cl_2 (2 x 50 ml). The organic phase was dried with Na_2SO_4 and filtered through a thin pad of basic alumina (Brockman I). The pad was then washed with CH_2Cl_2 (5 x 10 ml) and the combined organic phases was concentrated in vacuo at RT (dark oil, yield 1,87 g). The concentrate was dissolved in CHCl3 (20 ml) added $FeCl_3$ (5 mg, catalytic) and left stirring overnight. The next day $CHCl_3$ (5 ml) and the solution was cooled in an ice bath. Hydrazine hydrate (2 ml, 30% in THF) was added and the solution was slightly concentrated, before being poured in MeOH (100 ml) which affected precipitation of a brownish tacky solid. The MeOH was decanted and the solid rinsed with MeOH (2 x 75 ml) and dissolved in toluene (30 ml). The solution was run through a thin silica pad. The pad was washed with toluene (5 x 10 ml). The combined toluene phases was concentrated in vacuo and poured into MeOH (100 ml) which affected precipitation of a light brown-yellowish tacky solid. This was rinsed in MeOH (2 x 75 ml), dissolved in CH_2Cl_2 (20 ml) and added hydrazine hydrate (4 ml, 30% in THF) and stirred overnight.
Water (10mL) was added and the mixture stirred for 1 hours, where after the volatiles were removed in vacuo. The water was decanted and the tan solid was rinsed with water (3 x 10 mL) and methanol (3 x 50mL) and dried under ambient conditions. The polymer was then in CH_2Cl_2 (50mL) and added over 15 minutes to cold methanol (100 mL) and the solution was filtered under reduced pressure. The solid was washed with methanol (50mL) and dried in a vacuum oven overnight.

Yield: 0.78g (1.75 mmol, 51 %); Poly(N-octadecyl-(propylene-1,3-dioxy)-3,4-pyrrole-2,5-diyl; ^{1}H-NMR (500 MHz, $CDCl_3$) δ = 4.02 (4H), 3.49 (2H); 2.13 (2H); 1.59-0.73 (35H).

Scheme 10: Thienopyrazine synthesis [11-14]

Reaction 10a: Stannylation

To a flame dried was added anhydrous THF (15 ml), which was cooled to -78^{o}C. 2-bromo-3-octyl thiophene (3 g, 10.8 mmol, 1 eq) was added followed by dropwise addition of BuLi (2.5 M in hexane, 5 ml 12.4 mmol, 1.1 eq) during 2 hours. The solution was allowed to reach -30^{o}C and cooled again to -78^{o}C before addition of Me_3SnCl (2.5 g, 12.4 mmol, 1.1 eq). The solution was then allowed to reach RT. Diethyl ether (150 ml) was added and the solution was washed with brine (6 x 50 ml), dried with $MgSO_4$ and concentrated in vacuo.

Yield: 3.42 g (9.5 mmol, 88%); Trimethyl(3-octylthiophen-2-yl)stannane

Reaction 10b and c: Stille coupling and reduction

Trimethyl(3-octylthiophen-2-yl)stannane (3.42 g, 9.5 mmol, 2.5 eq) and 2,5-dibromo-3,4-dinitrothiophene (1.14 g, 3.8 mmol, 1 eq) was dissolved in anhydrous THF (20 ml) and degassed with argon for 30 minutes. $PdCl_2(PPh_3)_2$ (25 mg, catalytic) was added the solution was refluxed for 24 hours, where TLC (1:9 EtOAc:heptane) shows conversion of SM. THF was removed in vacuo and ether (150 ml) was added, which was washed with water(3 x 100 ml) and brine (150 ml). The organic phase was dried with $MgSO_4$ and concentrated in vacuo. ^{1}H-NMR shows formation of product. The crude product is suspended in ethanol (20 ml) and concentrated HCl (30 ml) and $SnCl_2$ (21g) in ethanol (30ml) was added. The mixture as stirred overnight at 30^{o}C, where after it was poured into cold NaOH (25%, 100 ml) which resulted in heavy precipitation. Toluene (50 ml) and the solution was tried filtered through celite, which was impossible. The celite and was extracted with water and toluene, but due to breakage of the funnel a substantial

amount of material was lost. The remaining solution was concentrated and the product purified by DCVC in 15 fraction of 25 eleuted with 0-50% EtOAc in heptane.

Yield: 500 mg (0.94 mmol, 10%); 3',4'-dinitro-3,3''-dioctyl-2,2':5',2''-terthiophene; ^{1}H-NMR (250 MHz, $CDCl_3$) δ = 7.26 (2H); 6.93 (2H); 3.48 (4H); 2.16 (4H); 1.58 (4H); 1.26 (20H); 0.87 (6H)

Reaction 10d and e: Lithiation and arylation

BuLi (2.5 M, 28.4 ml, 71 mmol, 1 eq) was added to 100 ml dry THF and cooled to -78^{o}C. 3-bromothiophene (11.6 g, 71 mmol, 1 eq) was added drop wise to this solution during 30 minutes and the solution was stirred at -78^{o}C for 2 hours. LiBr (6.2 g, 71 mmol, 1 eq) and CuBr (10.18 g, 71 mmol, 1 eq) was dissolved in anhydrous THF (400 ml) and cooled to -78^{o}C. The 3-lithiothiophene solution was added to the LiBr/CuBr solution, which increased the temperature to -60^{o}C. The solution was cooled again to -78^{o}C.

Oxalylchloride (4.05 g, 32 mmol, 0.9 eq) was dissolved in anhydrous THF 50 ml and cooled to -78^{o}C. 10 ml portions of this solution were added drop wise to the 3-lithiothiophene/CuBr/LiBr solution during 1.5 hours. Stirred at -78^{o}C for 2 hours and allowed to reach RT. Saturated (50 ml) was added, which affected precipitation. THF was removed in vacuo and heptane (200 ml) was added. The solution was washed with NH_4Cl (3 x 100 ml), water (2 x 100 ml) and brine (100 ml). The organic phase was added heptane (100 ml), filtered through celite pad and concentrated in vacuo. The crude product was purified by DCVC in 20 fraction of 50 ml eluted with 0-20% EtOAc in heptane.

Yield: 2.6 g (11.7 mmol, 36% in two steps); 1,2-di(thiophen-3-yl)ethane-1,2-dione; NMR (250 MHz, $CDCl_3$) δ = 8.36 (s, 2H); 7.71 (d, 2H; J=4.9 Hz); 7.39 (m, 2H)

Reaction 10f: Coupling and oxidative polymerization

3',4'-dinitro-3,3''-dioctyl-2,2':5',2''-terthiophene (280 mg, 0.52 mmol, 1 eq) and 1,2-di(thiophen-3-yl)ethane-1,2-dione (188 mg, 0.84 mmol, 1.5 eq) were dissolved in MeOH (30 ml) and left stirring for 6 days. MeOH removed in vacuo and the crude product was purified by DCVC in 15 fraction of 25 ml eluted with 0-12% EtOAc in hep-

tane. The product was dissolved in EtOAc (4 ml) and degassed with argon. $FeCl_3$ (0,17 g, 4 eq) was added and the solution stirred for 24 hours. The solution was slightly concentrated and poured into MeOH (50 ml). The solution was filtered and the precipitate dissolved in $CHCl_3$ (50 ml). Hydrazine hydrate (0.5 ml, 30% in THF) was added and the solution was stirred for 1 hour before being washed with water (2 x 150 ml). The organic phase was concentrated in vacuo and precipitated in MeOH. The solution was filtered and the solid dried in a vacuum oven overnight.

Yield: 120 mg (0.1 mmol, 33% in two steps); Poly(5,7-bis(3-octylthiophen-2-yl)-2,3-di(thiophen-3-yl)thieno[3,4-b]pyrazine); NMR (250 MHz, $CDCl_3$) δ = 7.69-6.99 (5H); 2.97 (4H); 1.75 (4H); 1.26 (10H); 0.87 (3H); 0.45 (1H)

Scheme 11: Synthesis of cyclopentadithiophene monomers and polymers[15-17]

Reaction 11a: Alkylation

Cyclopentadithiophene (2g, 11.2 mmol, 1eq) was dissolved in DMSO (50ml) and octylbromide (4.3 g, 22.4 mmol, 2 eq) and KI (50 mg) was added. The solution was cooled in an water/ice bath under argon. Crushed KOH (2g, 35.6 mmol, 3.2 eq) was added at the solution was stirred overnight by which TLC (1:4 DCM:heptane) shows conversion of starting materials. Water (50 ml) was added and the solution extracted with diethyl ether (2 x 75 ml). The ether phase was washed with water (50 ml), brine (50 ml) and NH_4Cl (50 ml). Dried with $MgSO_4$ and concentrated in vacuo. The crude product was purified by DCVC in 10 fractions of 100 ml eluted with 0-4% DCM in heptane.

Yield: 3.86 g (9.6 mmol, 86%); Dioctylcyclopentadithiophene; ^{1}H-NMR (250 MHz, $CDCl_3$) δ = 7.14 (d, 2H, J=5.1 Hz); 6.93 (d, 2H, J=5.0 Hz); 1.81 (m, 4H); 1.34-1.02 (m, 24H); 0.99-0.79 (m, 6H)

Reaction 11b: Stannylation

Dioctylcyclopentadithiophene (1.5 g, 3.7 mmol, 1 eq) was dissolved in anhydrous THF (45 ml) and cooled to -78^{o}C. BuLi (2.5 M in hexane, 3.69 ml, 9.2 mmol, 1.25 eq) was added drop wise during 2 hours. The solution was allowed to reach RT and stirred for 2 hours, before being cooled to -78^{o}C. Me_3SnCl (1.85 g, 9.25´6 mmol, 1.25 eq) dissolved

in anhydrous THF (3 ml) was added and the solution stirred at RT overnight. The reaction mixture was then poured into water (300 ml) and extracted with CH_2Cl_2 (3 x 150 ml) – adding a pinch of NaCl helped to separate the phases. The organic phase was washed with $NaHCO_3$ (150 ml). It was then added $MgSO_4$ and activated carbon and stirred for 10 minutes before being filtered through celite. It was then concentrated in vacuo using an oil pump. The crude product was purified by DCVC on a short colum pretreated with Et_3N in heptane. The eluent was 20% Et_3N in 5% EtOAc/heptane mixture. The first two fraction contained product.

Yield: 1.25g (1.25 mmol, 34%); 4,4-dioctyl-4H-cyclopenta[2,1-b:3,4-b']dithiophene-2,6-diyl)bis(trimethylstannane), ^{1}H-NMR (500 MHz, $CDCl_3$) δ = 6.94 (s, 2H); 1.78 (m, 4H); 1.33-0.93 (m, 28H); 0.85 (t, 6H, J=7.1 Hz); 9.38 (s, 18H)

Reaction 11c: Oxidative polymerization

Dry $CHCl_3$ (40 ml) was added to a flame dried flask and degassed with argon for 15 minutes before addition of $FeCl_3$ (2.4 g, 15 mmol, 4 eq). Dioctylcyclopentadithiophene (1.5 g, 3.7 mmol, 1 eq) was dissolved in $CHCl_3$ (4 ml) and added drop wise to the $FeCl_3$ solution. The solution was then stirred for 24 hours at RT and then concentrated in vacuo to a viscous liquid that was poured into MeOH (450 ml) and stirred for 20 minutes. The solution was filtered and the precipitate was washed with MeOH until the filtrate was clear (app. 600 ml). The solid was dissolved in $CHCl_3$ and hydrazine hydrate (6 ml, 30% in THF) was added. The solution was then refluxed for 22 hours and then washed with water (2 x 150 ml). The organic phase was concentrated in vacuo and added to MeOH (300 ml). The solution was filtered directly into a cotton thimble and Soxleth extracted (MeOH 1 day, acetone 1 day, heptane 2 days, $CHCl_3$ 1 day). The $CHCl_3$ phase was concentrated in vacuo and precipitated in MeOH (200 ml), filtered and the solid dried in a vacuum oven.

Yield: 0.5g (1.25 mmol, 33%); Poly(dioctylcyclopentadithiophene); ^{1}H-NMR (500 MHz, $CDCl_3$) δ = 7.02 (2H); 1.88 (4H); 1.30-0.97 (22H); 0.89 (6H)

Reaction 11d: Stille polymerization

4,4-dioctyl-4H-cyclopenta[2,1-b:3,4-b']dithiophene-2,6-diyl)bis(trimethylstannane) (1.2 g, 1.6 mmol, 1 eq) and 4,7-dibromobenzo[c][1,2,5]thiadiazole (0.48 g, 1.6 mmol, 1 eq) was dissolved in anhydrous DMF and degassed with argon for 30 minutes. $Pd(PPH_3)_4$ in anhydrous THF (3ml) was added and the reaction flask was sealed. The reaction was stirred at 120^{o}C under argon for 2 days. The solution was then filtered an the precipitate was washed with MeOH (2 x 50 ml) and DMF (2 x 50 ml). The DMF fractions were concentrated in vacuo and poured into MeOH (200 ml). The solution was filtered directly into a cotton thimble and Soxleth extracted (MeOH 1 day, EtOH 1 day, acetone 1 day, $CHCl_3$ 2 days) The $CHCl_3$ concentrated in vacuo to a dark solid that was dried in avacuum oven.

Yield: 580 mg (1.1 mmol, 67%), Poly(4-(4,4-dioctyl-4H-cyclopenta[2,1-b:3,4-b']dithiophen-2-yl)benzo[c][1,2,5]thiadiazole); ^{1}H-NMR (500 MHz, $CDCl_3$) δ = 8.10 (2H); 7.85 (2H); 1.95-0.75 (34H)

References

1 P. M. Beaujuge, C. M. Amb and J. R. Reynolds, *Adv Mater,* 2010, **22,** 5383-5387.

2 B. D. Reeves, C. R. G. Grenier, A. A. Argun, A. Cirpan, T. D. McCarley and J. R. Reynolds, *Macromolecules,* 2004, **37,** 7559-7569.

3 C. M. Amb, P. M. Beaujuge and J. R. Reynolds, *Adv Mater,* 2010, **22,** 724-728.

4 C. M. Amb, J. A. Kerszulis, E. J. Thompson, A. L. Dyer and J. R. Reynolds, *Polym. Chem.,* 2011, **2,** 812-814.

5 P. Shi, C. M. Amb, E. P. Knott, E. J. Thompson, D. Y. Liu, J. Mei, A. L. Dyer and J. R. Reynolds, *Adv Mater,* 2010, **22,** 4949-4953.

6 A. L. Dyer, M. R. Craig, J. E. Babiarz, K. Kiyak and J. R. Reynolds, *Macromolecules,* 2010, **43,** 4460-4467.

7 J. Jensen, A. L. Dyer, D. E. Shen, F. C. Krebs and J. R. Reynolds, *Advanced Functional Materials,* 2013, **23,** 3728-3737.

8 R. M. Walczak, J. -H. Jung, J. S. Cowart Jr. and J. R. Reynolds, *Macromolecules,* 2007, **40,** 7777-7785.

9 R. M. Walczak, J. K. Leonard and J. R. Reynolds, *Macromolecules,* 2008, **41,** 691-700.

10 E. P. Knott, M. R. Craig, D. Y. Liu, J. E. Babiarz, A. L. Dyer and J. R. Reynolds, *J. Mater. Chem.,* 2012, **22,** 4953-4962.

11 G. Sonmez, H. B. Sonmez, C. K. F. Shen, R. W. Jost, Y. Rubin and F. Wudl, *Macromolecules,* 2005, **38,** 669-675.

12 G. Sonmez, H. B. Sonmez, C. K. F. Shen and F. Wudl, *Adv Mater,* 2004, **16,** 1905-1908.

13 F. A. Arroyave, C. A. Richard and J. R. Reynolds, *Org. Lett.,* 2012, **14,** 6138-6141.

14 C. Kitamura, S. Tanaka and Y. Yamashita, *Chem. Mater.,* 1996, **8,** 570-578.

15 C. -G. Wu, M. -I. Lu, S. -J. Chang and C. -S. Wei, *Adv. Funct. Mater.,* 2007, **17,** 1063-1070.

16 C. -G. Wu, M. -I. Lu and P. -F. Tsai, *Macromol. Chem. Phys.,* 2009, **210,** 1851-1855.

17 P. Coppo, D. C. Cupertino, S. G. Yeates and M. L. Turner, *Macromolecules,* 2003, **36,** 2705-2711.

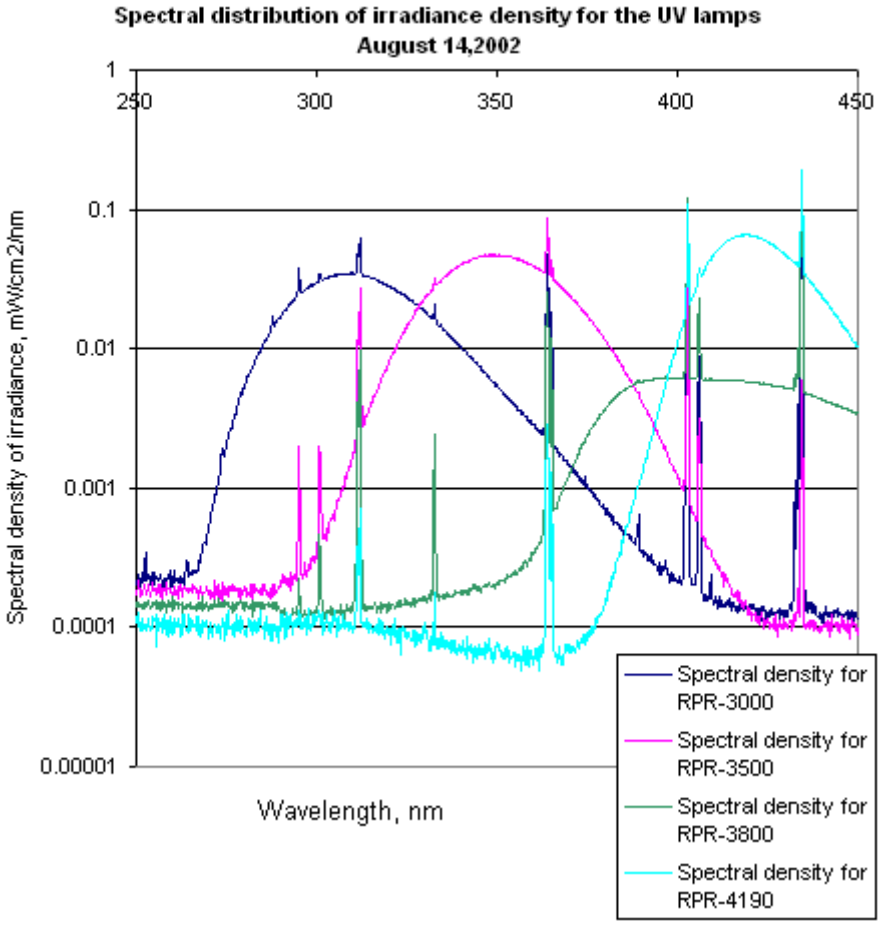
Spectral distribution of irradiance density for the UV lamps
August 14,2002
Spectral density of irradiance, mW/cm2/nm
1
0.1
0.01
0.001
0.0001
0.00001
250
300
350
400
450
Wavelength, nm
Spectral density for RPR-3000
Spectral density for RPR-3500
Spectral density for RPR-3800
Spectral density for RPR-4190

Manufacture and Demonstration of Organic Photovoltaic-Powered Electrochromic Displays Using Roll Coating Methods and Printable Electrolytes

Jacob Jensen,[1] Henrik F. Dam,[1] John R. Reynolds,[2] Aubrey L. Dyer,[2] Frederik C. Krebs[1]

[1]Department of Energy Conversion and Storage, Technical University of Denmark, Frederiksborgvej 399, DK-4000 Roskilde, Denmark

[2]The George and Josephine Butler Polymer Research Laboratory, Department of Chemistry, Center for Macromolecular Science and Engineering, University of Florida, Box 117200 Gainesville, Florida

Correspondence to: F. C. Krebs (E-mail: frkr@risoe.dtu.dk)

Received 15 November 2011; revised 16 December 2011; accepted 16 December 2011; published online 17 January 2012
DOI: 10.1002/polb.23038

ABSTRACT: Electrochromic devices (ECDs) were prepared on flexible substrates using spray coating and slot-die coating methods. The electrochromic materials were the conjugated electroactive polymers, poly((2,2-bis(2-ethylhexyloxymethyl)-propylene-1,3-dioxy)-3,4-thiophene-2,5-diyl) as a vibrantly colored active material (ECP-Magenta) and poly(*N*-octadecyl- (propylene-1,3-dioxy)-3,4-pyrrole-2,5-diyl) as a minimally colored, charge balancing material (MCCP). Two electrolyte systems were compared to allow development of fully printable and laminated devices on flexible substrates. Devices of various sizes, up to 7 × 8 cm^2, are demonstrated with pixelated devices containing pixel sizes of 4 × 4 mm^2 or 13 × 13 mm^2. The transmission contrast exhibited by the devices, when switched between the fully bleached and fully colored state, was 58% at a visible wavelength of 550 nm, and the devices exhibited switching times of <10 s. Additionally, we demonstrate the utilization of printed organic photovoltaic devices (with or without the use of a lithium-polymer battery) to power the devices between the colored and bleached state, illustrating a self-powered ECD. © 2012 Wiley Periodicals, Inc. J Polym Sci Part B: Polym Phys 50: 536–545, 2012

KEYWORDS: adhesion; conjugated polymers; coatings; electrochemistry; electrochromism; interfaces; processing; thin films

INTRODUCTION Thin, functional, organic, and polymeric films for electronic devices have attracted significant interest industrially due to the promise of enabling manufacture of equivalents to existing solutions much more efficiently and at much lower cost. Examples of this include organic light emitting diodes (OLEDs),[1] white OLEDs[2] and light emitting electrochemical cells,[3,4] light harvesting devices such as small molecule photovoltaics[5] and polymer photovoltaics (OPVs),[6] color changing devices for displays such as e-paper, LCDs, and electrochromics (ECs),[7] logic circuitry such as transistors,[8] diodes,[9] and memory elements,[10] and energy storage devices such as thin film batteries[11] and supercapacitors.[12] Advantages of the many organic-based materials discussed above, over their well-established inorganic counterparts, include processability to yield printable materials, mechanical flexibility to allow use of flexible and organic substrates, and lower power consumption in many cases.[13] Organic and polymeric ECs also fall into this category as, in the past decade, full classes of materials have been developed that are processable from common organic and aqueous solvents, the use of flexible and all-organic electrodes has been demonstrated, and the full color palette of polymeric electrochromes has been developed through use of structural modification to achieve the subtractive primaries, cyan–magenta–yellow and red–yellow–blue along with black.[14,15]

When considering organic materials for active devices, the use of roll coating and roll-to-roll printing methods is an advantage that would allow low-cost and high-throughput processing as demonstrated for OPV devices. These polymer solar cells have been demonstrated in product-integrated applications comprising the light energy harvesting polymer solar cell, a thin film battery for energy storage, and a LED as a light source.[16–18] The poor match between the relatively power hungry LED and low power density OPV is managed through the battery and the intentional use of the application where light is used intermittently.

In this work, we demonstrate the use of polymer solar cells to drive EC display devices. The EC devices (ECDs) were fabricated using roll coating methods onto indium tin oxide coated flexible substrates (ITO/polyethyleneterphthalate (PET)) and switch between a vibrantly colored magenta state and a near colorless bleached state with low current density. These devices exhibit switch times on the order of several

Additional Supporting Information may be found in the online version of this article.

seconds with use of a printed, crosslinked electrolyte. With the low current required to switch, combined with the bistability that the ECDs exhibit, we are able to show that there is a good match between the power density of an OPV and the power requirements of EC displays by integrating both into printed module devices wherein one OPV powers a switch to the colored state and a second OPV powers a switch to the bleached state. In situations where constant lighting is not available, modules were constructed and demonstrated where a lithium battery stores the charge harvested by the OPV and further powers the ECD.

EXPERIMENTAL

All chemicals and solvents were used as received unless otherwise noted. The polymer inks used for the poly(methylmethacrylate) (PMMA)/propylene carbonate (PC) devices had an electrolyte content equivalent to that of the electrolyte-binder layer (w/w) to avoid cracking in the polymer film. Chloroform was used as the solvent because of the solubility of both polymer and salt, while having a reasonably low vapour pressure for roll coating. The ElectroChromic Polymer (ECP)-Magenta had a M_n of 76 kDa and the MCCP had a M_n of 56 kDa. The concentrations of inks were varied according to coating method. Solutions of 5 mg/mL were used in the spray coating experiments. In the spin coating experiments, a 20 mg/mL concentration of polymer was used, whereas the concentration used for slot-die coating varied between 20 and 40 mg/mL in $CHCl_3$.

The electrolyte solution was a mixture of PMMA (M_n 80,000 kDa; 4.4 g), tetrabutylammonium-hexafluorophosphate ($TBAPF_6$; 2 g), and PC (40 mL). The suspension was stirred at 100 °C until the PMMA was completely dissolved (3–4 h). To this was added a UV curable binder mixture comprising of Ebecryl® 150 (44 g), Ebecryl® 116 (3.5 g), Additol® BCPK (tradename of Cytec) (2.5 g; all from Cytec), and Zonyl FSO (trade name of Dupont)-100 (1.5 g). A typical electrolyte:-binder solution was a 2:1 mixture, which was mixed well and sonicated before use.

The ionic liquid electrolyte solution was made according to Watanabe with a slight modification.[19] Methylmethacrylate (MMA) and the crosslinking agent ethyleneglycol-dimethacrylate was purified by distillation and degassed before use. Benzoylperoxide was recrystallized from chloroform/methanol before use. MMA (0.02 mol), the crosslinker ethylenedimethacrylate (2 mol %) and 1-ethyl-2-methyl-imidazolium-bis(triflouromethane sulfonyl)imide (0.02 mol) were mixed in a round-bottomed flask and benzoyl peroxide (BPO) (0.5 mol %) was added. A condenser was added and the solution stirred at 85 °C for 4 h, after which acetonitrile (10 mL) was added. Further stirring (12 h) at 85 °C yielded a slightly yellow viscous solution that was used without further purification.

Roll Coating

Roll coating was performed on a small-scale roll coater with PET foil substrates.[20] The foil came prepared with a 175 μm sputtered ITO layer, etched into stripes of 4 mm or 13 mm with a nominal sheet resistivity of 100 Ω/□. Lengths of 1 m were coated at a time and with a coating width of 50 mm, thereby overlapping three of the ITO stripes. ECP-Magenta, MCCP, and electrolyte were coated on the machine with a high degree of uniformity.

EC Assembly

The ECDs were assembled manually due to the adhesiveness of the electrolyte. The ITO covered PET substrate was cleaned with isopropanol prior to coating. After coating of the various layers, 1 cm of ITO was carefully made available for electrical contact by removing the polymer and electrolyte layer with isopropanol. The two films were assembled perpendicular to each other. After assembly, the device was run through a laminator effectively forming a laminate joint.

Polymer Solar Cells and Demonstrator Assembly

The polymer solar cell modules used in this study were fully roll-to-roll processed and has been described in use for the Organic Electronics Association (OE-A) demonstrator.[18] The typical performance when initially prepared comprised a power conversion efficiency of 2%, open circuit voltage of 7.5–8.5 V, a device short circuit current of 10–15 mA, and a fill factor of 30–35%.

RESULTS AND DISCUSSION

Over the last several decades, the availability of EC polymers exhibiting a wide range of neutral state colors, switching to highly transmissive, has made the use of these materials in vibrantly colored displays, such as e-paper and e-readers, a serious possibility.[14] What has advanced this possibility even further is that many of these materials are also solution processable, allowing for use of film casting and patterning methods not previously used, such as spray casting, inkjet printing, slot-die coating, and several others. However, as the processability has improved, the characterization methods have remained the same with application of the polymer film to a small transparent electrode (typically ITO/glass), immersed in a 1 cm cuvette, for electrochemical and optical characterization. Further application of these materials to device platforms has also remained relatively small, and on rigid substrates, while little effort has extended to the use of roll coating and roll-to-roll coating methods for large area, flexible devices, or demonstrators. Additionally, little effort has been put toward understanding the power and energy requirements for such devices regarding the needs for switching between extreme states or maintaining a constant state. It is expected that the energy requirements are relatively low, as these devices are redox devices and that they exhibit memory, in that a specific color state, after an initial voltage hold, will remain after taken to open circuit. [21–23] The extent of time allowed to pass at open circuit before a refresh pulse is needed can vary based on fabrication conditions and redox potential of the device, but the energy requirements are significantly lower than those seen for solution-based ECDs, such as viologens in solution.

Here, we present the development of a printed ECD in a demonstrator where the device is powered by printed OPVs. In general, there are several opportunities and challenges for EC technology as presented in Figure 1. We have these broken down into three main points (materials, addressability,

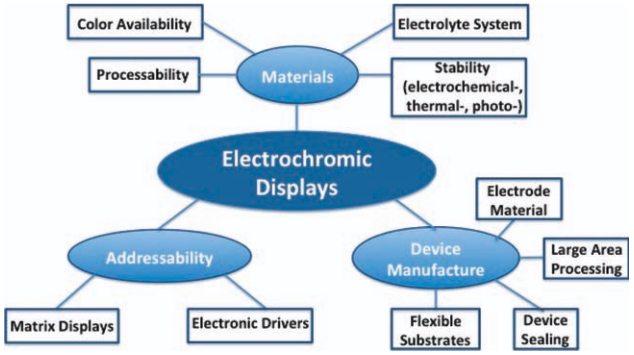

FIGURE 1 Challenges and possibilities in ECD development.

and device manufacture). As mentioned previously, recent work has addressed the challenges involving color availability and processing, allowing for a full color palette of solution processable polymers, not previously available. However, little effort has focused on using these materials in full device manufacture, looking at use of flexible substrates and large area processing, let alone addressability of matrix displays and integration of electronics drivers.[24] As an effort toward use of EC materials in commercial applications, such as currently available in auto mirrors, the development process for ECDs is at a stage where further progress has to center on efficient production methods combining high output, reliability, and low cost. To realize these important parameters, where conjugated polymers are concerned, the employment of roll coating onto flexible substrates emerges as the technique of choice. The success of using these techniques in polymer photovoltaics manufacture has stimulated the use of similar techniques in ECDs. The research presented in this article centers on the progress toward a demonstrator ECD with effort focused toward printable electrolyte development, printing methods, device lamination, and finally, incorporation into a photovoltaic-powered module, addressing several of the points illustrated in Figure 1.

Materials and Coating Methods

The EC polymers used in this work were reported previously by Reynolds et al. and were the poly((2,2-bis(2-ethylhexyloxymethyl)-propylene-1,3-dioxy)-3,4-thiophene-2,5-diyl) (ECP-Magenta) that switches between a vibrant magenta color when charge neutral and highly transmissive, nearly colorless when oxidized,[25] and the PProDOP-N-C18 (MCCP) was used as the counterpolymer wherein the polymer provides charge balance during device operation but lends minimal color to the device optical properties. Both polymers are highly soluble in common organic solvents and have been routinely processed from solution using spray casting. In this work, we examined use of spray processing and slot-die coating onto flexible substrates. We initially used spray casting, as this technique is known to create an open morphology in the film[14] and is advantageous as it easily allows ions from the electrolyte layer to be driven into the polymer film when a current is applied. In unpublished trials, slot-die coated films exhibited extensive cracking when switched between the two redox states. This is because the slot-die coated films are more dense than the spray cast films with a compact film morphology.[26] The observed cracking in slot-die coated films is explained by ions being forced into the dense polymer matrix on redox switching, causing swelling and creating stresses in the polymer film.[27] On reversal of the redox potential, the current reversed, and the matrix morphology collapses, resulting in cracking. Although the spray casting avoids this issue and is compatible with roll coating film formation, slot-die coating is a more reproducible method and was the method of choice for this work. The issue with film cracking was resolved by incorporating electrolyte ions into the polymer film during coating. A further advantage of incorporating ions in the polymer film during printing is minimization of the absorption change of the polymer when initially switched between the different redox states. This phenomenon, known as electrochemical annealing, results from the irreversible reorganization of the EC polymers caused by the initial applied current.[14,28] The setup used is shown in Figure 2(a–d) for roll coating, whereas the incorporation of spray processing on a roller is shown in Figure 2(e). For slot-die coating, the substrate is attached to the rotating drum and moved while the dispensing head is maintained stationary. The coating conditions are provided in the Experimental section. In short, both ECP-Magenta and MCCP were printed on ITO/PET films on a small-scale roll coater.[20] The coating solution contained the polymer dissolved to 20 mg/mL, $TBAPF_6$ to 4 wt % in chloroform. The electrodes consist of PET coated with 4 or 13 mm-wide ITO stripes or full ITO. The electrodes were coated with a layer of either MCCP or ECP-Magenta and afterward a layer of electrolyte mixed with a UV curable binder was applied.

Central to the preparation of an ECD that is flexible and roll-to-roll compatible is the development of a solid electrolyte system that enables laminate formation of the device while maintaining fast and robust switching. We explored two approaches in this work to establish advantages/disadvantages between the use of an electrolyte system comprised of a dissolved electrolyte salt in a printable/coatable photocurable prepolymer with a swelling agent and a system comprises a printable/coatable polymer mixed with ionic liquid. The need for a printable electrolyte is crucial if one wants to gain all the benefits of a roll coating process, where a liquid electrolyte will not work. The electrolyte layer in the ECD serves multiple purposes. The first being that it serves as a source of moveable charge carriers (i.e., ions), which are able to counterbalance the induced charges on the ECPs during redox switching. This is accomplished by dissolving an appropriate salt in an ion conducting solvent, typically PC. PC being a polar aprotic solvent is widely used in ECD studies, as it fulfils many of the requirements for an electrolyte solvent. The high polarity of PC allows it to dissolve the electrolyte salt and its high relative permittivity/dielectric constant introduces capacitance in the system allowing charge to build up on the ECPs. Additionally, its excellent properties as a plasticizer are used to modulate the plasticity of PMMA. The second role of the electrolyte in laminated devices is that it acts as an adhesive layer when sandwiched between

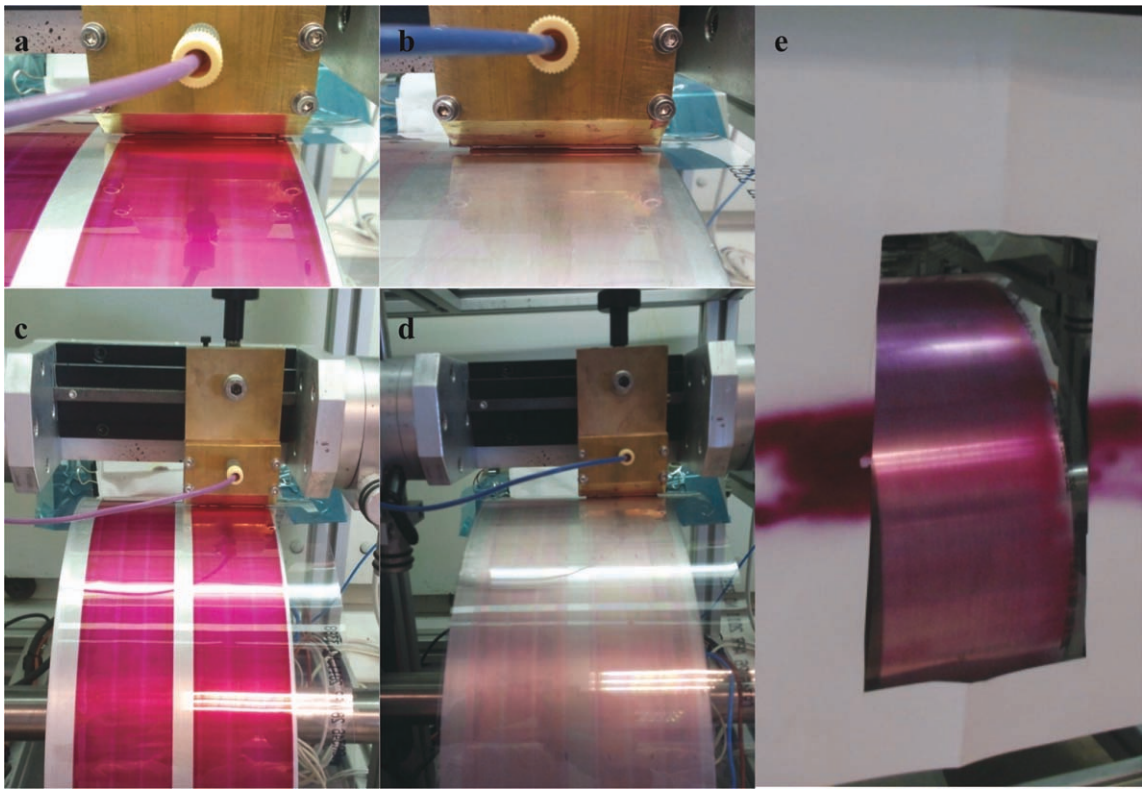

FIGURE 2 Roll coating of (a and c) ECP-Magenta from a 20 mg/mL solution and (b and d) MCCP from a 20 mg/mL solution. (e) A spray-coated substrate coated with 20 mg/mL ECP-Magenta.

the two active layers during lamination. The device presented in this report either made use of a PC/PMMA system or a PMMA/ionic liquid electrolyte. For the former, variation of the PC/PMMA ratio allows for an electrolyte system with a viscosity compatible with roll coating while enabling curing at a later stage for sealing. In the case of the PMMA/PC electrolyte system, the required viscosity was achieved by mixing of the PMMA/PC/salt system with an UV-curable acrylate oligomer, Ebecryl®. Subjecting this electrolyte layer to approximately 1700 mJ/cm^2 of UV light dosage made the surface adhesive, which allowed for curing of the laminate joint after lamination. When the devices were examined for function in outside light exposure (powered by OPVs), the curing process continued inside the device resulting in ECDs with limited switching abilities after full sun exposure for about an hour (1000 W/m^2, AM1.5G). The result was a hardened and brittle electrolyte layer with poor ion mobility and consequently poor switching. The challenge in using the electrolyte layer as a sealant in addition to the other required properties arises because of counteracting properties of ion mobility (switching speed) and adhesive properties. This was then addressed by exploring the use of ionic liquids as the swelling agent/plasticizer in combination with ion conducting properties of such agents. The latter approach proved superior due to the fact that the system was fully cured and no longer subject to photochemical crosslinking when the device was assembled, yet exhibited sufficient ion mobility to allow switching of the device. We thus present here data for the most successful method that uses a polymer (PMMA) mixed with ionic liquid where we found reliable and fast switching and good adhesion between the ECP-Magenta and MCCP electrodes. The binder mixture was used as a sealant as well, thereby avoiding the tedious and slow process of using double-sided adhesive or epoxy liner. When the binder was appropriately cured, as detailed in the Experimental section, the two electrodes were combined with the architecture detailed in the following section and shown in Figure 3.

ECD Assembly and Testing

One of the strengths in using polymers in ECDs lies in their mechanical flexibility and, as such, the electrode material ideally should posses this ability as well. The flexibility is challenged by use of inorganic oxides (i.e., ITO on PET) as electrode material, as cracking during extensive stressing can be a problem, in addition to availability of high quality coated ITO films.[29] In the literature, this has been addressed by use of polyethylenedioxythiophene-polystyrenesulphonate (PEDOT:PSS) as electrode material in all polymer ECDs.[30,31] However, as PEDOT:PSS electrodes exhibit a light blue hue and affect the ultimate bleached state achieved, as well as dissolving and cracking during processing and device curing, ITO/PET was chosen as the electrode material in this report.

The devices were assembled by coating individual layers onto the transparent ITO/PET electrodes from opposite sides, followed by sealing the device using a UV curable

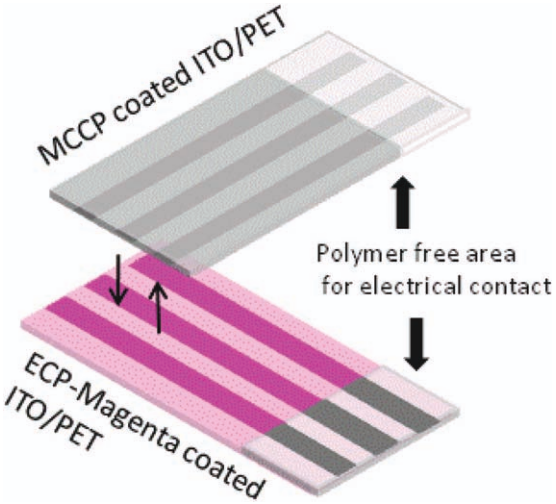

FIGURE 3 Assembly of the ECD. The foils consist of PET with ITO stripes or solid ITO. MCCP (top) and ECP-Magenta (bottom) is coated onto the foils followed by a layer of electrolyte. The foils are placed on top of each other with the ITO stripes perpendicular. An area of 1 cm on each foil is cleaned of polymer for connection to an external power source.

electrolyte binder. The electrolyte binder was chosen to act as a sealant for the device rather than peripheral adhesives as, from a production point of view, the use of double-sided adhesives is challenging in that they are not compatible with fast processing using batch methods (i.e., only a dedicated in-line machine can handle this efficiently). Fabricating the device in this way enables roll coating of the individual layers using either spray or slot-die coating as film forming techniques, followed by printing of the electrolyte-binder layer onto one electrode and laminating the two sides together. This multilayer approach is not without its limitations. Although it is possible to use roll coating with this assembly method, the multilayer approach is not directly roll-to-roll compatible, as the coated surfaces of two electrodes are to be joined through a lamination step with a sticky electrolyte. A "bottom-and-up" approach can solve this challenge but raises others regarding coating and manufacture. Building a device in one direction is the preferred method incorporating roll-to-roll coating techniques but the coating of individual layers needs to be orthogonal to each other.[32] This means that the coating of succeeding layers does not influence the already coated layer(s); typically by dissolution or oxidation. A typical challenge is dissolution of previous layers by the solvent as the materials used are often soluble in the same solvents. This can be solved by modification of the materials making them postcoating processable by hydrolysis[33] or heat[34] or by coating some layers from water and others from organic solvents.[32] Despite the aforementioned shortcomings, the multilayer approach was chosen as a starting platform for the development of the EC demonstrators.

The assembled devices switched efficiently with low current densities as illustrated for large area devices with an active area of >10 cm^2 as shown in Figure 4. As can be seen the initial voltage switch (± 2 V) induced a peak in the current with a maximum of 1 mA/cm^2, which decayed rapidly to a background current of $\sim$0.05 mA/cm^2. Between these two voltage extremes, the devices were switched from fully colored, vibrant magenta to fully bleached, nearly colorless, as shown in the photographs in Figure 4.

On monitoring the optical changes during switching, a change in transmission (ΔT) was found to be 44%, with a transmission in the clear state of $\sim$54% and a transmission as little as 10% in the colored state (at 550 nm) as shown in Figure 5(a). As seen in the figure, the response time remains constant for a period of 45 min with 30 s between switches (i.e., 90 switches), with minimal ΔT drop during that time.

To achieve 100% switching ($\Delta T = 44\%$), 10 s was required. As a substantial portion of the redox process occurs in the beginning of the voltage pulse, as seen by the initial current spike at the beginning of a switch, and the optical changes noticeable to the human eye are in the 90–95% range of the full switch, it is common to report the time periods required to reach these percentages of the full switch.[14] As shown in Figure 5(b), the full 100% switch is achieved in 10 s, whereas that for 95% of the full switch is reached in 5 s. These values are longer than those reported previously as we are using a crosslinked electrolyte with an expected ionic mobility less than that for the gel-type electrolytes. To determine the full ΔT across the visible region for this device type, a difference spectrum was measured and is shown in Figure 6. A difference spectral setup was used as there is difficulty in obtaining exactly matched sample and reference devices where optical effects (i.e., interference effects and reflective losses) are eliminated, especially where there are thin multilayer films as in these devices. We thus used a setup where two identical devices are counterdriven in, respectively, the reference and sample channel. We obtain the plot in Figure 6 that shows that the achievable ΔT with

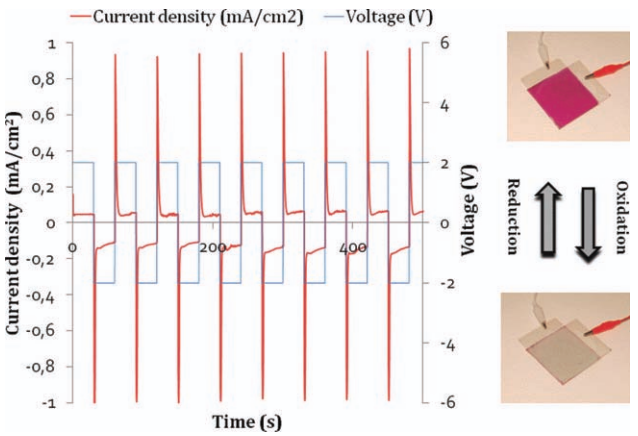

FIGURE 4 Current (left axis)/voltage (right axis) switching of a 10 cm^2 device, when switched between -2 and 2 V. The colored (reduced ECP-magenta) and bleached (oxidized ECP-Magenta) states for a device are shown in the photographs to the right.

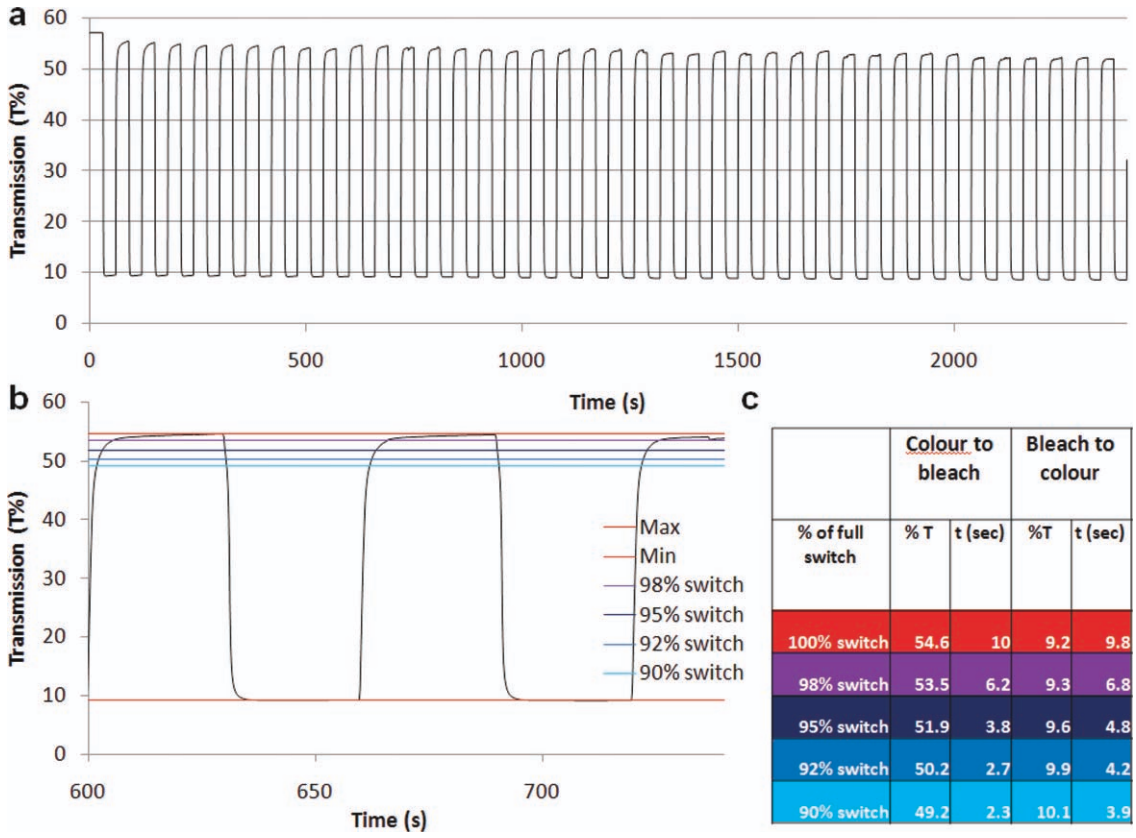

	Colour to bleach		Bleach to colour	
% of full switch	% T	t (sec)	%T	t (sec)
100% switch	54.6	10	9.2	9.8
98% switch	53.5	6.2	9.3	6.8
95% switch	51.9	3.8	9.6	4.8
92% switch	50.2	2.7	9.9	4.2
90% switch	49.2	2.3	10.1	3.9

FIGURE 5 Transmission of a device at 550 nm while switching from 2 to −2 V for 30 s at each potential. (a) Optical transmission data for a 45-min period (90 switches) causing a slight decrease in ΔT is observed. (b) Response times for the 600–750-s interval. The colors represent various degrees of switching. (c) Table showing response times corresponding to the lines in (b).

this device is around 58% at 550 nm. This value takes a bleached reference sample into account, thereby subtracting absorption by PET, ITO, reflections, and the polymeric electrolyte. The practically obtained ΔT of 44% [Fig. 5(a and b)] is obtained without a reference sample constituting the difference in transmission as seen by the eye. It is thus very satisfactory showing that our device is well constituted and unlikely to be improved much further. In addition, taking the inverse values of the plot where the reference is colored and the sample is clear (Fig. 6, green line), one should obtain values corresponding to a setup where the reference is bleached and the sample colored (Fig. 6, red line). Any difference between the values arises from nonmatched samples. For the values reported here, this corresponds to only 1%.

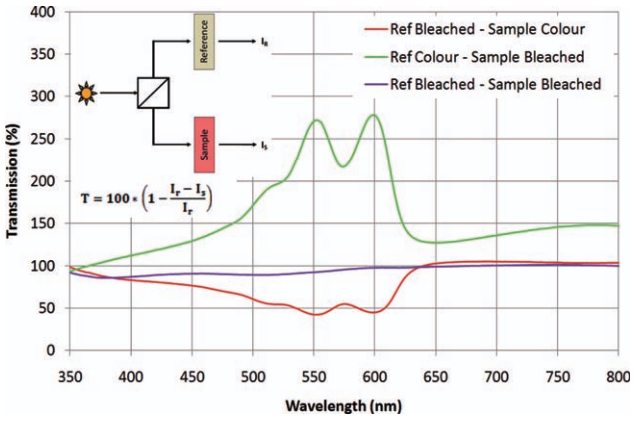

FIGURE 6 Difference plot. The green line results from the reference device being colored and the sample device bleached. The red line represents the opposite, that is, a bleached reference device and a colored sample device. The middle (purple) line results from both devices being bleached.

Demonstrator Assembly

As a large optical contrast can be effected by use of a relatively low voltage (+/−2 V) and low current (<100 μA/cm^2), use of polymer solar cells as power sources was ideal. The solar cell devices used in this study were prepared according to ProcessOne[35] following a device structure and outline as recently described for the OE-A demonstrator.[18] The polymer solar cell modules used to drive the ECDs in this study were prepared on a scale of more than 10,000 units and typically presented a V_{oc} in the range of 7.5–8.5 V and an I_{sc} in the range of 5–10 mA under illumination with 1 sun (AM1.5G, 1000 W/m^2). The solar cells were directly laser cut from the roll and used for direct incorporation into the prototypes developed here.

The demonstrator was prepared using printed electronic circuitry and assembly that was previously developed in an earlier study for an OPV/lithium-polymer battery powered

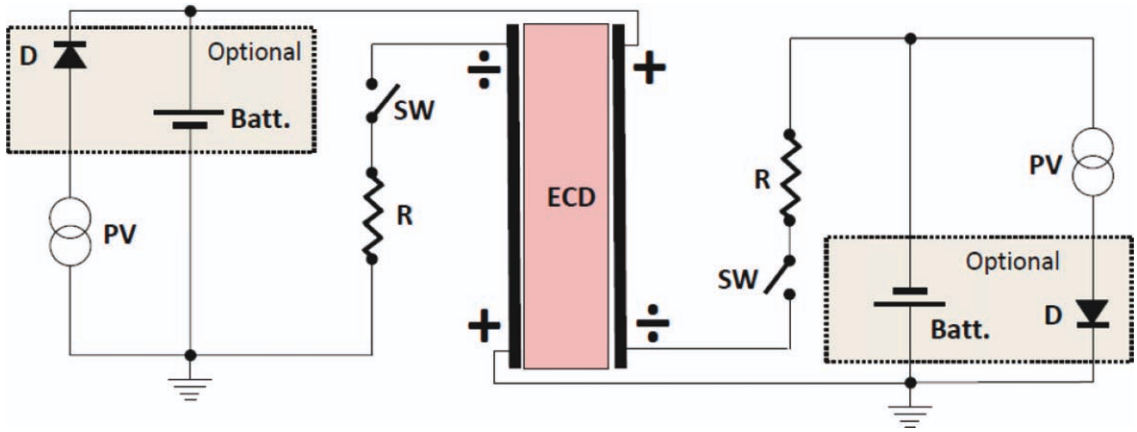

FIGURE 7 The electrical diagram for the demonstrator showing how the two independent circuits can be used to switch the ECD between the colored and transparent state. The switches are push buttons that are pressed alternately. In the case where the device is powered solely by the OPVs, the circuit elements marked optional are not included (top). The flexible printed circuitry is shown below for the version with battery and blocking diode (in dashed square box). The display area measures 40 × 40 mm^2.

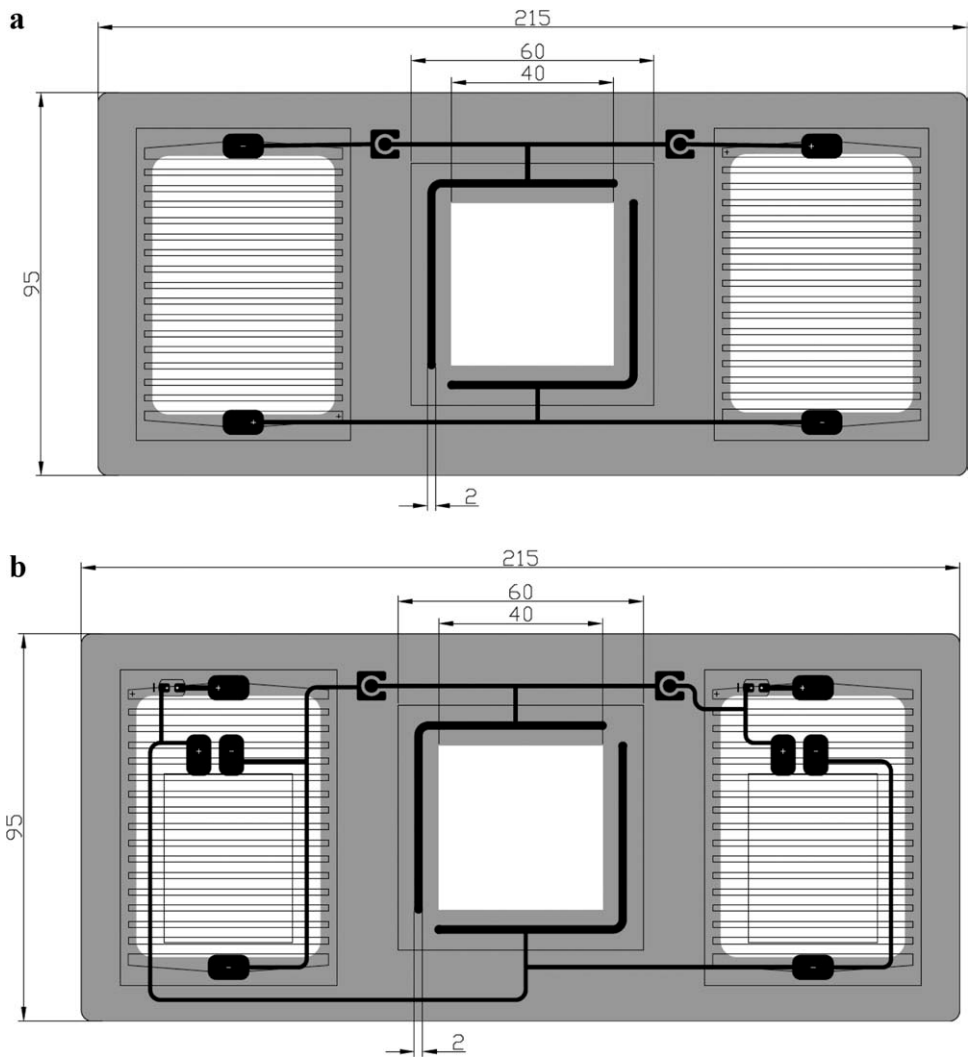

FIGURE 8 Illustration of the schematic circuit diagrams for devices powered by OPV alone (top) or OPV/lithium-polymer battery (bottom).

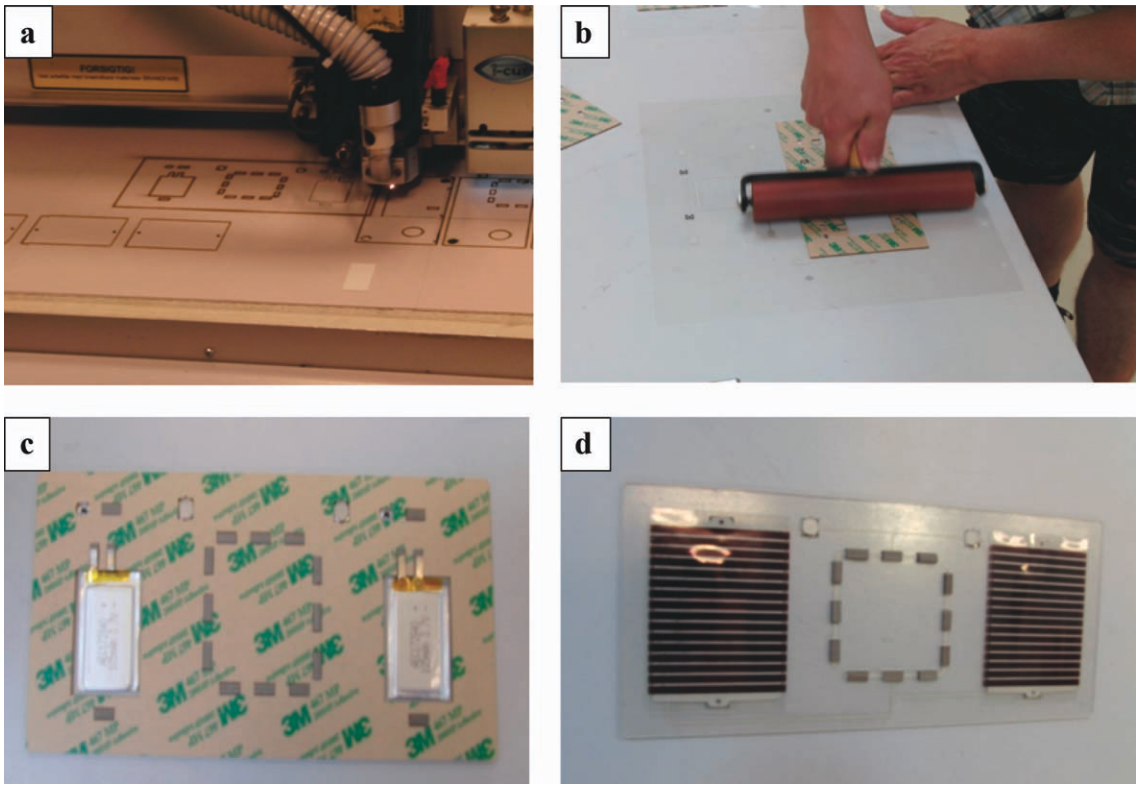

FIGURE 9 Demonstrator assembly. (a) Laser cutting of electrical circuit. (b) Lamination of adhesive polyester. (c) Polyester plate with lithium batteries and nickel sponges. (d) OPV module with on/off switches.

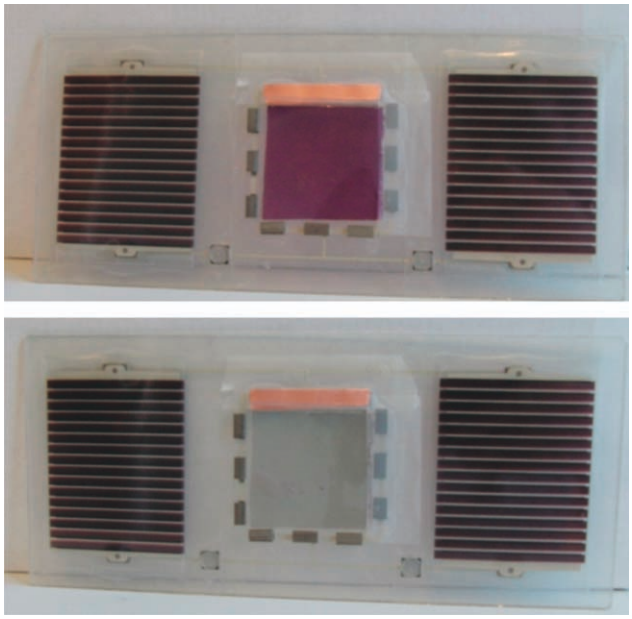

FIGURE 10 Demonstrator device, powered by polymer solar cells (far left and far right), with ECP-Magenta/MCCP ECD in the center. Contact to the ECD is made with printed circuitry from the solar cells to nickel sponges (seen around the periphery of the ECD), and the device is switched by pressing of buttons located at the bottom of the device.

flashlight[17] by replacing the white LED with the ECD. As the ECD needs to be driven electrically to switch states by passing a current through the device in opposite directions, we powered the ECD through two independent OPV circuits or OPV/lithium-polymer battery circuits as illustrated in Figure 7 where the circuit diagram is shown. The lithium-polymer battery presents a voltage in the range of 3.7–4.2 V depending on the state of charging and can supply a large current at this voltage. This resulted in fast switching times on the order of 2 s, but such large voltages can also lead to degradation of the various components in the device.[36] The switching times when powered by the solar cell alone depend on the incident light intensity and at full sun the switching time was on the order of 3 s.

The demonstrator circuitry was prepared by printing silver lines using sheet fed screen printing of a silver paste (Dupont 5007E) onto an optically clear polyester foil with a thickness of 130 μm that was cured at 140 °C for 10 min. A graphite paste was subsequently printed over the areas of the switch and the material again cured at 140 °C for 10 min. The circuit diagram for the devices is shown in Figure 8 for the demonstrators with the OPV alone [Fig. 8(a)] or with the OPV/lithium-polymer battery combination [Fig. 8(b)].

A 2.5-mm thick polyester plate was then prepared on each side with a 50-μm thick lined pressure sensitive adhesive (MP467 from 3M). The polyester sheets carrying the

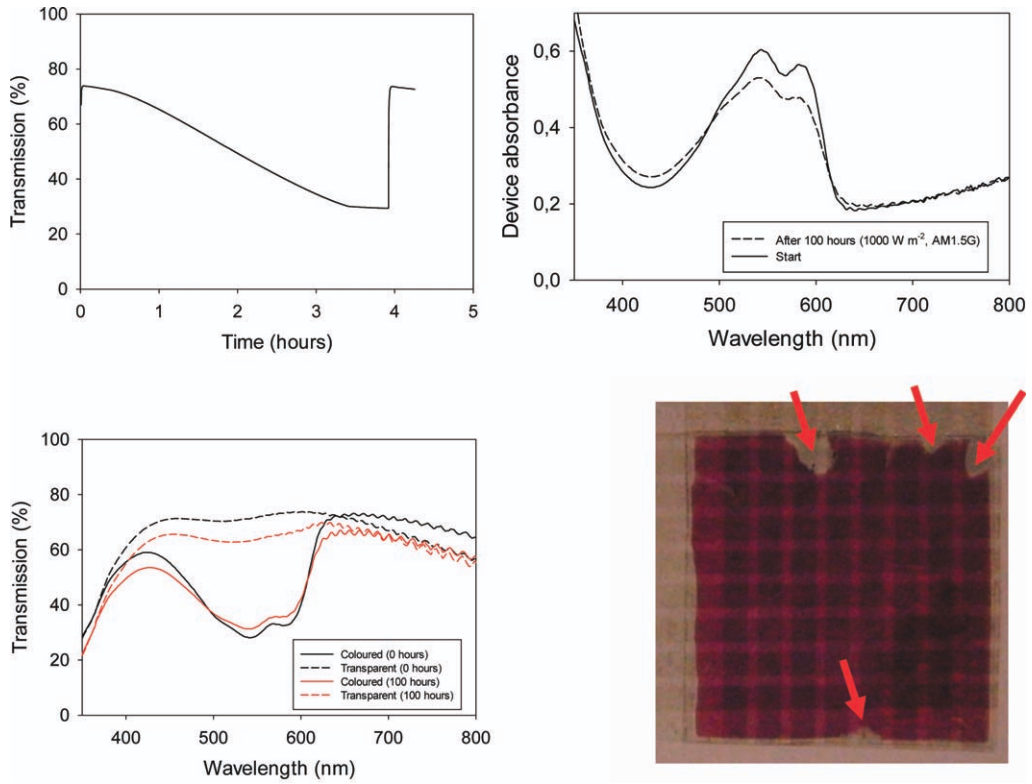

FIGURE 11 The hold time for a bleached device showing the gradual loss in transmission due to reversion from the oxidized to the reduced (colored) state when the electrical supply is removed (top left). A photobleaching experiment for a complete device under continuous illumination (AM1.5G, 1000 W/m^2, 45 °C) for 100 h leading to a 20% loss in absorbance (top right). The loss in switching capacity as a consequence of the 100-h illumination condition was 25% (lower left). The effect of photobleaching is shown with red arrows on a photograph of the photobleached device. It is also observed as ingress all around the edge (lower right).

adhesive was laser cut [Fig. 9(a)] into the desired shape of the demonstrator by cutting holes for the batteries, discrete component (1N4148 blocking diode), switches, and the nickel sponge via connections. The adhesive liner was then removed at one side and the printed circuit was applied to the adhesive [Fig. 9(b)] followed by mounting of the nickel via connections and the batteries [Fig. 9(c)]. Finally the solar cells [Fig. 9(d)] were applied over the batteries, the switch components inserted, and the ECD mounted followed by a final lamination to complete the device.

The completed device is shown in Figure 10 and movies of the device switching indoors (powered by the batteries) and outdoors (powered solely by solar cells) is supplied as Supplementary Information. Future work should address the possibility for crosslinking the electroactive polymers and electrolyte system or some other means of in-solubilization thus enabling both the bottom-and-up approach and ensure better thermomechanical properties such that the final devices become robust toward delamination during processing, handling, and operation. Although devices could be delaminated in the laminate joint by manual force, they are quite well joined and we estimate the fracture energy (G_c) to be significantly above >1 J/m^2 based on earlier studies for delamination of polymer solar cells.[37] Development of electrolyte systems with higher fracture energies would be a valid research goal.

Of significant importance is also the hold time and the temporal and photochemical stability of the devices during operation as these devices would be intended for use as variable shading of sunlight (e.g., in a window) or as a display unit (e.g., a billboard applied outdoors with backlight). We performed experiments to establish how long the bleached state is maintained after the power supply is removed from the device. The stable state for the ECD is the colored (reduced) state. Here, it is stable for extended periods of time. After bleaching, it takes on the order of 4 h to revert to the colored state (Fig. 11). This is of some importance for large area applications as a short hold time would use constant power consumption. Based on this result, it would seem that these ECDs have a large potential for display and shading applications with very low power consumption either through self powering using a solar cell as demonstrated here or through brief updates of the color state every 30 min. The devices prepared here were not encapsulated in a barrier to oxygen and water and in spite of that seem quite stable. We illuminated an operational device with a solar simulator (AM1.5G, 1000 W/m^2, 45 °C) for 100 h continuously and found that the degree of photobleaching was limited.

The device lost 20% in absorbance and when switching about 25% of the transmission change was lost (Fig. 11). The photobleaching was just visible to the eye and most significant in areas around the edges where slight delamination had occurred allowing for ingress of water and oxygen. This is a convincing result and we estimate that operation for many years is possible provided that water and oxygen are excluded from the ECD through a suitable barrier material. The shelf life is encouragingly long for practical development and use. We were unable to detect any decrease in absorbance or performance for devices stored or cycled in the dark for 4 months.

CONCLUSIONS

In this report, we have demonstrated that large area EC displays with high contrast and relatively fast response times can be achieved using EC polymers in combination with a printed and cured adhesive electrolyte. The devices were prepared by using roll coating methods on flexible substrates followed by lamination. The devices exhibited 58% ΔT when fully switched and $\sim$44% ΔT with switch times of $<$5 s. The power required for the devices were low with $+/-2$ V applied and <100 $\mu A/cm^2$ max current with a 5 $\mu A/cm^2$ background current. These low energy requirements paired well with the power output of printed polymer photovoltaic devices, allowing fabrication of a self-powered OPV/ECD module. We also established a preliminary assessment of the photochemical and temporal stability for the devices and found that full sun illumination (AM1.5G, 1000 W/m^2, 45 °C) of an ECD for 100 h led to a decrease in absorbance of 20% and a loss in ΔT of 25%.

ACKNOWLEDGMENTS

The authors thank Jan Fyenbo at Mekoprint A/S for technical assistance during manufacture of the demonstrator and also acknowledge the funding of the electrochromics program at UF by BASF and for their supply of the two EC polymers used in this work.

REFERENCES AND NOTES

1 Greenham, N. C.; Moratti, S. C.; Bradley, D. D. C.; Friend, R. H.; Holmes, A. B. *Nature* **1993,** *365*, 628–630.

2 Reineke, S.; Lindner, F.; Schwartz, G.; Seidler, N.; Walzer, K.; Lüssem, B.; Leo, K. *Nature* **2009,** *459*, 234–238.

3 Pei, Q.; Yu, G.; Zhang, C.; Yang, Y.; Heeger, A. J. *Science* **1995,** *269*, 1086–1088.

4 Fang, J.; Matyba, P.; Edman, L. *Adv. Funct. Mater.* **2009,** *19*, 2671–2676.

5 Uchida, S.; Xue, J.; Rand, B. P.; Forrest, S. R. *Appl. Phys. Lett.* **2004,** *84*, 3013–3015.

6 Brabec, C. J.; Sariciftci, N. S.; Hummelen, J. C. *Adv. Funct. Mater.* **2001,** *11*, 15–26.

7 Mortimer, R. J.; Dyer, A. L.; Reynolds, J. R. *Displays* **2006,** *27*, 2–18.

8 Dimitrakopoulos, C. D.; Malenfant, P. R. L. *Adv. Mater.* **2002,** *14*, 99–117.

9 Katsia, E.; Huby, N.; Tallarida, G.; Kutrzeba-Kotowska, B.; Perego, M.; Ferrari, S.; Krebs, F. C.; Guziewicz, E.; Godlewski, M.; Osinniy, V.; Luka, G. *Appl. Phys. Lett.* **2009,** *94*, 143501.

10 Katsia, E.; Tallarida, G.; Kutrzeba-Kotowska, B.; Ferrari, S.; Bundgaard, E.; Søndergaard, R.; Krebs, F. C. *Org. Electron.* **2008,** *9*, 1044–1050.

11 Meyer, W. H. *Adv. Mater.* **1998,** *10*, 439–448.

12 Jayalakshmi, M.; Balasubramanian, K. *Int. J. Electrochem. Sci.* **2008,** *3*, 1196–1217.

13 Forrest, S. R. *Nature* **2004,** *428*, 911–918.

14 Amb, C. M.; Dyer, A. L.; Reynolds, J. R. *Chem. Mater.* **2011,** *23*, 397–415.

15 Dyer, A. L.; Thompson, E. J.; Reynolds, J. R. *ACS Appl. Mater. Interfaces* **2011,** *3*, 1787–1795.

16 Krebs, F. C.; Nielsen, T. D.; Fyenbo, J.; Wadstrøm, M.; Pedersen, M. S. *Energy Environ. Sci.* **2010,** *3*, 512–525.

17 Krebs, F. C.; Fyenbo, J.; Jørgensen, M. *J. Mater. Chem.* **2010,** *20*, 8994–9001.

18 Krebs, F. C.; Fyenbo, J.; Tanenbaum, D. M.; Gevorgyan, S. A.; Andriessen, R.; van Remoortere, B.; Galagan, Y.; Jørgensen, M. *Energy Environ. Sci.* **2011,** *4*, 4116–4123.

19 Susan, M. A.; Kaneko, T.; Noda, A.; Watanabe, M. *J. Am. Chem. Soc.* **2005,** *127*, 4976–4983.

20 Dam, H. F.; Krebs, F. C. *Sol. Energy Mater. Sol. Cells* **2012,** *97*, 191–196.

21 Heckner, K.-H.; Kraft, A. *Solid State Ionics* **2002,** *152–153*, 899–905.

22 Lampert, C. M. *Sol. Energy Mater. Sol. Cells* **2003,** *76*, 489–499.

23 Mortimer, R. J. *Annu. Rev. Mater. Res.* **2011,** *41*, 241–268.

24 Andersson, P.; Forchheimer, R.; Tehrani, P.; Berggren, M. *Adv. Funct. Mater.* **2007,** *17*, 3074–3082.

25 Reeves, B. D.; Grenier, C. R. G.; Argun, A. A.; Cirpan, A.; McCarley, T. D.; Reynolds, J. R. *Macromolecules* **2004,** *37*, 7559–7569.

26 Krebs, F. C. *Sol. Energy Mater. Sol. Cells* **2009,** *93*, 394–412.

27 Rajesh; Pandey, S. S.; Kumar, D.; Takashima, W.; Kaneto, K. *Thin Solid Films* **2004,** *467*, 227–230.

28 Welsh, D. M.; Kloeppner, L. J.; Madrigal, L.; Pinto, M. R.; Thompson, B. C.; Schanze, K. S.; Abboud, K. A.; Powell, D.; Reynolds, J. R. *Macromolecules* **2002,** *35*, 6517–6525.

29 Ginley, D. S.; Bright, C. *MRS Bull.* **2000,** *25*, 15–18.

30 Mecerreyes, D.; Marcilla, R.; Ochoteco, E.; Grande, H.; Pomposo, J. A.; Vergaz, R.; Sánchez Pena, J. M. *Electrochim. Acta* **2004,** *49*, 3555–3559.

31 Argun, A. A.; Cirpan, A.; Reynolds, J. R. *Adv. Mater.* **2003,** *15*, 1338–1341.

32 Larsen-Olsen, T. T.; Andersen, T. R.; Andreasen, B.; Böttiger, A. P. L.; Bundgaard, E.; Norrman, K.; Andreasen, J. W.; Jørgensen, M.; Krebs, F. C. *Sol. Energy Mater. Sol. Cells* **2012,** *97*, 43–49.

33 Reeves, B. D.; Unur, E.; Ananthakrishnan, N.; Reynolds, J. R. *Macromolecules* **2007,** *40*, 5344–5352.

34 Hagemann, O.; Bjerring, M.; Nielsen, N. C.; Krebs, F. C. *Sol. Energy Mater. Sol. Cells* **2008,** *92*, 1327–1335.

35 Krebs, F. C.; Gevorgyan, S. A.; Alstrup, J. *J. Mater. Chem.* **2009,** *19*, 5442–5451.

36 Ma, C.; Taya, M.; Xu, C. *Electrochim. Acta* **2008,** *54*, 598–605.

37 Dupont, S. R.; Oliver, M.; Krebs, F. C.; Dauskardt, R. H., *Sol. Energy Mater. Sol. Cells* **2012,** *97*, 171–175.

Materials Views
www.MaterialsViews.com

ADVANCED FUNCTIONAL MATERIALS
www.afm-journal.de

Fast Switching ITO Free Electrochromic Devices

*Jacob Jensen, Markus Hösel, Inyoung Kim, Jong-Su Yu, Jeongdai Jo, and Frederik C. Krebs**

Indium-doped tin oxide free electrochromic devices are prepared by coating electrochromic polymers onto polyethylene terephthalate substrates encompassing two different silver grids as electrodes. One design comprises a flexoprinted highly conductive silver grid electrode, yielding electrochromic devices with a response time of 2 s for an optical contrast of 27%. The other design utilizes an embedded silver grid electrode whereupon response times of 0.5 s for a 30% optical contrast are realized when oxidizing the device. A commercially available conductive poly(3,4-ethylenedioxythiophene):poly(4-styrenesulfonate acid) formulation (PEDOT:PSS) is coated onto the silver grids as a charge balancing polymer, and is in this setting found to be superior to a polypyrrole previously employed in electrochromic devices. In addition, the PEDOT:PSS layer increases the conductivity in the hexagonal grid structure.

1. Introduction

The development of electrochromic devices (ECDs) has moved from laboratory conditions into pilot plants; whereby, new challenges have emerged that include avoidance of vacuum processing steps and use of simple printing, coating, and lamination methods for deposition and assembly of the devices. If these challenges are successfully addressed, polymer based electrochromic devices will be commercially attractive and competitive to existing solutions. A main obstacle is the replacement of indium-doped tin oxide (ITO) as the transparent electrode material. ITO has been widely used as electrode material in organic electronics, but due to the scarcity of indium, substituting this material for a less expensive one would significantly reduce production costs of ECDs.[1–3] Another incitement to replace ITO is the vast amount of energy used in the sputtering process employed in the production of ITO covered substrates. By avoiding such energy consuming processes, one would be able to manufacture ECDs with limited energy consumption from materials, to manufacturing and operation.

From an operational point of view, the use of ITO as electrode material in ECDs is problematic since a low concentration of charge carriers in ITO gives rise to a large sheet resistance. It has been established that the electrode resistance has a marked effect on the response time and optical contrast of an ECD,[4] and high electrode resistance leads to a non-uniform potential across the electrode (Ohmic loss), and a non-uniform current distribution in the electrolyte.[5] By using electrodes of moderate conductivity, increasing potentials are needed to achieve satisfactory response times and optical contrast, as the ionic mobility (already impeded by the semisolid gel electrolyte) partly depends on the electric field between the two electrodes. Due to several other chemical components, increasing the potential conflicts with the voltage limits, outside of which side reactions are likely to occur. These could be redox reactions of water due to moisture in the device or irreversible oxidation or reduction of the polymer films.[6–9] Such reactions can lead to reduced optical contrast, increased response times, and ultimately render the ECD non-functional.

One approach is using thin metal grids as electrode material. Such grids have been utilized as counter electrodes in inorganic based ECDs, and we have previously shown how ITO can be replaced by flexoprinting a silver based conductive hexagonal grid onto a transparent polyethylene terephthalate (PET) substrate.[5,10] Other reports show successful substitution of ITO by organic semiconductors (mostly poly(3,4-ethylenedioxythiophene), PEDOT) for fabrication of all-organic or fully printable ECDs.[11–14] Development of ITO free ECDs is an interesting academic accomplishment, as well as a major cost reducing factor, in line with our development of commercially attractive ECDs; combining flexibility, efficient production, high operational stability and good electrochromic properties. The achievements in developing ITO free electrochromic devices are shown in **Table 1**.

In this report, we show improved polymer based ECDs, comprising thin metal grid electrodes and we address several challenges;[15,16] a) Slow and uneven switching of flexoprinted silver grid based devices: by employing a hexagonal grid pattern (as opposed to a full ITO covered surface) lateral charge transport in the resulting cells produce a blooming effect within each cell. This effect is caused by differences in surface resistance, and areas in close proximity to the metal grid lines respond faster than those in the center of a hexagon. The difference in conductivity across the electrode surface cause switching of the devices in the order of 5–10 min. This is sufficient for applications such as shading or other light-management devices, but a limiting factor for other applications. b) Electrochemical decomposition of organic material: upon switching of the silver

J. Jensen, M. Hösel, Prof. F. C. Krebs
Department of Energy Conversion and Storage
Technical University of Denmark
Frederiksborgvej 399, DK-4000, Roskilde, Denmark
E-mail: frkr@dtu.dk
Dr. I. Kim, Dr. J.-S. Yu, Dr. J. Jo
Department of Printed Electronics
Korea Institute of Machinery and Materials
Daejeon, 305–343, Korea

DOI: 10.1002/adfm.201302320

Table 1. Response times for ITO free electrochromic devices.

Electrode material[a)]	Primary ECP[b)]	Abs_{max} [nm]	ΔT	Voltage range [V]	Response time – oxidizing [s]	Response time – reducing [s]	Refs.
PEDOT:PSS	PEDOT	650	14%	0.0 to 3.0	20	16	[12]
PEDOT:PSS	PProdot-Me_2[c)]	540	40%	–1.2 to 1.2	8[d)]	8[d)]	[11]
PEDOT:PSS	PEDOT	–[e)]	22–35%	0.0 to 2.0	–[e)]	–[e)]	[13]
Flexoprinted Ag grid/PEDOT	PProdot-$EtHx_2$[f)]	550	24%	–0.5 to 1.0	2	3.4	This work
Embedded Ag grid/PEDOT	PProdot-$EtHx_2$[f)]	550	29%	–0.5 to 1.0	0.3	2.5	This work

[a)]Material used for both electrodes; [b)]ECP: Electrochromic polymer; [c)]Poly((2,2-bis-methyl-propylene-1,3-dioxy)-3,4-thiophene-2,5-diyl); [d)]It is unclear whether the response time given is for both redox processes; [e)]Abs_{max} and response time where not available. The report presented ECDs showing a range of ΔT values; [f)]Poly((2,2-bis(2-ethylhexyloxymethyl)-propylene-1,3-dioxy)-3,4-thiophene-2,5-diyl).

grid based ECD, a discoloring of the device was observed, that was initially attributed to electrochemical decomposition of surfactants in the silver nanoparticle based ink used for printing the hexagonal grid structure. By using post-treated Ag-grid foils using intensive pulsed light (photonic sintering of the silver) the surfactants were satisfactorily removed,[12] but further investigation revealed that decomposition of the charge balancing polypyrrole used in the ECDs was partly responsible for the discoloration. c) Macroscopic gridlines: as the flexoprinted gridlines are currently of dimensions that cause some optical distortion when viewed at a close distance, an embedded grid having line widths of just 15 microns was explored as a less visible semi-transparent electrode grid material.

2. Results and Discussion

The two electrodes in ECDs must be able to accommodate the charge species that migrate to them during device operation in order to ensure electrochemical stability. If not protected by an electroactive species that can balance the charged species, irreversible redox reactions can occur directly on the electrode surface, with the risk of gradually lowering device performance.[21] Naturally, one electrode is coated with the primary ECP that ensures charge balance by reversible redox reactions. The other electrode should likewise by coated with an electroactive species, that ideally operate within the same potential range to ensure optimal response time and contrast.[22,23] Since most absorptive-transmissive (A/T) devices require the viewer to see through the device in the transmissive state, both electrodes need to be transparent. One way of resolving this is by using polymers that change color complementary too each other, which implies that one polymer is cathodically coloring and the other is anodically coloring. While using a color complementary polymer enhances the optical density in the colored state, the optical contrast in the ECD is lowered.[24] Another drawback using this approach is that two polymers are seldom exactly color complementary, which yields devices that has colored transmissive states.[25–27]

Instead of the color complementary approach, the secondary ECP can be an electroactive compound that has minimal absorbance in the potential region employed. Such a polymer is the recently published polypyrrole: poly(N-octadecyl-(propylene-1,3-dioxy)-3,4-pyrrole-2,5-diyl), nicknamed minimally color changing polymer (MCCP).[17,27] As the name implies MCCP lends limited absorption to the visible region and we have previously made use of this polymer as a counter polymer in ECDs, due to good solubility and processing properties that allows a wide range of coating applications.[10,20] These properties qualified MCCP to be one of the best choices as counter polymer for a grid based device. Unfortunately, we found that employing MCCP in a flexoprinted grid based device produced a slight reddish taint following repeated switches at –1 V to +1 V. By carefully taking the device apart, the discoloring was found to reside on the electrode coated with MCCP. It should be noted that we have never observed discoloring of MCCP in devices employing MCCP coated onto ITO in this potential range, and MCCP films are reported to retain 50% electroactivity (measured as current density) during 325 000 redox cycles between –0.5 V and 0.5 V for 5 s each in an argon purged electrolyte solution. In electrochromic devices, however, the chemical environment and operating conditions is different from standard laboratory test conditions. ECDs encompassing MCCP and poly((2,2-bis(2-ethylhexyloxymethyl)-propylene-1,3-dioxy)-3,4-thiophene-2,5-diyl (ECP-magenta) have been found to require potentials between –2 V and +2 V or –0.6 V and +1.4 V, depending on electrolyte composition and response time requirements.[17,20]

A second obstacle in using MCCP in combination with the silver grid electrodes is the blooming effect previously reported and shown in **Figure 1**A.[10] As the areas between the grid lines are non-conductive, the hexagonal grid structures result in an inhomogeneous electrical field between the two electrodes. This requires lateral charge transport for redox switching to occur, and the results is a slow uneven switching, as shown in Figure 1A.

2.1. Dual Functionality of PEDOT:PSS

To address the problems in using MCCP in combination with the silver grid design, a commercially available PEDOT:PSS formulation was employed as the counter polymer. PEDOT:PSS is well characterized, and polythiophenes are known to possess

Adv. Funct. Mater. **2013**,
DOI: 10.1002/adfm.201302320

www.MaterialsViews.com

ADVANCED FUNCTIONAL MATERIALS
www.afm-journal.de

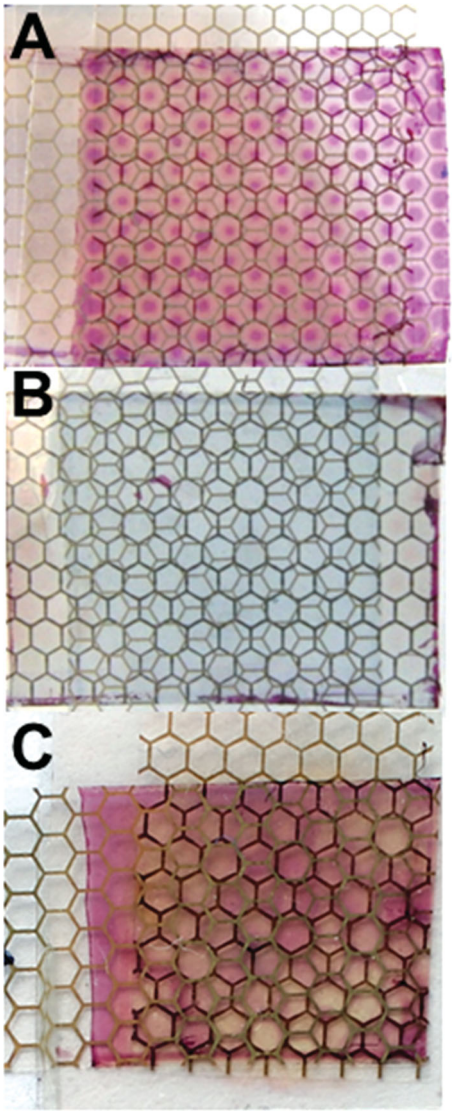

Figure 1. Flexoprinted silver grid electrodes. A) The blooming effect due to an inhomogeneous electrical field for an ECD comprising MCCP and ECP-magenta. B) ECD (in the oxidized state) where MCCP has been substituted by a conductive PEDOT:PSS formulation. The blooming effect is not observed in this device. The grid substrate has been post treated with IPL. C) ECD encompassing a flexoprinted silver grid that has not been post-treated using intensive pulsed light (IPL). This causes brown patches to form around the grid lines.

higher electrochemically stability than polypyrroles.[6,28–30] In addition to the charge balancing function, the coating of PEDOT on top of the silver grid increased the conductivity in the hexagonal grid patterns. The conductive PEDOT:PSS coating homogenized the electrical field such that the blooming effect was not observed and the devices switched evenly between the two redox states (compare Figure 1A and 1B). While both PEDOT and ECP-magenta are cathodically coloring polymers, the absorption that the thin PEDOT:PSS layer lends to the device is very limited as shown by Figure S2 in the Supporting Information. Figure S2A shows the absorption spectra (350–800 nm) for a device comprising only PEDOT:PSS on both electrodes layers switched at –0.5 V and +1.5 V, while Figure S2B shows the transmittance at 550 nm (Abs_{max}) for the same device switched between –0.5 V and 1.5 V. ΔT at 550 nm was found to be 2%.

2.2. Photonic Flash Sintering vs Non-Flashed Grid Electrodes

Figure 1B,C shows the difference in appearance after 20 switches at –1 V/+ 1.5 V between two ECDs based on flexoprinted silver-grid electrodes, with the only difference being that the grid in (B) has been post-treated using intensive pulsed light (IPL, photonic flash sintering) with a voltage setting of 3.6 kV (Sinteron 2000, Xenon Corp.) in a roll-to-roll process at 1 m min^{-1} prior to coating of polymers and electrolyte.[15] It should be noted that the silver grid was already fully sintered during the drying process while printing and the additional effect of an increased conductivity is small for the specific silver ink used here. As seen from Figure 1C, brown patches form around the grid lines that have not been post-treated. We believe the origin of this discoloring to be redox byproducts from the surfactants in the silver based ink caused by electrochemical oxidation and reduction of the device, possibly having reacted with the polymer layer coated directly on top. These byproducts are not to be seen in the devices comprising post-treated foils (Figure 1B).

2.3. Response Time

The response time partly defines the application possibilities of an electrochromic device. Since a common protocol on how to report response time have not been defined, response times are reported for a variety of ΔT values. The fastest response times are naturally linked to the smallest changes in optical contrast; however, it does make sense to report a series of response times based on different levels of optical contrast. As the majority of the redox reactions (and hence color change) occur in the beginning of a switch, 90% of a full switch might occur in two seconds while the remaining 10% of the switch takes 10 s to complete. In reporting response time, we focus on the optical contrast obtainable in relation to a given switch length rather than in relation to a percentage of a complete switch. This means that the 100% switch reported in **Figure 2** is 100% of the transmittance change achievable during a period of 10 s. In order to ease comparison with other ECDs, a full response time investigation is provided in the Supporting Information, Figure S3, which shows a full switch (maximum obtainable optical contrast) of 33% in 44 s at –0.5 V/+1.5 V. But fully switching an ECD lowers the long term stability, most likely due to electrochemically initiated side reactions. Figure 2 shows the response times for a 2 cm × 2 cm ECD based on the flexoprinted hexagonal silver grid and PEDOT:PSS coating to be 10 s for an optical contrast of 30% (550 nm) at –0.5 V and +1.5 V. Also of interest is the 26% optical contrast obtainable in approximately 2 s (depending on direction of the switch) at the same potentials, and the graph shows that a ΔT of 24% is obtainable in 10 s at –0.5 V and + 1 V.

% switch	Colour	to	Bleach	ΔT (%)	Time (s)
100	8.5		37.6	29.1	10.0
98	8.5		37.0	28.5	7.0
95	8.5		36.1	27.6	4.1
90	8.5		34.7	26.2	1.8

% switch	Bleach	to	Colour	ΔT (%)	Time (s)
100	37.6		8.5	29.1	9.5
98	37.6		9.1	28.5	6.0
95	37.6		10.0	27.6	3.8
90	37.6		11.4	26.2	2.5

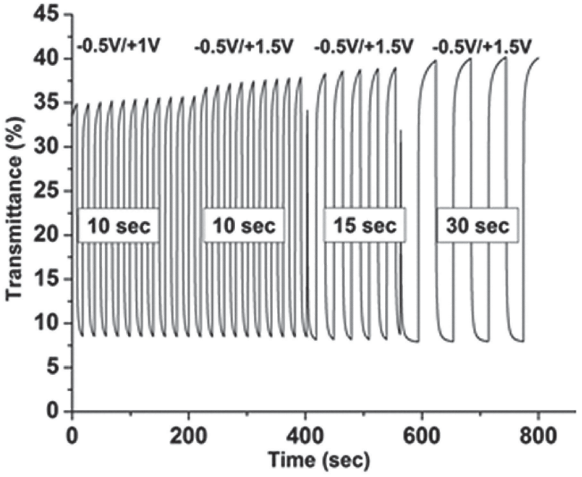

Figure 2. Response time for a 2 cm × 2 cm ECD employing a flexoprinted silver grid. The graph shows the transmittance at 550 nm for a device in response to switching at various potentials (above the graph) and switch lengths (inside the graph). The table shows the response time for the device switched between –0.5 V and +1.5 V with a switch length of 10 s.

Even though the silver grid lines in the flexoprinted silver grid are barely visible at distances beyond a few meters, a PET foil having embedded silver grid lines was employed to minimize optical distortion when the devices was viewed up close.[16,19] The line width in these foils was 15 micrometers and just noticeable as a slight blur. PEDOT:PSS coatings of a thickness similar to the flexoprinted grid devices were also employed for these devices. **Figure 3**A shows the a device employing flexoprinted Ag grid as electrodes alongside the dimensions of the gridlines, while Figure 3B shows that of a device employing embedded silver grid as electrode material. **Figure 4** shows the response times for a 1 cm × 1 cm ECD comprising the embedded silver grid. The transmittance recorded during "break in" of the device at –0.5 V/+0.5 V (the first 120 s) is included in the graph. During the break-in the optical contrast is limited to a few percent, but upon increasing the anodic potential to +1.0 V the optical contrast reaches 32%. When the potential is again lowered, the device reaches an optical contrast of 23% when switched between –0.5 V and +0.5 V. Looking at the table in Figure 4, the device generally exhibit fast response times with an optical contrast of 29% obtainable in 2.5 s when coloring and just 0.3 s when bleaching. By extending the switch to 0.8 s the optical contrast is increased to 31%, and these sub-second response times open up new possibilities for electrochromic devices. The low potentials sufficient for switching are encouraging as they serve to minimize unwanted side reactions in these devices.

2.4. Device Coloration Efficiency

The number of color centers formed as function of the charge used to evoke this change is described by the coloration efficiency, η. While high values are desirable for primary electrochromes, low values are wanted for the charge balancing polymer on the secondary electrode. Coloration efficiencies are reported in several ways, and the absence of a suitable device characteristic make comparison of devices incorporating identical polymers difficult.[31,32] Therefore, we have herein introduced the device coloration efficiency, η_d, which take the complex chemical environment of an ECD into account (compared to a standard ECP test cuvette set-up). Similar to the standard coloration efficiency, η, the device coloration efficiency η_d is given by the change in optical density at the maximum absorbing wavelength (Equation 2 divided by the charge density during that change (Equation 3). η_d is related to η by a device correction factor w, that include contributions due to electrode substrate, electrolyte matrix, and Faradaic side reactions occurring in the device (Equation 1). Knowing η_d is beneficial when designing electronic circuitry for device applications. Similar to the response time given above, η_d values are reported in relation to ΔT and not as percentages of a full switch.

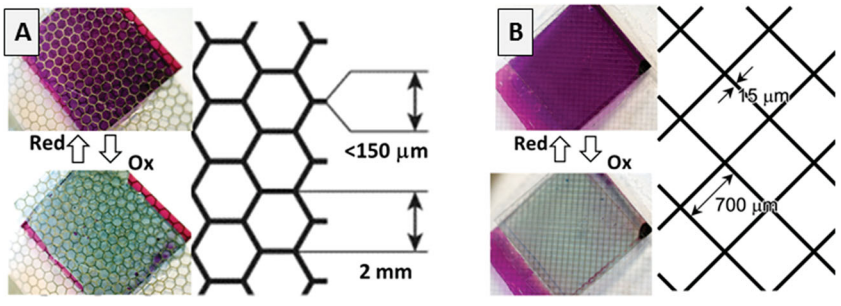

Figure 3. Dimensions of silver grid design. A) The two redox states of an ECD employing flexoprinted silver grid along a schematic showing the dimensions of the grid lines. B) A similar device, where the electrodes are from an embedded silver grid. Dimensions of the embedded grid are shown to the right.

Adv. Funct. Mater. 2013,
DOI: 10.1002/adfm.201302320

www.MaterialsViews.com

ADVANCED FUNCTIONAL MATERIALS
www.afm-journal.de

% switch	Colour	to	Bleach	ΔT (%)	Time (s)
100	5.8		37.8	32	10
98	5.8		37.2	31.4	0.8
95	5.8		36.2	30.4	0.5
90	5.8		34.6	28.8	0.3

% switch	Bleach	to	Colour	ΔT (%)	Time (s)
100	37.8		5.8	32	10
98	37.8		6.4	31.4	6.8
95	37.8		7.4	30.4	4.4
90	37.8		9.0	28.8	2.5

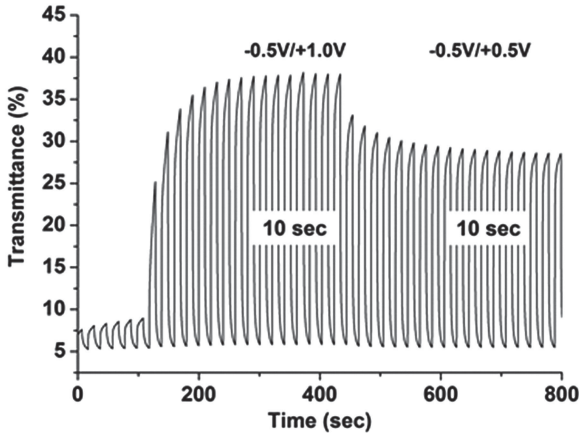

Figure 4. Response time for a 1 cm × 1 cm ECD employing an embedded silver grid. The graph shows the transmittance at 550 nm for a device in response to switching at various potentials (above the graph) for switch lengths of 10 s. The table shows the response time for the device switched between –0.5 V and +1.0 V with a switch length of 10 s.

$$\eta_d = \eta w \quad (1)$$

$$\Delta OD = \log(\%T_1/\%T_2) \quad (2)$$

$$\eta_d = (\log(\%T_1)\%T_2))/(Q_d) \quad (3)$$

Figure 5 shows η_d for a device employing ECP-magenta as the primary electrochromic polymer and flexoprinted hexagonal silver grid as transparent electrodes (solid line). The figure shows a decrease in η_d as the switch length is increased, which is to be expected as most of the color change occurs in the beginning of the switch. The most drastic change occurs during the first 10 s of the switch length where η_d drops from 310 C^{-1} cm^2 for a 1.8 s switch to 114 C^{-1} cm^2 for a 10 s switch at a potential of +1.5 V. After this the curve flattens out ending with a η_d of 20 C^{-1} cm^2 for a 60 s switch. The η_d obtained when reducing the device at –0.5 V is slightly lower for switches shorter than 10 s, but as the switch length is increased both redox reactions yield similar η_d values (additional η_d values for the two grid designs can be found in the Supporting Information, Figure S4). In devices comprising the embedded silver grid, the η_d was 391 C^{-1} cm^2 after 0.3 s, which fell to 79 C^{-1} cm^2 for a 10 s switch. For comparison, an optical contrast of 80% obtained in 0.57 s was reported for spray cast film of ECP-magenta, which gave a composite coloration efficiency of more than 1200 C^{-1} cm^2 and while such values are indeed impressive, it is worth noting they are obtained under conditions that characterize the polymer material but not devices.[18] The dashed line in Figure 5 shows the optical contrast (ΔT%) as a function of switch length, that is, the switch length required to reach a certain optical contrast. Since η_d and ΔT are connected by Equation 3, a decrease in η_d is observed as ΔT saturate.

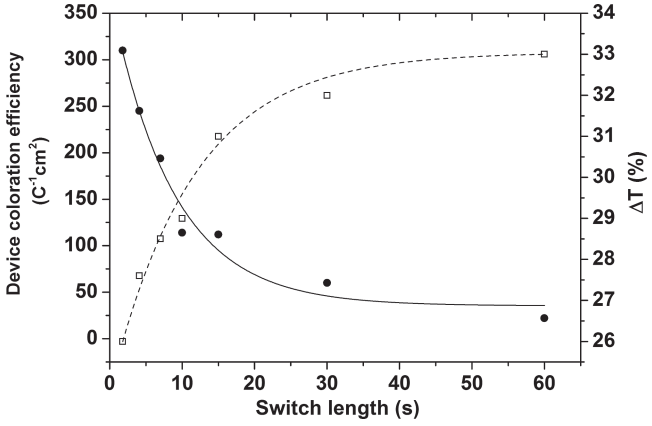

Figure 5. Device coloration efficiency as a function of switch length for an ECD employing flexoprinted silver grid as electrodes and ECP-magenta as the primary electrochromic polymer (solid line and solid circles, left *y*-axis). The dashed line shows the optical contrast as a function of switch length (open squares, right *y*-axis). Transmittance was measured at 550 nm for a device oxidized at +1.5 V. Both curves were fitted to an exponential function (R^2 values of 0.95 and 0.96).

3. Conclusion

We have shown that fast switching ITO free electrochromic devices can be manufactured on flexible substrates, by substituting ITO with a highly conducting printed silver grid as electrode material. Photonic sintering of the flexoprinted silver grid electrodes is required in order to decompose residual organic surfactants prior to coating of the electroactive polymers. PEDOT:PSS was found useful as both a stable charge balancing polymer and to increase the conductivity in the grid electrodes. By coating a conductive PEDOT:PSS formulation onto the silver grids, the electric field in the devices was homogenized and the ECDs were found to switch evenly and with appreciable speed, which is an improvement compared to previously published reports. As the length of the flexoprinted Ag web is infinite and the width is only limited by the size of the printing machine (1 m wide substrates are currently realizable, but wider substrates are not unrealistic), large area ECDs based on these substrates is certainly within reach. Flexible substrates comprising embedded silver grid electrodes were also explored and devices employing these showed better optical contrast and

faster response times compared to their flexoprinted counterparts. PEDOT:PSS lowered the optical contrast of the grid based devices by 2%, which was found acceptable in comparison to the electrochemical stability induced. In perspective, this report shows that EC parameters such as response time and coloration efficiency are influenced by the setting in which they are evaluated. The standard way of characterizing EC materials can be considered a theoretical limit for a given material, while device equivalents more fully describe the practical values that can be achieved in operational devices.

4. Experimental Section

Instrumentation: Absorption/transmission spectra in the 900–300 nm range were determined using a Pharma Spec UV-1700 from Shimadzu. A Keithley 2440 Sourcemeter were used for switching the devices, and custom made software were used for logging data.

Electrochromic Polymers: poly((2,2-bis(2-ethylhexyloxymethyl)-propylene-1,3-dioxy)-3,4-thiophene-2,5-diyl) (ECP-Magenta) and poly(N-octadecyl-(propylene-1,3-dioxy)-3,4-pyrrole-2,5-diyl) (MCCP) was synthesized according to literature (with minor modifications).[17,18] The conductive PEDOT:PSS formulation was a Clevios F010 from Heraeus.

Grid Manufacture: The hexagonal grid pattern was flexo printed on a 72 µm thick PET barrier foil (Amcor) using a water-based silver ink (PChem, PFI-722) and an anilox cylinder with a volume of 3 mL m^{-2}. The printing speed was 20 m min^{-1} whereas the nanoparticle-based ink was fully dried and sintered during the printing run using IR and hot air (140 °C).[15]

For the embedded Ag grid pattern, a 15 µm line width was employed. The PET film was thermally imprinted at 110 °C using custom made machinery. The manufacturing process is described in detail elsewhere,[19] but the basic steps are summarized here: A flexible electroformed nickel-cobalt stamp holding the grid mesh is mounted on a heating roll, and heated to 200 °C. The foil is then fed through the heating roll and an impression roller during which the imprinting force and speed are 450 kgf and 0.96 m min^{-1}, respectively. Following this a water-based silver ink is filled into the engraved mesh patterns by a doctor-blade and sintered at 140 °C for 3 min. Finally residue ink is removed by a roll cleaning process.

ECD Manufacture: Prior to deposition of the ECPs the silver grid substrates was cleaned with isopropanol. The primary electrode was manufactured as follows. A PEDOT:PSS film was spincoated from a 1:2 (w:w) Clevios F010: isopropanol solution at an angular velocity of 1200 RPM. ECP-magenta (poly((2,2-bis(2-ethylhexyloxymethyl)-propylene-1,3-dioxy)-3,4-thiophene-2,5-diyl) was spincoated on top of the PEDOT:PSS layer from a 20 mg mL^{-1} toluene solution at 800 RPM. Following this a previously employed PMMA based electrolyte was spincoated at 1500 RPM.[20] The secondary electrode was manufactured as follows: A PEDOT:PSS film was spincoated from a 1:1 (w:w) Clevios F010: isopropanol solution at an angular velocity of 1000 RPM, this was followed a PMMA based electrolyte layer spincoated at 1500 RPM. Devices of 1 cm × 1 cm (embedded grid) and 2 cm × 2 cm (flexoprinted grid) were manufactured by assembling the two electrodes. A schematic depicting the layered device structure is found in the Supporting Information, Figure S1.

Supporting Information

Supporting Information is available from the Wiley Online Library or from the author.

Received: July 10, 2013
Revised: September 13, 2013
Published online:

[1] European Commission, **2010**, Critical raw materials for the EU: Report of the Ad-hoc Working Group on defining critical raw materials.
[2] R. L. Moss, E. Tzimas, H. Kara, P. Willis, J. Kooroshy, **2011**, Critical Metals in Strategic Energy Technologies (JRC 65592).
[3] C. J. M. Emmott, A. Urbina, J. Nelson, *Sol. Energy Mater. Sol. Cells* **2012**, *97*, 14.
[4] H. Kaneko, K. Miyake, *Appl. Phys. Lett.* **1986**, *49*, 112.
[5] K. Ho, D. E. Singleton, C. B. Greenberg, *J. Electrochem. Soc.* **1990**, *137*, 3858.
[6] A. A. Pud, *Synth. Met.* **1994**, *66*, 1.
[7] H. Harada, T. Fuchigami, T. Nonaka, *J. Electroanal. Chem.* **1991**, *303*, 139.
[8] E. W. Tsai, S. Basak, J. P. Ruiz, J. R. Reynolds, K. Rajeshwar, *J. Electrochem. Soc.* **1989**, *136*, 3683.
[9] F. Beck, P. Braun, M. Oberst, *Ber. Bunsenges. Phys. Chem.* **1987**, *91*, 967.
[10] R. R. Søndergaard, M. Hösel, M. Jørgensen, F. C. Krebs, *J. Polym. Sci. Part B* **2013**, *51*, 132.
[11] A. A. Argun, A. Cirpan, J. R. Reynolds, *Adv. Mater.* **2003**, *15*, 1338.
[12] D. Mecerreyes, R. Marcilla, E. Ochoteco, H. Grande, J. A. Pomposo, R. Vergaz, J. M. Sánchez Pena, *Electrochim. Acta* **2004**, *49*, 3555.
[13] P. Andersson, R. Forchheimer, P. Tehrani, M. Berggren, *Adv. Funct. Mater.* **2007**, *17*, 3074.
[14] J. Kawahara, P. Andersson Ersman, D. Nilsson, K. Katoh, Y. Nakata, M. Sandberg, M. Nilsson, G. Gustafsson, M. Berggren, *J. Polym. Sci. Part B* **2013**, *51*, 265.
[15] M. Hösel, F. C. Krebs, *J. Mater. Chem.* **2012**, *22*, 15683.
[16] J.-S. Yu, I. Kim, J.-S. Kim, J. Jo, T. T. Larsen-Olsen, R. R. Søndergaard, M. Hösel, D. Angmo, M. Jørgensen, F. C. Krebs, *Nanoscale* **2012**, *4*, 6032.
[17] E. P. Knott, M. R. Craig, D. Y. Liu, J. E. Babiarz, A. L. Dyer, J. R. Reynolds, *J. Mater. Chem.* **2012**, *22*, 4953.
[18] B. D. Reeves, C. R. G. Grenier, A. A. Argun, A. Cirpan, T. D. McCarley, J. R. Reynolds, *Macromolecules* **2004**, *37*, 7559.
[19] J.-S. Yu, G. H. Jung, J. Jo, J.-S. Kim, J. W. Kim, S.-W. Kwak, J.-L. Lee, I. Kim, D. Kim, *Sol. Energy Mater. Sol. Cells* **2013**, *109*, 142.
[20] J. Jensen, H. F. Dam, J. R. Reynolds, A. L. Dyer, F. C. Krebs, *J. Polym. Sci. Part B* **2012**, *50*, 536.
[21] D. M. De Leeuw, M. M. J. Simenon, A. R. Brown, R. E. F. Einerhand, *Synth. Met.* **1997**, *87*, 53.
[22] S. Sindhu, K. Narasimha Rao, E. S. R. Gopal, *Bull. Mater. Sci.* **2008**, *31*, 15.
[23] H. C. Ko, S. Park, H. Lee, *Synth. Met.* **2004**, *143*, 31.
[24] J. Padilla, T. F. Otero, *Electrochem. Commun.* **2008**, *10*, 1.
[25] S. A. Sapp, G. A. Sotzing, J. R. Reynolds, *Chem. Mater.* **1998**, *10*, 2101.
[26] A. Kumar, D. M. Welsh, M. C. Morvant, F. Piroux, K. A. Abboud, J. R. Reynolds, *Chem. Mater.* **1998**, *10*, 896.
[27] I. Schwendeman, R. Hickman, G. Sönmez, P. Schottland, K. Zong, D. M. Welsh, J. R. Reynolds, *Chem. Mater.* **2002**, *14*, 3118.
[28] H. Yamato, M. Ohwa, W. Wernet, *J. Electroanal. Chem.* **1995**, *397*, 163.
[29] L. Groenendaal, F. Jonas, D. Freitag, H. Pielartzik, J. R. Reynolds, *Adv Mater* **2000**, *12*, 481.
[30] F. Louwet, L. Groenendaal, J. Dhaen, J. Manca, J. Van Luppen, E. Verdonck, L. Leenders, *Synth. Met.* **2003**, *135*, 115.
[31] P. M. S. Monk, R. J. Mortimer, D. R. Rosseinsky, *Electrochromism and Electrochromic Devices*, Cambridge (UK), Cambridge University Press, **2007**.
[32] C. L. Gaupp, D. M. Welsh, R. D. Rauh, J. R. Reynolds, *Chem. Mater.* **2002**, *14*, 3964.

Adv. Funct. Mater. **2013**,
DOI: 10.1002/adfm.201302320

FULL PAPER

Direct Photopatterning of Electrochromic Polymers

Jacob Jensen, Aubrey L. Dyer, D. Eric Shen, Frederik C. Krebs, and John R. Reynolds*

Propylenedioxythiophene (ProDOT) polymers are synthesized using an oxidative polymerization route that results in methacrylate substituted poly(ProDOTs) having a M_n of 10–20 kDa wherein the methacrylate functionality constitutes from 6 to 60% of the total monomer units. Solutions of these polymers show excellent film forming abilities, with thin films prepared using both spray-casting and spin-coating. These polymers are demonstrated to crosslink upon UV irradiation at 350 nm, in the presence of an appropriate photoinitiator, to render the films insoluble to common organic solvents. Electrochemical, spectroelectrochemical, and colorimetric analyses of the crosslinked polymer films are performed to establish that they retain the same electrochromic qualities as the parent polymers with no detriment to the observed properties. To demonstrate applicability for multi-film processing and patterning, photolithographic patterning is shown, as is desired for fully solution processed and patterned devices.

1. Introduction

Electrochromic materials are promising for a variety of applications that span dynamic tinting windows and mirrors, color-changing displays, smart cards, and e-paper.[1] Electrochromic compounds constitute a group of chemical species and may be categorized by their solubility in different redox states[2] or by their chemical origin as either inorganic or organic.[3,4] Of the organic compounds having electrochromic properties, conjugated polymers (CP) are ideal candidates for printable large area displays, windows, mirrors and e-paper.[2,5–8] The synthetic flexibility in designing CPs is one of their merits and band-gap engineering has allowed color tuning of electrochromic polymers (ECPs). Just as important is the ability to make organic conducting polymers processable from organic, and in some cases, aqueous solutions.[9–13] While conjugated polymers such as poly(pyrrole)s, poly(aniline)s and poly(thiophene)s have been subject to intense investigation for their electrochromic properties,[1] a majority of those studies involve use of film preparation methods such as electrochemical polymerization (in the case of polypyrrole and polythiophene) and spin-casting (in the case of cationic dispersions with anionic polymers such as poly(styrene sulfonate)), which limits their applicability as full solution processability and patterning is desired for most device applications.

Alkyl and alkoxy substituted poly(propylenedioythiophene)s (PProDOTs) are electrochromic conducting polymers that have excellent film forming abilities, which allow for a wide range of processing methods from solution.[10] Their relative ease and scale-up of synthesis make them ideal candidates for future electrochromic devices (ECDs). As films of PProDOTs are mechanically formable, they can be coated onto flexible substrates for use in a variety of flexible devices and displays.[6,14] We have recently shown that it is indeed possible to exploit these mechanical advantages by using roll coating processes to develop electrochromic devices that rely on PProDOTs as the active electrochrome.[15] By use of PProDOTs, and ProDOT monomer units in combination with various other heterocycles and aryl units, the full color palette, desired for non-emissive displays, is now accessible.[16] Further research in ECPs should now focus on the processing of these materials to allow development into commercially viable applications. As such, understanding the electrochromic properties and advances in process development of PProDOTs have been a focus since ProDOTs were investigated as effective electrochromic polymers more than a decade ago.[17,18]

By taking advantage of the C2 symmetry in the ProDOT structure it is possible to functionalize the central bridging carbon atom twice while preserving the regiosymmetry of the monomer, and by extension, affording regioregular polymers. Functionalization at the bridging carbon affords two main advantages–improved electrochromic properties and solubility. It has been shown that this substitution gives rise to a less compact morphology, thereby allowing faster incorporation of counter ions and faster switching rates.[9,18–20] The advantage of solution processable polymers cannot be understated and by appending various alkyl and alkoxy chains to the ProDOT monomer, spray processable polymers (namely PProDOT-$(CH_2OEtHx)_2$) with a transmittance contrast (Δ%T) approaching 80% were synthesized and devices fabricated.[9,21] In further advancing the processability of PProDOTs, ester functionalities have been incorporated that, after conversion to the corresponding salts, allow for processing from more environmentally benign solvents such as alcohols and water. These carboxylate substituted PProDOTs permit a short post-processing acid treatment yielding solvent resistant films.[22] The possibility of such orthogonal processing steps is advantageous in device fabrication.[20,23]

J. Jensen, Prof. F. C. Krebs
Department of Energy Conversion and Storage
Technical University of Denmark
Frederiksborgvej 399, DK-4000 Roskilde, Denmark
Dr. A. L. Dyer, Dr. D. E. Shen, Prof. J. R. Reynolds
School of Chemistry and Biochemistry
and School of Materials Science and Engineering
Georgia Institute of Technology
Atlanta, GA 30332, USA
E-mail: aubrey.dyer@chemistry.gatech.edu

DOI: 10.1002/adfm.201203005

www.MaterialsViews.com

ADVANCED FUNCTIONAL MATERIALS
www.afm-journal.de

In addition to introducing processability through synthetic methods, there is the possibility of utilizing functionalities that allow for photolithographic patterning of CPs, a method commonly utilized in the semiconductor industry. Several methods of photolithographic patterning exist,[24–26] with the two main approaches employed being: Chemically Amplified Photolithography (CAP) and Non Chemically Amplified Photolithography (NCAP). The former relies on photochemical reactions that do not occur in the resist material, but rather triggers a response, upon irradiation, that induces a solubility change in the resist material. For polythiophenes this has been exploited with the use of thermally cleavable tetrahydropyranyl functionalities: upon exposure to a photogenerated acid, the deprotection temperature decreases and consequently the polymer becomes insoluble.[27] By employing CAP procedures, it is possible to avoid likely photobleaching of the thiophene backbone, that would lead to altering of the polymer optical properties, as the amplifier molecule absorbs the radiation during the liberation of the amplifying species (e.g. the acid in the above example). A NCAP approach, which has also been explored in relation to patterning of polythiophenes, is a method of photo-induced crosslinking.[26] In general, however, the irradiation source used in the direct procedure approach (laser, UV lamp, etc) generates free radicals, consequently damaging the thiophene ring by causing irreversible photobleaching, rendering the photoresist useless as an electroactive component.[28–31] This has, in some cases, been solved by attaching acrylate or methacrylate groups to the alkyloxy bridge of the thiophene ring.[33] By incorporation of a photoinitiator to absorb the radiation and appending C=C bonds to crosslink, it is possible to use lower doses of UV light, thereby sparing the thiophene ring.[32,33] An elegant way of preventing photooxidation of the parent thiophene ring was presented by Sotzing et al.[34] whereby, relying on crosslinking of methacrylate groups, the authors employ a precursor polymer that is already crosslinked prior to oxidative polymerization of the thiophene rings, allowing them to avoid harsh radiation procedures that have the potential of damaging the polymer backbone.

To achieve more than just academic value, the patterning of conducting polymers should be simple and avoid tedious post-processing steps such as etching, peeling of solid layers, etc. Conventional photolithography requires multiple steps and, while each step in itself is not complicated, the use of direct photopatterning to generate negative tones is facile and complementary to large scale manufacturing procedures. Depending on the usage of the electrochromic film, several coating methods are available and include spray-casting, slot-die coating, screen printing, and others.[35] In this report, we utilize drop-casting, spin-coating and spray-coating. While drop-casting was exclusively utilized for electrochemistry measurements and spin-coating reserved for solubility demonstrations, the technique utilized for the majority of this work was airbrush spraying. All of the above techniques are preferred for lab scale experiments, but if one desires to manufacture electrochromic displays on a larger scale, it is necessary to employ line-coating procedures, of which roll coating is advantageous and requires that the substrate to be coated is flexible. Here, it is helpful to turn to the various coating methods utilized in the extensive research surrounding organic and polymeric solar cells, including the recent demonstration of the manufacturing of roll coated organic solar cells by one of our groups.[36]

Of the many roll coating techniques available, we have recently shown that electrochromic devices can be made by utilizing slot-die coating onto flexible substrates.[15,37] In this context, we report here a complementary method that will allow extension of the zero- and one-dimensional coating techniques previously demonstrated. Direct photopatterning of slot-die coated electrochromic films will transform this fast and reliable coating technique into a two dimensional method, which is traditionally associated with contact printing techniques such as flat bed screen printing, rotary screen printing, flexographic printing, gravure printing[38] and, to some extent, ink jet printing.[39]

However, compared to traditional photoresists, the photoresists used in electrochromic devices must preserve the electronic and optical properties of the materials. A simplified example of direct photopatterning, as demonstrated in this report, is depicted in **Figure 1**, wherein a solution processable polymer is cast onto a transparent conductive electrode (typically ITO/glass or ITO/plastic). This is followed by application of a photomask and irradiation (step A - Figure 1). The irradiation initiates crosslinking within the exposed areas of the polymer film. After irradiation, the mask is removed and the non-crosslinked (i.e., non irradiated) areas of the film are dissolved, leaving behind a negative image of the pattern (step B–Figure 1). Finally the electrochromic film is submerged in an appropriate electrolyte and electrochemically switched between the different oxidation states (step C–Figure 1).

In this paper, we report on the synthesis of a series of methacrylate substituted PProDOTs where the relative content of methacrylate functionality is varied. By varying the relative amounts of alkyl substituted-ProDOT and methacrylate substituted-ProDOT units, it was possible to synthesize random

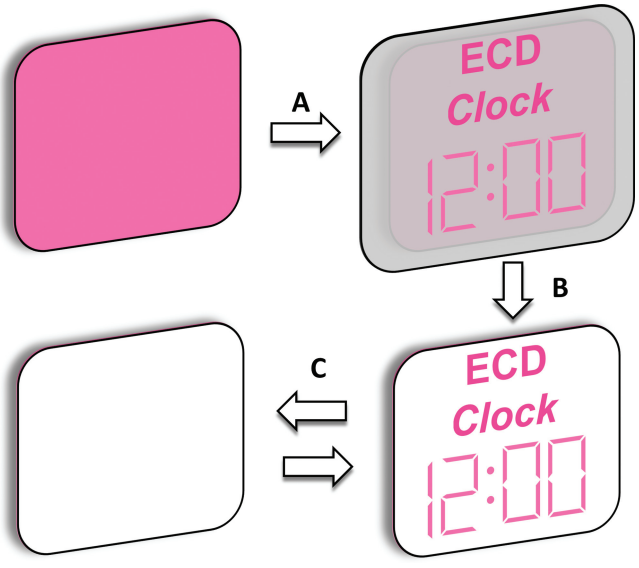

Figure 1. Principles of direct ECP photopatterning, starting from a conducting surface coated with ECP. A) Application of a photomask and irradiation. B) Dissolution of non-irradiated polymer. C) Electrochromic switching of crosslinked polymer.

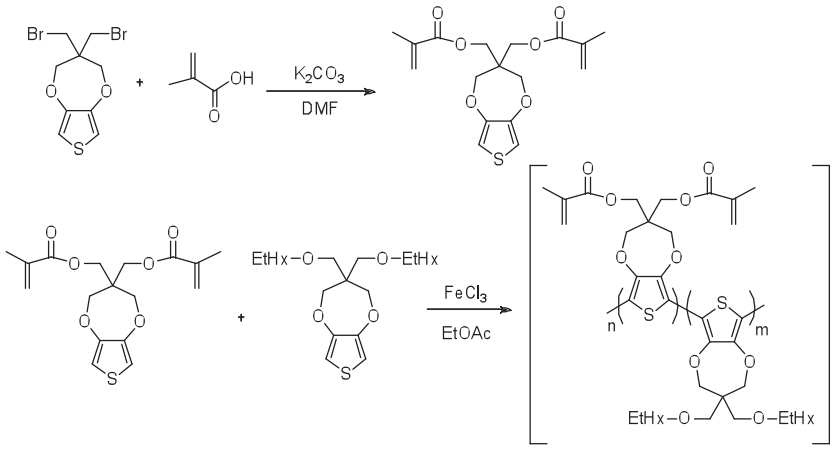

Scheme 1. Synthetic route to bis-methacrylate containing comonomer and copolymers.

copolymers containing from 6% to 60% of bis-methacrylate monomers (e.g. copolymer 30 contains 30% bis-methacrylate monomer). The straightforward synthesis route leads to a set of polymers prepared via an oxidative polymerization route with number average molecular weights (M_n) between 10 and 20 kDa that are highly soluble in common organic solvents. Utilizing photo-crosslinking results in thin polymer films that are rendered insoluble in common organic solvents, allowing patterning of electrochromic polymer thin films that switch between a highly colored and near colorless transmissive state. Most importantly, we demonstrate that photo-crosslinking of the polymers is possible with conservation of the electrochromic properties such that redox potentials, color, optical properties, contrast, and switching speeds are retained.

2. Results and Discussion

2.1. Synthesis

Scheme 1 shows the synthetic route to the bis-methacrylate ProDOT–poly(3,4-dihydro-2H-thieno[3,4-b][1,4]dioxepine-3,3-diyl)bis(methylene)bis(2-methylacrylate), starting from available 3,3-bis(bromomethyl)-3,4-dihydro-2H-thieno[3,4-b][1,4]dioxepine. The starting material was reacted with methacrylic acid under basic conditions in dry DMF affording the bis-methacrylate thiophene, **1**, after purification by dry column vacuum chromatography (DCVC).[40]

Table 1. Polymer composition and molecular weight estimation by GPC.

Monomer 1 in reaction	Monomer 1 in polymer	Yield	M_n [Da]	M_w [Da]	PDI
10%	6%	36%	10500	22000	2
20%	12%	50%	15700	33500	2.1
50%	30%	31%	16900	31700	1.9
80%	60%	30%	7300[a)]	15400	2.1

[a)]Crosslinking of the polymer was observed during analysis, which might cause a lower M_n to be detected.

By varying the amounts of the two monomers, we synthesized random copolymers containing from 6 to 60% (see **Table 1**) of the bis-methacrylate monomer by use of oxidative polymerization with ferric chloride in ethyl acetate. This method afforded copolymers in reasonable yields (30–50%) and with molecular weights ranging from 10 to 20 kDa. Compared to homopolymers of the bis-ethylhexyl monomers, which yield an M_n of 35 kDa when prepared under the same conditions, we believe that the acrylate groups impose steric hindrance during the polymerization resulting in lower M_n values. The composition of the copolymers was determined by FT-IR and ^{1}H NMR. The ^{1}H-NMR spectra of homopolymer (herein referred to as ECP-magenta) (A) and the copolymers containing various amounts of the bis-methacrylate monomer (B-E) are found in the Supporting Information (Figure S1). The difference between the homopolymer of ECP-magenta and the copolymers is the peak at 1.97 ppm (methacrylate CH_3) and the two peaks at 6.14 and 5.61 ppm (C=C protons) indicated by arrows. The increase in intensity of these peaks, in proceeding from A to E, is a consequence of a higher content of bis-methacrylate monomer in the copolymer, which was determined by integration to be from 6–60%. On comparison of the incorporated bis-methacrylate content in the copolymers to the percent of the bis-methacrylate utilized in the reaction mixture, it is noted that this polymerization favors incorporation of the bis-ethylhexyl monomer. We were able to estimate that the bis-methacrylate content of the copolymer to be consistently 60% of that in the reaction mixture, except for the highest content where it is 75% (column 1 and 2 in Table 1).

The FT-IR absorption spectrum of the copolymer containing 6% bis-methacrylate substituted monomer (copolymer 6) is shown in **Figure 2** and that for the bis-methacrylate monomer

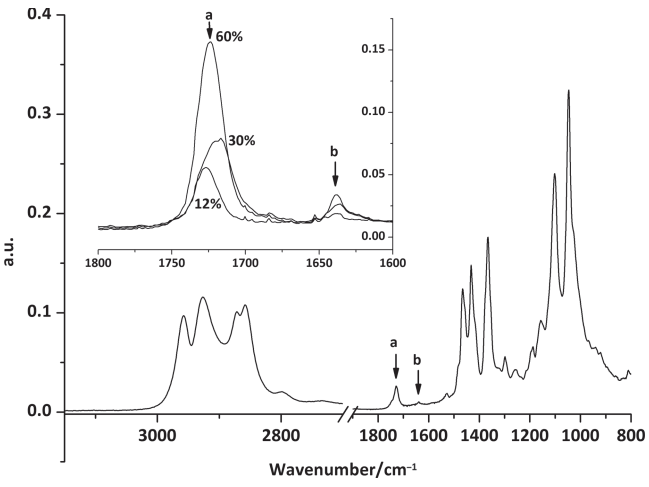

Figure 2. FT-IR of the bis-methacrylate copolymer A/Absorption spectra of the 6% copolymer (the 1800–1600 cm^{-1} region for 12%, 30%, and 60% is shown in the inset). The arrows marked a and b indicate the C=O and C=C stretch respectively.

www.MaterialsViews.com

ADVANCED FUNCTIONAL MATERIALS
www.afm-journal.de

is available in the Supporting Information (Figure S2) for reference. In the latter, the band at 3103 cm^{-1} is assigned to the C–H stretch on the 2- and 5-positions on the thiophene ring of the monomer and the band at 2974 cm^{-1} is the methyl C–H stretch. The 2- and 5- C–H stretch from the thiophene monomer is not present in the polymer spectra (compare Supporting Information Figure S2 to Figure 2 and Supporting Information Figure S3), which indicates polymerization. Of particular interest is the intense sharp band at 1712 cm^{-1} from the C=O stretch of the ester and the less intense band at 1643 cm^{-1} from the C=C stretch in the acrylate (marked a and b respectively in Figure 2). These bands do not occur in IR spectra of the homopolymer ECP-magenta and confirms that the desired copolymer was synthesized. Preservation of the C=C stretches confirm that the acrylate groups are intact after the oxidative polymerization. The band at 2974 cm^{-1} originating from the C–H stretch in the methyl group of the methacrylate does not show in Figure 2, as this region is populated by signals from various aliphatic groups. In the spectrum of the 100% bis-methacrylate homopolymer this band is visible. However, as the homopolymer was completely insoluble in common organic solvents it was considered not useful from a practical point of view (see Supporting Information Figure S3). The inset in Figure 2 shows the increasing absorption of the C=O and C=C bands as a result of increasing the bis-methacrylate monomer content in the feed. As the intensity of absorption bands is directly proportional to the content of the group resonating at that wavelength, the FT-IR and NMR data presented support each other satisfactorily.

2.2. Coating

To perform electrochemical measurements, thin films of the polymers were prepared by drop-casting the polymer solutions onto platinum button electrodes. While this is an often-used method of thin film formation for electrochemical measurements on small area electrodes, it should be noted that drop-casting is not well-suited for large area processing of polymer films as issues arise from inhomogeneous film drying and lack of control over dry film thickness. To prepare polymer films on larger area substrates for solubility studies, spin-coating was employed. This casting method is highly reproducible, affording films equivalent in thickness, density and morphology.[41] However, it should be noted that we did encounter inhomogeneous films when the methacrylate content of the copolymers was 60%. We ascribe this to a higher surface tension of the bis-methacrylate resulting in de-wetting (the acrylate functionality is more polar compared to the saturated alkyl functional groups). This issue was circumvented by switching the processing solvent for this particular polymer, allowing the formation of visually homogeneous films as detailed in the experimental section. To demonstrate a more practical method for large area processing, we employed airbrush spray-casting and utilized these films for spectroelectrochemical measurements and for the patterned electrochromic films. This method of preparing films of processable electrochromic polymers has been demonstrated to be ideal to produce electrochromic films with an open morphology that is believed to enhance optical contrasts and switching speeds.[42] Details regarding solution compositions and photoinitiators used in crosslinking are found in the experimental methods section.

2.3. Crosslinking

In order to avoid photooxidation of the electrochromic polymer films, we used as mild conditions as possible in terms of irradiance and temperature exposure. This was addressed using several approaches: employing azobisisobutyronitrile (AIBN) as a photoinitiator and incorporation of a high degree of polymerizable acrylate sites. In regards to the first approach, AIBN was found to be a reliable photoinitiator and is soluble in the organic solvents used in formulating the polymer solutions. AIBN is a well-known azo-radical initiator that decomposes upon irradiation at wavelengths of 300–360 nm, yielding the 2-cyanoprop-2-yl radicals responsible for initiating the polymerization of the methacrylate groups. An additional product of the reaction is gaseous nitrogen, which is expected to evaporate from the polymer film with no observable damage due to nitrogen diffusion.

Another strategy to decrease the irradiance necessary for crosslinking was successfully realized by employing polymers containing a high degree of polymerizable acrylate sites. This was done by synthesizing bis-methacrylate monomers. As described in the introduction, the aliphatic groups in the 2-position on the ProDOT propylene bridge play a key role in controlling solubility and processability of these polymers, and by substituting the ethylhexyl groups with methacrylates, the solubility of the resulting polymers could be compromised. Indeed, an insoluble polymer was observed when the bis-methacrylate homopolymer was synthesized. However, by synthesizing copolymers comprising both monomers (see Scheme 1), it was possible to tune the solubility of the polymer, such that high quality films retaining full electrochromic properties could be cast, and subsequently crosslinked. This was accomplished by having the crosslinkable groups on the polymer backbone (as opposed to end groups). The resulting M_n ensured the favorable qualities of the polymers (saturated colors, processability, high film quality, etc.) without sacrificing the degree of crosslinking.

To monitor the crosslinking process, FT-IR spectroscopy was performed whereby thin polymer films were spin-cast onto freshly pressed KBr pellets and transmission spectra recorded after irradiation of the films at regular intervals. **Figure 3** shows the results for copolymer 30, where depletion of the acrylate double bonds can be seen as the decrease of the band at 1643 cm^{-1} upon irradiation. What is also observed is no change in the other bands present (especially the band at 1712 cm^{-1} originating from the ester functionality), which demonstrates that the crosslinking proceeds exclusively through the carbon-carbon double bonds of the acrylate, without disrupting the ester functionality nor the ProDOT backbone. It can be seen from the time progression shown in Figure 3 that the majority of the crosslinking occurs within the first 240 seconds of irradiation. It should be noted that even upon longer exposures, the small peak at 1643 cm^{-1} is not fully depleted. While the exposed surface of the polymer film is relatively uniform, the underlying structure is not due to the KBr pellet, on which the film is cast,

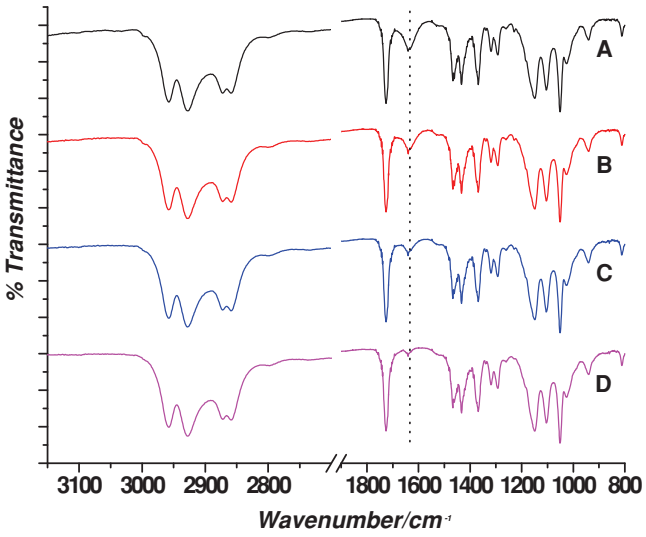

Figure 3. IR transmission spectra of the 30% copolymer during irradiation. A) 0 s, B) 60 s, C) 240 s, D) 960 s.

not being a flat surface, causing non-uniformity in crosslinking through the thickness of the polymer film.

In order to assess the effect of crosslinking on solubility in toluene, polymer solutions of the various copolymers were cast onto ITO-coated glass (as described in the Experimental Section), and irradiated. They were then submerged in a solution of stirring toluene at room temperature for 1 min and allowed to dry. Following this, the transmission profiles of the films were measured and compared to spectra obtained prior to toluene treatment as shown in **Figure 4**.

To be of interest in electrochromic devices, the optical properties of the conjugated polymer should be retained after irradiation and crosslinking, as is demonstrated in Figure 4. The as-cast films are shown as the traces labeled as 'A' for the 30% copolymer (left) and 60% copolymer (right). The films were then irradiated for 600 seconds and immersed in stirred toluene for 60 s to remove any polymer not rendered insoluble by crosslinking. The spectra labeled as 'B' are of the films after this treatment. It can be seen that a relatively small fraction of material was removed in the 30% copolymer film as indicated by a 20% increase in transmission at the λ_{max}. For the 60% copolymer, even less material was removed as shown in the spectra on the right by a minimal 2% increase in transmission. A difference in extent of crosslinking is expected as the 60% copolymer has twice as many acrylate functional groups to allow for reaction upon irradiation, allowing for a higher extent of crosslinking. When films of the alkoxy homopolymer (ECP-Magenta) were subjected to the same conditions, the films fully dissolved in under 10 s. Likewise, the 6% and 12% copolymers exhibited a slight decrease of solubility on crosslinking, compared to the alkyloxy homopolymer and were not further studied. In further work, it is expected that the extent of crosslinking can be increased in the copolymers containing 6% to 30% acrylate functionality by varying the relative concentration of the diacrylate additive or utilizing an additive with a longer chain or increased functionality (e.g., tetraethyleneglycoldiacrylate or pentaerythritol triacrylate).

It should be noted that there is a small extent of crosslinking occurring under normal laboratory conditions as shown in the spectra labeled as 'C' that are of spin cast films of the acrylate functionalized polymer films not irradiated in the photoreactor, followed by immersion in stirring toluene. This is attributed to a combination of emission of UV radiation from the fluorescent room lighting and thermal initiation of the AIBN. As the focus of this work is the synthesis of newly functionalized electrochromic polymers that allow photoinduced crosslinking and their characterizations in regards to preserving electrochromic properties post-processing, it is understood that further work remains in regards to optimization of the photoinitiator and crosslinking conditions. For example, AIBN is known to decompose thermally at 65 °C. While it was found stable to handling at standard atmospheric conditions, the relatively low decomposition temperature does pose a challenge upon selective irradiation as the substrate material and/or photomask may reach temperatures approaching the AIBN decomposition temperature, resulting in crosslinking non-irradiated areas of the film. Furthermore, future work should include use of appropriate UV light filters, as is typically utilized in photopatterning-intensive laboratories, to selectively block UV emission from typical laboratory fluorescent lamps as the irradiation from room lighting can initiate crosslinking.

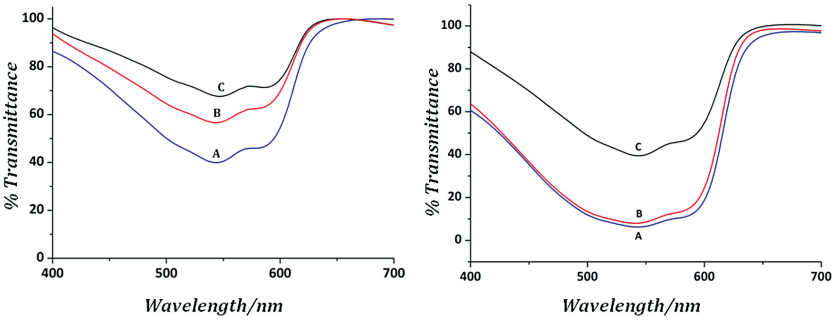

Figure 4. Transmission profiles for spin-cast polymer films after various treatments. The left hand graph was normalized to compensate for reflections in the glass substrate (resulting in transmittance above 100%). The spectra on the left are of copolymer 30 and on the right of copolymer 60. The A curves show the transmittance profile of the pristine films, while the B curves are of films cured for 600 s and then immersed in toluene for 60 s, and the C curves are of the uncured film after dissolution in stirring toluene for 60 s.

2.4. Electrochemistry

The electrochemical behavior of the polymer films was investigated by use of cyclic voltammetry. Of particular interest were differences in redox activity that may result from replacement of the ethylhexyloxy groups at the C2 carbon of the propylene bridge with methacrylate groups, and upon crosslinking of polymer films. **Figure 5**A provides the CV scans for the 50th cycle for both copolymer 30 and 60 with that of the homopolymer ECP-Magenta presented in the Supporting Information (Figure S4). While there are several similarities in the current–voltage profiles

www.MaterialsViews.com

ADVANCED FUNCTIONAL MATERIALS
www.afm-journal.de

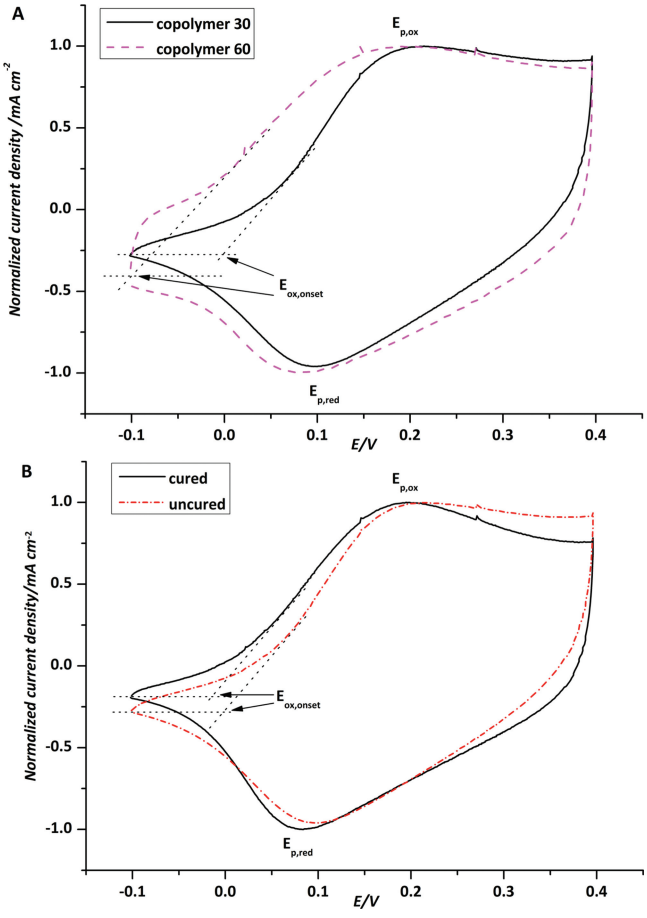

Figure 5. Cyclic voltammetry analysis of ECP films. A) CV of copolymer 30 (solid line) and copolymer 60 (dotted line). B) CV before (dotted line) and after (solid line) 600 s of irradiation (crosslinking) of copolymer 30. Normalized current density is displayed to counterbalance any effects of inhomogeneity of film thickness drop-casting might have. All reported potentials are relative to Ag/Ag^+.

between these three polymers, there are several differences that can be ascribed to the acrylate functionality. The redox switching windows were similar for all three polymers with the onset of oxidation, E_{ox}, observed to be 0 V and –0.1 V for the copolymers 30 and 60 respectively, while E_{ox} was 0.1 V for ECP-Magenta. A consequence of the acrylate functionality is a broader redox process and higher level of charging current during cycling due to the acrylate functionality that can lightly crosslink under ambient conditions. The broad redox process for the acrylate-functionalized polymers is similar to that seen for the first CV scan of the alkyloxy homopolymer in Supporting Information Figure S5. The homopolymer has been shown to undergo an 'electrochemical annealing' process on the first cycle, resulting in a reordering of the polymer chains to adopt a more ordered conformation (this can also be observed in the spectral data discussed later), which can be seen by the sharper redox peaks for the second (and subsequent) CV scans. However, in the acrylate-functionalized polymers, a low level of crosslinking causes the polymer chains to lock in their conformation and not reorder on redox switching. This semi-locked conformation can also lead to a larger component of the current resulting from diffusional-dependent double-layer charging as the solvated counter ions are more restricted in their ability to diffuse through the polymer film. This is further supported by the higher background charging current observed in copolymer 60 than in copolymer 30 as shown in Figure 5A, where copolymer 60 has a higher density of acrylate functionality and, hence, a larger amount of ambient crosslinking occurring. We can exclude any differences between the copolymers and homopolymer being due to electrochemical crosslinking as there is an absence of additional redox peaks within the potential window scanned and therefore conclude that no electrochemical polymerization of the acrylate functionality occurs in addition to no additional insolubilization observed. This indicates that the acrylate functionality is stable within the potential window scanned.

In utilizing crosslinkable functionalities, the retention of electroactivity in the polymer films after photo-induced crosslinking, is essential. In Figure 5B below, we present a CV scan of a pristine copolymer 30 film overlaid with that of a polymer film after photo-induced crosslinking after 600 s of irradiation, as detailed in the experimental section. This demonstrates that the polymer electroactivity is preserved in the crosslinked film as there is essentially no change in the redox peaks indicating that there are no detrimental side reactions on UV exposure.

2.5. Spectroelectrochemistry and Colorimetry

Films were spray-cast from toluene solutions as detailed in the experimental section and spectroelectrochemistry was performed *in situ* by measuring the absorbance spectrum at a desired applied potential with the potential stepped in increasing increments of 50 mV. **Figure 6** shows the absorbance spectra of films of copolymer 30 and homopolymer ECP-Magenta in the fully neutral and fully oxidized states (the

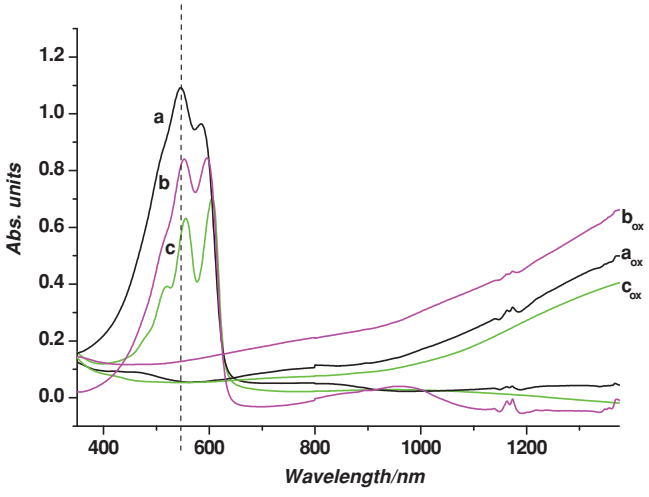

Figure 6. Spectroelectrochemistry of methacrylate copolymers and ECP-Magenta homopolymer. The graphs a and a(ox) show the absorbance of copolymer 30 at 0 V and 0.4 V, respectively, prior to crosslinking. Graph b and b(ox) are copolymer 30 at 0 V and 0.4 V after irradiation for 600 s (crosslinking). Graphs c and c(ox) show homopolymer ECP-Magenta.

full spectroelectrochemical series is provided as Supporting Information, Figure S6). By comparing spectra a, b, and c, the onsets of absorption are observed to occur at similar wavelengths, with only minor differences between the spectra in regards to relative peak intensities. The copolymer before and after crosslinking (spectra a and b, respectively), show similar absorption profiles in the neutral state with a λ_{max} centered at 548 nm and an absorption onset at 620 nm. The homopolymer ECP-Magenta exhibits a slightly red-shifted spectra in addition to a higher degree of vibronic coupling, which is typical of this polymer.[9] This is not unexpected in light of the electrochemical data, given that the homopolymer has the conformational freedom to reorder on electrochemical cycling to form a highly ordered structure, resulting in the vibronic coupling. However, the acrylate polymer, with a low level of crosslinking occurring under ambient conditions, is partially locked in conformation and is not able to order, resulting in a broader absorption profile in the neutral state. On oxidation, the absorbance in the visible region decreases due to depletion of the π–π* transition while absorptions at longer wavelengths begin to appear due to the introduction of lower energy electronic transitions (polarons and bipolarons). Upon full oxidation, the polymer has little absorption in the visible region as nearly all of the absorption is now occurring in the near infrared, with little tailing into the visible region as is also seen for the alkoxy-substituted homopolymer. This indicates that there is no loss of electrochromic switching on UV exposure and the copolymer retains a high level of optical contrast before and after crosslinking.

To quantitatively describe the color of the electrochromic films as perceived by the human eye, colorimetry was employed using a Minolta colorimeter and a standard background illumination as detailed in the experimental section. The 1976 CIE LAB (L*a*b*) method was utilized to represent colors measured *in situ* at different applied potentials, shown in **Figure 7**A. As the potential applied to the film was progressively stepped from fully neutralizing to fully oxidizing values, the a*, b* values decreased from 46, −32 when colored (indicating a color with a blue-red component as expected for a magenta film) at −0.1 V to −1, −1 when fully bleached (indicating a highly achromatic film) at the applied potential of 0.35 V. These values are very similar to those previously reported for the ECP-Magenta homopolymer.

The lightness, or L*, is a measure of the weighted response of the eye to light intensity variations (whereas transmittance is a linear response of a photodetector) and was simultaneously measured as shown in Figure 7B as a function of applied voltage. In the fully neutralized state at −0.1 V, the polymer is in a colored, absorptive state, transitioning to a near colorless, high lightness state between 0.1 and 0.2 V until fully oxidized when the L* maximizes at 93. This is also seen in the inset photographs. Similarly with the a* and b* values there is negligible difference in the L* values between the films before and after photo-crosslinking, except for a slightly higher L* value in the neutral state, which can be ascribed to a slight loss of non-crosslinked material in the film after crosslinking and rinsing, as was also observed in the spectra. This minimal difference of the L*a*b* values measured between the pristine and crosslinked films supports the analysis that crosslinking does not affect the optical and color properties of the polymer films in either the neutral or oxidized states.

3. Patterning

To realize the full potential of electrochromic conjugated polymers, the development of practical processing and patterning methods is of major importance. To demonstrate this, we have previously shown that large area devices incorporating electrochromic polymers and semi-solid ionic gels can be achieved by coating onto flexible substrates using commonly used coating techniques such as slot-die coating. When considering these practical printing and processing methods, the ability to directly pattern a material is highly desirable; especially fine, detailed patterns. However, with the zero- and one-dimensional methods previously mentioned, direct patterning is not possible. The ability to print a soluble material using roll-to-roll methods, followed by photolithographic patterning will allow for large area processing with small feature patterning as desired for display applications. To that end, we preliminarily demonstrate the use of photolithographic patterning using the 30% copolymer as shown in **Figure 8**. In this method, we have spray-cast a thin polymer film from toluene, followed by 600 s of irradiation through a shadow mask as shown in Figure 8B. The irradiated

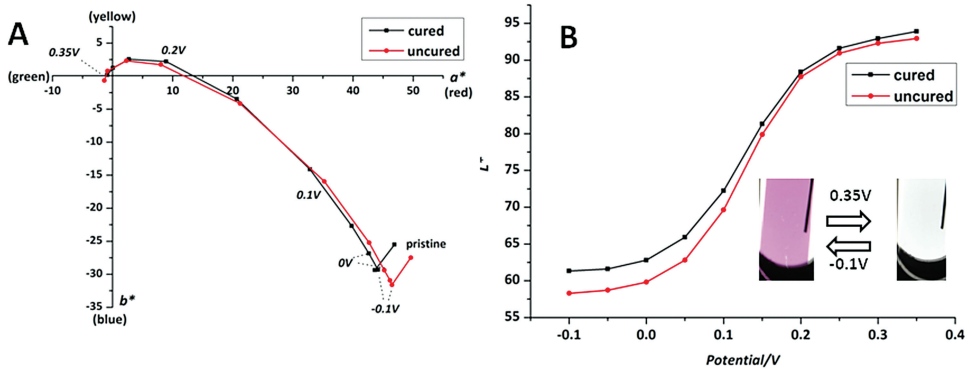

Figure 7. Colorimetry measurements of cured and uncured copolymer 30. A) Development of a* and b* at increasing potentials. B) Lightness (L*) as a function of applied potential. Inset photographs show the film switched at the oxidized and neutral state. All reported potentials are relative to Ag/Ag^+.

www.MaterialsViews.com

ADVANCED FUNCTIONAL MATERIALS
www.afm-journal.de

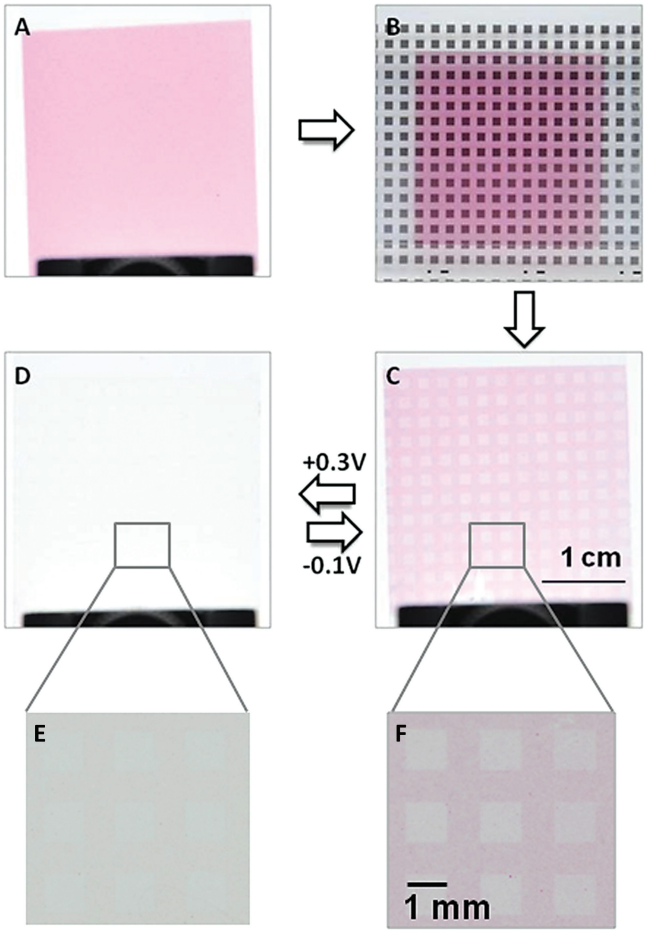

Figure 8. Direct photopatterning of methacrylate-substituted ECP-Magenta. A) An ECP-coated ITO/glass substrate. B) Application of a photomask followed by 600 s of irradiation. C) Film in the neutral state following dissolution of non-irradiated polymer in toluene and repeated switching. D) Film in the oxidized state following repeated switching. E,F) Optical microscope enlargements of the pattern.

film is then rinsed in toluene, leaving a patterned film behind with dimensions on the order of 1 mm shown in Figure 8C. After drying, the film was immersed in electrolyte and oxidized at 0.35 V, to bleach the patterned areas shown in Figure 8D. As mentioned previously, this photolithographic patterning was performed under standard laboratory conditions and, as expected, light crosslinking of the masked areas occurred. We expect that a higher contrast and finer detail can be achieved under rigorous lithographic conditions such as filtered light and controlled temperature in a cleanroom setting as is used for most photolithographic printing. It is understood that this is a first demonstration of this concept in regards to electrochromic conjugated polymers and that further optimization of processing and patterning are needed, but are beyond the scope of this paper.

Additionally, as with other polymer and organic electronic devices, such as organic photovoltaics (OPVs), organic light emitting diodes (OLEDs) and light emitting electrochemical cells (LEECs), most electrochromic devices consist of several successively deposited organic layers, with many of those layers soluble in common solvents. By employing orthorgonal processing methods, subsequent layers are processed (and the solvents used) without dissolving underlying layers. Several strategies have been explored within the area of OPVs and PLEDs,[22,43] that rely on a post-processing step where the coated layer is made insoluble in the next processing solvent. Ultimately this would enable the fabrication of devices from the bottom-up, a further step towards roll-to-roll processing. To that end, the copolymers presented here show promise where both the 30 and 60% copolymer are rendered insoluble in toluene after crosslinking suggesting they can additionally be ideal candidates for large area orthogonal coating.

4. Conclusion

In this report, we have presented a conjugated electroactive copolymer based on an alkoxy-substituted ProDOT and an acrylate-substituted ProDOT where the relative amount of monomer unit containing acrylate functionality relative to alkoxy was varied. This material is unique in that it allows solution processability of an electrochromic material from common organic solvents, followed by photo-crosslinking to render the film insoluble, while maintaining electrochemical, spectroscopic, and colorimetric properties. We have also shown the utility of such materials for printing and patterning by utilizing photolithographic methods whereby we created a patterned surface with millimeter-sized dimensions as a first demonstration. This opens the way for printing and patterning of fully solution processed and roll-to-roll coated conjugated electrochromic polymers for patterned displays as desired for applications such as e-readers, smart-cards, and information displays.

5. Experimental Section

Instrumentation: ^{1}H and ^{13}C NMR spectra were recorded on a Gemini 300 FT-NMR. IR spectroscopy was performed on an IRAffinity-1 from Shimadzu. The IR spectra were obtained using either Attenuated Total Reflectance (ATR) technique on the pure solids or transmission IR on polymer films spin-cast onto KBr pellets. Gel-permeation chromatography (GPC) was performed at 35 °C in THF to determine molecular weight(s). A combination of a Waters HPLC pump 1515, UV-vis Detector 2487, and a Refractive Index Detector 2414 were used. A Waters column (4.6 mm × 300 mm; Styragel HR 5E) and polystyrene standards from Fluka were used. The polymer solution (1 mg mL^{-1} in THF) was prepared and filtered through a Mini-UniPrep PTFE vial with a 0.45 µm filter. 20 µL of each polymer solution was injected and molecular weights were calculated using Waters Breeze II software. Electrochemical analysis was performed using a Princeton Applied Research (PAR) model 273A Potentiostat/Galvanostat. Absorption profiles and spectroelectrochemical measurements were carried out on a Cary 5000 model UV-Vis-NIR from Agilent. Colorimetry studies were performed with a Konica Minolta CS-100 Chromameter.

Crosslinking: The polymer films were crosslinked using a Rayonet RPR-100 Photoreactor equipped with RPR-3500 lamps. The total irradiance was measured to 12 mW cm^{-2} using a Thorlabs PM100 and individual wavelengths were measured using a Newport Optical Power Meter 1830C employing a 818-UV detector (SN2009). The irradiance at 350 nm was determined to be 0.7 mW cm^{-2}.

Film Formation: For solubility studies, films of the various copolymers were spin-coated from 20 mg mL^{-1} solutions of toluene or $CHCl_3$. In addition, films subject to irradiation contained 6 mg mL^{-1} AIBN and

~42 mg mL^{-1} ethyleneglycoldimethacrylate (EGDMA). Films were cast onto ITO-coated float glass (1" × 1"; Delta Technologies, R_s < 20 Ω/sq.) at an angular velocity of 800 rpm using a Laurell WS-400-6NPP spin-coater. For cyclic voltametry, films were drop-cast onto a Pt-button electrode from a 0.5 mg mL^{-1} toluene solution and allowed to evaporate leaving a thin film. Irradiated films contained 0.25 mg mL^{-1} AIBN and ~2.1 mg mL^{-1} EGDMA. For spectroelectrochemical measurements and direct photopatterning, thin films were spray-cast from a 2 mg/mL toluene solution using either a GREX genesis xg or Iwata-eclipse HP-BS airbrush, onto ITO-coated glass (Delta Technologies, CG-50IN-10V, Rs = 5–10 Ω). Irradiated films contained 1 mg/mL AIBN and ~6.3 mg mL^{-1} EGDMA.

Solubility Studies: Thin films were spin cast onto ITO-coated glass as described above. The absorbance of the individual slides was measured using a Cary 5000 prior to irradiation. The samples were then irradiated for 0–600 s and the absorbance measured a second time after irradiation. The slides were then emerged into a stirring solution of toluene at room temperature for 60 s. After drying, the absorbance was measured a third time and the spectra plotted. In some instances the temperature of the toluene solution was raised to 100 °C.

Spectroelectrochemical and Colorimetric Analysis: Films were spray-cast, as described above, onto cuvette-size ITO-coated glass, and used as the working electrode (WE). The WE was submerged in a solution of 0.5 M tetrabutylammonium hexafluorophosphate ($TBAPF_6$) in acetonitrile in a cuvette. A standard Ag/Ag^+ (10 mM $AgNO_3$ in 0.5 M $TBAPF_6$/acetonitrile) was used as a reference electrode and a Pt flag was used as the counter electrode. The absorption spectrum was taken of the pristine film prior to any electrochemical switching. The films were electrochemically cycled between –0.1 and 0.4 V until a stable voltammetric response was obtained (typically 5 cycles), to allow incorporation of electrolyte into the polymer film. Potentiostatic experiments were then performed between 0 and 0.4 V and the absorbance spectra recorded at each potential. The same setup and procedure were used for colorimetric analysis. The ITO-coated glass was sprayed with the ECP so that the absorbance was between 0.79 and 0.84. After the initial break-in of the films, potentiostatic experiments were performed and the Y, x and y values measured using a Minolta Chromameter CS-100 colorimeter with a GraphicLite LiteGuard II standard D50 light source illuminating the sample from behind. The light source and the sample to be measured were placed in a color viewing booth. The interior of the light booth is coated with a standard gray neutral 8 (GTI Graphic Technology Inc.) matte latex enamel (equivalent to Munsell N8) to allow for accurate assessment of color of the sample during measurement. These values were subsequently used to calculate L*a*b* values.

Synthesis of (3,4-dihydro-2H-thieno[3,4-b][1,4] dioxepine-3,3-yl) bis(methylene)bis(2-methylacrylate): Into a dry 250 mL round-bottomed flask was added anhydrous DMF (100 mL) in which ProDOT(CH_2Br)$_2$ (5.0 g; 14,6 mmol) was dissolved. To this solution was added methacrylic acid (3.75 g; 43.8 mmol) and K_2CO_3 (7.3 g; 52.8 mmol). A condenser was attached and the frothing solution was stirred under argon at 100 °C for 21 h, by which TLC (10% EtOAc in hexane) confirmed conversion of starting material. The solution was allowed to cool and water (150 mL) was added. The solution was extracted with DCM (3 × 100 mL), and the combined organic phases were washed twice with brine (2 × 100 mL). The organic phase was dried using $MgSO_4$ and concentrated in vacuo yielding a yellow-brownish oil. The crude compound was purified by dry column vacuum chromatography (DCVC) using EtOAc in hexane as the eluent (0 to 50%) in 50 mL fractions.[40] The pure compound appeared as a white solid with a blue hue. Yield 2.35 g (45%): mp 49–50 °C ^{1}H NMR (300 MHz, $CDCl_3$): δ ppm 6.46 (s, 2H); 6.09 (s, 2H); 5.58 (s, 2H); 4.28 (s, 4H); 4.06 (s, 4H); 1.93 (s, 6H). ^{13}C NMR (300 MHz, DMSO-d_6): 166.6, 149.5, 136.9, 127.9, 106.7, 72.6, 63.0, 46.2, 18.4; EIMS (*m*/*z* (%)): 352.1 (80) [M^+], 353.1 (20) [M^+ + H], 83 (40); calc.: 352.098; found: 352.097.

Synthesis of Poly(3,3-bis(((2-ethylhexyl)oxy)methyl)-3,4-dihydro-2H-thieno[3,4-][1,4]dioxepine)-co(3,4-dihydro-2H-thieno[3,4-b][1,4]dioxepine-3,3-yl)bis(methylene)bis(2-methylacrylate): Copolymers with various amounts of bis-methacrylate monomer were synthesized by varying the amount of individual monomers in the reaction mixture. In a typical synthesis, a total of 2.8 mmol of monomers were added to a 50 mL round bottomed flask and dissolved in ethyl acetate (15 mL). The solution was bubbled thoroughly with argon for 60 min while stirred. The flask was placed in a water bath (20 °C). $FeCl_3$ (14 mmol, 2.2 g, 5 eq) was added to a small beaker of ethyl acetate (5 mL) and bubbled with argon for 1 min. The resulting yellow solution was added by syringe in one portion to the monomer solution resulting in an immediate color change to dark green/blue. The reaction flask was covered in foil and the water bath removed after 5 min. During the polymerization the reaction mixture was continuously bubbled with argon and stirred. The reaction was considered complete when the mixture was black and almost solid (around 3 h). The viscous dark mixture was transferred to a solution of MeOH (200 mL) and stirred for 60 min. Hereafter, it was filtered and the residue washed with MeOH until the filtrate became clear. The solid was dissolved in toluene (200 mL) and reduced with hydrazine (THF solution) until the resulting solution became bright purple (around 0.25 mL). The mixture was transferred to a separatory funnel and washed twice with water (2 × 200 mL), and the organic phase was concentrated in vacuo. The concentrate was precipitated in stirring MeOH (200 mL) and transferred to a cotton thimble. The precipitate was Soxhlet extracted with MeOH (24 h), hexanes (24 h) and $CHCl_3$ (24 h). The $CHCl_3$ fraction was concentrated in vacuo and reprecipitated in MeOH (200 mL). The solution was filtered and the solid dried under vacuum for 24 h yielding a magenta colored solid.

Supporting Information

Supporting Information is available from the Wiley Online Library or from the author.

Acknowledgements

J.R., A.D., and E.S. gratefully acknowledge support of BASF.

Received: October 15, 2012
Revised: December 29, 2012
Published online: March 6, 2013

[1] P. M. S. Monk, R. J. Mortimer, D. R. Rosseinsky, *Electrochromism and Electrochromic Devices*, Cambridge University Press, Cambridge **2007**.
[2] R. J. Mortimer, A. L. Dyer, J. R. Reynolds, *Displays* **2006**, *27*, 2–18.
[3] C. G. Granqvist, *Sol. Energy Mater. Sol. Cells* **2000**, *60*, 201–262.
[4] C. G. Granqvist, *Sol Energ Mater. Sol. Cells* **2012**, *99*, 1–13.
[5] F. C. Krebs, *Nat. Mater.* **2008**, *7*, 766–767.
[6] D. Mecerreyes, R. Marcilla, E. Ochoteco, H. Grande, J. A. Pomposo, R. Vergaz, J. M. Sánchez Pena, *Electrochim. Acta* **2004**, *49*, 3555–3559.
[7] A. A. Argun, P.-H. Aubert, B. C. Thompson, I. Schwendeman, C. L. Gaupp, J. Hwang, N. J. Pinto, D. B. Tanner, A. G. MacDiarmid, J. R. Reynolds, *Chem. Mater.* **2004**, *16*, 4401–4412.
[8] H. W. Heuer, R. Wehrmann, S. Kirchmeyer, *Adv. Funct. Mater.* **2002**, *12*, 89–94.
[9] B. D. Reeves, C. R. G. Grenier, A. A. Argun, A. Cirpan, T. D. McCarley, J. R. Reynolds, *Macromolecules* **2004**, *37*, 7559–7569.
[10] C. M. Amb, P. M. Beaujuge, J. R. Reynolds, *Adv. Mater.* **2010**, *22*, 724–728.
[11] A. L. Dyer, M. R. Craig, J. E. Babiarz, K. Kiyak, J. R. Reynolds, *Macromolecules* **2010**, *43*, 4460–4467.
[12] P. M. Beaujuge, S. Ellinger, J. R. Reynolds, *Nat. Mater.* **2008**, *7*, 795–799.
[13] G. Gunbas, L. Toppare, *Chem. Commun.* **2012**, *48*, 1083–1101.

[14] A. A. Argun, A. Cirpan, J. R. Reynolds, *Adv. Mater.* **2003**, *15*, 1338–1341.
[15] J. Jensen, H. F. Dam, J. R. Reynolds, A. L. Dyer, F. C. Krebs, *J. Polym. Sci., Part B* **2012**, *50*, 536–545.
[16] C. M. Amb, A. L. Dyer, J. R. Reynolds, *Chem. Mater.* **2011**, *23*, 397–415.
[17] M. Dietrich, J. Heinze, G. Heywang, F. Jonas, *J. Electroanal. Chem.* **1994**, *369*, 89–92.
[18] A. Kumar, D. M. Welsh, M. C. Morvant, F. Piroux, K. A. Abboud, J. R. Reynolds, *Chem. Mater.* **1998**, *10*, 896–902.
[19] D. M. Welsh, A. Kumar, E. W. Meijer, J. R. Reynolds, *Adv. Mater.* **1999**, *11*, 1379–1382.
[20] D. M. Welsh, L. J. Kloeppner, L. Madrigal, M. R. Pinto, B. C. Thompson, K. S. Schanze, K. A. Abboud, D. Powell, J. R. Reynolds, *Macromolecules* **2002**, *35*, 6517–6525.
[21] A. Cirpan, A. A. Argun, C. R. G. Grenier, B. D. Reeves, J. R. Reynolds, *J. Mater. Chem.* **2003**, *13*, 2422–2428.
[22] P. M. Beaujuge, C. M. Amb, J. R. Reynolds, *Adv. Mater.* **2010**, *22*, 5383–5387.
[23] N. R. De Tacconi, K. Rajeshwar, R. O. Lezna, *Chem. Mater.* **2003**, *15*, 3046–3062.
[24] Z. Nie, E. Kumacheva, *Nat. Mater.* **2008**, *7*, 277–290.
[25] Y. Xu, F. Zhang, X. Feng, *Small* **2011**, *7*, 1338–1360.
[26] S. Holdcroft, *Adv. Mater.* **2001**, *13*, 1753–1765.
[27] J. Yu, M. Abley, C. Yang, S. Holdcroft, *Chem. Commun.* **1998**, *15*, 1503–1504.
[28] M. S. A. Abdou, Z. W. Xie, A. M. Leung, S. Holdcroft, *Synth. Met.* **1992**, *52*, 159–170.
[29] M. S. A. Abdou, S. Holdcroft, *Macromolecules* **1993**, *26*, 2954–2962.
[30] J. Kim, J. You, E. Kim, *Macromolecules* **2010**, *43*, 2322–2327.
[31] J. Kim, J. You, B. Kim, T. Park, E. Kim, *Adv. Mater.* **2011**, *23*, 4168–4173.
[32] K. S. Schanze, T. S. Bergstedt, B. T. Hauser, *Adv. Mater.* **1996**, *8*, 531–534.
[33] J. Lowe, S. Holdcroft, *Macromolecules* **1995**, *28*, 4608–4616.
[34] A. Kumar, S.-Y. Jang, J. Padilla, T. F. Otero, G. A. Sotzing, *Polymer* **2008**, *49*, 3686–3692.
[35] F. C. Krebs, *Sol. Energy Mater. Sol. Cells* **2009**, *93*, 394–412.
[36] R. Søndergaard, M. Hösel, D. Angmo, T. T. Larsen-Olsen, F. C. Krebs, *Mater. Today* **2012**, *15*, 36–49.
[37] H. F. Dam, F. C. Krebs, *Sol. Energy. Mater. Sol. Cells* **2012**, *97*, 191–196.
[38] F. C. Krebs, M. Jørgensen, K. Norrman, O. Hagemann, J. Alstrup, T. D. Nielsen, J. Fyenbo, K. Larsen, J. Kristensen, *Sol. Energy. Mater. Sol. Cells* **2009**, *93*, 422–441.
[39] H. Sirringhaus, T. Kawase, R. H. Friend, T. Shimoda, M. Inbasekaran, W. Wu, E. P. Woo, *Science* **2000**, *290*, 2123–2126.
[40] D. S. Pedersen, C. Rosenbohm, *Synthesis* **2001**, *16*, 2431–2434.
[41] K. Norrman, A. Ghanbari-Siahkali, N. B. Larsen, *Annu. Rep. Prog. Chem., Sect. C* **2005**, *101*, 174–201.
[42] R. J. Mortimer, K. R. Graham, C. R. G. Grenier, J. R. Reynolds, *ACS Appl. Mater. Interfaces* **2009**, *1*, 2269–2276.
[43] T. T. Larsen-Olsen, B. Andreasen, T. R. Andersen, A. P. L. Böttiger, E. Bundgaard, K. Norrman, J. W. Andreasen, M. Jørgensen, F. C. Krebs, *Sol. Energy. Mater. Sol. Cells* **2012**, *97*, 22–27.

Journal of Materials Chemistry C

RSC Publishing

PAPER

View Article Online
View Journal | View Issue

Photochemical stability of electrochromic polymers and devices†

Cite this: *J. Mater. Chem. C*, 2013, **1**, 4826

Jacob Jensen, Morten V. Madsen and Frederik C. Krebs*

The stability of fully printed flexible organic electrochromics based on 11 different conjugated polymers is explored from the fundamental chemical degradation level to the operational device level. The photochemical stability of the electrochromic polymers (ECPs) is studied enabling an analysis of the influence that the chemical constitution of the conjugated polymer backbone has on the photochemical stability. Based on changes in the UV-visible absorption and IR spectra, the polymers were categorized into two distinct groups, each with a separate degradation mechanism. During irradiation (1000 W m^{-2}, AM 1.5G) under ambient conditions the majority of the polymers degraded within 4–5 hours. Three polymers showed increased stability with degradation rates from 0.44 to 1.58% per hour measured as loss of absorption. Application of oxygen and UV barrier foils was found to drastically slow the photochemical decomposition of the polymer films, such that after 2200 hours of continuous irradiation the less stable polymer films were degraded 27% on average, while the degradation of the most stable polymer films was immeasurable thus indicating that such materials can be sufficiently stable for device operations for many years under indoor conditions and for a few years under outside conditions. Finally, functioning electrochromic devices (ECDs) were made and the effect of illumination on the response time and optical contrast was established. This report shows that encapsulated electrochromic devices based on flexible barrier substrates exhibit increased stability and are indeed viable in devices such as shading elements, light management systems, displays with low switching speed requirements and signage.

Received 22nd April 2013
Accepted 16th June 2013

DOI: 10.1039/c3tc30751d

www.rsc.org/MaterialsC

Introduction

Electrochromic conjugated polymers have for several decades been promising candidates for a variety of optical devices such as billboard displays, matrix displays, e-paper and light management devices such as "smart" windows, sun glasses and other forms of shading elements.[1] As fundamental studies on synthesis, colour control, *etc.* have progressed during this time,[1–8] research towards commercial exploitation of ECPs and development of ECDs should now be regarded as the next step in advancing this technology beyond academic interest. Following this line of thought large area EC displays are suitable candidates for introducing electrochromics on a commercial basis. To be commercially attractive emerging technologies that are meant to replace existing ones already in the market face several challenges to be competitive. New technologies must show improvements on parameters such as cost, efficiency, production speed, environmental impact, *etc.* In that context we believe that electrochromic polymers have potential since they have low power consumption, show a multitude of vibrant colours and can be processed on flexible substrates using fast processes and abundant elements. The latter is a prerequisite for keeping the production costs low. We have previously reported on the development of processing ECPs on flexible substrates integrated in an organic photovoltaic driven circuit, large area ITO free displays and patterning of electrochromic films, as we see the efficient processing of ECPs on flexible substrates as central in realizing the potential of ECPs.[9,10] In this respect, stability of the polymer films is a key element.

The basic principle of an electrochromic device is the ability to change colour by application of a suitable electric potential (shown in Fig. 1) that will oxidize the polymer films if the electrode potential is higher (more positive) than the equilibrium potential of the cell or reduce/neutralize the film if the electrode potential is lower (more negative). The working principle governs the architecture which subsequently affects the stability of ECDs: Since redox reactions occur in the polymer films they need to be in contact with the electrodes, and so the ECPs are coated onto separate transparent conductive substrates (usually flexible substrates or glass coated with ITO). For electrical insulation and ion storage an electrolyte layer is sandwiched between the polymer coated electrodes, which are put (facing inwards) on top of each other. Though other ECD

Department of Energy Conversion and Storage, Technical University of Denmark, Frederiksborgvej 399, DK-4000 Roskilde, Denmark

† Electronic supplementary information (ESI) available. See DOI: 10.1039/c3tc30751d

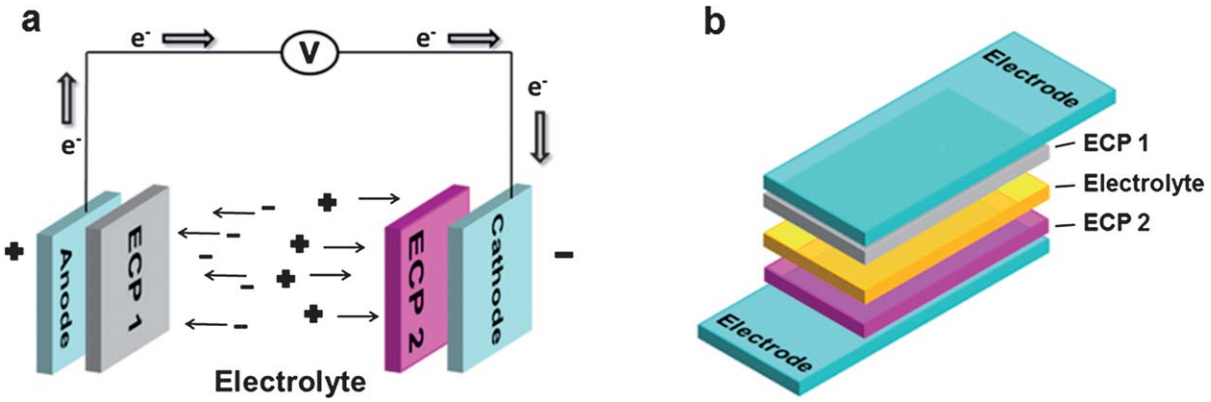

Fig. 1 Working principle and architecture of an ECD. (a) Two ECPs are coated on electrodes connected to an external power source. For electrical insulation and ion storage, an electrolyte layer is sandwiched between the two polymers. By application of a suitable potential **ECP 1** is oxidized at the anode and **ECP 2** is reduced/neutralized at the cathode. Due to the electric field created between the two electrodes anions and cations move towards the anode and the cathode respectively, where they are injected into the polymer film thereby doping the polymer and compensating for the developing charge (*i.e.* formation of polarons and bipolarons). (b) The working principle governs the architecture of ECDs. The layer structure presented here is encountered in a majority of devices. The ECPs are coated onto electrode substrates facing inwards with an electrolyte layer sandwiched in between.

approaches using conjugated polymers are being investigated, multilayer structures such as that shown in Fig. 1b are currently used in a majority of ECDs.[11–13]

The mechanical stability of a polymeric ECD has two weak points, the electrolyte layer and the conductive substrate. Liquid electrolytes are difficult to process and the resulting ECDs need to be meticulously sealed to prevent leakage. To circumvent this, the electrolyte needs to be in the form of a gel or solid.[14] Using a solid electrolyte compromises the switching time, which is dependent on the ionic mobility. This drops as a function of increased electrolyte viscosity. By using an ionic liquid/PMMA based polymeric gel, we have previously shown that the electrolyte layer can be efficiently deposited onto a polymeric layer using slot die or spray coating, with response time in the order of seconds.[9] Transparent electrodes are vital to ECDs, and because no better alternative exists, so far indium doped tin oxide (ITO) has been widely used as an electrode material. This can be problematic in large area devices since ITO presents a large sheet resistance. A large sheet resistance can cause an ohmic drop across the substrate, with uneven switching and higher potential near the external contacts as a result.[15,16] Furthermore, the mechanical stability (*i.e.* risk of cracking and scratching) of the ITO layers can be low, and from a commercial perspective the cost of ITO is high, owing to the scarcity of indium, and the embedded energy associated with sputter deposition.[17] Since electrochromic polymers are to be electrically switched between redox states, newly developed ECPs customarily have their redox properties evaluated using cyclic voltammetry (CV).[1,3,18] CV is also the basis for evaluation of electrochemical stability along with spectroelectrochemistry and measurement of long-term optical contrast (ΔT). From an electrochemical stability perspective the valence band and conduction band are of significance, as they give an electrochemical window in which to operate. Outside of this the polymers are prone to electrochemical degradation by irreversible electrochemical oxidation or reduction. Polymers with relatively high HOMOs are easily oxidized and as a result "doped" with anions (p-doping) from the electrolyte layer. A high HOMO level is advantageous when operating an ECD, as a low potential is sufficient to drive the device between the two redox states.

The combination of oxygen, moisture and light is known to be the reason for photochemical breakdown of polymers at large.[19,20] By analysing poly(3-hexylthiophene) (P3HT) in oxygen saturated solutions, Holdcroft found a linear relationship between irradiation time and decrease in optical density, which was seen as an indication of a reduced number of conjugated π-electrons.[21] The absorbance maximum was also slightly shifted, and this was attributed to a decrease in the average conjugation length. Oxygen, solvent and irradiation wavelength were identified as the three main components responsible for photodegradation. Further studies identified photobleaching and photolytic chain scission as two separate mechanisms of photodegradation in solution.[22] It was concluded that singlet oxygen was responsible for the majority of photo bleaching, by ring opening of the thienyl residue through a 1,4-Diels–Alder addition. A free radical pathway of chain scission was proposed, in which residual transition metal salts from the polymerization reactions (mainly Fe^{3+}) were photolysed to radicals. These were believed to initiate proton abstraction from the alkyl side chain, leading to addition of ground state oxygen and subsequently chain scission through multiple pathways. In thin polymer films of P3HT photo bleaching has also been observed, but instead of chain scission, network formation by crosslinking of the alkoxy radicals produced was identified.[23,24] Recently the involvement of singlet oxygen in the degradation of P3HT films has been rejected by Manceau *et al.* and a mechanism proposed wherein photobleaching is attributed to oxidation of the alkyl side chains, while oxidation of the thiophene backbone is believed to cause chain scission and loss of conjugation.[25–27] Both pathways involve radical chain mechanisms where the α-protons on the side chains play a significant role in the degradation, and the observation that decreasing the irradiation wavelength will increase the photooxidation supports

this.[28] Other studies propose that the polymer is mainly attacked at the terminal thiophene rings and at points of broken conjugation.[29,30] A rule of thumb for the photochemical stability of a large range of donor–acceptor polymers was recently published and herein alkyl side chains, quaternary sites and C–N/C–O bonds were identified as leading to poor photochemical stability while aromatic polycyclic units stabilized the polymers.[31] The position of the HOMO was also addressed, but the conclusion on this matter was less clear.

The aspect of photochemical stability has been largely ignored for ECPs and the literature is scarce. This can to a large extent be attributed to the fact that so far, photochemical stability has not been the limiting factor for the stability of ECDs. In this report we evaluate the photochemical stability of ECPs. We first establish a rate of degradation based on chemical motifs and thicknesses of the polymer films. Then we analyse ECDs by successively adding layers such as electrolyte, barrier film, *etc.* to establish their effect on the photochemical stability. Finally we examine the effect that irradiation has on the response time of an ECD and evaluate the photochemical stability of a fully operating electrochromic device. We do this by exposing the targeted ECPs and ECDs to artificial solar irradiation (AM 1.5) in a custom made degradation setup that allows for fast and reliable analysis. This is correlated with infrared (IR) spectroscopy of the polymer films at various stages of degradation.

Experimental

Instrumentation

^{1}H and ^{13}C NMR spectra were recorded on a BRÜKER 250 or 500 MHz FT-NMR. IR spectroscopy was performed on a Spectrum One from Perkin-Elmer. Transmission/absorption IR spectra of the polymer films were obtained from ECPs spin-cast onto KBr pellets from toluene solutions. Absorption/transmission profiles in the 800–300 nm range were determined using a Pharma Spec UV-1700 from Shimadzu. The film thickness was measured on a Dektak 3030 from Veeco Instruments Inc. scanning 500 μm with a stylus force of 0.05 mN.

Film formation

ECP films were spin-coated from 20 mg mL^{-1} solutions of toluene or chlorobenzene (**ECP 5** and **ECP 6**). The **ECP 2** solution additionally contained 6 mg mL^{-1} AIBN and 2 drops per millilitre ethyleneglycol dimethacrylate (EGDMA, 1 drop $\sim$ 21 mg). Films were cast onto ITO-coated glass (2.5 cm $\times$ 5 cm; $R_s \sim 20$ ohms per sq) or onto ITO covered PET foil (2.5 cm $\times$ 5 cm; $R_s \sim 30$ ohms per sq) at angular velocities of 500–1400 rpm using a Laurell WS-400-6NPP spin-coater.

Film degradation

A fully automated, high-throughput photo-chemical degradation setup was used for the degradation of all materials in this study as described elsewhere.[32] The setup utilizes a Steuernagel solar simulator with an Osram 1200 W metal halide arc lamp providing an approximate AM1.5G spectrum with an intensity of 1000 W m^{-2}. The sample exchanger has a capacity of 22 samples and a UV-vis spectroscopic probe based on an optical fiber-based CCD spectrometer (Avantes AvaSpec 1024) and a halogen/deuterium light source (Avantes AvaLight-DHc) were used to measure the evolution in the absorbance of the samples.

Long term stability measurements

Samples were constructed by spincoating ECPs onto ITO coated PET and sealing them by covering the substrate on both sides with a PET multilayer foil comprising a PTA adhesive (3M, MP467, cut-off 320 nm) that functioned as an oxygen barrier foil.

Half the sample was further covered with a UV barrier foil (Amcor, thickness 72 μm, cut-off 400 nm), see Fig. 3B and C. A second set of samples were constructed that in addition contained a PMMA based electrolyte previously employed in ECDs,[9] see Fig. 3D and E. Samples were irradiated for 2200 hours using a solar simulator as described above. Absorption spectra were measured at weekly intervals, relative to an appropriate reference that was similarly exposed. It should be noted that blisters in the protective foil (following 500 hours of illumination) might cause reflections different from the reference.

Response time

Functional electrochromic devices were constructed by spincoating **ECP 1** and **ECP 9** onto ITO/PET substrates (1.5 cm $\times$ 3 cm; $R_s \sim 80$ ohms per sq) as previously reported.[9] Prior to assembly, the **ECP 1** coated substrates were irradiated (AM 1.5G, 1000 W m^{-2}) for 0, 30, 60 and 90 minutes respectively. Potential square wave absorptiometry experiments were done from -0.6 V to +1.5 V with a 60 second hold at each of the two potentials. After an initial "break in" of 35 double switches, the response time was obtained.

Results and discussion

The polymers presented in this study are depicted in Fig. 2, and were synthesized in our laboratories for this report according to the literature.[32–41] Polymer structures were confirmed by NMR and IR spectroscopy. The selected polymers are all solution processable from common organic solvents, as a prerequisite for efficient film formation. Polymers encompassing several colours were chosen, since a wide range of colours are used in commercial billboards, signs, displays, *etc.*

On this basis it is of interest to know the rate of degradation of the individual polymer films, when designing such displays. And although colour mixing by subtractive primary colours (red-blue-yellow) or cyan-magenta-yellow produces the full colour spectrum, it has yet to be sufficiently demonstrated in functioning ECDs.[36] Furthermore polymers encompassing different chemical motifs were synthesized, to study the effect of these on the photochemical stability. **ECP 1** and **ECP 9** are both magenta coloured in the neutral state. **ECP 1** has been extensively studied over the last decade, and in addition to being a homopolymer with distinct characteristics, it also serves as a point of reference since the structure is part of several of the copolymers explored.[35] The crosslinkable analogue **ECP 9** is capable of network formation, and the effect of this on the photochemical stability was observed.[41] **ECP 3** is a random copolymer, with a

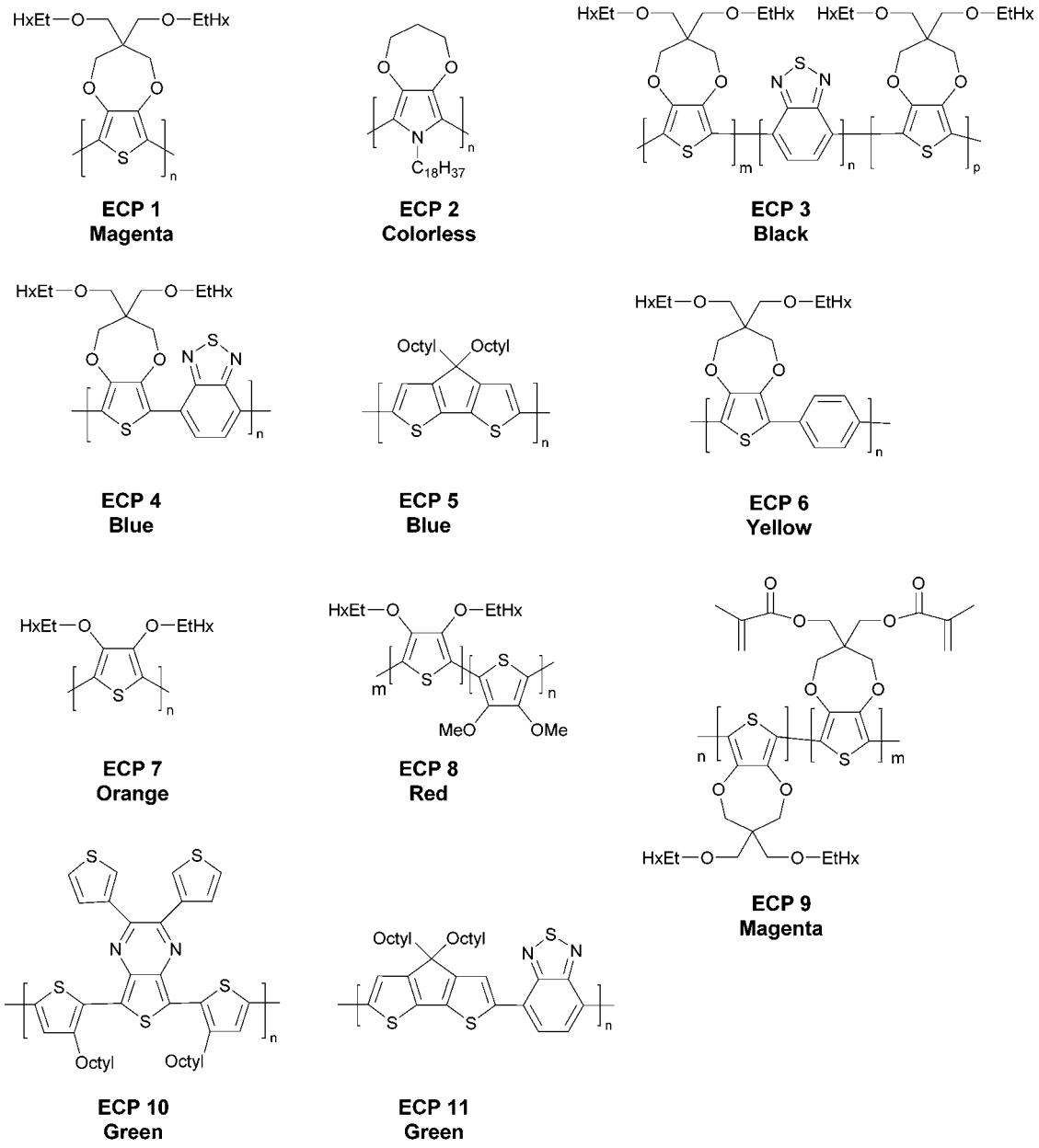

Fig. 2 Electrochromic polymers analysed in these trials. Note the names have been changed compared to the original literature. EtHx = 2-ethylhexyl.

structure that gives rise to several absorption peaks within the visible spectrum. The result is a black colour which is of interest in relation to e-paper, shading and black/white displays.[37] **ECP 4** and **ECP 5** are both blue in their neutral state but comprise different chemical motifs.[30,42] The blue colour in **ECP 4** is a result of the donor–acceptor approach, with ProDOT(OEtHx)$_2$ and benzothiadiazole as the donor moiety and acceptor moiety respectively.[8] The steric effect of the phenyl ring in **ECP 6** is another approach by which to alter absorption of ECPs. By a combination of steric and acceptor properties the absorption is blueshifted and therefore **ECP 6** appears yellow in the neutral state.[36] Polymer **ECP 7** is orange in the neutral state and has a higher band gap than **ECP 8** that has methoxysubstituted thiophenes randomly incorporated. These substituents relax the steric repulsion between the substituents and lower the band gap to 2.0 eV, which redshift the absorption to 525 nm producing a red polymer.[31] **ECP 10** is green in the neutral state and was selected based on the different chemical motif compared to the other polymers.[43] **ECP 11** is green as well and encompasses a BTD acceptor group that results in an additional absorption peak compared to **ECP 5**, typical of donor–acceptor polymers.[8,39] **ECP 2** is an almost colourless polymer in both redox states, which is advantageous in ECDs, where it can function as a charge balancing polymer with minimal effect on the optical contrast.[38] The effect of the structural difference of **ECP 2** and the other polymers (polypyrrole *vs.* polythiophenes), and the near absence of absorption in the visible spectrum was explored.

Photochemical degradation of ECPs

To determine the rate of degradation of the ECPs, the polymer films were subjected to solar irradiation under different conditions, as depicted in Fig. 3. In order to correlate film thickness with absorption, ECPs were spin coated on ITO covered glass at different angular velocities. Following this, a thickness dependent rate of photochemical degradation was established by illuminating the samples while recording the absorption spectra, as detailed in the Experimental section. Fig. 4a shows the absorption spectra recorded during continuous irradiation of **ECP 1**. During this time (0–5 h) a pronounced decrease in absorbance is observed in the visible region, while a slight increase in absorbance is seen in the ultraviolet region. The latter is caused by degradation products absorbing in that part of the spectrum. Due to the position of the HOMO, oxidation of the polymer under ambient conditions might influence the degradation. To ensure that the polymer was in its fully natural state, the polymer film was switched between the two redox states (+1.5 V/−1.0 V) leaving it in the neutral state prior to irradiation. As there was no observable difference in the absorption spectra following this treatment, it was considered an unnecessary source of experimental error. Fig. 4b shows the maximum absorbance (abs_{max}) as a function of illumination time for three different polymers along with the fitted curves. The slope of these curves is the degradation rate given as the percentage decrease of abs_{max} per hour. For similar information on the other polymers the reader is directed to the ESI (Fig. S1–S11† – b graphs, note the difference in time scale for various polymers).

The comparison of degradation rates for different polymers can be challenging and reports have shown an order of magnitude difference in the degradation of P3HT.[29,44,45] The explanation for this discrepancy is that the film thickness influences the observed degradation rate, and in addition the comparison of degradation rate for different polymers of equal thickness is questionable since the extinction coefficient can be vastly different. Using the absorption maximum has been suggested as a better alternative. For this reason all degradation experiments were conducted with a series of thicknesses for each polymer. Fig. S1–S11† (d graphs) in the ESI show the correlation between thickness and absorption. It is noted that it was not possible to obtain the exact same thicknesses for all polymers. However, initial absorption values as close to 0.5 as possible have been used for comparing the degradation rate of the polymers in this report. Consistent with previous findings, degradation rates cannot be determined on scales better than a factor of five for comparison of different polymers.[32] This, however, still allows us to organize the polymers in a hierarchy based on their relative degradation rates. This is shown in Table 1. **ECP 11**, the most photo stable polymer, is more stable than **ECP 8**, the most photo unstable polymer, by a factor of 200. The degradation behaviour of the different polymers clearly divides them into distinct degradation classes, see Fig. 4 and ESI.† Some polymers exhibit a linear decline of absorption during degradation (**ECP 1–4**, **10** and **11**) while others exhibit a sublinear decline (**ECP 5–8**). Based on these observations, the polymers can be classified into two groups according to their photochemical stability and degradation modes. Group 1 includes all polymers with linear degradation behaviour. Group 2 includes all polymers with sublinear degradation behaviour. In Table 1 the group assignment is indicated in column 4. From this point it is clear that all polymers in group 1 are more photochemically stable than the polymers in group 2. The grouping of the polymers is indicative of the underlying degradation mechanism governing the degradation of the polymers. Linear degradation behaviour as exhibited by group 1 can be explained by a simple hypothesis. If one imagines that the polymers of this group only degrade by a mechanism attacking terminal positions on the polymer chain, the degradation would be linear since the number of reaction sites is constant, as seen for group 1. On the other hand if there is no preferred attack point on the polymer the degradation rate would decelerate since the number of reaction sites diminishes, as seen for group 2. A mixed state where the polymer is preferably degraded at terminal positions, but also at intermediate points would result in an accelerating degradation behaviour which is not observed for any of the groups, this does however depend on the respective rates of the two degradation mechanisms. The terminal attack point hypothesis infers that the conjugation must be preserved for the majority of the degradation period; that is the absorption peak position must remain near constant for the major part of the degradation. When plotting the peak position as a function of the degradation state, as can be seen in the ESI for all polymers, a peak shift rate can be established (Fig. S1–S11,†c graphs). As is evident from Table 1 all polymers in group 1 exhibit a slower peak shift than the polymers in group 2; an observation consistent with the terminal attack point hypothesis. We have already established that if the polymer is attacked at terminal positions the

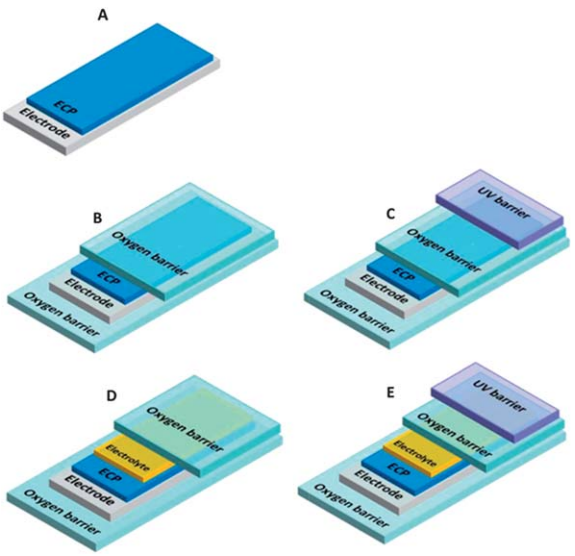

Fig. 3 Sample structures. (A)–(E) depict the layer structure under which the polymer films were irradiated. (A) shows the ECP coated on an ITO covered glass substrate in the absence of barrier foils. (B) shows the polymer coated onto ITO covered PET and encapsulated in oxygen barrier foil. (C) shows a sample additionally covered with a UV barrier foil. (D) and (E) are similar to (B) and (C) but comprise a PMMA/ionic liquid electrolyte layer.

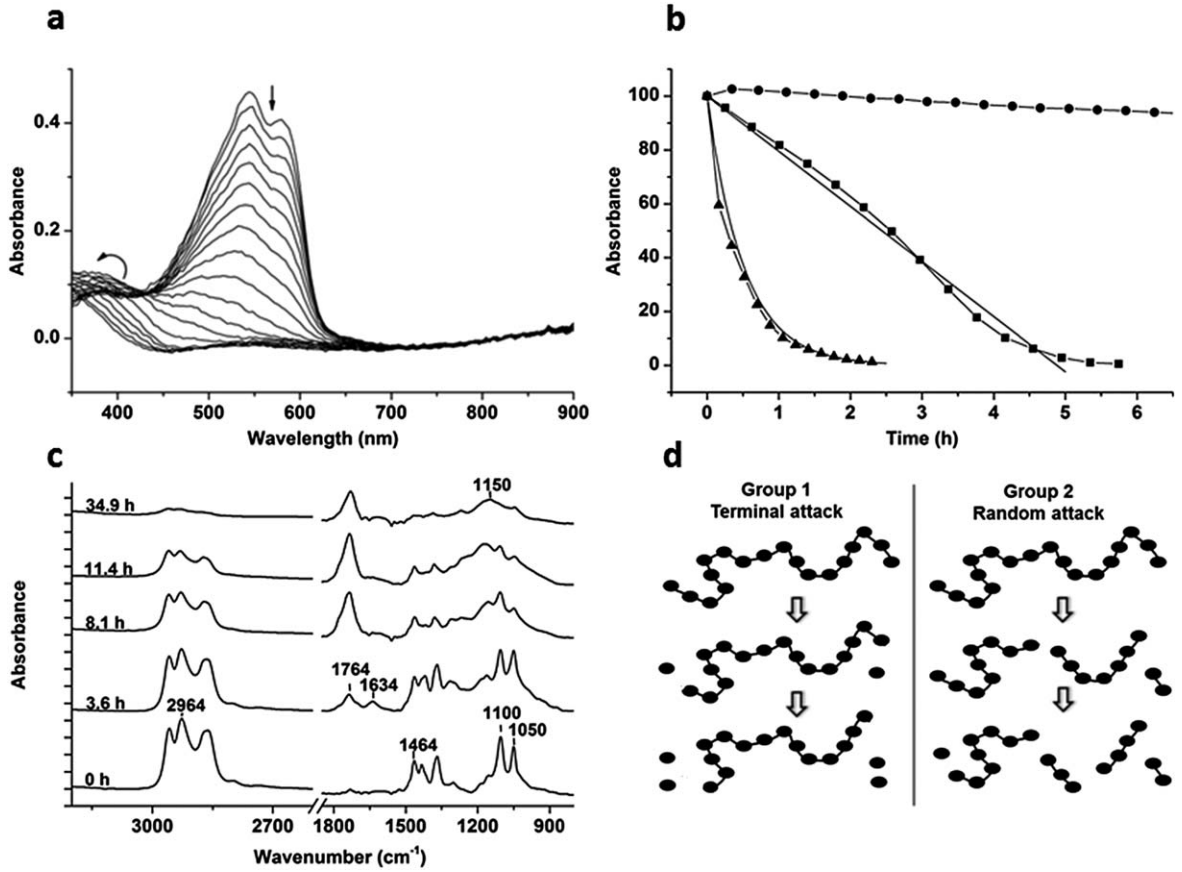

Fig. 4 Irradiation of polymer films. (a) Absorption profiles of **ECP 1** in the UV-visible region from $t = 0$ (top) to $t = 6$ h (bottom). (b) The maximum absorbance as a function of irradiation time for polymer films. The absorbance has been normalized to allow for comparison of the degradation rate. For clarity two examples, ■ **ECP 1** (magenta) and ▲ **ECP 7** (orange), of the two distinct groups are depicted along with the second most stable polymer ● **ECP 4** (blue). Next to **ECP 1** and **ECP 7** are shown the fitted curves. (c) Development in the infrared region during 35 hours of irradiation of **ECP 1**. (d) Schematic showing photochemical degradation of polymer chains by the two different mechanisms proposed.

Table 1 Degradation and peakshift rate for electrochromic polymers. Abs_{max} is the wavelength where the absorption is at a maximum in the pristine film. *Peakshift rate* describes how much the maximal absorbing peak shifts during irradiation. *Degradation rate* refers to the decrease of the maximal absorbing peak per hour of irradiation

Polymer	Abs_{max} (nm)	Peakshift rate (nm/%)	Degradation rate (%/h)	Group
ECP 11 (green)	670	0.10	0.44	1
ECP 4 (blue)	645	0.39	1.17	1
ECP 10 (green)	717	0.49	1.58	1
ECP 9 (magenta)[a]	544	0.10	3.85	1
ECP 3 (black)	539	0.37	7.32	1
ECP 2 (colorless)[b]	302	—	7.93	1
ECP 9 (magenta)[c]	545	0.15	8.48	1
ECP 1 (magenta)	546	0.26	16.95	1
ECP 5 (blue)	584	1.41	34.91	2
ECP 6 (yellow)	445	0.75	43.49	2
ECP 7 (orange)	460	0.62	81.48	2
ECP 8 (red)	504	0.72	81.70	2

[a] The polymer film comprised ethyleneglycol dimethacrylate (EGDMA) crosslinker and AIBN photoinitiator. [b] Peakshift rate could not be determined as the spectrum does not contain any distinct peaks. [c] The polymer film did not contain any additional components.

degradation would be linear, but if the polymer is attacked at completely random positions we can also predict the shape of the degradation. If it is assumed that the degradation is not oxygen limited or limited by light shielding, the only rate-determining factor is the number of attack points.[30] The rate will be given by the recurrence equation $f(n + 1) = (1 - a)f(n)$, where n represents the numbered time intervals and a is the percentage loss of attack points per time iteration. The solution to this equation can be written in the form $f(n) = c(1 - a)^n$. By letting $f(1) = 100$ and then optimizing to the degradation state values this function can be fitted to the experimental data. In Fig. 4 a fit for **ECP 8** along with the experimental values is depicted. It is found that all polymers in group 2 can be described with an r-squared value better than $R^2 = 0.98$. This is a very strong indication that the degradation mechanism is indeed targeting random positions on the polymer chain. The fact that a faster peakshift is observed for this group also strengthens the hypothesis, since the conjugation length would change faster in the random attack mode.

From the data in Table 1, it is seen that the two most photochemically stable polymers **ECP 11** and **ECP 4** contain a benzothiadiazole (BTD) group. There are, respectively, 80 and 14 times increase in photochemical stability between these two

copolymers and the homopolymers **ECP 1** and **ECP 5** that have similar chemical motifs but do not comprise BTD groups. Being an electron-deficient group, the incorporation of the BTD group is expected to lower the oxidation potential of the polymer, due to a relatively lower lying HOMO level of the resulting polymer.[45,46] While the electrochemical stability of conjugated polymers depends on the electrode potentials (and consequently HOMO/LUMO levels),[47] the photon energy from sunlight is so high that other reactions such as radical initiated side-chain scission contribute to the degradation of conjugated polymers. The third most photo-stable polymer was the thienopyrazine **ECP 10**, which is in good accordance with previously published results.[31,48] The position of the HOMO is not necessarily correlated with photochemical stability, but in this case the effect is observable. Looking at Table 1, one can note the difference in stability between the magenta coloured polymers **ECP 1** and **ECP 9**. The increased stability of **ECP 9** is attributed to the methacrylate functionalities present in the polymer. When crosslinked, **ECP 9** shows a two fold increase in stability (see footnote a in Table 1) compared to **ECP 1**, which is presumably due to absorption of photons by the carbonyl group formed by crosslinking. In the absence of a photoinitiator and crosslinker in the polymer film (see footnote c in Table 1), **ECP 9** shows a fourfold increase in stability compared to **ECP 1**. This increase was ascribed to a higher degree of photon absorption by the methacrylate group compared to the carbonyl moiety in the crosslinked species.

Infrared spectroscopy

As UV-visible absorbance spectroscopy is based on π–π^* transitions and related features such as charge transfer, conjugation length and regioregularity of the polymer films, infrared spectroscopy was used to monitor the chemical alterations of functional groups and correlate with the results obtained using UV-visible spectroscopy. Fig. 4c shows the assignment of the major peaks in the infrared spectrum of **ECP 1**. Since all, but one, of the polymers are polythiophenes with similar structural components, they show analogous infrared spectral features. For the assignments of the other polymer films the reader is directed to the individual spectra in the ESI (Fig. S1–S11, † e graphs). The peaks from 2960 cm^{-1} to 2860 cm^{-1} are assigned to C–H stretching mainly from the aliphatic side chains. The intensity of these peaks progressively decreased during irradiation as a result of photolytic scission of the aliphatic side chains. The peaks from 1500 cm^{-1} to 1434 cm^{-1} are assigned to symmetric and asymmetric C=C stretching in the thiophene rings. These signals disappear during exposure which is ascribed to changes in the ring structure and conjugation. The decrease in the intensity of these peaks was found in accordance with the UV-visible absorption spectra. The peaks at 1100 cm^{-1} to 1050 cm^{-1} likewise decreased during irradiation of the film. These peaks are assigned to the C–O–C stretch from the ether groups. During exposure two bands appeared in the carbonyl region at 1764 cm^{-1} and 1634 cm^{-1}. The appearance and increase in these peaks is a strong indication of C=O formation. The intensity of the former band increased up to a certain point whereafter it decreased slowly. This band has, under similar conditions, previously been assigned to anhydride species. The latter band can be assigned to an aromatic ketone that is photochemically unstable, which is in accordance with the disappearance of this band on continuous irradiation. A broad band centred at 1150 cm^{-1} also appeared during exposure, which previously has been assigned to sulphur–oxygen oxidation products such as sulfinic acids or esters *i.e.* a breakdown/opening of the thiophene ring.[26] In the hydroxyl region a broad signal between 3200 and 3700 cm^{-1} increased during progressive irradiation. The appearance of bands in this region indicates formation of hydroxyl or peroxy adducts.

The infrared spectrum obtained from the polypyrrole **ECP 11** was similar to those of the polythiophenes with minor differences. The peaks at 1462 and 1373 cm^{-1} are assigned to C=C stretching in the pyrrole ring. The peak at 1434 cm^{-1} corresponds to a C–N stretching vibration and the peaks 1163 and 1139 cm^{-1} are assigned to C–O–C stretching from the ether bindings. All of the above peaks decreased in intensity during irradiation. A peak appeared in the carbonyl region at 1723 cm^{-1} during irradiation, and increased continuously until a slight drop was observed after 10 hours of exposure. Fig. 5 shows the (normalized) development in the intensity of various bands in the infrared spectrum of **ECP 1** as a function of irradiation time along with the absorption at 545 nm. The signals corresponding to aliphatic side chains (2964 cm^{-1}) and the thiophene ring (1464 cm^{-1}) decrease in intensity at the same rate, while the visible absorbance at 545 nm decreased at a rate four times as fast during the first 5 hours, whereafter the curve reached a minimum. As visible absorbance requires a minimum conjugation length to be detectable, this explains why the IR signals from the thiophene ring are detectable long after 5 hours. For the carbonyl signal at 1734 cm^{-1}, the trend is the opposite. The signals increase during the first eleven hours, whereafter the intensity slightly decreases, suggesting formation of a carbonyl containing oxidation product that subsequently decomposes. The occurrence and development of the

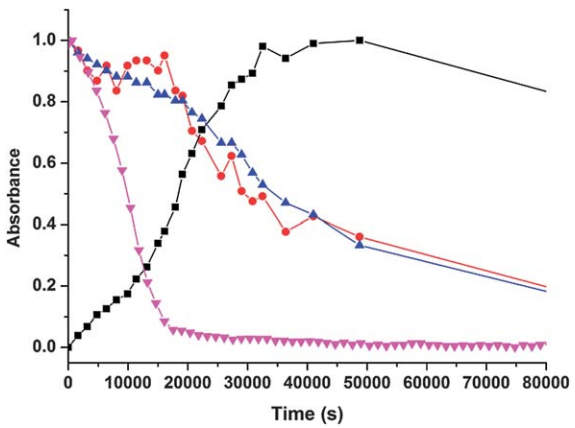

Fig. 5 Peak development during photochemical degradation. The absorbance has been normalized to allow for comparison of the signals. ● 1464 cm^{-1}; C=C stretching in thiophene rings ▲ 2964 cm^{-1}; C–H stretching in alkyl groups at ■ 1734 cm^{-1}; C=O stretching from carbonyl moiety ▼ absorbance measured at 545 nm.

signals during irradiation show trends much alike those obtained for P3HT, which implies that the ECPs degrade *via* similar intermediates.[26]

Operational stability

In addition to the diminished absorbance due to photochemical alterations of the polymer films, the operational characteristics, response time and optical contrast, of a photo exposed ECD were obtained. To confine the effect of irradiation to the primary ECP film (the more strongly coloured ECP),[1] these were illuminated prior to device assembly, as detailed in the Experimental section. Electrochemical stability was ensured by keeping the applied potentials at −0.6 V to +1.5 V, which is fairly low for an electrochromic device. The low potentials naturally compromised the response time and optical contrast of the devices, but as focus was on changes in response time due to illumination (relative to a non-exposed device), the extended response time was of no concern. Fig. 6a shows the optical contrast (ΔT) and response time of photo exposed ECDs potentiostatically switched between −0.6 V and +1.5 V. As seen in the figure, illumination affected both redox states of the device, with a pronounced effect on the coloured state of the devices. After 30 minutes of exposure the minimum transmission (T_{min}) obtainable increased from 45% (non-exposed) to 47% (30 min), 62% (60 min) and following 90 minutes of irradiation T_{min} was 73%. Exposing the samples to irradiation had a less pronounced effect on the bleached state, since photodegradation involves oxidation of the film. The difference in maximum transmission (T_{max}) between the non-exposed and the film exposed for 90 minutes was only 3%. As a consequence, ΔT decreased from 35% in the non-exposed device to 33% (30 min), 17% (60 min) and 6% (90 min). The absence of plateaus, due to incomplete oxidation reactions, on the oxidized parts of transmission curves is noted. A further increase in transmission should therefore be possible, but as shown in Fig. 6b the slope of the current response only very slowly approaches zero during the end of the 60 second potential step, indicative of a very slow electrochemical reaction at this stage. Extending the potential step to three minutes merely resulted in a minor transmission increase (results not shown), and the 60 second potential steps were considered reasonable for measuring changes in response time. In Table 2 the response times for the ECDs are shown. Since a substantial part of the redox reaction occurs at the beginning of the voltage pulse (as seen by the initial current spike in Fig. 6b), the changes in response time due to exposure for 90% and 95% of a full switch are expected to be most notable. Going from left to right in the "coloured to bleached" columns, a slight decrease in response time is observed between the non-exposed sample and the one exposed for 30 min. We suggest this being caused by the larger optical contrast of the non-exposed sample. The opposite (*i.e.* increased response time) seen for films exposed for 60 and 90 minutes is attributed to

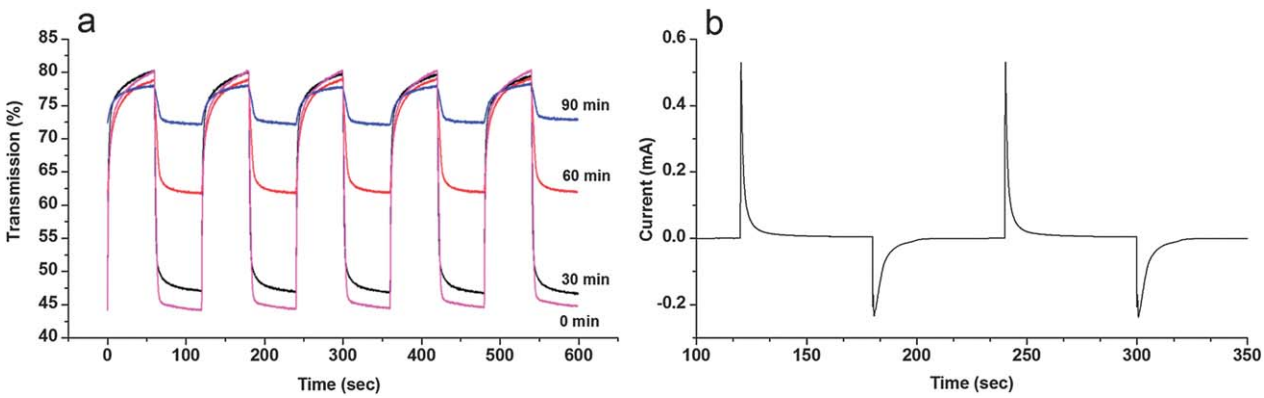

Fig. 6 (a) Response time and optical contrast of irradiated electrochromic devices using potential square wave absorptiometry from −0.6 V to +1.5 V with 60 seconds hold at each potential. The time of exposure is marked to the right of the curves. The transmission was measured at 545 nm. (b) Device current in response to applied potential of the non-exposed sample.

Table 2 Response time of irradiated ECDs. The "coloured to bleached" and "bleached to coloured" columns show the response time when oxidizing (+1.5 V) and reducing (−0.6 V), respectively, ECP films irradiated for 0, 30, 60 and 90 minutes. For every film the response time for a 100% (full) switch is given along with the response time for a 90%, 95% and 98% switch. The optical contrast (ΔT) for a full switch is shown in parentheses on the bottom line

	Colored to bleached				Bleached to colored			
	Exposure time				Exposure time			
% of full switch	0 min	30 min	60 min	90 min	0 min	30 min	60 min	90 min
90%	19.6s	14.1s	19.4s	25.6s	4.0s	5.7s	10.5s	9.4s
95%	34.7s	30.8s	40.3s	34.5s	6.1s	14.0s	18.2s	12.4s
98%	48.8s	43.3s	49.0s	45.2s	11.2s	28.0s	31.2s	19.4s
100%	58.8s (35.9%)	59.2s (33.0%)	59.1s (17.2%)	51.8s (5.8%)	49.3s (35.7%)	55.3s (33.1%)	59.9s (17.3%)	55.1s (5.5%)

widespread degradation of the polymer chains, not yet occurring in the 30 min. exposed film. It is also worth noting that although the difference in response time between *e.g.* the non- and 90 minute exposed samples at 95% of a full switch is negligible, the optical contrast of the former is roughly six times as large as the latter; hence more chemical reactions occur during the same time interval. The response time when reducing the polymers was, as expected, faster compared to the corresponding oxidation reactions. Such discrepancy in response time is common for p-dopable electrochromic polymers and could be explained by a lower reduction potential relative to the oxidation potential, and secondly charge balancing anions are intercalated in the solid polymer films upon oxidation, while exiting into a semisolid electrolyte upon reduction. On extending the exposure time of the samples, a generally slower response time when reducing the devices is observed. As the illuminated polymer films contain oxidized functional groups, these may impede delocalization of pi-electrons and formation of polarons. In conclusion the response time in both directions is affected by illumination. Even though the response time is faster when reducing the polymer films, this reaction is slowed relatively more by light exposure than the corresponding oxidation reaction.

Long term stability

The relatively poor stability of the ECP films under ambient conditions is incompatible with ECDs that are supposed to function for long periods of time. For ECDs that operate indoors under artificial illumination, this degradation is negligible, but for ECDs operating outside (*e.g.* ECDs driven by a photovoltaic cell or an outdoor electrochromic display) the lifetime of the ECDs has to be long to be useful. It is realized that operational ECDs will have a multi-layered structure, different from Fig. 3A, which will confer some degree of protection to the ECP films. But even with an optimistic prediction of a magnitude increase in lifetime gained from the layered structure, the lifetime of the ECDs is still too short. By employing barrier foils capable of protecting the ECP films from atmospheric oxygen and/or UV irradiation (see Fig. 3B–E), this was addressed. The barrier foils were applied directly onto the ECP samples, and as the foils are equally flexible, this was done without compromising the flexibility of the samples. The oxygen barrier comprised a polyethylene terephthalate (PET) multi-layered foil and a pressure sensitive adhesive (PSA) that facilitated encapsulation of the sample. As the encapsulation was done under ambient conditions, small amounts of oxygen were intrinsically trapped inside the samples, but the effects of this were considered limited.

After 2200 hours of continuous illumination the average level degradation for group 1 polymers was so limited that it was immeasurable, while the group 2 polymers showed a degradation rate of 0.027% per hour on average. This amounts to a drastic 1300–3300 fold increase in lifetime for group 2 polymers. To observe the effect of the PMMA electrolyte, a second set of samples comprising the electrolyte gel were investigated (see Fig. 3D and E).[49] The PMMA based gel did in some instances confer additional protection from photochemical degradation, and did in any instance not enhance degradation.

The UV barrier foil did not seem to have any direct effect on the stability of the ECPs, as the oxygen already conferred UV protection, but the additional UV barrier did protect the oxygen barrier from UV induced decomposition, thereby extending device lifetime.

Conclusions and outlook

In this report we have established that the majority of electrochromic polymers tested degraded within 1–5 hours of irradiation in an ambient atmosphere. Based on the degradation profile, the polymers can be grouped into two distinct groups, each with a separate mechanism. The mechanisms are based on fitted models, which were shown to match the experimental data very well. In one mechanism the polymer chains are attacked at terminal positions only and this leads to a linear loss of absorption. In the second mechanism the polymer chains are attacked at random positions during irradiation, with a logarithmic decrease in the degradation rate as a consequence. The relatively photo unstable ECPs were protected with oxygen and/or UV barrier foils, which prolonged the lifetime of the polymers. With a yearly average of 2.8 sun peak hours per day at northern latitudes (*e.g.* Copenhagen) and 4.9 sun peak hours at subtropical latitudes (*e.g.* Miami), 2200 hours of illumination (AM 1.5G, 1000 W m^{-2}) amount to exposure for more than two years at northern latitudes and a year and a half for southern latitudes. These numbers show that photochemically stable ECDs with convincing operational lifetimes can be constructed by a relatively simple process. This facile manner of protection is encouraging for the further development and use of electrochromic polymers in devices, and by increasing the barrier foil stability (*e.g.* using thicker foils) a further increase in lifetime can be expected. By analysing operational performance of exposed polymer films it was found that both response time and optical contrast were compromised.

In a broader context, this is to the best of our knowledge the first published research paper that thoroughly analyses the photochemical stability of conjugated electrochromic polymers. As stability issues are very important, they need to be addressed as part of the on-going development of operational electrochromic devices. Continuing the work on stability issues would further enhance development within the area of electrochromic devices. Research on electrochemically stable electrodes and electrolyte materials is strongly needed, alongside the improvement of robust manufacturing processes.

Acknowledgements

This work was supported by the Eurotech Universities Alliance project “Interface science for photovoltaics (ISPV)”.

References

1 P. M. S. Monk, R. J. Mortimer and D. R. Rosseinsky, *Electrochromism and Electrochromic Devices*, Cambridge University Press, 2007.
2 G. Gunbas and L. Toppare, *Chem. Commun.*, 2012, **48**, 1083–1101.

3 C. M. Amb, A. L. Dyer and J. R. Reynolds, *Chem. Mater.*, 2011, **23**, 397–415.
4 R. J. Mortimer, *Annu. Rev. Mater. Res.*, 2011, **41**, 241–268.
5 R. J. Mortimer, A. L. Dyer and J. R. Reynolds, *Displays*, 2006, **27**, 2–18.
6 M. Sassi, M. M. Salamone, R. Ruffo, C. M. Mari, G. A. Pagani and L. Beverina, *Adv. Mater.*, 2012, **24**, 2004–2008.
7 P. M. Beajuge, S. Ellinger and J. R. Reynolds, *Nat. Mater.*, 2008, **7**, 795–799.
8 P. M. Beaujuge, C. M. Amb and J. R. Reynolds, *Acc. Chem. Res.*, 2010, **43**, 1396–1407.
9 J. Jensen, H. F. Dam, J. R. Reynolds, A. L. Dyer and F. C. Krebs, *J. Polym. Sci., Part B: Polym. Phys.*, 2012, **50**, 536–545.
10 R. Sondergaard, M. Hösel, M. Jørgensen and F. C. Krebs, *J. Polym. Sci., Part B: Polym. Phys.*, 2013, **51**, 132–136.
11 S. Percec and S. Tilford, *J. Polym. Sci., Part B: Polym. Phys.*, 2011, **49**, 361–368.
12 D. Mecerreyes, R. Marcilla, E. Ochoteco, H. Grande, J. A. Pomposo, R. Vergaz and J. M. Sánchez Pena, *Electrochim. Acta*, 2004, **49**, 3555–3559.
13 M. Mallouki, P. Aubert, L. Beouch, F. Vidal and C. Chevrot, *Synth. Met.*, 2012, **162**, 1903–1911.
14 H. J. Byker, *Electrochim. Acta*, 2001, **46**, 2015–2022.
15 K. Ho, D. E. Singleton and C. B. Greenberg, *J. Electrochem. Soc.*, 1990, **137**, 3858–3864.
16 H. Kaneko and K. Miyake, *Appl. Phys. Lett.*, 1986, **49**, 112–114.
17 C. J. M. Emmott, A. Urbina and J. Nelson, *Sol. Energy Mater. Sol. Cells*, 2012, **97**, 14–21.
18 A. A. Pud, *Synth. Met.*, 1994, **66**, 1–18.
19 M. Day and D. M. Wiles, *J. Appl. Polym. Sci.*, 1972, **16**, 203–215.
20 P. Gijsman, G. Meijers and G. Vitarelli, *Polym. Degrad. Stab.*, 1999, **65**, 433–441.
21 S. Holdcroft, *Macromolecules*, 1991, **24**, 4834–4838.
22 M. S. A. Abdou and S. Holdcroft, *Macromolecules*, 1993, **26**, 2954–2962.
23 M. S. A. Abdou, G. A. Diaz-Guijada, M. I. Arroyo and S. Holdcroft, *Chem. Mater.*, 1991, **3**, 1003–1006.
24 M. S. A. Abdou, Z. W. Xie, A. M. Leung and S. Holdcroft, *Synth. Met.*, 1992, **52**, 159–170.
25 M. Manceau, A. Rivaton and J. Gardette, *Macromol. Rapid Commun.*, 2008, **29**, 1823–1827.
26 M. Manceau, A. Rivaton, J. Gardette, S. Guillerez and N. Lemaître, *Polym. Degrad. Stab.*, 2009, **94**, 898–907.
27 M. Koch, R. Nicolaescu and P. V. Kamat, *J. Phys. Chem. C*, 2009, **113**, 11507–11513.
28 H. Hintz, H. Egelhaaf, L. Lüer, J. Hauch, H. Peisert and T. Chassé, *Chem. Mater.*, 2011, **23**, 145–154.
29 H. Hintz, H. Egelhaaf, H. Peisert and T. Chassé, *Polym. Degrad. Stab.*, 2010, **95**, 818–825.
30 M. V. Madsen, T. Tromholt, A. Böttiger, J. W. Andreasen, K. Norrman and F. C. Krebs, *Polym. Degrad. Stab.*, 2012, **97**, 2412–2417.
31 M. Manceau, E. Bundgaard, J. E. Carlé, O. Hagemann, M. Helgesen, R. Søndergaard, M. Jørgensen and F. C. Krebs, *J. Mater. Chem.*, 2011, **21**, 4132–4141.
32 T. Tromholt, M. V. Madsen, J. E. Carlé, M. Helgesen and F. C. Krebs, *J. Mater. Chem.*, 2012, **22**, 7592–7601.
33 C. M. Amb, P. M. Beaujuge and J. R. Reynolds, *Adv. Mater.*, 2010, **22**, 724–728.
34 A. L. Dyer, M. R. Craig, J. E. Babiarz, K. Kiyak and J. R. Reynolds, *Macromolecules*, 2010, **43**, 4460–4467.
35 B. D. Reeves, C. R. G. Grenier, A. A. Argun, A. Cirpan, T. D. McCarley and J. R. Reynolds, *Macromolecules*, 2004, **37**, 7559–7569.
36 C. M. Amb, J. A. Kerszulis, E. J. Thompson, A. L. Dyer and J. R. Reynolds, *Polym. Chem.*, 2011, **2**, 812–814.
37 P. Shi, C. M. Amb, E. P. Knott, E. J. Thompson, D. Y. Liu, J. Mei, A. L. Dyer and J. R. Reynolds, *Adv. Mater.*, 2010, **22**, 4949–4953.
38 E. P. Knott, M. R. Craig, D. Y. Liu, J. E. Babiarz, A. L. Dyer and J. R. Reynolds, *J. Mater. Chem.*, 2012, **22**, 4953–4962.
39 C. Wu, M. Lu and P. Tsai, *Macromol. Chem. Phys.*, 2009, **210**, 1851–1855.
40 P. Coppo, D. C. Cupertino, S. G. Yeates and M. L. Turner, *Macromolecules*, 2003, **36**, 2705–2711.
41 J. Jensen, A. L. Dyer, D. E. Shen, F. C. Krebs and J. R. Reynolds, *Adv. Funct. Mater.*, 2013DOI: 10.1002/adfm.201203005.
42 C. Wu, M. Lu, S. Chang and C. Wei, *Adv. Funct. Mater.*, 2007, **17**, 1063–1070.
43 G. Sonmez, H. B. Sonmez, C. K. F. Shen, R. W. Jost, Y. Rubin and F. Wudl, *Macromolecules*, 2005, **38**, 669–675.
44 S. Schuller, P. Schilinsky, J. Hauch and C. J. Brabec, *Appl. Phys. A: Mater. Sci. Process.*, 2004, **79**, 37–40.
45 N. Blouin, A. Michaud, D. Gendron, S. Wakim, E. Blair, R. Neagu-Plesu, M. Belletête, G. Durocher, Y. Tao and M. Leclerc, *J. Am. Chem. Soc.*, 2008, **130**, 732–742.
46 Y. Liang and L. Yu, *Acc. Chem. Res.*, 2010, **43**, 1227–1236.
47 D. M. De Leeuw, M. M. J. Simenon, A. R. Brown and R. E. F. Einerhand, *Synth. Met.*, 1997, **87**, 53–59.
48 J. C. Bijleveld, M. Shahid, J. Gilot, M. M. Wienk and R. A. J. Janssen, *Adv. Funct. Mater.*, 2009, **19**, 3262–3270.
49 Y. Fu and F. Tsai, *Org. Electron.*, 2011, **12**, 179–184.

Solar Energy Materials & Solar Cells 95 (2011) 2949–2958

Contents lists available at ScienceDirect

Solar Energy Materials & Solar Cells

journal homepage: www.elsevier.com/locate/solmat

Review

Flexible substrates as basis for photocatalytic reduction of carbon dioxide

Jacob Jensen, Mette Mikkelsen, Frederik C. Krebs *

Risø National Laboratory for Sustainable Energy, Technical University of Denmark, Frederiksborgvej 399, DK-4000 Roskilde, Denmark

ARTICLE INFO

Article history:
Received 21 June 2011
Accepted 22 June 2011

Keywords:
Photocatalysis
Titanium dioxide
Nanoparticles
Flexible substrates
Spray coating
Surfactants

ABSTRACT

A photocatalytic system for converting carbon dioxide into carbon monoxide was designed and constructed. The system relies on thin films of the photocatalyst prepared at low temperature using spray coating. We formulated inks based on the well-known photocatalyst titanium dioxide and characterized the performance in this setting. Glass substrates were used for model studies with an active area of 100 cm^2 and flexible substrates based on polyethyleneterphthalate (PET), polyethylene-naphtalate (PEN) and polyethylene (PE) with a similar area for prototypes of photocatalytic converters. The results from this new setup are presented and the challenges herein compared with other research results which address the sub processes involved—photoinduced degradation of polymers, decomposition of catalyst surfactant and inactivation of the catalyst efficiency by carbonaceous residues, etc.

Contents

* Corresponding author. Tel.: +45 46 77 47 99.
E-mail address: frkr@risoe.dtu.dk (F.C. Krebs).

0927-0248/$ - see front matter © 2011 Elsevier B.V. All rights reserved.
doi:10.1016/j.solmat.2011.06.040

1. Introduction

The largest chemical challenge in terms of scale is undoubtedly the control and management of carbon dioxide in the atmosphere. Currently, there is around 1 tera ton excess carbon dioxide in the atmosphere which is man-made and stemming mainly from the combustion of fossil fuels [1]. The annual man-made emission of carbon dioxide amounts to 24 gigaton. There is broad recognition worldwide that the emission of carbon dioxide must be brought down and preferably reverted such that a situation of a negative man-made carbon dioxide emission is reached. The former challenge is simply too huge to fathom and the latter exceeds our capacity for handling materials by several orders of magnitude. This is a result of a very efficient and a highly distributed system for conversion of reduced forms of carbon into carbon dioxide (cars, households, etc.). Thus, there is an enormous challenge of scale in finding a solution to the problem. An efficient laboratory scale catalyst is therefore not particularly useful unless it can be scaled to the required level without any carbon footprint. In addition to this problem it is impossible to extract carbon dioxide directly from the atmosphere without generating more carbon dioxide in the process (i.e. the sequestration of 1 kg of carbon dioxide from the atmosphere will emit more than 1 kg of carbon dioxide). This fundamental problem has resulted in the passive view that man-made carbon dioxide emissions should be reduced but not reverted. This is done most efficiently by reducing carbon dioxide emissions where they are largest such as flue gasses from coal fired power plants, iron smelters and concrete factories. The added cost of extracting the carbon dioxide from the flue gasses is very significant and the carbon sequestration and storage (CSS) costs can be as high as 50% of the electricity costs. In order to propose an efficient solution to the problem one must use a renewable energy source to convert atmospheric carbon dioxide either for reuse of the stored energy or for sequestration thus reducing the amount of carbon dioxide in the atmosphere. The most abundant source of renewable energy is in the form of sunlight, and the most rational approach is thus one where sunlight is used to convert carbon dioxide to some other reduced form of carbon. The only foreseeable way to realize systems that efficiently address this challenge is through the use of fast printing or coating of low cost photocatalysts on flexible substrates using roll-to-roll processing at low temperatures.

In recent years, the area of transition metal oxides has gained considerable interest and stimulated research with a wide range of applications. Especially, but not limited to, titanium dioxide, iron oxide and zinc oxide have received a lot of attention. With regard to titanium dioxide, a considerable amount of attention has been devoted within three areas of interest—photooxidation, device components and photoreduction. The photooxidation of organic compounds have been exploited in environmental management such as wastewater treatment and self-cleaning surfaces [2–6]. The area of device components has seen extensive research using TiO_2 in dye-sensitized solar cells [7–10]. The area of photoreduction of carbon dioxide using transition metal oxides as catalysts has also been the topic of an increasing number of research papers during the last 20 years, with reported results steadily improving [11–13]. But, as is the case in many other areas of research, results are difficult to compare, because of differences in reported experimental setups. Recently, papers have been published that question some earlier results [14], and as our own research indicates, the results obtained in photocatalytic conversion of carbon dioxide need to be critically evaluated.

The focus of this paper is to briefly review the area of photocatalytic carbon dioxide reduction with focus on the pitfalls that may be encountered, in the context of low cost scalable manufacture of photocatalytic surfaces, with the aim of furthering the development of this important field.

2. Experimental

2.1. Materials and setup

Titaniumtetraisopropoxide (Ti(OPr^i)) 97%, oleic acid ($C_{18}H_{33}CO_2H$ or OLEA, 90%), carbon-^{13}C dioxide (99 atom% ^{13}C, 3 atom% ^{18}O) and carbon-^{13}C monoxide (99 atom% ^{13}C, <5 atom% ^{18}O) were purchased from Aldrich. All other gases were purchased from Air Liquid. Trimethylamine N-oxide dehydrate was purchased from Fluka. All solvents were of analytical grade and purchased from Aldrich. All chemicals were used as received without further purification.

The reaction chamber is depicted in Fig. 1 and is comparable to those reported by other groups [15,16]. It comprises a lathed aluminum chamber with an inner diameter of 110 mm ϕ and a depth of 31 mm. This gave a chamber volume of 290 cm^3. Blocks of aluminum were lathed to fit the inside, enabling a variation of the chamber volume. The chamber had a gas inlet and a gas outlet with Swagelock™ valves. The chamber construction allowed for two modes of usage. The front of the chamber could be used as the window material (float glass, quartz or flexible substrates) coated with catalyst material. Compared to other reports this setup differs in that the photocatalyst is coated directly onto the substrate used as the chamber window. The challenge in this setup lies in controlling the catalyst layer thickness and harvest enough light for the photocatalytic reaction to proceed satisfactorily. This could be obstructed by catalyst particles closest to the coated substrate that shade particles in lower layers, thereby reducing the amount of excited electrons and catalytic yield. Another use of the setup is to monitor volatile degradation products formed inside the chamber upon illumination of the polymer substrates (PET, PE, etc.), when these are inserted as windows.

Additionally, the substrate could be placed inside the reaction chamber, where after the chamber was closed using a quartz window, or some other impermeable substrate as window material. By choosing the appropriate material the window could function as a solar filter.

The chamber also had two zinc selenide windows allowing for in-situ recording the IR-spectrum of the gaseous components inside the chamber. The path length was 17 cm.

2.2. IR detection system

The detection system made use of a FT-IR spectrometer (Perkin-Elmer Spectrum One) with the chamber prepared in such

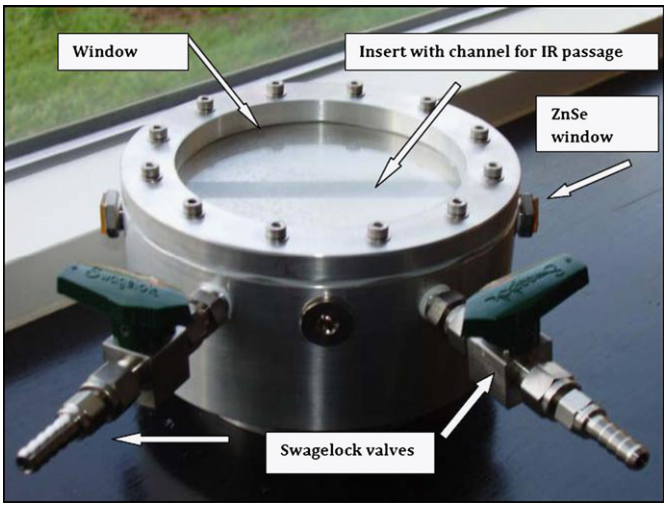

Fig. 1. A photograph of the test chamber.

a way that it could be removed from the solar simulator during the photocatalytic experiment and then placed back under the solar simulator to continue the experiment. The use of infrared spectroscopy was found particularly useful as it combines a reasonable sensitivity with a highly chemical fingerprinting enabling the detection of many different materials. The detection limit of CO of our instrument was ~0.01%, and by making calibration curves of the absorbance of known components such as methane, formic acid, methanol and carbon monoxide in carbon dioxide it became a quantitative analytical tool for determining the amount of photocatalytic products formed per area per time. By using isotopically labeled $^{13}CO_2$ it was possible to distinguish between reaction products formed from the introduced carbon dioxide or other sources (flexible film, surfactant, etc.), as the reduction products would contain ^{13}C. In the case of ^{12}CO vs. ^{13}CO the difference is shown in Fig. 2.

2.3. Flexible substrates

For the experiments involving flexible substrate, films of PET, PEN and PE were used. The substrates for the model cells were laser cut using a 90 W CO_2 laser. They were cut at 15 W with a 33% duty cycle and had the following thicknesses: PET (130 μm), PEN (130 μm), PE/Nylon (130 μm). As reported elsewhere (manuscript under construction) and described in Sections 4.1 and 5, to establish the rate of degradation the plastic substrate was first illuminated using a solar simulator powered by an Osram light bulb, single ended providing 1200 W m^{-1} equipped with a solar filter (AM1.5G) without the photocatalyst to measure the amount of photolytic/photooxidized CO formed.

2.4. Glass substrates

2.4.1. Coatings onto laboratory glass slides

The general procedure was as follows. TiO_2 nanorods were synthesized according to a procedure by Cozzoli et al. [17], with the minor modification that the NPs were dissolved in chlorobenzene. The particles were coated onto laboratory glass slides using a simple spray coating technique, creating a semitransparent film. Hereafter, the substrates were annealed at 500 °C for 4 h with an initial heating ramp of 10 °C min^{-1}. After cooling to room temperature, the glass slides were placed in the reaction chamber, which was closed with a quartz window (0.3 mm) screwed against an o-ring gasket in the housing. To remove as many unwanted adsorbed components as possible, the chamber was heated to 60 °C and subsequently evaporated and flushed with hydrogen gas. This cleaning cycle was repeated twice. The chamber was then flushed with a mixture of carbon dioxide and hydrogen (v/v 25/75) and a reference IR-spectrum was recorded. The photocatalyst was illuminated through the window using a UV lamp (Osram, HTT 150-211). The temperature of the setup under the lamp was 35 ± 5 °C. The chamber was illuminated for up to 230 h. Prior to this an experiment was conducted with the above reactants, but the reaction chamber was kept in the dark for 72 h.

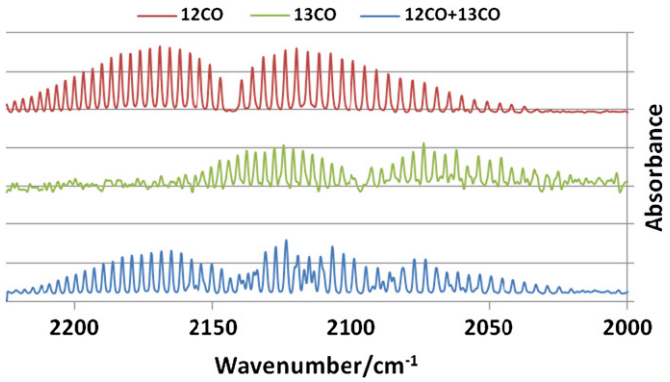

Fig. 2. IR spectra of carbon monoxide isotopes in the 2200–2000 cm^{-1} region (1 cm^{-1} resolution).

Alternatively, the NPs were precipitated from the chlorobenzene solution by adding EtOH. The resulting precipitate was washed and isolated by centrifugation. This procedure was repeated 3 times to remove any unbound surfactant residues. The resulting solid was dried at 100 °C for 1 h yielding a light yellow solid that was annealed using the above conditions. A small sample of the resulting white powder was analyzed by FT-IR, to confirm removal of the surfactant groups; the results are shown in Fig. 4. The remaining part was pestled in a mortar and dispersed in EtOH yielding a thick paste. This was coated onto laboratory glass slides by the doctor-blade technique, creating a nontransparent layer of TiO_2. Hereafter, the procedure was similar to the spraycoated slides.

3. Coatings onto the illuminated window

These experiments employed solutions of TiO_2 NP's spraycoated directly onto the illuminated window as described in Section 4.1. Float glass (0.2 mm) was used as window material, allowing the transmission of wavelengths above 320 nm. The rest of the procedures were as previously described. In another experiment, the NPs were spraycoated onto float glass and then subjected to UV light (Osram, HTT 150-211). Samples were analyzed by FT-IR at 30 min intervals to determine the degree of surfactant removal. The results are shown in Fig. 4.

4. Degradation of flexible substrates

One of the reasons for undertaking this study was to examine the possibilities of employing flexible polymers as substrates for coating of photocatalysts. By using flexible substrates it is possible to process the catalysts onto the substrate using R2R, slot-die coating, spray coating or other fast coating technique. Using these techniques enable that large area manufacture of catalyst-covered film can be achieved in very short time and at a reasonable production cost.

As polymeric films degrade under outdoor conditions [18], where they are ultimately to be in operation, knowledge of the degradation as a function of time is important. This information is vital in the life cycle assessment of devices containing polymeric components, and as the degradation products include volatiles such as CO and CO_2, it is a necessity to know the concentration when evaluating catalytic systems, where these gasses are reaction components. As the group of T.A. Egerton showed, using an IR setup very similar to our reaction chamber, the degradation of PET, PE and PP could be monitored using infrared spectroscopy [15]. They monitored the evolution of the volatiles CO and CO_2, thereby confirming the results made by Day and Wiles who used GC/LC-MS to elucidate the composition of volatiles and proposed a reaction mechanism for the formation of degradation products [15]. Both groups state that UV degradation of polymer substrates is a combination of two reactions; photolysis and photocatalytic oxidation where the latter can be suppressed, but not avoided, by using oxygen free conditions (i.e. non-atmospheric).

4.1. Polyolefins

The reaction mechanism for degradation depends on whether the substrate is a polyolefin (PE, PP, etc.) or polyester (PET, PBT,

etc.). In polyolefins, the process classified as a photocatalytic oxidation (Scheme 1) is the UV generation of active intermediates on the surface [19]. This is the main reaction for substrates under the influence of sunlight (AM1,5) and oxygen. Chemically, polyolefins such as polyethylene or polypropylene do not contain any chromophoric groups capable of absorbing energy from terrestrial sunlight (>290 nm), leading to insufficient energy for bond cleavage. The degradation of such compounds demands, in principle, the presence of oxygen to initiate reaction. During processing and storage of polyolefins, certain light absorbing chromophores can develop in the films [15], which can make them prone for photolysis, i.e. the absorbance of sunlight by chromophores domains within the molecule (aromatic ring, conjugated double bound, etc.). Under simulated conditions/UV light (<300 nm) they degrade by direct photolysis, absorbing light at these wavelengths [18].

The process is further influenced by the coating of pigments or nanoparticles (TiO_2) onto the polyolefin substrates. Even though TiO_2 can be used to protect PE from UV degradation by light absorption and light scattering, there is a duality as the opposite effect (i.e. enhanced decomposition) of the PE by heterogeneous catalytic oxidation on the surface of the TiO_2 particles results [15]. This changes the reaction mechanism from being primarily photolytic to being photooxidative. The effect is further enhanced (relative to the uncoated substrates) by increasing humidity [20].

The above results were obtained in an atmosphere containing oxygen, but as mentioned polyolefins show degradation even without oxygen present [15], which is in agreement with our own findings. As did the cited authors, we speculated that, apart from impurities, this might be caused by the reduction of TiO_2 or the involvement of water. The latter corresponds well with the findings that humidity affects the rates of oxidation.

4.2. Polyesters

The decomposition of PET, PEN and similar aromatic polyesters differs from the olefins in some ways. The primary difference relates to the chemical composition, where the aromatic rings adjacent to the carbonyl groups enable the polymers to absorb light with a longer wavelength (<330 nm). As the ester moieties are converted to carboxylic groups in the degradation, they are capable of further catalyzing the ongoing degradation [15].

Of interest in our research is the difference in oxygen and CO_2 diffusion between the olefins and the polyesters. The lower diffusion constant for O_2 into PET [21] makes it suitable for our experimental setup. Whereas higher diffusions constants of O_2 and CO_2 in PE [22] supposedly leads to oxidation in all regions of the film, the lower diffusion of O_2 in PET restricts the degradation to the surface regions [23–25]. The thickness dependence of the "backside"/non-irradiated contribution to the total degradation could be used to our advantage, since our setup physically separates the irradiated from the non-irradiated side of the film. The main question here was whether enough light was transmitted through the film to be able to excite the photocatalyst.

Concerning PET and related polyesters, there is some debate about the photolytic degradation mechanism. Day and Wiles [19] based on GC/LC-MS results suggest that the carboxylic end groups detected is a result of a Norrish type II rearrangement (Scheme 2). Among others, Hurley and Leggett, through the use of XPS, FFM and contact angle goniometry, proposed that the COOH end groups are formed via a Norrish type I radical pathway (Scheme 3), though they conducted their experiments in atmospheric air [19], and that could explain the different mechanism proposed, even though Grossetête et. al. claim that the presence or absence of oxygen only have minor impact on the mechanism[26]. But as Fechine et al. point out, the presence of oxygen affects the chemical degradation indicated by differences in degradation progression between the surface and the lower layers in PET films [27].

Both groups believe the formation of CO originates from chain scission radical pathways of the Norrish type I category. This furthermore produces several radicals that form non-volatile species in low concentrations [28].

The CO_2 produced in the photolytic degradation is believed to appear as a secondary reaction product. We base this conclusion on the findings of a longer induction period than found for CO and RCOOH, and whereas formation of the latter is independent of atmospheric conditions, the formation of CO_2 is strongly dependent on oxygen, suggesting a formation via peroxide radicals [27] (Scheme 4).

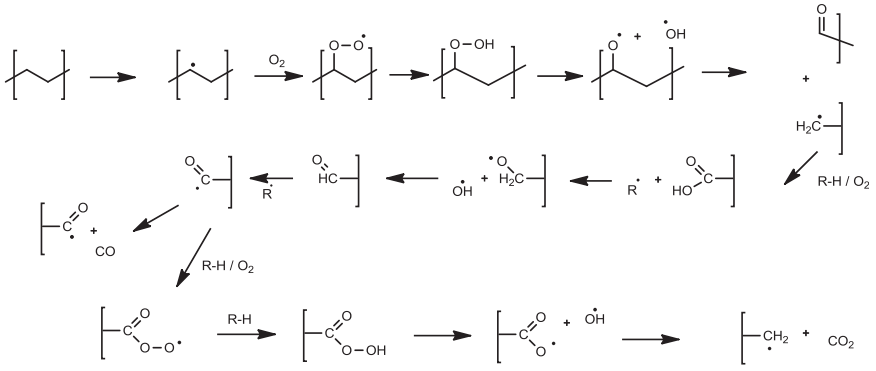

Scheme 1. Photocatalytic oxidation of PE.

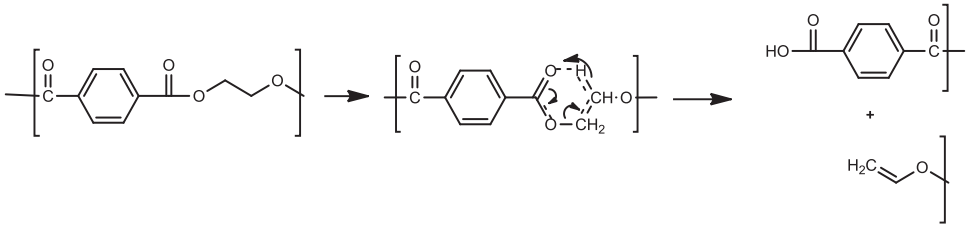

Scheme 2. Norrish type II rearrangement.

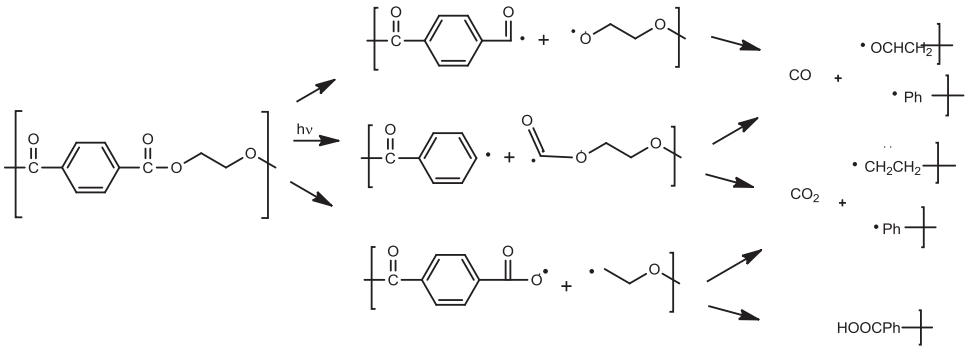

Scheme 3. Norrish type I reaction pathways.

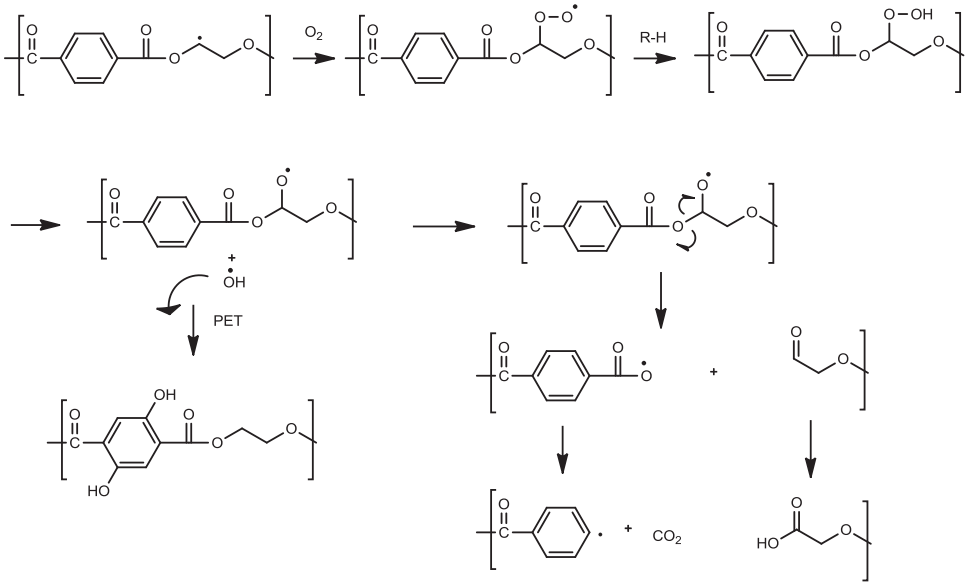

Scheme 4. Photoxidation of PET.

4.3. Reductive atmosphere

The TiO_2 nanoparticles were coated directly on the substrates (PEN, PET, PE/Nylon), even though this could enhance oxidative degradation of the substrates in question. But as the atmosphere in the reaction chamber as a starting point did not contain any molecular oxygen, it was assumed that this effect would be limited. The atmosphere comprises a mixture of 25% CO_2 and 75% H_2 saturated with water vapor. As this mixture would hinder the monitoring of CO_2 evolution, experiments were made using pure gaseous hydrogen, with and without water vapor.

The degradation of flexible films were monitored by measuring the peak height for CO_2 absorbance for the band at 2360 cm^{-1} and CO from the peak 2176 cm^{-1}, as this has been shown to be a reliable way to monitor the reaction [18,19]. The experimental setup allowed for a differentiation between backside and total contribution of volatiles.

Another possibility of limiting heterogeneous photocatalytic oxidation would be to physically separate the catalyst from the polymeric substrate. The physical contact between the nanoparticles and the films was already limited compared to the above reference, as the particles were not part of the polymeric material/inside the film, but coated onto the surface. Furthermore, an intermediate inactive transparent layer could be applied before coating the catalyst effectively separating the two components.

5. Decomposition of surfactants

The surfactants are in many synthetic procedures vital to the correct growth of the metal oxide nanoparticles, suppressing aggregation, agglomeration and precipitation[15], but relatively few studies have specifically concentrated on the degradation products of these surfactants/capping groups. The analysis concerning the annealing procedure primarily focuses on the temperature effect concerning particle morphology and possible phase transformation of the transition metal oxides in question [17,29–31]. And even though this is of major importance to photocatalytic reactions, it also worthwhile to analyze the degradation products of the surfactants, as these possibly have an impact on the interpretation of the results [32,33]. The aim of using surfactants is stabilizing the metal oxide nanoparticles in the solution during their synthesis. When soluble, the nanoparticles are processable with a wide range of coating techniques. The list of surfactants is extensive, but a few examples are given in Fig. 3 [14].

5.1. Thermal degradation of oleic acid

The majority of studies reporting on the decomposition of surfactants focus on the temperature dependent degradation (as opposed to the photolytic degradation described later) that occurs during the annealing process [31,34–36]. It is generally accepted

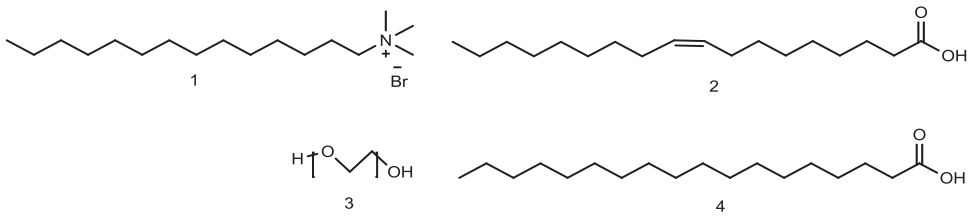

Fig. 3. Examples of surfactants. 1—cetyltrimethylammonium bromide, 2—oleic acid, 3—polyethylene glycol, 4—stearic acid.

that oleic acid is removed from the metal oxide surface at around 400–500 °C in air ([37,38], which is in good correspondence with our own findings using FT-IR. As oleic acid is presumed to bind to the both iron oxide and titanium dioxide in similar ways—as a bidentate and a bridging ligand [32,37,38], it is assumed that any effect that this has on the release and decomposition of surfactant is equivalent. DSC and TG analyses suggest that the decomposition mechanism differs depending on whether oleic acid is heated in an oxygen or a non-oxygen contained atmosphere. In the former, a double bound cleavage is indicated at 240 °C, whereas in the latter a release of hydrogen bonded water peaks at 200 °C, and CO_2 and H_2 formation begins at 280 °C. In both cases, the weight loss stops at around 450 °C [37], which is in good agreement with another study done by Bronstein et al. [37].

5.2. Photolytic degradation of oleic acid

Of particular interest when working with flexible substrates coated with surfactant containing catalyst is the removal of surfactant at low temperatures. Ideally this allows for the exposure of the catalytic surface to reactants without thermal degradation of the polymer substrate. The photooxidative abilities of TiO_2 have among a lot of things been exploited in self-cleaning surfaces [6,38–40], where decomposition of dirt by photolytic oxidation yields oxygenated compounds, which are easily removed. One such study describes very well the photocatalytic decomposition of oleic acid using UV light [40], and many of the reaction pathways have been made probable by a combination of quantum-chemical calculations and gas chromatographic analysis. The main photolytic intermediates are found to be nonanal and 9-oxononaic acid. The volatile products detected were heptanal, decanal and octanal.

5.3. Carbonaceous residues

A wide range of both thermal and photolytic cleavage products of oleic acid is possible [41], but of importance in photocatalysis are the leftover residues on the catalyst surface. It has been suggested that some sort of carbon residues is left on Fe catalyst (in the case of Fe_xO_y catalysts) surfaces after thermal decomposition of oleic acid in air. FT-IR reveals these carbonic species as CO_x complexes giving rise to absorption in the carbonyl region (2200, 2259, 2330 cm^{-1}) [42]. In addition to these oxygen containing species, amorphous carbon/graphite residues are also suggested on the basis of FT-IR, when the decomposition takes place under an argon atmosphere. Beneath this graphite shell alkane residues are believed to adsorb on the metal oxide surface [37]. Other reports state that a wide range of hydrocarbons constitutes the carbonaceous deposits on zeolite catalysts after cracking [43]. Rathouský et. al report on the photolytic removal of thin layers of carbonized oleic acid residues, stating that moisture and elevated temperatures enhance reaction [44]. Regardless of the origin of these carbonic species, it is clear that they are present and that they influence the photocatalytic process and the evaluation of the products formed [41], and we consider the effect of such carbonized layers important.

6. Adsorption of volatiles

The detection of isotopically labeled $^{13}CO_2$ and ^{12}CO in the reaction chamber devoid of any catalyst and after prolonged flushing with pure hydrogen gas and subsequent UV illumination shows that a very critical evaluation of the obtained results is necessary. In our case an empty reaction chamber was flushed with hydrogen for 30 min, the chamber was closed using a 2 mm float glass as the window. The chamber was filled with gaseous argon/nitrogen and illuminated under the solar simulator in the absence of solar filtration. The detected $^{13}CO_2$ is believed to originate from earlier experiments performed in that reaction chamber, as we see no other explanation to its presence. Jin et al. encountered a similar presence of CO_2 depending on the chamber age [45].

Evaluating the chemical species in the reaction chamber, we deduced an explanation for our observations. During the course of experiments, the aluminum surface has been subject to water vapor, oxygen and light. These reaction conditions might result in the formation of alumina [15] and aluminum hydroxide on the chamber surface. Alumina showing both basic and acidic characteristics is capable of adsorbing volatiles such as CO_2 and CO, through multiple forms of bindings [46]. Alumina has been widely used for adsorption of carbon dioxide and has among other things been used in carbon dioxide capture and sequestration (CCS) processes. It has also been shown that a range of carbon–oxygen containing species possibly resides on the alumina surface [47]. The complete desorption of carbon dioxide from alumina has been shown to take place at around 200 °C for mesoporous alumina [48] and γ-alumina [49,50], and even though we have not characterized the surface species of alumina, it seems plausible that flushing the chamber with hydrogen at room temperature does not ensure complete removal of carbon dioxide. To ensure removal of this bound CO_2, we introduced a cycle of heating to 65 °C for 60 min, flushing with hydrogen and evaporation at reduced pressure. This was repeated twice before each experiment.

Carbon monoxide likewise binds to Lewis acid sites on alumina, albeit to a lesser degree than carbon dioxide [47].

Mao et al. reported in agreement with our observations that a short period of degassing was not sufficient to remove the entire CO present.

As it remained outside the scope of our research to determine the type of adsorption or morphology of the alumina species, we conclude that both carbonaceous gasses can be adsorbed onto the chamber surface to be desorbed at a later time, possibly obscuring the interpretation of results if precautions are not taken.

7. Results and discussion

7.1. Removal of surfactant group

Fig. 4 shows the FT-IR spectrum of the TiO_2 nanoparticles before and after UV illumination and annealing at 500 °C.

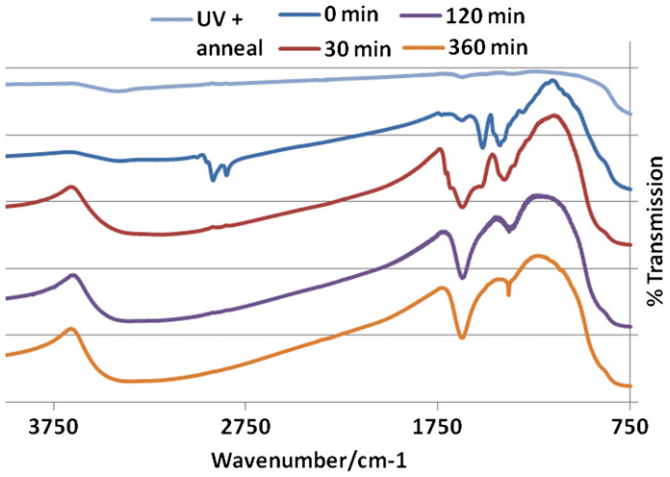

Fig. 4. Removal of oleic acid surfactant by UV light (4 cm^{-1} resolution).

The characteristic bands of oleic acid capped TiO_2 at 2924, 2852, 1523 and 1433 cm^{-1} are clearly visible in the spectrum. The disappearance of these bands after annealing is in agreement with Kang et al. [51–53].

As seen from Fig. 4, the removal of oleic acid by UV light at low temperatures seems to be a viable process. The disappearance of the characteristic bands after a relatively short while (~60 min) is promising, leaving a broad band centered at 3433 cm^{-1} and one at 1626 cm^{-1}. The former is attributed to absorbed water or titanol, the latter is attributed to adsorbed water in the pellets. The presence of these bands is not disturbing, since water is introduced in the reaction chamber prior to the photochemical reaction.

7.2. Catalyst efficiency

As it proved to be the most efficient method, quartz glass was used as window material with TiO_2 catalyst coated onto laboratory glass slides using the doctorblading technique. The catalytic performance was monitored by measuring the increasing absorbance of isotopically labeled carbon species formed (notably ^{13}CO).

The reference experiment conducted in the dark did not show any conversion of $^{13}CO_2$ and only a slight increase in $^{12}CO_2$, but no trace of ^{12}CO.

After 1/2 h of illumination a buildup of $^{12}CO_2$ was observed; the content remained steady throughout the experiment with only minor fluctuations. The formation of $^{12}CO_2$ in the reaction chamber is attributed to pre-adsorbed carbonaceous species on the catalyst [33] or chamber surface, and was monitored by measuring the band centered at 2360 cm^{-1}.

After 1 h of illumination, the formation of gaseous ^{12}CO was observed, which is interesting as no $^{12}CO_2$ was introduced into the reaction vessel. After 130 h, the peak height at 2183 cm^{-1} shows that approximately 0.074% (0.19 μmol) of the chamber volume is ^{12}CO.

After 2 h, the formation of ^{13}CO is vaguely visible in the spectrum as indicated by the IR pattern (compare Fig. 2 with Fig. 7), which becomes clearly visible further on in the experiment (Fig. 8). The amount of ^{13}CO increases during the first 11 h of illumination, where after the characteristic IR-motive disappears, leaving "only" a ^{12}CO spectrum. This situation continues for 50 h, after which the detection of ^{13}CO is possible again as a ^{12}CO–^{13}CO motif. The additional increment in ^{12}CO during the 11–50 h period is marked in Fig. 5 with red dots. As can be seen, these lie off the curve formed by the other observations. A plausible

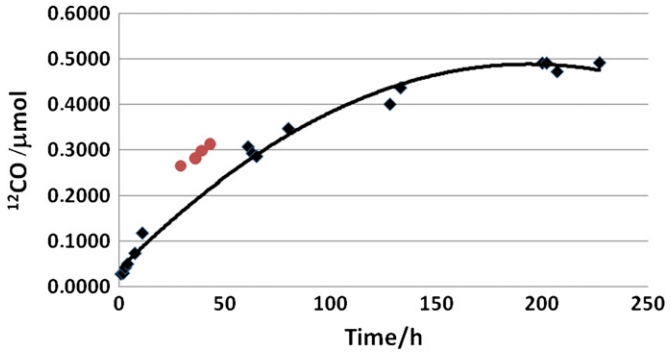

Fig. 5. ^{12}CO content in reaction chamber during UV illumination. (For interpretation of the references to color in this figure legend, the reader is referred to the web version of this article.)

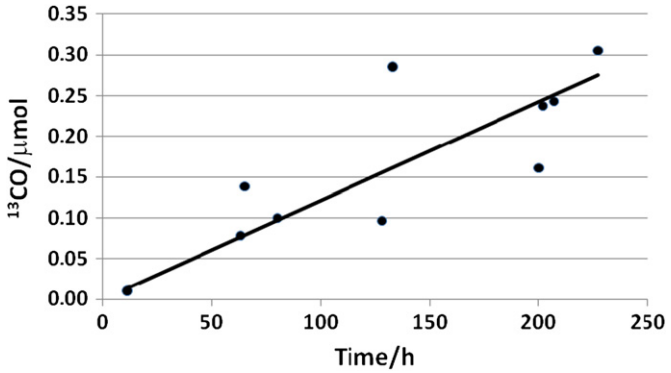

Fig. 6. ^{13}CO content in reaction chamber during UV illumination.

explanation is that these observations might be several reactions contributing to the contents of the chamber. During the first hours of illumination two reactions could take place simultaneously—the photocatalytic reduction of the introduced $^{13}CO_2$ and the UV induced release of $^{12}CO_2$ from the outer layers of the catalyst. The $^{12}CO_2$ is photocatalytically converted to ^{12}CO giving rise to an IR spectrum of both isotopes. After 11 h a third reaction is presumed to take place. This is the release of carbon–oxygen containing species from deeper within the catalyst, which is activated due to the prolonged UV exposure. This saturates the catalyst surface, thereby excluding $^{13}CO_2$ from the catalytic sites and henceforth photocatalytic transformation. From an analytical point of view, the relatively large increase in ^{12}CO obscures the detection of the small amount of the ^{13}C isotope. After this amount of $^{12}CO_2$ has been converted, the catalyst returns to an equilibrium state, converting both $^{12}CO_2$ and $^{13}CO_2$.

To determine the concentration of ^{13}CO the peak height at 2127 cm^{-1} was measured and the contribution from ^{12}CO subtracted. The contribution from ^{12}CO was found by comparing the peak height at 2183 cm^{-1} with standard curves for this species. The content of ^{13}CO was found to rise linearly with time at a rate of 0.0019 μmol h^{-1} during the experiment. This amounts to an efficiency for converting $^{13}CO_2$ into ^{13}CO of 0.0013 μmol h^{-1} g^{-1} (catalyst) (Fig. 6).

The formation of methane is observed after 4 h of illumination, and hereafter the content of methane increases linearly with time up to 150 h. By comparing the peak heights at 3017 and 1306 with standard curves for methane in the chamber, the concentration of methane was found to be 2.6%, which equals 6.7 μmol after 130 h (Fig. 7). This corresponds to a formation of 0.36 μmol h^{-1} g^{-1} catalyst. However, as the peaks centered around 3017 and 1306 cm^{-1} corresponds to $^{12}CH_4$, the formed methane must have other origins than the introduced $^{13}CO_2$.

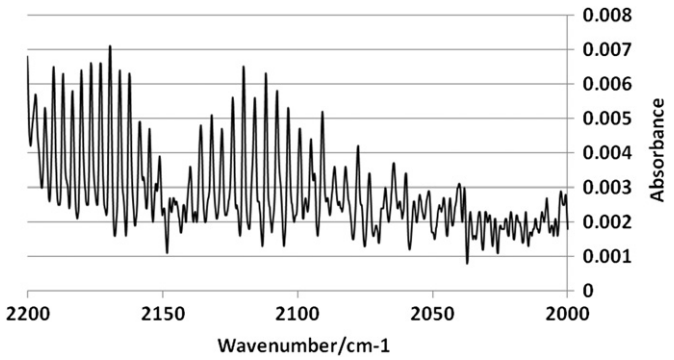

Fig. 7. IR spectra after 2 h of the 2200–2000 cm^{-1} region (1 cm^{-1} resolution).

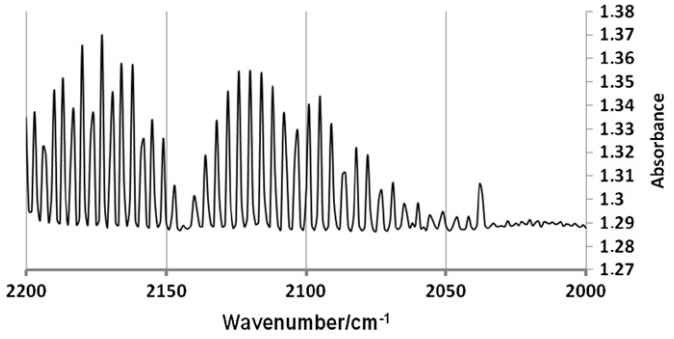

Fig. 8. IR spectra after 63 h of the 2200–2000 cm^{-1} region (1 cm^{-1} resolution).

We presume that the observed methane is the 8-electron reduction product [54] of carbon–oxygen containing species in the reaction chamber (Fig. 8).

As seen from Figs. 5 and 6, the ratio of ^{12}CO to ^{13}CO in the reaction chamber is approximately 2:1, with concentrations of both species increasing linearly as a function of time, for the first 150 h of UV illumination. This ratio of formation is in good agreement with the detection of ^{12}CO after 1 h followed by observation of ^{13}CO after 2 h. The observed linearity could indicate that both species follow the same reaction mechanism. In that case, it is surprising to find the content of ^{12}CO to be twice as high as ^{13}CO. A reason for this might be that ^{12}CO is the reduction product of carbon containing species on the catalyst surface (surfactant, carbonate). The closer proximity of these compounds to the catalyst surface might favor their reduction compared to the introduced $^{13}CO_2$.

Another option proposed by Yang et al.[55] suggests that the observed CO species are the products of a reverse Bourdard reaction and a water induced photocatalytic surface carbon gasification, with the latter being the predominant, as seen from a 1:6 ratio of ^{13}CO to ^{12}CO in that study:

$$^{13}CO_2 + \text{“}^{12}C\text{”} \rightarrow {}^{13}CO + {}^{12}CO$$

$$H_2O + \text{“}^{12}C\text{”} \rightarrow {}^{12}CO + H_2$$

It cannot be ruled out that we might experience similar reactions, but as the observed ratio between the two CO isotopes is different (1:2 compared to 1:6), other reactions will possibly contribute as well. As hydrogen gas is introduced as part of the reactant mixture, the gasification reaction might be suppressed by counteracting the disturbed equilibrium. The presence of H_2 in the reaction chamber makes the formation of methane achievable, and could account for the higher ^{13}CO:^{12}CO ratio observed. It is puzzling though that only $^{12}CH_4$ is observed. We find it highly unlikely that only the ^{12}CO isotope is reduced if both isotopes are present, hence methane is supposedly formed via other reaction pathways that does not include desorption/adsorption of gaseous CO Fig. 9.

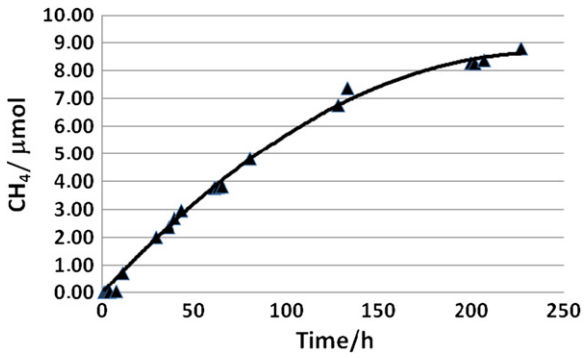

Fig. 9. Methane content in reaction chamber during UV illumination.

$$2CO_2 + h\nu \rightarrow 2CO + O_2 \qquad \Delta H = 565.98 \text{ kJ mol}^{-1}$$

Scheme 5. CO_2 conversion. CO formation $\Delta H = -110.53$ kJ mol^{-1}, CO combustion $\Delta H = -283.0$ kJ mol^{-1}, CO_2 formation $\Delta H = -393.52$ kJ mol^{-1}. 3600 kJ m^{-2} h^{-1} = 12.72 mol m^{-2} h^{-1} of CO_2 or 560 g m^{-2} h^{-1} of CO_2 or 1120 kg m^{-2} $year^{-1}$ of CO_2.

Another interesting observation is the blackening of the catalyst, indicating that elemental carbon could be formed on the catalyst surface. If this is the case, it could explain the decrease in catalyst efficiency observed after 150 h. The formation of elemental carbon on the surface could poison the catalyst by decreasing the available surface area for catalytic reaction. A similar observation, albeit under slightly different conditions, is made by Jin et. al. [15], who suggest that the blackening/graying effect might result from a reduction of TiO_2. This observation is made likely in that upon exposure to atmospheric air, the blackening effect is partially negated indicating re-oxidation of Ti(III) to Ti(IV). Whatever the cause, this “destruction” of the catalyst is coherent with the decreased reaction rate and awaits further investigation.

When evaluating the catalytic efficiency, it is in this context necessary to evaluate the fate of the flexible substrates used. Our studies show that both CO and CO_2 are formed in varying concentrations during the UV degradation of the flexible films in a hydrogen/carbon dioxide atmosphere, in quantities that for now exceed the capability of the catalytic system. These findings suggest that we need to use a material that do not degrade via photolytic mechanism, i.e. less capable of absorbing UV light. Future work in this direction is warranted.

7.3. Energy considerations

The most well-known photocatalysts for conversion of carbon dioxide into various other products such as carbon monoxide, formic acid, methanol, methane are titanium dioxide, zinc oxide and iron oxide. Common for those catalysts is that a proton source is generally needed. The proton source may be water or hydrogen. In this study, we chose to focus on the simplest reaction comprising photocatalytic conversion of carbon dioxide into carbon monoxide and oxygen as shown in Scheme 2.

The energy available at the surface of the earth is around 1000 W m^{-2} (AM1.5G), and depending on the local climate one can expect to receive between 1000 and 2000 kWh m^{-2} $year^{-1}$. From Scheme 5 it is clear that if all the solar energy impinging on a 1 m^2 surface solely went into converting carbon dioxide to

carbon monoxide and oxygen, about 560 g pr. h^{-1} of carbon dioxide could be converted. To match the annual man-made emissions of 24 gigaton under the assumption that one has available landmass with an annual irradiance of 2000 h of sunlight ($\sim$1120 kg m^{-2} $year^{-1}$ of CO_2) one would require an area of 21.5×10^9 m^2=21,500 km^2=146.6×146.6 km^2. This is a large area but manageable. Especially since such a system would inherently store the energy in the form of carbon monoxide. With significantly lower performance of the catalyst to levels in the range of 0.1–1%, the required area would be correspondingly larger, but compared to the globally available land mass 148,939,063 km^2 where 20–30% is estimated as desserts, it is not an unrealistic scenario from this point of view. It is thus clear that an efficient solution to this problem will have to involve fast and low cost manufacturing of large areas, low thermal budget, low cost materials and low cost photocatalysts.

On a scale of 1 m^2 with a layer thickness and a UV light source equal to that reported here, a conversion of 0.34 μmol m^{-2} h^{-1} or 680 μmol m^{-2} $year^{-1}$ CO_2 to CO is possible (assuming 2000 h of sunlight pr. year). For comparing this to real working conditions (the system is to function outside) the contribution of the natural sunlight that is absorbed by the catalyst has to be calculated. The catalyst absorbs wavelength below 320 nm. The irradiance from the lamp below 320 nm is 500 W m^{-2}, whereas the energy contribution from natural sunlight below 320 nm from is 1.56 W m^{-2}. This is a 320-fold reduction compared to the UV lamp, meaning that under natural sunlight 1 m^2 of catalyst covered surface is able to convert 2.1 μmol m^{-2} $year^{-1}$. If this energy is converted by combustion of the CO formed, one would be able to generate a meager 0.6 J m^{-2} $year^{-1}$.

7.4. Future work

As seen from the above calculations the results are clearly very poor and underline the urgent need for a better understanding of these catalysts with respect to their preparation, operation and stability. It is clear that more effective catalysts are necessary for a catalytic system to be effective on a usable scale. One approach to this is the development of catalysts with a lower band gaps, such that a larger percentage of the energy from sunlight can be made available for photochemical reactions. Secondly work towards using flexible substrates as basis for this is vital to obtain the large areas necessary.

8. Conclusion

A system for photocatalytic reduction of CO_2 was designed and evaluated. By using FT-IR we have demonstrated that our photocatalyst was capable of reducing isotopically labeled $^{13}CO_2$ with the product being ^{13}CO. In addition to ^{13}CO, ^{12}CO and $^{12}CH_4$ were observed as reaction products, both in relatively large amounts. Since these compounds did not contain any ^{13}C, we conclude that they cannot have come from the introduced starting material, but that they more likely originate from carbonates or other carbonaceous residues that reside on the chamber or catalyst surface. Nevertheless, the observation of these reduced forms of carbon dioxide makes it likely that our catalytic system is capable of reducing oxidized carbon.

Furthermore, we have shown that necessary precautions must be taken when evaluating the outcome of photocatalytic systems, and a key factor herein is using isotopically labeled starting materials. By coating our photocatalyst onto flexible substrates we have shown that a challenge exists in finding or developing flexible substrates with the required photostability to be used as substrates for photocatalysis.

Acknowledgments

We would like to thank Kristian Larsen and Torben Kjær for providing us technical assistance in preparing the test chambers. This work was supported by The Solar Energy Program at Risø DTU.

References

[1] M. Mikkelsen, M. Jørgensen, F.C. Krebs, The teraton challenge. A review of fixation and transformation of carbon dioxide, Energy Environ. Sci. 3 (2010) 43–81.
[2] M.N. Chong, B. Jin, C.W.K. Chow, C. Saint, Recent developments in photocatalytic water treatment technology: a review, Water Res. 44 (2010) 2997–3027.
[3] S. Ahmed, M.G. Rasul, W.N. Martens, R. Brown, M.A. Hashib, Advances in heterogeneous photocatalytic degradation of phenols and dyes in wastewater: a review, Water Air Soil Pollut. 215 (2011) 3–29.
[4] D. Hufschmidt, L. Liu, V. Selzer, D. Bahnemann, Photocatalytic water treatment: fundamental knowledge required for its practical application, Water Sci. Technol. 49 (2004) 135–140.
[5] A. Fujishima, X. Zhang, D.A. Tryk, TiO_2 photocatalysis and related surface phenomena, Surf.Sci. Rep. 63 (2008) 515–582.
[6] I.P. Parkin, R.G. Palgrave, Self-cleaning coatings, J. Mater. Chem. 15 (2005) 1689–1695.
[7] B. O'Regan, M. Grätzel, A low-cost, high-efficiency solar cell based on dye-sensitized colloidal TiO_2 films, Nature 353 (1991) 737–740.
[8] S.R. Gajjela, K. Ananthanarayanan, C. Yap, M. Grätzel, P. Balaya, Synthesis of mesoporous titanium dioxide by soft template based approach: characterization and application in dye-sensitized solar cells, Energy Environ. Sci. 3 (2010) 838–845.
[9] M. Grätzel, Solar energy conversion by dye-sensitized photovoltaic cells, Inorg. Chem. 44 (2005) 6841–6851.
[10] H. Hafez, Z. Lan, Q. Li, J. Wu, High efficiency dye-sensitized solar cell based on novel TiO_2 nanorod/nanoparticle bilayer electrode, Nanotechnol. Sci. Appl. 3 (2010) 45–51.
[11] T.-V. Nguyen, J.C.S. Wu, Photoreduction of CO_2 to fuels under sunlight using optical-fiber reactor, Sol. Energy Mater. Sol. Cells 92 (2008) 864–872.
[12] C.-C. Lo, C.-H. Hung, C.-S. Yuan, J.-F. Wu, Photoreduction of carbon dioxide with H_2 and H_2O over TiO_2 and ZrO_2 in a circulated photocatalytic reactor, Sol. Energy Mater. Sol. Cells 91 (2007) 1765–1774.
[13] M. Anpo, M. Takeuchi, The design and development of highly reactive titanium oxide photocatalysts operating under visible light irradiation, J. Catal. 216 (2003) 505–516.
[14] C.-C. Yang, Y.-H. Yu, B. Van Der Linden, J.C.S. Wu, G. Mul, Artificial photosynthesis over crystalline TiO_2-based catalysts: fact or fiction, J. Am. Chem. Soc. 132 (2010) 8398–8406.
[15] C. Jin, P.A. Christensen, T.A. Egerton, E.J. Lawson, J.R. White, Rapid measurement of polymer photo-degradation by FTIR spectrometry of evolved carbon dioxide, Polym. Degrad. Stab. 91 (2006) 1086–1096.
[16] A.J. Robinson, J.R. Searle, D.A. Worsley, Novel flat panel reactor for monitoring photodegradation, Mater. Sci. Technol. 20 (2004) 1041–1048.
[17] P.D. Cozzoli, A. Kornowski, H. Weller, Low-temperature synthesis of soluble and processable organic-capped anatase TiO_2 nanorods, J. Am. Chem. Soc. 125 (2003) 14539–14548.
[18] P. Gijsman, G. Meijers, G. Vitarelli, Comparison of the UV-degradation chemistry of polypropylene, polyethylene, polyamide 6 and polybutylene terephthalate, Polym. Degrad. Stab. 65 (1999) 433–441.
[19] M. Day, D.M. Wiles, Photochemical degradation of poly(ethylene terephthalate). III. Determination of decomposition products and reaction mechanism, J. Appl. Polym. Sci. 16 (1972) 203–215.
[20] N.S. Allen, H. Khatami, F. Thompson, Influence of titanium dioxide pigments on the thermal and photochemical oxidation of low density polyethylene film, Eur. Polym. J. 28 (1992) 817–822.
[21] D.N. Bikiaris, G.P. Karayannidis, Effect of carboxylic end groups on thermooxidative stability of PET and PBT, Polym. Degrad. Stab. 63 (1999) 213–218.
[22] J.B. Brolly, D.I. Bower, I.M. Ward, Polym. J. Sci. Part B Polym. Phys. 34 B (1966) 769–780.
[23] R.E. Kesting, Synthetic Polymeric Membranes: A Structural Perspective, second edition, John Wiley & Sons, 1985.
[24] J.F. Rabek, Photostabilization of polymers: principles and applications, Appl. Sci., 1990.
[25] S.S. Fernando, P.A. Christensen, T.A. Egerton, R. Eveson, S.M. Martins-Franchetti, D. Voisin, J.R. White, Carbon dioxide formation during initial stages of photodegradation of poly(ethyleneterephthalate) (PET) films, Mater. Sci. Technol. 25 (2009) 549–555.
[26] C.R. Hurley, G.J. Leggett, Quantitative investigation of the photodegradation of polyethylene terephthalate film by friction force microscopy, contact-angle goniometry, and X-ray photoelectron spectroscopy, ACS Appl. Mater Interfaces 1 (2009) 1688–1697.
[27] T. Grossetete, A. Rivaton, J.L. Gardette, C.E. Hoyle, M. Ziemer, D.R. Fagerburg, H. Clauberg, Photochemical degradation of poly(ethylene terephthalate)-modified copolymer, Polymer 41 (2000) 3541–3554.

[28] G.J.M. Fechine, M.S. Rabello, R.M. Souto Maior, L.H. Catalani, Surface characterization of photodegraded poly(ethylene terephthalate). The effect of ultraviolet absorbers, Polymer 45 (2004) 2303–2308.
[29] A.L. Willis, N.J. Turro, S. O'Brien, Spectroscopic characterization of the surface of iron oxide nanocrystals, Chem. Mater. 17 (2005) 5970–5975.
[30] S. Satapathy, P.K. Gupta, H. Srivastava, A.K. Srivastava, V.K. Wadhawan, K.B.R. Varma, V.G. Sathe, Effect of capping ligands on the synthesis and on the physical properties of the nanoparticles of $LiTaO_3$, J. Cryst. Growth. 307 (2007) 185–191.
[31] G.Q. Liu, Z.G. Jin, X.X. Liu, T. Wang, Z.F. Liu, Anatase TiO_2 porous thin films prepared by sol–gel method using CTAB surfactant, J. Sol. Gel. Sci. Technol. 41 (2007) 49–55.
[32] J. Kehres, J.W. Andreasen, F.C. Krebs, A.M. Molenbroek, I. Chorkendorff, T. Vegge, Combined in situ small- and wide-angle X-ray scattering studies of TiO_2 nanoparticle annealing to 1023 K, J. Appl. Crystallogr. 43 (2010) 1400–1408.
[33] K.S. Kang, Y. Chen, K.H. Yoo, N. Jyoti, J. Kim, Cause of slow phase transformation of TiO_2 nanorods, J. Phys. Chem. C 113 (2009) 19753–19755.
[34] B. Hao, Y. Li, S. Wang, Synthesis and structural characterization of surface-modified TiO_2, Adv. Mater. Res. 129–131 (2010) 154–158.
[35] X. Shi, R. Rosa, A. Lazzeri, On the coating of precipitated calcium carbonate with stearic acid in aqueous medium, Langmuir 26 (2010) 8474–8482.
[36] X. Liang, W. Huan, X. Jia, H. Ding, Y. Yang, X. Liu, Preparation, characterization and magnetic properties of nano-Fe_3O_4 and cobalt-doped nano-Fe_3O_4 by CO-precipitation method, Nano 5 (2010) 203–214.
[37] P. Roonasi, A. Holmgren, A Fourier transform infrared (FTIR) and thermogravimetric analysis (TGA) study of oleate adsorbed on magnetite nanoparticle surface, Appl. Surf. Sci. 255 (2009) 5891–5895.
[38] L.M. Bronstein, X. Huang, J. Retrum, A. Schmucker, M. Pink, B.D. Stein, B. Dragnea, Influence of iron oleate complex structure on iron oxide nanoparticle formation, Chem. Mater. 19 (2007) 3624–3632.
[39] M. Gohin, E. Allain, N. Chemin, I. Maurin, T. Gacoin, J.-P. Boilot, Sol–gel nanoparticulate mesoporous films with enhanced self-cleaning properties, J. Photochem. Photobiol. A Chem. 216 (2010) 142–148.
[40] Q. Kuai, H.-Q. Ye, Y. Gao, Preparation of aluminum titanium pigments and its application in self-cleaning coating, Mater. Sci. Eng. Powder Metal. 15 (2010) 283–287.
[41] J. Rathouský, V. Kalousek, M. Kolář, J. Jirkovský, P. Barták, A study into the self-cleaning surface properties—the photocatalytic decomposition of oleic acid, Catal. Today 161 (2011) 202–208.
[42] H.J. Harwood, Reactions of the hydrocarbon chain of fatty acids, Chem. Rev. 62 (1962) 99–154.
[43] V. Pérez-Dieste, O.M. Castellini, J.N. Crain, M.A. Eriksson, A. Kirakosian, J.-L. Lin, J.L. McChesney, F.J. Himpsel, C.T. Black, C.B. Murray, Thermal decomposition of surfactant coatings on Co and Ni nanocrystals, Appl. Phys. Lett. 83 (2003) 5053–5055.
[44] A.R. Pradhan, J.F. Wu, S.J. Jong, T.C. Tsai, S.B. Liu, An ex situ methodology for characterization of coke by TGA and 13C CP-MAS NMR spectroscopy, Appl. Catal. A Gen. 165 (1997) 489–497.
[45] W. Lin, H. Han, H. Frei, CO_2 splitting by H_2O to CO and O_2 under UV light in TiMCM-41 silicate sieve, J. Phys. Chem. B 108 (2004) 18269–18273.
[46] K.L.I. Kobayashi, Y. Shiraki, Y. Katayama, Study of adsorption phenomena on aluminium by interatomic Auger transition spectroscopy I. Initial oxidation of Al, Surf. Sci. 77 (1978) 449–457.
[47] N.D. Parkyns, The surface properties of metal oxides. Part II. An infrared study of the adsorption of carbon dioxide on γ-alumina, J. Chem. Soc. A: Inorg. Phys. Theor. Chem. (1969) 410–417.
[48] C. Morterra, G. Magnacca, A case study: surface chemistry and surface structure of catalytic aluminas, as studied by vibrational spectroscopy of adsorbed species, Catal. Today 27 (1996) 497–532.
[49] Z. Zhou, T. Zeng, Z. Cheng, W. Yuan, Preparation and characterization of titania–alumina mixed oxides with hierarchically macro-/mesoporous structures, Ind. Eng. Chem. Res. 50 (2011) 883–890.
[50] C. Chen, W.-S. Ahn, CO_2 capture using mesoporous alumina prepared by a sol–gel process, Chem. Eng. J. 166 (2011) 646–651.
[51] C.-F. Mao, M.A.s Vannice, High surface area a-alumina. I. Adsorption properties and heats of adsorption of carbon monoxide, carbon dioxide, and ethylene, Appl. Catal. A Gen. 111 (1994) 151–173.
[52] Y. Shiraki, K.L.I. Kobayashi, Y. Katayama, Study of adsorption phenomena on aluminium by interatomic Auger transition spectroscopy. II CO adsorption onto Al, Surf. Sci. 77 (1978) 458–464.
[53] N.D. Parkyns, Surface properties of metal oxides. Part I. Infrared studies of the adsorption and oxidation of carbon monoxide on alumina, J. Chem. Soc. A: Inorg. Phys. Theor. Chem. (1967) 1910–1913.
[54] J.C.S. Wu, C.-W. Huang, In situ DRIFTS study of photocatalytic CO_2 reduction under UV irradiation, Front. Chem. Eng. China 4 (2010) 120–126.
[55] V.P. Indrakanti, J.D. Kubicki, H.H. Schobert, Photoinduced activation of CO_2 on Ti-based heterogeneous catalysts: Current state, chemical physics-based insights and outlook, Energy Environ. Sci. 2 (2009) 745–758.